

Transient and Stability Tests at Peach Bottom Atomic Power Station Unit 2 at End of Cycle 2 PECo Library Copy

EPRI

EPRI NP-564
Project 1020-1
Topical Report
June 1978

Keywords:

BWR Turbine Trip
BWR Stability
BWR Pressure Transient
BWR Pressure Perturbation Test

RESEARCH DIVISION
E. S. HALFMANN
SEP 27 1978
Note:
Referred:

Prepared by
General Electric Company
San Jose, California



ELECTRIC POWER RESEARCH INSTITUTE

Transient and Stability Tests at
Peach Bottom Atomic Power Station Unit 2
at End of Cycle 2

NP-564
Research Project 1020-I

Topical Report, June 1978



Prepared by

GENERAL ELECTRIC COMPANY
Nuclear Energy Engineering Division
175 Curtner Avenue
San Jose, California 95125

Principal Investigators
L. A. Carmichael
R. O. Niemi

Prepared for

Electric Power Research Institute
3412 Hillview Avenue
Palo Alto, California 94304

EPRI Project Manager
Robert N. Whitesel

LEGAL NOTICE

This report was prepared by General Electric /GE/ es an account of work done in conjunction with Philadelphia Electric Company (PECo) and sponsored by both the Electric Power Research Institute, Inc. (EPRI) and the General Electric Company. Neither EPRI, members of EPRI, PECo, GE, nor any person acting on behalf of either: (a) Makes any warranty or representation, express or implied, with respect to the accuracy, completeness, or usefulness of the information contained in this report, or that the use of any information, apparatus, method, or process disclosed in this report may not infringe privately owned rights; or (b) Assumes any liabilities with respect to the use of, or for damages resulting from the use of, any information, apparatus, method or process disclosed in this report.

FOREWORD

This report is a description of the results from the transient and stability tests conducted at the Peach Bottom-2 reactor in April 1977 at end of Cycle 2. The project has been aimed at measuring both the stability of a BWR core when subjected to small pressure oscillations and the response of the reactor to large pressure transients. The data from such tests are important not only to the technical base of the licensing of BWR plants, but also as reference data for the qualification of reactor transient and stability computer codes.

A companion report, NP-563, *Core Design and Operating Data for Cycles 1 and 2 of Peach Bottom-2*, provides a compilation of reactor design and operating data for use in the qualification of reactor core analysis methods and provides a source of plant design geometric inputs for the transient and stability computer codes.

BRUCE W. CRAWFORD
Program Manager
Nuclear Energy Engineering Division
General Electric Company

ROBERT N. WHITESEL
Project Manager
Electric Power Research Institute

ABSTRACT

Turbine trip transient and low flow stability tests were performed at the Peach Bottom-2 BWR/4 nuclear power plant prior to shutdown for refueling at end of Cycle 2 in April 1977. The turbine trip transient tests were conducted to investigate the effect of the pressure transients generated in the reactor vessel following a turbine trip on the neutron flux in the reactor core. The purpose of the low-flow stability testing was to determine the power-to-void feedback stability margin of the BWR core at an operating condition above the rated power-flow control line, and to investigate the sensitivity of core stability to changes in reactor operating conditions. These tests were also intended to demonstrate the practicality of using small pressure perturbation tests to determine the stability margin of a large B WR core.

The results of the turbine trip transient tests showed that the fundamental mode of the acoustical pressure oscillation generated in the main steam piping propagates with relatively little attenuation into the reactor core. The magnitude of the neutron flux transient taking place in the BWR core was found to be strongly affected by the initial rate of pressure rise caused by the pressure oscillation. The measured neutron flux transients showed a strong spatial variation along the axis of the reactor core. Very little radial variation in the neutron flux transient was observed.

The low-flow stability tests demonstrated that the Peach Bottom-2 Cycle 2 core exhibited a high degree of stability at the limiting test condition above the rated power-flow control line. The measured reactor stability margins showed the expected sensitivity to core power changes at minimum reactor core flow. The Peach Bottom-2 tests showed that the small pressure perturbation stability testing offers a useful and practical method of measuring core stability margins in operating BWR reactors. The actual core stability margin was determined from the measured closed-loop pressure to average neutron flux transfer function data based on maximum likelihood estimates of the parameters in a relatively simple transfer function model determined from nonlinear regression analysis.

Both static and dynamic error estimates were taken into consideration in evaluating the test results.

ACKNOWLEDGMENT

We would like to acknowledge the help and cooperation of the Peach Bottom staff, without which the Peach Bottom transient and stability tests could not have been run successfully. We would like to thank station superintendent W. T. Ullrich for guiding the operating and engineering staff in balancing the often conflicting requirements of generating power and conducting the tests. Ms. Robbie Kankus provided the liaison between the PECO and GE engineers. Bruce Clark guided the sensitive operation of connecting special instrumentation while maintaining the plant operation. Roman Cyhan and Fred Polaski provided the nuclear engineering talent for maneuvering the plant through the numerous restrictions to achieve the test conditions.

The contributions of the above individuals to the achievement of a successful test are gratefully acknowledged.

TABLE OF CONTENTS

	Page
1. INTRODUCTION	I-1
1.1 Background.	I-1
1.2 Objectives	I-1
1.3 Test Plan	I-1
1.4 Expected Application of Test Results	I-2
2. SUMMARY OF RESULTS AND CONCLUSIONS.	2-I
2.1 Transient Tests.	2-I
2.2 Low-Flow Stability Tests	2-I
3. PLAN OF THE EXPERIMENT..	3-1
3.1 Basis for Test Conditions	3-1
3.2 Planned Test Sequence.	3-1
3.3 Actual Test Conditions.	3-2
4. PLANT AND TEST EQUIPMENT DESCRIPTION	4-1
4.1 Plant Description.	4-1
4.2 Special Transducer Installation.	4-1
4.3 Data Acquisition System.	4-1
4.4 Measurement System Calibration	4-2
5. TEST PROCEDURES	5-I
5.1 Turbine Trip Transient Tests	5-1
5.2 Small Pressure Perturbation Tests.	5-2
6. EXPERIMENTAL RESULTS	6-I
6.1 Turbine Trip Transient Tests.	6-1
6.2 Low-Flow Stability Tests	6-4
7. REFERENCES.	7-1

APPENDICES

A. DATA REDUCTION METHODS.	A-I
B. MEASUREMENT ERROR ANALYSIS.	B-I
C. PROCESS COMPUTER EDITS	C-I
D. ADDITIONAL TURBINE TRIP TEST MEASUREMENTS.	D-I
E. ADDITIONAL LOW-FLOW STABILITY FREQUENCY RESPONSE MEASUREMENTS.	E-I

LIST OF ILLUSTRATIONS

Figure		Page
3-1	Peach Bottom-2 Low-Flow Stability Tests: Planned Test Conditions.	3-7
3-2	Peach Bottom-2 EOC-2 Test Planned Test Operational Time Line.	3-7
3-3	Peach Bottom-2 EOC-2 Turbine Trip Test (TT1) Initial Control Rod Pattern	3-8
3-4	Peach Bottom-2 Turbine Trip Test (TT1) Average Axial Power Distribution.	3-8
3-5	Peach Bottom-2 EOC-2 Turbine Trip Test (TT2) Initial Control Rod Pattern	3-9
3-6	Peach Bottom-2 Turbine Trip Test (TT2) Average Axial Power Distribution.	3-9
3-7	Peach Bottom-2 EOC-2 Turbine Trip Test (TT3) Initial Control Rod Pattern	3-10
3-8	Peach Bottom-2 Turbine Trip Test (TT3) Average Axial Power Distribution.	3-10
3-9	Peach Bottom-2 Low-Flow Stability Test (PT1) Control Rod Pattern	3-11
3-10	Peach Bottom-2 Low-Flow Stability Test (PT1) Average Axial Power Distribution. . . .	3-11
3-11	Peach Bottom-2 Low-Flow Stability Test (PT2) Control Rod Pattern	3-12
3-12	Peach Bottom-2 Low-Flow Stability Test (PT2) Average Axial Power Distribution. . . .	3-12
3-13	Peach Bottom-2 Low-Flow Stability Test (PT3) Control Rod Pattern	3-13
3-14	Peach Bottom-2 Low-Flow Stability Test (PT3) Average Axial Power Distribution. . . .	3-13
3-15	Peach Bottom-2 Low-Flow Stability Test (PT4) Control Rod Pattern	3-14
3-16	Peach Bottom-2 Low-Flow Stability Test (PT4) Average Axial Power Distribution. . . .	3-14
3-17	Peach Bottom-2 Low-Flow Stability Tests: Actual Test Conditions.	3-15
4-1	LPRM Power Supply Signal Tap.	4-6
4-2	Special Pressure Transducer Installation.	4-7
4-3	Digital Data Acquisition System Hardware Configuration	4-8
6-1	Peach Bottom-2 EOC2 Test Turbine Trip Test TT1 Transient Pressure Measurements. .	6-9
6-2	Peach Bottom-2 EOC2 Test Turbine Trip Test TT2 Transient Pressure Measurements .	6-10
6-3	Peach Bottom-2 EOC2 Test Turbine Trip Test TT3 Transient Pressure Measurements .	6-11
6-4	Peach Bottom-2 EOC2 Test Turbine Trip Test TT1 Filtered Pressure Measurements (5 Hz Lowpass Filter).	6-12

LIST OF ILLUSTRATIONS (Continued)

Figure		Page
6-5	Peach Bottom-2 EOC2 Test Turbine Trip Test TT2 Filtered Pressure Measurements (5 Hz Lowpass Filter).	.6-13
6-6	Peach Bottom-2 EOC2 Test Turbine Trip Test TT3 Filtered Pressure Measurements (5 Hz Lowpass Filter).	.6-14
6-7	Peach Bottom-2 EOC2 Test Turbine Trip Test TT1 Reactor Core Response	.6-15
6-8	Peach Bottom-2 EOC2 Test Turbine Trip Test TT2 Reactor Core Response	.6-16
6-9	Peach Bottom-2 EOC2 Test Turbine Trip Test TT3 Reactor Core Response	.6-17
6-10A	Peach Bottom-2 EOC2 Test Turbine Trip Test TT1 Core Local Power Monitor Response	.6-19
6-10B	Peach Bottom-2 EOC2 Test Turbine Trip Test TT1 Core Local Power Monitor Response	.6-21
6-10C	Peach Bottom-2 EOC2 Test Turbine Trip Test TT1 Core Local Power Monitor Response	.6-23
6-11A	Peach Bottom-2 EOC2 Test Turbine Trip Test TT1 Control Rod Drive Response	.6-25
6-11B	Peach Bottom-2 EOC2 Test Turbine Trip Test TT1 Control Rod Drive Response	.6-26
6-11C	Peach Bottom-2 EOC2 Test Turbine Trip Test TT1 Control Rod Drive Response	.6-27
6-11D	Peach Bottom-2 EOC2 Test Turbine Trip Test TT1 Control Rod Drive Response	.6-28
6-12	Peach Bottom-2 EOC2 Test Turbine Trip Test TT1 Control Rod Scram Speed Summary	.6-29
6-13	Peach Bottom-2 EOC2 Test Turbine Trip Test TT1 Reactor Feedwater and Level Response	.6-30
6-14	Peach Bottom-2 EOC2 Test Turbine Trip Test TT1 Reactor Jet Pump and Core Pressure Drop Response	.6-31
6-15	Peach Bottom-2 EOC2 Test Turbine Trip Test TT1 Reactor Recirculation Loop Response	.6-32
6-16	Peach Bottom-2 EOC2 Test Turbine Trip Test TT2 Reactor Feedwater and Level Response	.6-33
6-17	Peach Bottom-2 EOC2 Test Turbine Trip Test TT2 Reactor Jet Pump and Core Pressure Drop Response	.6-34
6-18	Peach Bottom-2 EOC2 Test Turbine Trip Test TT2 Reactor Recirculation Loop Pressure	.6-35
6-19	Peach Bottom-2 EOC2 Test Turbine Trip Test TT3 Reactor Feedwater and Level Response	.6-36
6-20	Peach Bottom-2 EOC2 Test Turbine Trip Test TT3 Reactor Jet Pump and Core Pressure Drop Response	.6-37
6-21	Peach Bottom-2 EOC2 Test Turbine Trip Test TT3 Reactor Recirculation Loop Response	.6-38

LIST OF ILLUSTRATIONS (Continued)

Figure	Title	Page
6-22	Peach Bottom-2 EOC2 Test Low-Flow Stability Tests Periodic Pressure Regulator Setpoint Steps.	.6-39
6-23	Peach Bottom-2 EOC2 Test Low-Flow Stability Test PRBS Pressure Regulator Setpoint Steps.	.6-40
6-24	Power Spectrum Core Exit Pressure Periodic Setpoint Input6-41
6-25	Power Spectrum Core Exit Pressure PRBS Setpoint Input.6-42
6-26	Peach Bottom-2 EOC2 Low-Flow Stability Test (PT3) Power Spectrum Core Exit Pressure.6-43
6-27	Peach Bottom-2 EOC2 Low-Flow Stability Test (PT3) Power Spectrum Average Neutron Flux (APRM A).6-44	
6-28	Peach Bottom-2 EOC2 Low-Flow Stability Test PT3 Measured Transfer Function Magnitude Average Neutron Flux (APRM A)/Core Pressure.6-45
6-29	Peach Bottom-2 EOC2 Low-Flow Stability Test PT3 Measured Transfer Function Phase Average Neutron Flux (APRM A)/Core Pressure6-46
6-30	Peach Bottom-2 EOC2 Low-Flow Stability Test (PT3) Coherence Between Average Neutron (APRM A) and Core Pressure Response.	.6-47
6-31	Peach Bottom-2 EOC2 Stability Test PT3 Transfer Function Model Comparison (1 Zero/2 Pole Model)6-48
6-32	Peach Bottom-2 EOC2 Stability Test PT3 Transfer Function Model Comparison (1 Zero/3 Pole Model)6-49
6-33	Peach Bottom-2 EOC2 Stability Test PT1 Transfer Function Model Comparison (1 Zero/2 Pole Model)6-50
6-34	Peach Bottom-2 EOC2 Stability Test PT2 Transfer Function Model Comparison (1 Zero/2 Pole Model)6-51
6-35	Peach Bottom EOC2 Low Flow Stability Test PT4 Transfer Function Model Comparison (1 Zero/2 Pole Model)6-52
6-36	Peach Bottom-2 EOC2 Test Low Flow Stability Tests Core Stability Margin Versus Core Flow6-53
6-37	Peach Bottom-2 Low-Flow Stability Test PT3 Axial Local Flux Response (LPRM String 32-41)6-54
6-38	Peach Bottom-2 Low-Flow Stability Test PT4 Axial Local Flux Response (LPRM String 32-41)6-55

LIST OF TABLES

Table	Title	Page
3-1	Turbine Trip Transient Tests Planned initial Conditions	3-4
3-2	Turbine Trip Transient Tests Planned APRM Trip Set Points.	3-4
3-3	Interim Technical Specification Fuel Thermal Operating Limits	3-4
3-4	Interim Technical Specification Rod Block and APRM Scram Lines	3-5
3-5	Peach Bottom-2 End-of-Cycle 2 Test Actual Turbine Trip Transient Test Conditions	3-5
3-6	Turbine Trip Transient Tests Actual APRM High Flux Scram Set Point.	3-6
3-7	Peach Bottom-2 End-of-Cycle Test Actual Low-Flow Stability Test Conditions.	3-6
4-1	Peach Bottom-2 Signal Range and Conditioning	4-5
6-1	Peach Bottom-2 EOC-2 Turbine Trip Transient Tests Event Timing.	6-7
6-2	Peach Bottom-2 Turbine Trip Transient Test Peak Measured Responses.	6-7
6-3	Low-Flow Stability Test PT3 Results of Empirical Transfer Function Model Parameter Identification.	6-8
6-4	Low-Flow Stability Tests Core Stability Margin Estimates.	6-8

1. INTRODUCTION

1 .1 BACKGROUND

1.1.1 Large-Transient Tests

During the 40-year expected lifetime of a boiling water reactor power plant, the frequency of occurrence of pressurization transients is expected to be 1 to 2 per year on the average. In addition, it can be expected that about once in the lifetime of the plant a complete and sudden isolation of the reactor from its heat sink could occur through the failure of the steam bypass system during a turbine trip or generator load rejection. The consequences of this type of transient are analyzed with large-scale system transient computer codes which must predict the dynamic behavior of the reactor core and nuclear steam supply system. Prior to the Peach Bottom-2 tests no data base existed for benchmarking these transient design codes at conditions approaching the limiting transients for which they are employed in safety and design analysis. Of the test data that were available, the majority were obtained at beginning-of-life (BOL) conditions during startup testing. Generally these tests are conducted for plant performance evaluation and are not specifically designed and instrumented for collecting model qualification test data. Also the beginning-of-life core condition can differ considerably from the limiting operating conditions expected for design and safety analysis.

1 .1.2 Core Stability Tests

The possibility of instability in the core of a boiling water reactor induced by thermal-hydraulic and void reactivity feedback has been the subject of many analytical and experimental investigations since the startup of early boiling water power reactors.^{1,2} The analytical methods available to the designer have become increasingly more sophisticated; however, the uncertainty in the prediction of boiling water reactor core stability behavior still contributes to the imposition of design constraints on the low-flow operating range of commercial boiling water reactor nuclear power plants. The amount of test data taken to improve this situation for modern higher-power-density reactor cores is, in fact, quite limited due to the high cost of the conventional control rod oscillator experiments in commercial power plants and the lower quality of the data because of poor signal-to-noise ratios in large reactor cores.³

1.2 OBJECTIVES

1.2.1 Large-Transient Tests

The main objective of these tests is to provide a data base for the utility industry for the qualification of transient design methods used for reactor analysis at operating conditions. An important requirement in these tests was that the test conditions approach the design basis conditions as closely as practicable. The results of such comparisons are expected to provide a high degree of confidence in the conservatism of the transient methods which are employed in the safety and licensing analysis of large nuclear reactor transients.

1.2.2 Core Stability Tests

The purposes of these tests are: (1) to demonstrate that the stability margin of a boiling water reactor core can be determined through a series of small pressure perturbation tests, with minimal disturbance to plant operation, and provide superior test data to that obtained from rod oscillator testing in large boiling water reactor cores; (2) to increase the data base for the qualification of core stability design methods which will, hopefully, serve to improve the confidence and identify conservatism in the current stability design methods; (3) to demonstrate safe operation at low flow conditions above the rated power/flow rod line.

1.3 TEST PLAN

Arrangements with Philadelphia Electric Company (PECo) were made for conducting up to three turbine trip tests and one or more series of low-flow stability tests at Peach Bottom, Unit 2 BWR during the first quarter of 1977. The selection of this reactor was based on its being a large BWR/4 with relatively small turbine bypass capacity which would reach the end of its reload fuel cycle early in 1977.

For both types of tests, the dynamic measurements were taken with a high-speed digital data acquisition system capable of sampling over 150 signals every 6 milliseconds. For both types of tests the core power distribution measurements were taken from the plant's local in-core flux detectors. Special fast response pressure and differential pressure transducers were installed in parallel with existing plant instruments to measure the response of important variables in the nuclear steam supply system. Control rod position information was available from a significant sample of drives to determine the scram speed during the transient tests.

The basis for selection of the test conditions is presented in Section 3. The criteria used in their selection were generally based on a combination of previous testing experience, evaluation of expected end-of-cycle BWR core stability and large pressurization transient limitations, and conditions required by PECo in performing the tests.

1.4 EXPECTED APPLICATION OF TEST RESULTS

The transient tests were not intended to give a direct demonstration of a design basis transient; hence, use of these results will depend on analytical modeling to relate the results to design basis transient calculations. The low-flow stability tests were intended to measure reactor core stability margins at the limiting conditions used in design and safety analysis, providing a one-to-one comparison to design calculations.

The test results were specified to consist of engineering transient data recorded on magnetic tape and process computer drum dumps for core power determination calculations at each test conditions. The transient data was to be available for direct comparison or resimulation using transient design codes for model qualification benchmark analysis. The results of the low-flow stability tests were to be derived from a Fourier time-series analysis in terms of an experimentally determined transfer function between core pressure and average neutron flux. From this transfer function the stability margin of the core in terms of a decay ratio of the fundamental oscillatory mode of response can be determined.

2. SUMMARY OF RESULTS AND CONCLUSIONS

2.1 TRANSIENT TESTS

The three core pressurization transient tests were conducted by manually tripping the turbine at three reactor power levels and near rated core flow. The tests were performed in order of ascending reactor power levels. The initial power conditions ranged from 48 to 69% of rated power. The turbine stop valve position input signal to the reactor protection system for scram initiation was intentionally delayed to allow a limited neutron flux transient to take place in the core. The neutron flux rise in the reactor was terminated by a trip of the reactor protection system on high neutron flux.

From the results of these tests, the following conclusions can be drawn:

1. An acoustical pressure wave (oscillation) can exist in the reactor main steam piping due to the combined compressibility and momentum effects in the steam line.
2. The fundamental mode of the acoustical pressure oscillation is strongly excited as a result of a turbine trip, which causes a sharp initial pressure rise in the reactor as the first pressure wave enters the reactor vessel.
3. The fundamental acoustical mode propagates in the main steam piping, entering the reactor vessel, and through the steam separators into the reactor core with relatively little attenuation.
4. The magnitude of the neutron flux peak during the turbine trip is strongly affected by the initial rate of pressure rise in the reactor core.
5. These tests demonstrate that the spatial effects of the neutron flux response are clearly in evidence in the axial core dimension. They also show essentially no radial dependence on the local neutron flux response. (The radial flux amplitude function is independent of radial position.)
6. The termination of the neutron flux transient was observed to be strongly dependent on the time at which the flux scram occurred. The effect of having both deep and shallow rods in the control rod pattern was demonstrated by the almost immediate termination of the flux transient at all levels in the core after only a small rod movement following the reactor scram.

2.2 LOW-FLOW STABILITY TESTS

Stability tests were conducted along the low-flow end of the rated power-flow line, and along the power-flow line corresponding to minimum recirculation pump speed. The reactor core stability margin was determined from an empirical model fitted to the experimentally derived transfer function measurement between core pressure and the APRM, average neutron flux signals. The effectiveness of two types of input test signals based on periodic and pseudo-random switching of the plant pressure regulator set point, was investigated.

The important conclusions reached as a result of the low-flow stability testing at Peach Bottom-2 are as follows:

1. The Peach Bottom-2 Reload Cycle-2 core design exhibited a large degree of stability in the power-to-void closed-loop response at each test condition.
2. Safe and stable operation of the reactor at a stability test condition above the rated power-flow line has been verified.
3. The experimental determination of the reactor core pressure to neutron flux transfer function is adequately modeled by a simple, empirical transfer function.
4. The small pressure perturbation tests have been shown to offer an operationally simple and precise technique for determining boiling water reactor core stability margins.

3. PLAN OF THE EXPERIMENT

3.1 BASIS FOR TEST CONDITIONS

3.1.1 Transient Tests

In the selection of the test conditions for the turbine trip transient tests it was required that the following three important constraints must be simultaneously satisfied:

1. The peak pressure rise transient should gradually approach the inception of relief valve operation through a series of three turbine trip tests.
2. The turbine trip test should cause an initial rate-of-pressure rise which would result in a significant neutron flux transient in the reactor core, providing adequate qualification data for benchmark comparisons of transient design models.
3. Sufficient operating margin must be maintained with regard to the initial core thermal operating limits so that an occurrence of a postulated limiting licensing transient during the tests will not result in a violation of the plant safety limit.*

These requirements were satisfied at each test condition by the choice of initial reactor power level and the APRM high neutron flux scram set point.

3.1.2 Low-Flow Stability Tests

The criteria for the selection of the test conditions for the low-flow stability tests were:

1. To investigate the relative sensitivity of the stability margin of the boiling water reactor core** to changes in core power and flow near the least stable core operating conditions.
2. To demonstrate the safe and stable operation of the reactor at low-flow operating conditions above the rated power-flow line. The test conditions were designated so that the sensitivity to core power and flow along the constant control rod line, and as close to the rated power-flow lines as practicable, could be examined. A test condition above the rated power-flow line, close to the design reference condition for boiling water reactor core stability licensing analysis, was to be conducted for direct comparison of the experimentally determined reactor core stability margin at this condition to the calculational results in the Reload Cycle-2 Licensing Submittal.⁵ Test points PT1, PT2, and PT3 were selected in order of decreasing stability so that data from each test could be evaluated prior to continuing to the next test condition.

3.2 PLANNED TEST SEQUENCE

The transient turbine trip test conditions were planned for the test conditions in Table 3-1. To ensure test data showing significant core pressure to power response from the initial pressure rise following the turbine trip, an interim change in the plant's technical specification to disable or delay the anticipatory reactor scram initiation from turbine stop valve closure was requested from the NRC. However, to minimize relief valve operation following the turbine trip, the initial core power level was reduced from rated and the high neutron flux trip set point was set down closer to the initial reactor operating power level. The planned APRM trip set points for the three test conditions in Table 3-1 are given in Table 3-2.

The initial operating limits on MCPR, which were imposed in the plant interim Technical Specification change for the duration of the turbine trip transient tests, were determined so that the postulated occurrence of the licensing basis transient occurring during the testing would not result in a violation of the plant safety limit.

*See the special licensing submittal⁴ prepared for the Peach Bottom-2 stability and transient tests for a description of the postulated limiting transient.

**The principal feedback path affecting boiling water reactor core stability is the power-to-void reactivity transfer function.⁶

The interim Technical Specification fuel thermal operating limits for the turbine trip tests are given in Table 3-3.

The four test conditions for the low-flow stability tests were planned to be as close as possible to one of the following reactor operating conditions:

1. points along the rated power-flow control line (PT1 and PT2);
2. points along the natural circulation power-flow control line (PT2, PT3, and PT4);
3. extrapolated rod-block natural circulation power (test point PT3).

The planned test conditions are shown in Figure 3-1.

In order to conduct reactor core stability tests at the low-flow test conditions, interim changes in the plant's Technical Specification of the APRM Rod Block and Scram Lines were requested from the NRC. The changes proposed for the duration of low-flow testing are given in Table 3-4.

An operational time line was developed for the test program in order to minimize the impact of the testing on the Peach Bottom-2 power production. The planned test sequence is shown in Figure 3-2. The strategy for the testing was to conduct the tests on a tightly controlled time schedule which allowed for the xenon transient effects. By testing at the maxima or minima in xenon concentration, the waiting time for stable power level and flux distribution in the core could be reduced from 24 to about 5 hours prior to each test.

3.3 ACTUAL TEST CONDITIONS

The actual test conditions for which the turbine trip transient tests were conducted are given in Table 3-5. Because of difficulties encountered with maneuvering to the control rod line, corresponding to a power level at or below that planned for TT2, reactor power was reduced to the planned level through flow control during the xenon soak." The APRM high flux scram set points for the three test conditions are given in Table 3-6. The process computer average axial power distribution calculation and the corresponding control rod patterns for the three turbine trip tests are plotted in Figures 3-3 through 3-8.**

The actual reactor operating conditions at which the low-flow core stability testing was conducted are listed in Table 3-7.** The minimum core flow that could be achieved at test conditions PT2, PT3, and PT4 was limited to that corresponding to about 20% of rated recirculation pump speed, rather than natural circulation core flow.[†] The reactor power level which could be attained above the rated rod line, PT3, was lower than that which was initially planned. The maximum power level which could be attained was found to be limited by the actual number of high-worth blades which could be withdrawn, under constraints of allowable flux peaking, at this point in the fuel cycle. The process computer average axial power distribution calculations for the low-flow stability test conditions, and the corresponding control rod patterns, are plotted in Figures 3-9 through 3-16.

The strong effect of the xenon transient occurring during the stability testing can be determined from a plot of the test conditions on a power-flow map in Figure 3-17. The skewing of the rated rod line between test conditions PT1 and PT2 from the equilibrium xenon calculated line gives an indication of the effect of the xenon transient. The average axial power distribution in the core was found to be stable following the B-hour xenon soak.^{††}

*This was intended to minimize the effect of local xenon transients on the axial power distribution, without requiring an additional 6-hour xenon soak.

**The process computer P1 edits from the core power calculations are reproduced in Appendix C. Calculated individual bundle nodal powers were stored on magnetic tape from the process computer drum dump and are available from General Electric Co.

[†]Operational problems with the reactor cleanup system limited the duration of natural circulation operation to approximately 20 minutes before vessel bottom head differential temperature limits would be exceeded; this is insufficient time to conduct one stability test.

^{††}Hourly tests of the average axial power distribution indicated local power changes of less than ~1/2% taking place.

During the Peach Bottom-2 testing, unforeseen changes in plant operation and utility load demand dictated some modification of the planned test sequence plotted in Figure 3-2. It was still possible, however, to utilize the strategy of waiting only for the maxima or minima of the xenon concentration to occur after plant maneuvering before proceeding with the testing. The first turbine trip test, TT1, was conducted 6 days prior to the low-flow stability test series, and the following two turbine trip tests were conducted 10 and 13 days after the stability testing.

Table 3-1
TURBINE TRIP TRANSIENT TESTS
PLANNED INITIAL CONDITIONS

Test Number	Thermal Power (MWt)	Core Flow (10⁶ lb/h)
TT1	1646	102.5
TT2	1975	102.5
TT3	2634	102.5

Table 3-2
TURBINE TRIP TRANSIENT TESTS
PLANNED APRM TRIP SET POINTS

Test Number	Initial Power Level (% Rated)	APRM Trip Set Point (% Rated)
TT1	50	85
TT2	60	95
TT3	80	100

Table 3-3
INTERIM TECHNICAL SPECIFICATION
FUEL THERMAL OPERATING LIMITS

	Operating MCPR	
	7X7 Fuel	8X8 Fuel
Current	1.28	1.31
Required for Test	1.31	1.39

Table 34
INTERIM TECHNICAL SPECIFICATION
ROD BLOCK AND APRM SCRAM LINES

Current	Planned
APRM Flux Scram Line	
$S = (0.66 \times W + 54) \times (A/\text{MTPF})$	$S = (0.45 \times W + 75) \times (A/\text{MTPF})$
APRM Rod Block Line	
$S = (0.66 \times W + 42) \times (A/\text{MTPF})$	$S = (0.58 \times W + 50) \times (A/\text{MTPF})$
where:	
S = setting in % of rated thermal power (3293 MWt).	
W = loop recirculating flow rate in % of rated (rated loop recirculation flow equals 34.2×10^6 lb/hr).	
A = design value of the total core peaking factor (2.63 for 7X7 and 2.44 for 8X8 fuel).	
MTPF = operating maximum total peaking factor if greater than A ; if less than or equal to A , $\text{MTPF} = A$.	

Table 3-5
PEACH BOTTOM-Z END-OF-CYCLE 2 TEST
ACTUAL TURBINE TRIP TRANSIENT TEST CONDITIONS

Test Number	Reactor (MWt)	Power (% Rated)	Core Flow Rate (10^6 lb/h)	Core Pressure ^a (psia)	Core Inlet Enthalpy (Btu/lb)
TT1	1562	47.4	101.3	98.8	528.4
TT2	2030	61.6	82.9	80.9	519.8
TT3	2275	69.1	101.9	99.4	523.6

^aBased on process computer edit (P1), corrected for steam separator pressure drop.

Table 3-6
TURBINE TRIP TRANSIENT TESTS
ACTUAL APRM HIGH FLUX SCRAM SET POINT

Test Number	Initial Power Level (% Rated)	APRM Trip Set Point (% Rated)
TT1	47.4	85
TT2	61.6	95
TT3	69.1	77

Table 3-7
PEACH BOTTOM-2 END-OF-CYCLE 2 TEST
ACTUAL LOW-FLOW STABILITY TEST CONDITIONS

Test Number	Reactor Power (MWt)	Core Flow Rate (10^6 lb/h)	Core Pressure ^a (psia)	Core Inlet Enthalpy (Btu/lb)
	(% Rated)	(% Rated)	(psia)	
PT1	1995	60.6	52.6	508.9
PT2	1702	51.7	43.0	505.0
PT3	1948	59.2	38.9	528.4
PT4	1434	43.5	38.9	507.2

^aBased on process computer edit (P1), corrected for steam separator pressure drop

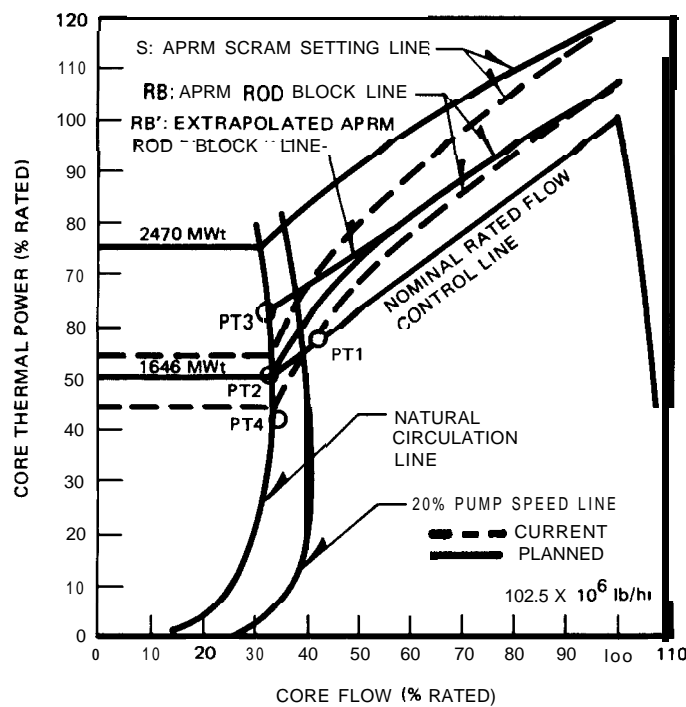


Figure 3-1. Peach Bottom-Z Low-Flow Stability Tests. Planned Test Conditions

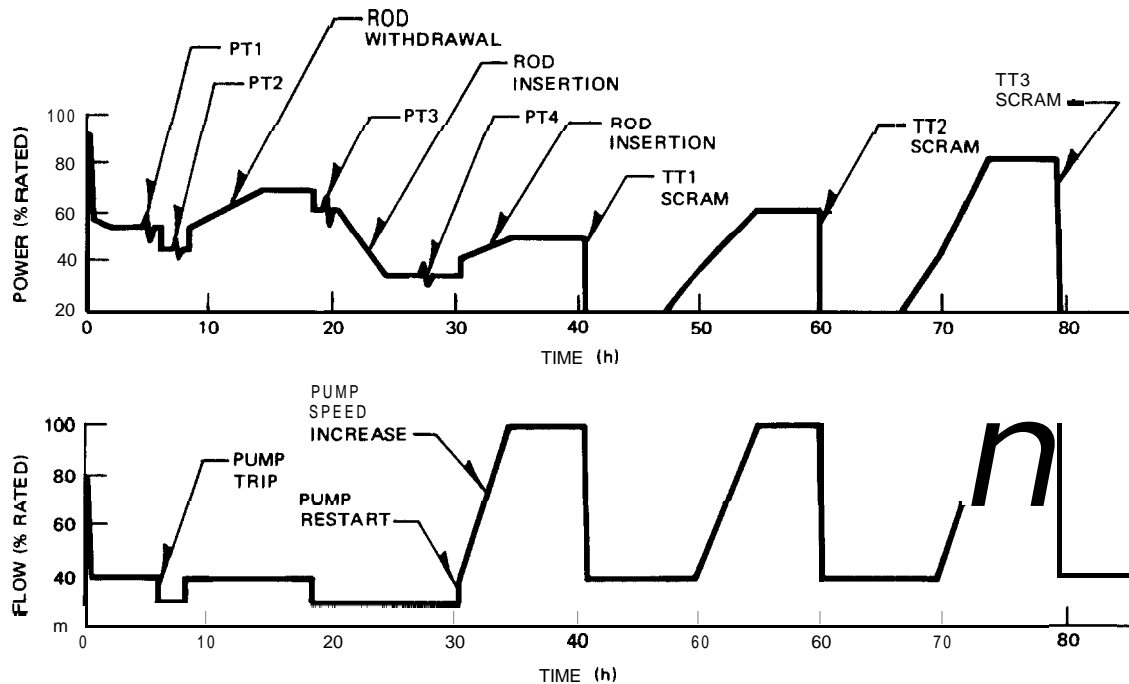


Figure 3-2. Peach Bottom-2 EOC-2 Test Planned Test Operational Time Line

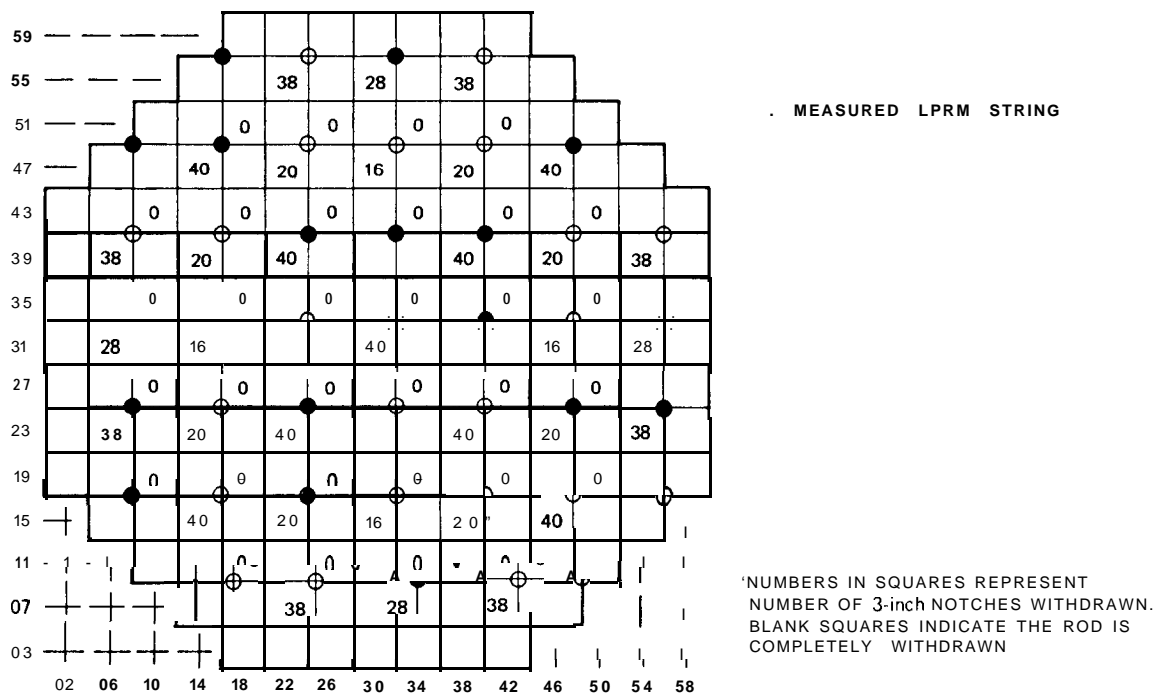


Figure 3-3. Peach Bottom-Z EOC-2 Turbine Trip Test (TT1) initial Control Rod Pattern •

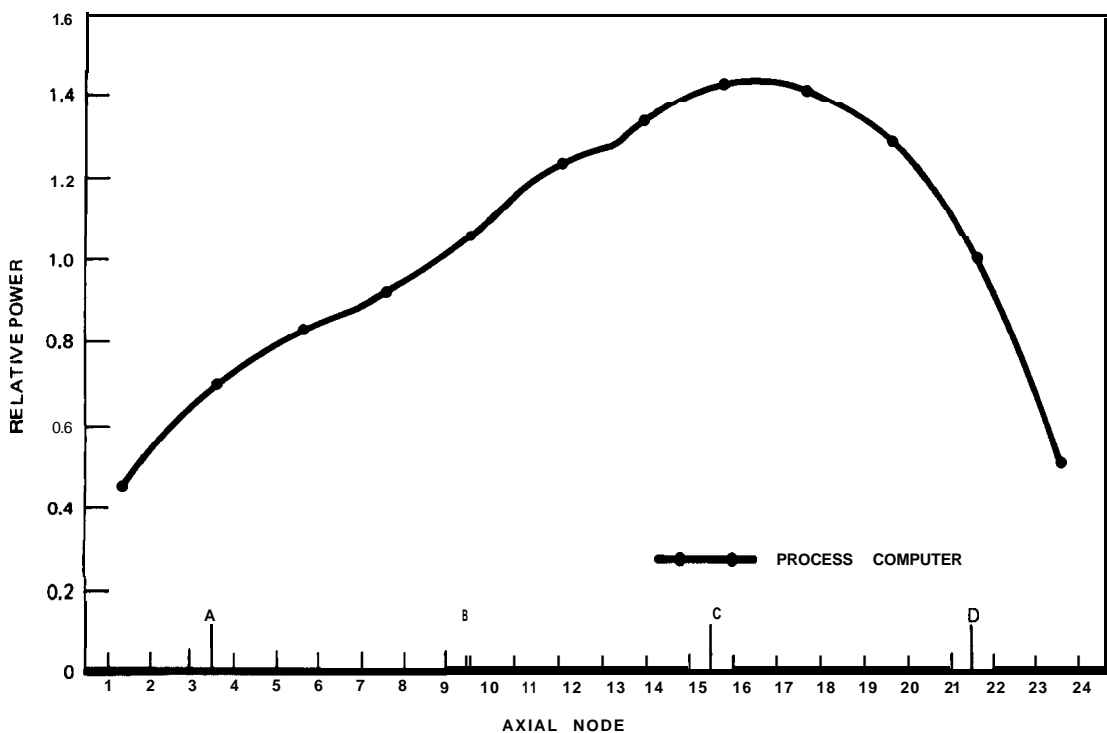


Figure 3-4. Peach Bottom-2 Turbine Trip Transient Test (TT1) Average Axial Power Distribution

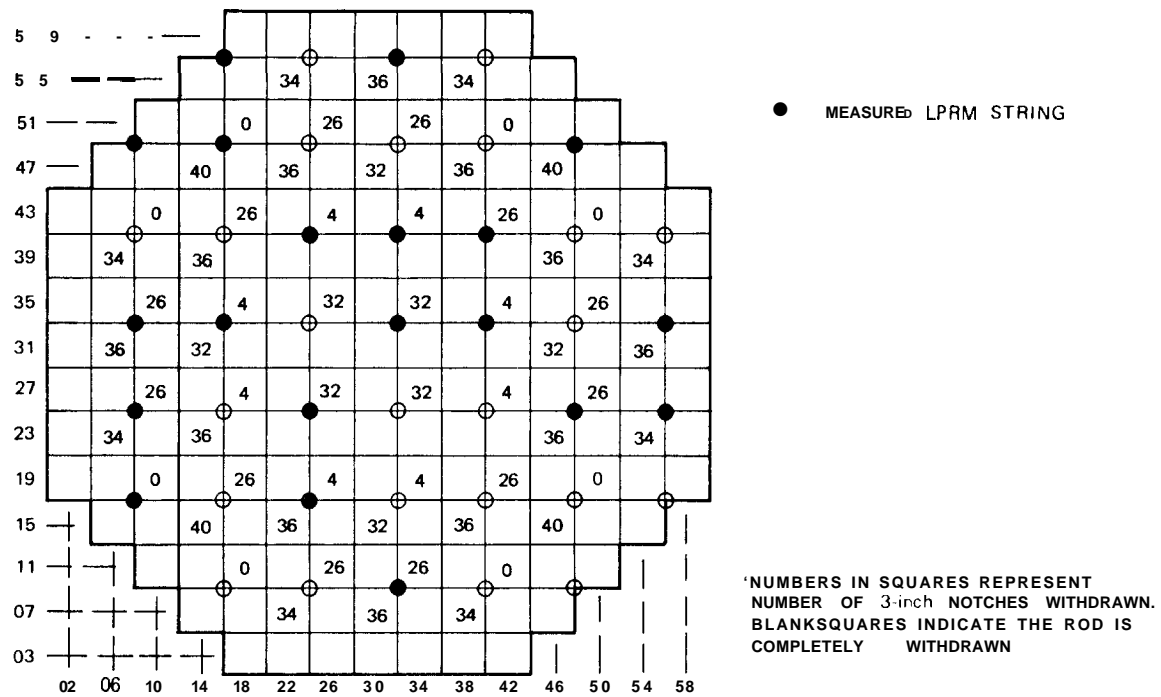


Figure 3-5. Peach Bottom-2 EOC-2 Turbine Trip Test (TT2) Initial Control Rod Pattern *

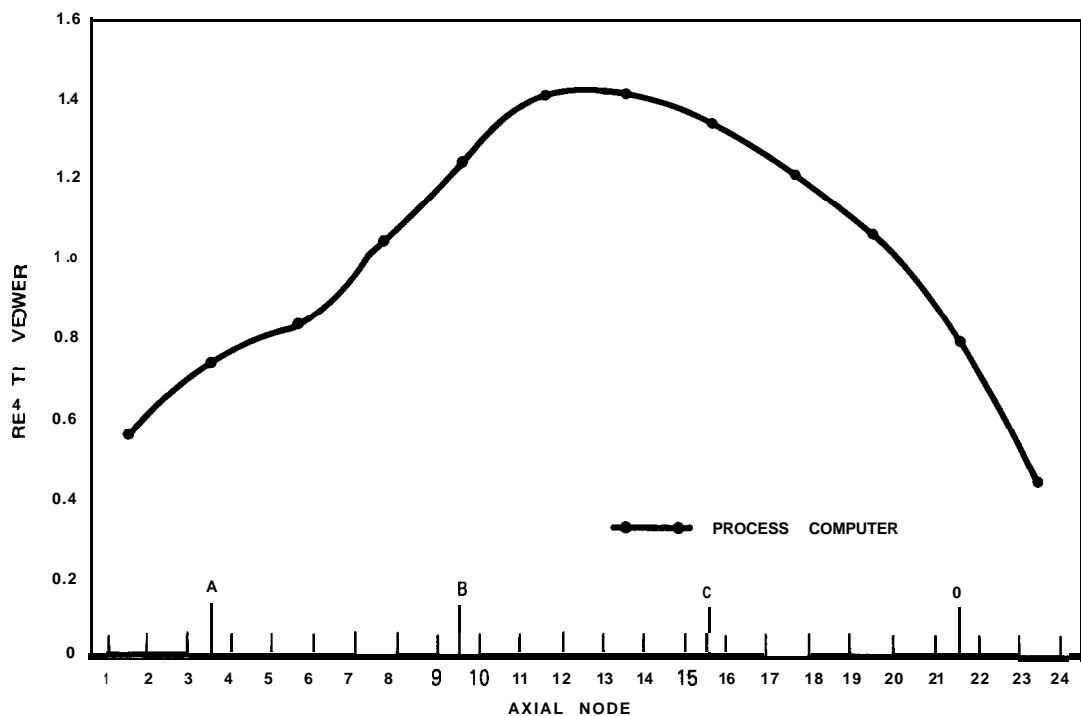


Figure 3-6. Peach Bottom-2 Turbine Trip Test (TT2) Average Axial Power Distribution

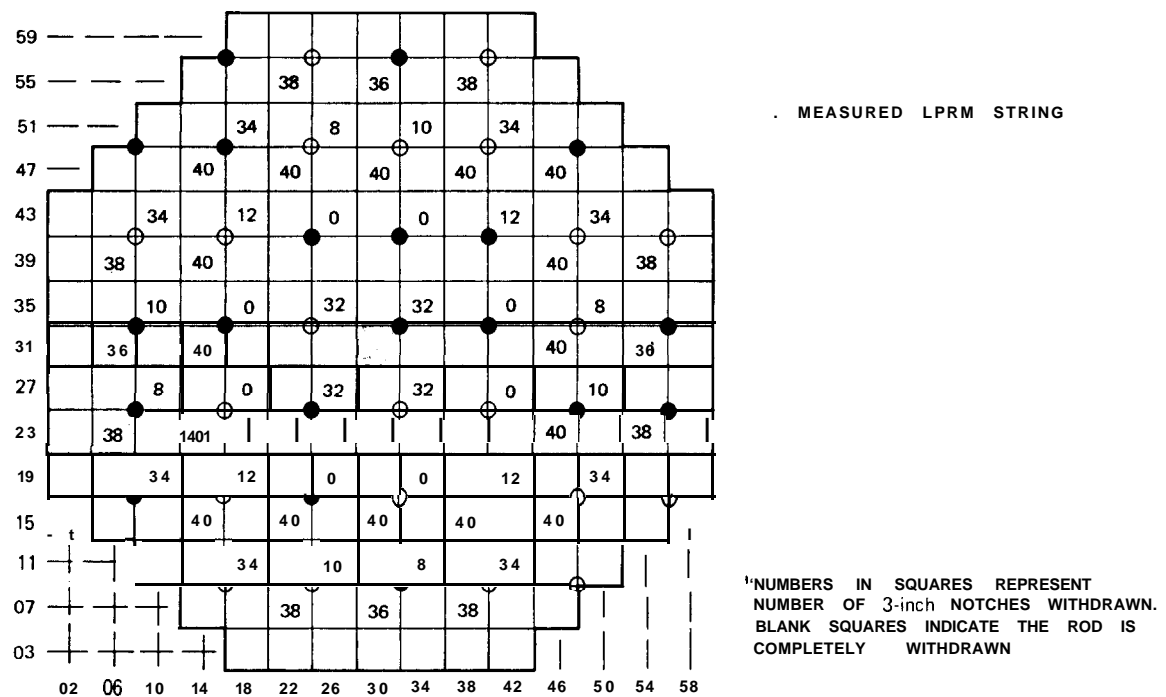


Figure 3-7. Peach Bottom-2 EOC-2 Turbine Trip Test (TT3) Initial Control Rod Pattern •

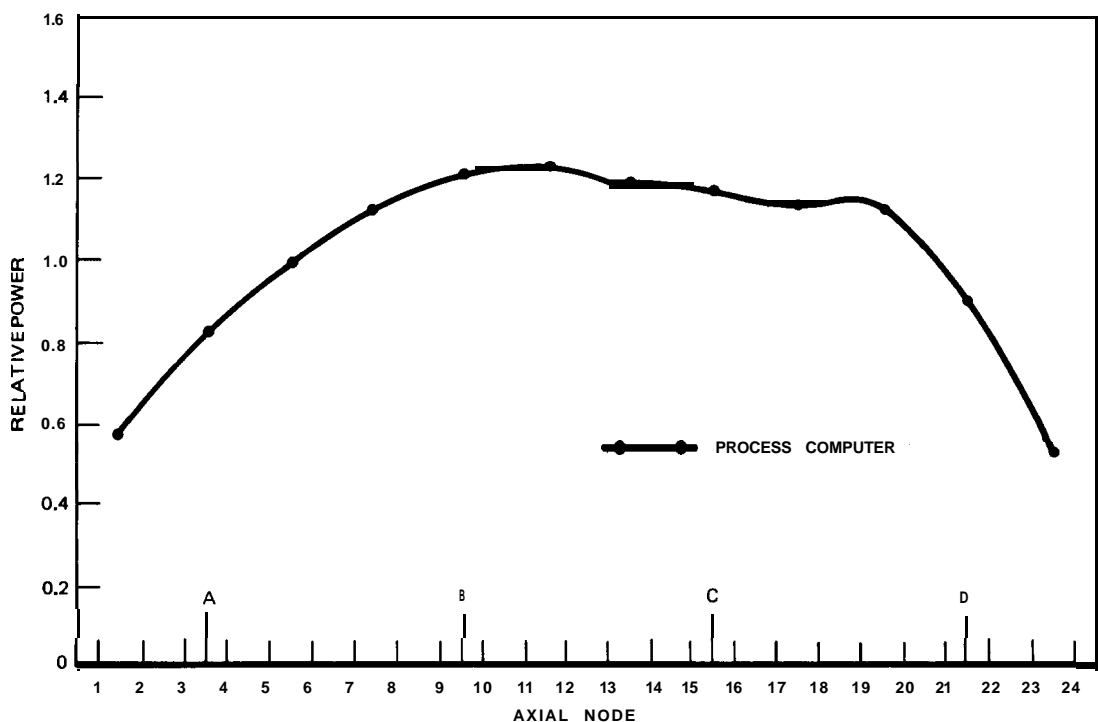


Figure 3-8. Peach Bottom-2 Turbine Trip Test (TT3) Average Axial Power Distribution

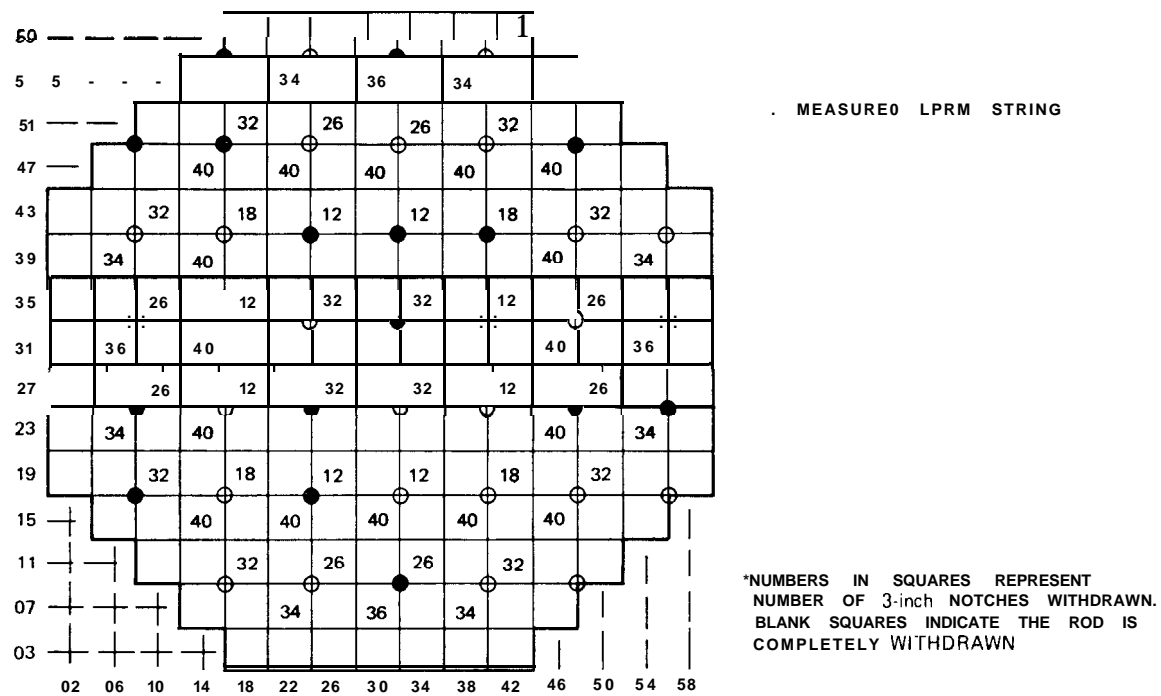


Figure 3-9. Peach Bottom-2 Low-Flow Stability Test (PT1) Control Rod Pattern .

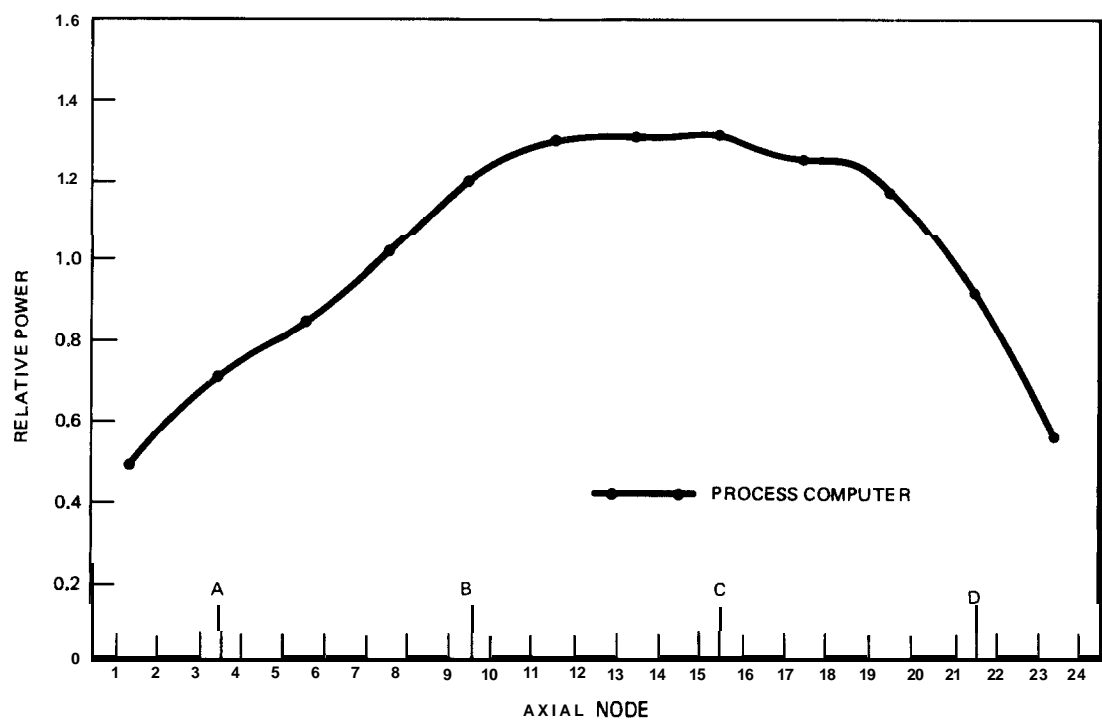


Figure 3- 10. Peach Bottom-2 Low-Flow Stability Test (PT1) Average Axial Po wer Distribution

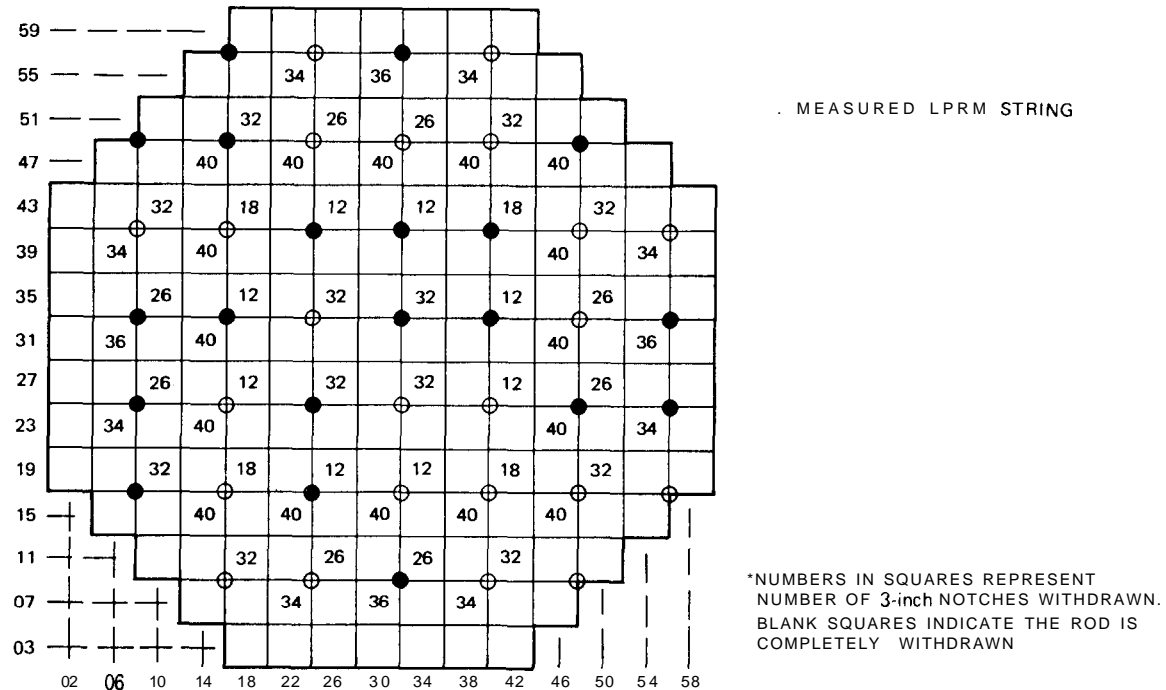


Figure 3-11. Peach Bottom-Z Low-Flow Stability Test (PT2) Control Rod Pattern'

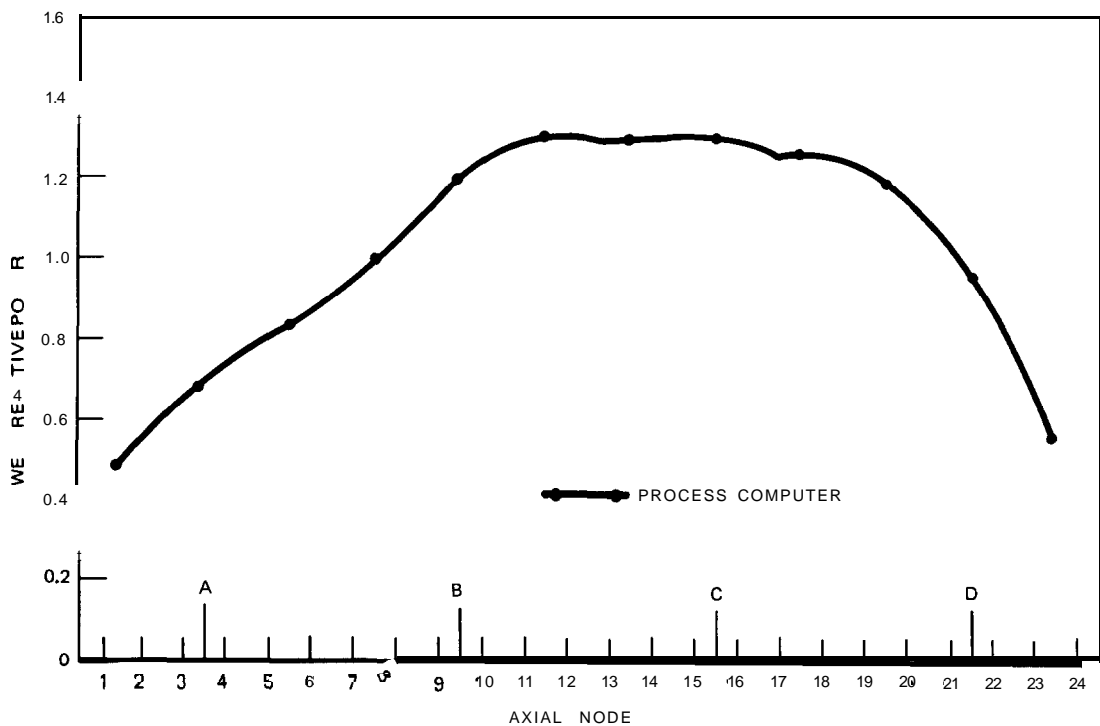


Figure 3-12. Peach Bottom-2 Low-Flow Stability Test (PT2) Average Axial Power Distribution

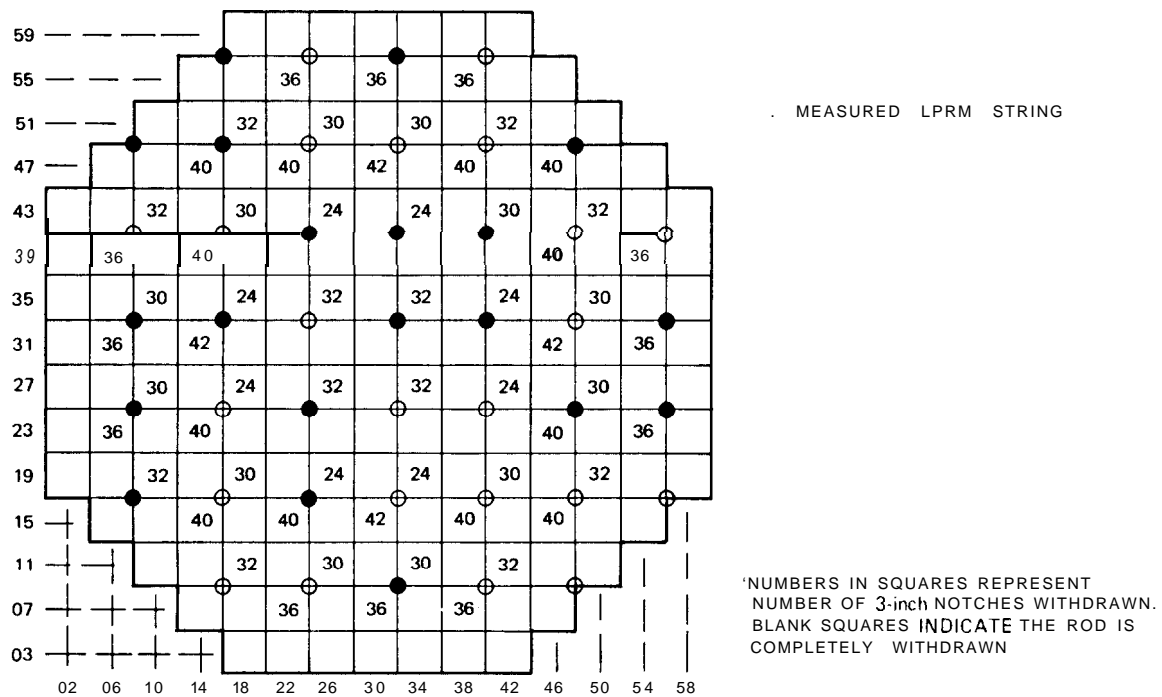


Figure 3-13. Peach Bottom-2 Low-Flow Stability Test (PT3) Control Rod Pattern *

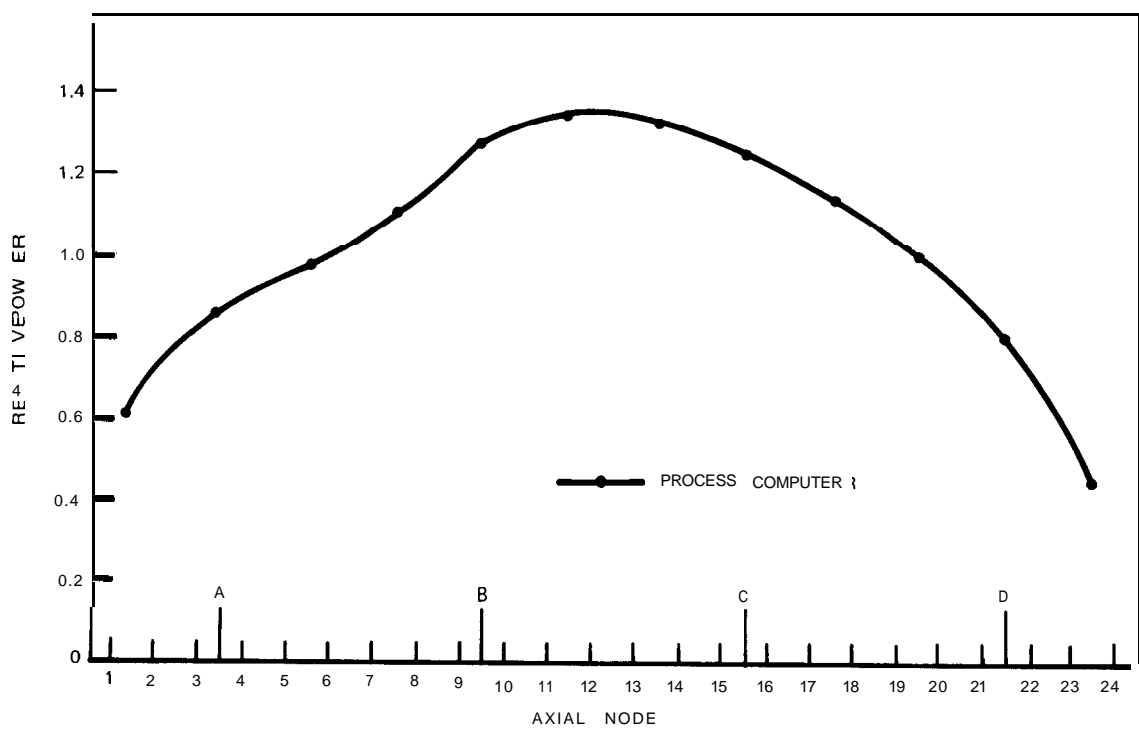


Figure 3-14. Peach Bottom-2 Low-Flow Stability Test (PT3) Average Axial Power Distribution

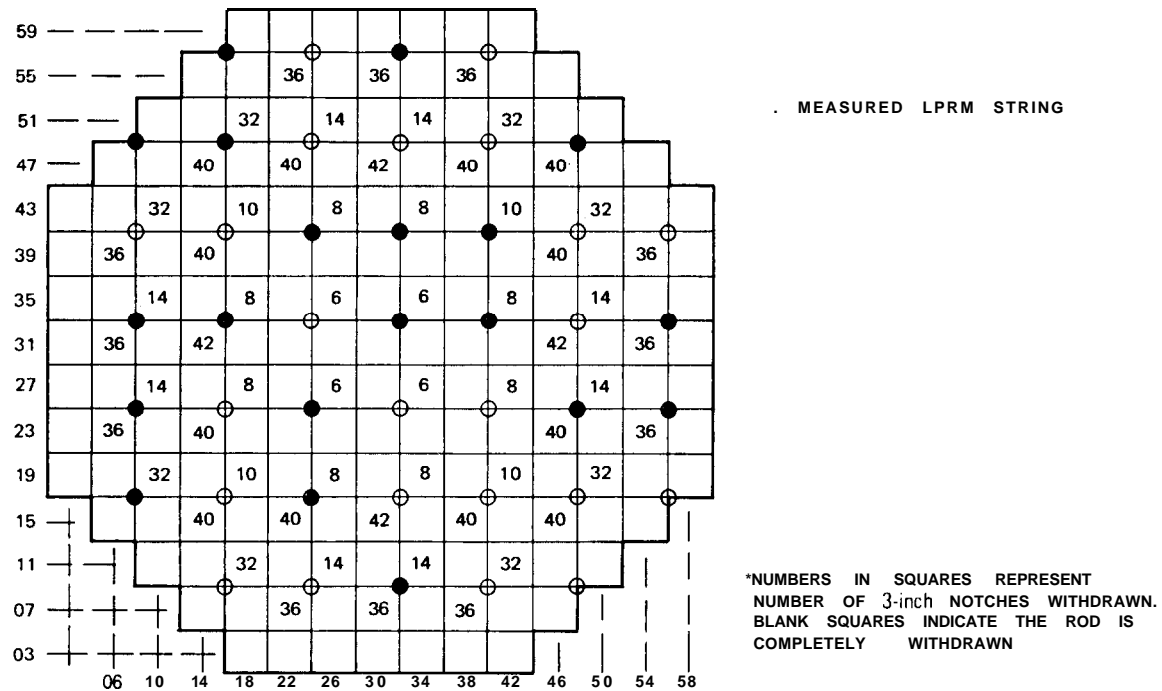


Figure 3-15. Peach Bottom-2 Low-Flow Stability Test (PT4) Control Rod Pattern.

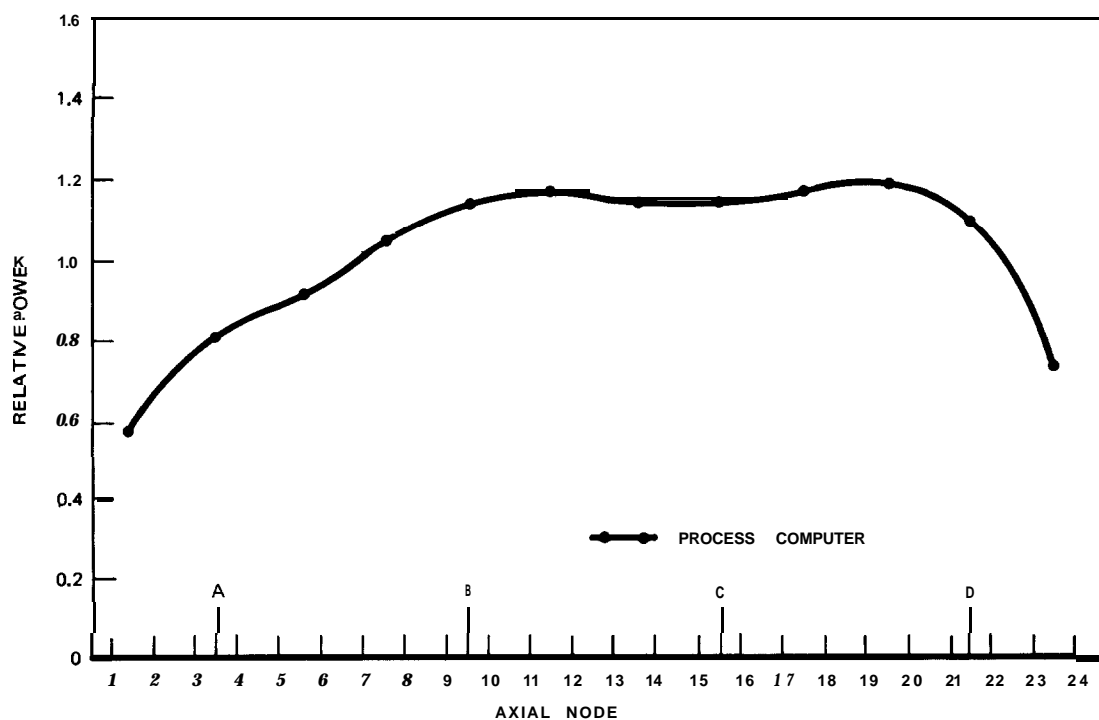


Figure 3-16. Peach Bottom-2 Low-Flow Stability Test (PT4) Average Axial Power Distribution

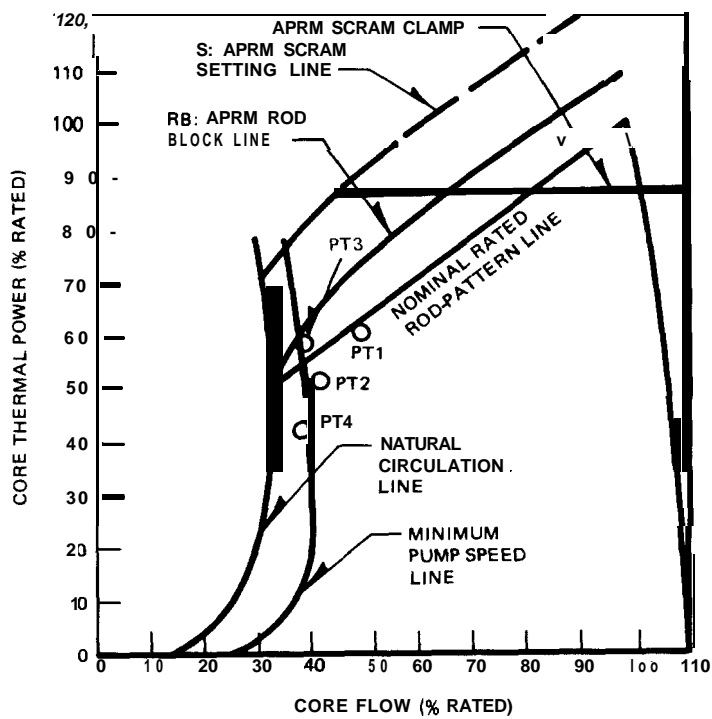


Figure 3-17. Peach Bottom Low-Flow Stability Tests: Actual Test Conditions

4. PLANT AND TEST EQUIPMENT DESCRIPTION

4.1 PLANT DESCRIPTION

Peach Bottom-Z is a single-cycle boiling water reactor (BWR/4) supplied by General Electric Company. The architect-engineer work was performed by Bechtel Power Corporation. The plant is owned and operated by Philadelphia Electric Company. The plant is located on the Susquehanna River 3 miles northeast of Delta, Pennsylvania, and 60 miles southwest of Philadelphia, Pennsylvania. The reactor vessel has a diameter of 251 inches, and contains 764 fuel bundles in a "D" lattice. The active core length is 144 inches. The vessel also contains 172 local power range detectors (LPRM), 4 source range detectors, 8 intermediate range detectors, and 5 traversing in-core probes. The total core flow is 102.5×10^6 lb/h; licensed power is 3293 MWe and 1098 MWe. The plant was accepted by Philadelphia Electric in July 1974. The tests were conducted in April 1977, at which time the plant was at the end of its Number 2 reload fuel cycle with an accumulated average core exposure of 12.7 GWd/t.

Details of the Peach Bottom-2 Nuclear Steam Supply System and Containment, as well as its various instrumentation, control, and safety system are provided in the plant Final Safety Analysis Report.⁷ A complete characterization of the Peach Bottom-2 Reload Cycle-2 core, and the requisite detailed plant layout data for the resimulation of the transient and stability tests, has been prepared and reported elsewhere.⁸

4.2 SPECIAL TRANSDUCER INSTALLATION

In order to measure effectively some of the faster-responding plant variables and to prevent signal saturation during the transient and stability tests, the following instrumentation was installed at Peach Bottom-2 specifically for the tests.

1. Direct measurements of local neutron detector power supply currents to provide a linear flux signal which is not affected by possible saturation of the LPRM current amplifiers during the transient testing. A schematic of a power supply installation is shown in Figure 4-1.
2. There were thirteen Viatran pressure transducers, providing fast-response measurements of absolute and differential pressures in the reactor vessel and main steam line piping. There were six model 218-15 0-1500 psia, five model 220-15 0-50 psid, and two model 220-15 0-100 psid transducers mounted in parallel with the existing plant instruments at the locations shown in Figure 4-2.*
3. A Rosemont type 115 differential pressure transducer, 0-200 inches H₂O, was placed in parallel with the plant safety system wide-range water level Yarway transducers to provide a continuous reactor bulk water level measurement.

4.3 DATA ACQUISITION SYSTEM

The data acquisition system used at Peach Bottom-2 consisted of the following equipment (refer to Figure 4-3).

1. HP 21MX computer (32K memory, 16 bit).
2. HP 2313A analog subsystem (45 kHz, 12 bit A/D, 160 channels).
3. HP 7970A magnetic tape (45 ips, 800 BPI).
4. HP 7970E magnetic tape (45 ips, 1600 BPI).
5. HP 7900A disc subsystem (25M word).
6. HP 2615A CRT terminal.
7. Versatec D1 110A printer/plotter.
8. NEFF Model 620 differential amplifiers (128 channels).
9. General Electric attenuation box (51-to-1 attenuation, 32 channels).

*Detailed diagrams of the individual pressure transducer installations are given in Appendix B

The data throughput rate to magnetic tape is 30 kHz. The number of data points per second per channel is dependent upon the number of channels being scanned.

4.4 MEASUREMENT SYSTEM CALIBRATION

At Peach Bottom-2, there were 13 signal types which required calibration. These expand to 17 different signals including overlap. These are listed in Table 4-1. All signals were digitized and recorded on magnetic tape.

- 1.. **Signal Type** — Local Power Range Monitor

Channel Numbers — 0-79

Signal Description — The equivalent of a $500\ \Omega$ resistor (one $1\ k\Omega$ resistor in parallel with a $1\ k\Omega$ potentiometer) was placed in series between the power supply and the flux amplifier input. The voltage developed across this resistor was amplified at the data acquisition system (DAS).

Calibration Description — Using the latest LPRM current values determined by PECo instrumentation technicians during the calibration of the flux amplifiers, the pre-test voltage developed across the resistor was calculated. This was multiplied to determine the voltage which would be present at the DAS amplifier input for a reading corresponding to $750\ W/cm^2$. The potentiometer was adjusted to yield a 0-IO Vdc output for a 0- $750\ W/cm^2$ scale. Readings from the DAS were then compared to the readings from a current process computer printout from the OD8 program.

2. **Signal Type** — Control Rod Position

Channel Numbers — 128-I 58

Signal Description — The control rod drive position drift sensing relay output from the rod position information system (RPIS) was attenuated at the DAS.

Calibration Description — The 5 Vdc drift relay output from the RPIS was attenuated at the DAS by $50\ k\Omega$ and $1\ k\Omega$ resistors in series. The voltage across the $1\ k\Omega$ resistor being 0 indicates an open relay and a 0.1 Vdc indicates a closed relay.

3. **Signal Type** — Average Power Range Monitor and Traversing In-Core Probe

Channel Numbers — 80-85

Signal Description — The recorder output was amplified at the DAS.

Signal Calibration — The 0-I Vdc recorder output was delivered to the DAS amplifier configured for a gain of 10. The amplifier was calibrated for a 0-IO Vdc output corresponding to a 0-125% scale.

4. **Signal Type** — Special Pressure Transducers, Wide Range and Special Differential Pressure Transducers. Jet pump AP, steam line A and D flow element AP, core AP, reactor pressure, core exit pressure, steam line A and D flow element upstream pressure, turbine inlet pressure steam lines A and D.

Channel Numbers — 92-98, 116, 118, 120, 122, 124, 126

Signal Description — Special pressure transducers were installed in parallel with existing plant instruments. Refer to Figure 4-2 for additional details. Signals from the transducers were amplified at the DAS.

Calibration Description — Each transducer was calibrated over its full range, and adjusted, if required, for a 0-5 Vdc output. The DAS amplifiers with a gain of 2 were calibrated for a 0-IO Vdc output corresponding to a scale of 0-1 500 psig, 0-1 00 psid, or 0-50 psid, depending on the transducer range.

5. **Signal Type** — Special Pressure Transducers, Narrow Range for reactor pressure, core exit pressure, steam line A and D flow element upstream pressure, turbine inlet pressure steam lines A and D.

Channel Numbers — 117, 119, 121, 123, 125, 127

Signal Description — The amplified signal from the O-1500 psig transducers was used as the high input to a second differential amplifier with an offset voltage being used as the low input, giving an expanded-scale output.

Calibration Description An offset equivalent to 6.666 Vdc from a stable power supply was supplied to the low input of the differential amplifier with a gain of 10. At the input of the first amplifier (gain of 2), an input voltage corresponding to 1000 psig was applied. The output of the narrow-range amplifier (gain of 10) was adjusted to give 0.00 Vdc output. Then an input voltage corresponding to 1150 psig was applied to the gain of 2 amplifier and the output adjusted to 10.000 Vdc for the first calibration. For the second calibration point, an input corresponding to 850 psig was applied but no amplifier adjustments were made. The output range of -10.000 to 10.000 Vdc corresponded approximately to 850 to 1150 psig.

6. *Signal Type* — Reactor Water Level, Narrow Range

Channel Number — 91

Signal Description A resistor was placed in the Reactor Level C circuit between the power supply and differential pressure transmitter. The voltage developed across this resistor was amplified at the DAS.

Calibration Description The scale for the narrow-range level is 0-60 inches. From the calibration data, 0 inch = 10.02 mA and 60 inches = 50.00 mA. Based on this data, the voltage drop across the 10 Ω resistor placed in series with differential pressure transmitter (6-52C) and the power supply (6-124) negative side was calculated to be 0.100 Vdc for 0 inch and 0.500 Vdc for 60 inches. The amplifier with a gain of 10 was calibrated for an output of 1-5 Vdc for a 0-60 inch scale.

7. *Signal Type* — Reactor Water Level, Wide Range

Channel Number — 100

Signal Description — A Rosemount type 115 differential pressure transmitter was installed in parallel with the existing level switch LITS 2-3-59A.

Calibration Description — The Rosemount transmitter has a 4-20 mA span. A 100 Ω resistor was used producing a 0.4-2 Vdc signal. The equivalent hot calibrated range was +50.42 to -162.3 inches H₂O. The DAS amplifier with a gain of 5 was calibrated to produce a 2.000 Vdc output for -162.3 inches and 10.000 Vdc for 50.42 inches.

8. *Signal Type* — Recirculation Flow Element Differential Pressure A and E

Channel Numbers — 86, 87

Signal Description — A 10 Ω resistor was placed in series with the power supply negative (2-162B) and flow transmitters (2-110B & D).

Signal Calibration — Based on the calibrated data, the following were calculated for 0 psid = 0.100 Vdc at the lower end of the scale and 24.664 psid = 0.501 Vdc for RC "A" and 0.502 Vdc for RC "B" at the upper end of the scale. These inputs were used to calibrate the DAS amplifiers with a gain of 10 for a 1-5.000 Vdc output.

9. *Signal Type* — Feedwater Differential Pressure A, B, and C

Channel Numbers — 88-90

Signal Description — The 3.2 Ω resistors used for the process computer which are in series with the power supply negative (FW "A" 6-93, FW "B" 6-92, and FW "C" 6-91) and the differential pressure transmitters (FW "A" 6-50A, FW "B" 6-50B, and FW "C" 6-50C) were tapped for these signals.

Signal Calibration -- Based on the calibration data, the following were calculated for 0 psid = 0.032 Vdc for all instruments at the lower end of the scale and 17.745, 17.926 and 17.781 psid = 0.160 Vdc for FW "A", "B", and "C". These inputs were used to calibrate the DAS amplifiers with a gain of 10 for a 0.32 - 1.60 Vdc output range.

10. *Signal Type* Recirculation Loop Suction Temperature, A and B.

Channel Numbers 114, 115

Signal Description The temperature signals are tapped off the process computer signal.

Signal Calibration -- The calibration data were 420° F = 0.03 mV, and 570° F = 150.0 mV. With an amplifier gain of 10, the outputs were set to 0 and 1.500 volts respectively.

11. *Signal Type* = Feedwater Temperature, Loop A.

Channel Number = 99

Signal Description -- The temperature signals were tapped off the process computer signal.

Signal Calibration -The calibration data were: 320° F = 39.92 mV; 350° F = 69.90 mV, 380° F = 99.92 mV. The slope from 320° F to 380° F was used and the curve was passed through 350° F.

12. *Signal Type* = Stop Valve Position

Channel Number = 102

Signal Description = Plant data signal was tapped.

Signal Calibration -- Open position signal was -0.390 Vdc; closed position was assumed to be 0.0 Vdc.

13. *Signal Type* = Total BPV position

Channel Number 104

Signal Description = Signal taken from plant signal output from total BPV position.

Signal Calibration -- The BPV signal is for 9 valves. The first valve nominally operates from 0 to approximately $5/9 = 0.555$ volts, where 5 volts is maximum output voltage when BPV9 is fully open. Table 4-I gives the voltages at which bypass valves 2 and 9 are scheduled to open initially and be fully open.

Table 4-1
PEACH BOTTOM-2 SIGNAL RANGE AND CONDITIONING

Signal	Units	Low End of Range		High End of Range		Filter Cutoff (Hz)
		Engineering Units	output Voltage	Engineering Units	output Voltage	
LPRM	W/cm ²	0	0	750	10	100
CR Position	Logic	0	0	1	0.1	None
APRM	% Rated	0	0	125	10	100
Pressure-Wide	psia	14.7	0	1514.7	10	10
Pressure-Narrow	psia	864.7	-10	1164.7	10	10
RWL-Narrow	inch	0	1	60	5	100
RWL-Wide	inch	-162.3	2	50.42	10.0	100
RC AP	psid	0	1	24.664	5.0	100
FW AP	psid	0	0.32	17.745	1.60	100
FW Temperature	°F	320	0.399	380	0.999	100
RC Temperature	°F	420	0	570	1.50	100
BPV 2	% of Stroke	0	0.555	100	1.166	100
BPV 9	% of Stroke	0	4.444	100	5.000	100
BPV Total	% of Stroke	0	0	100	5.0	100
Stop Valve Position	% of Stroke	0	0	100	-0.39	100
Jet Pump AP	psid	0	0	50	5.0	10
Scram Backup Solenoid	Logic	0	0	1	0.1	None

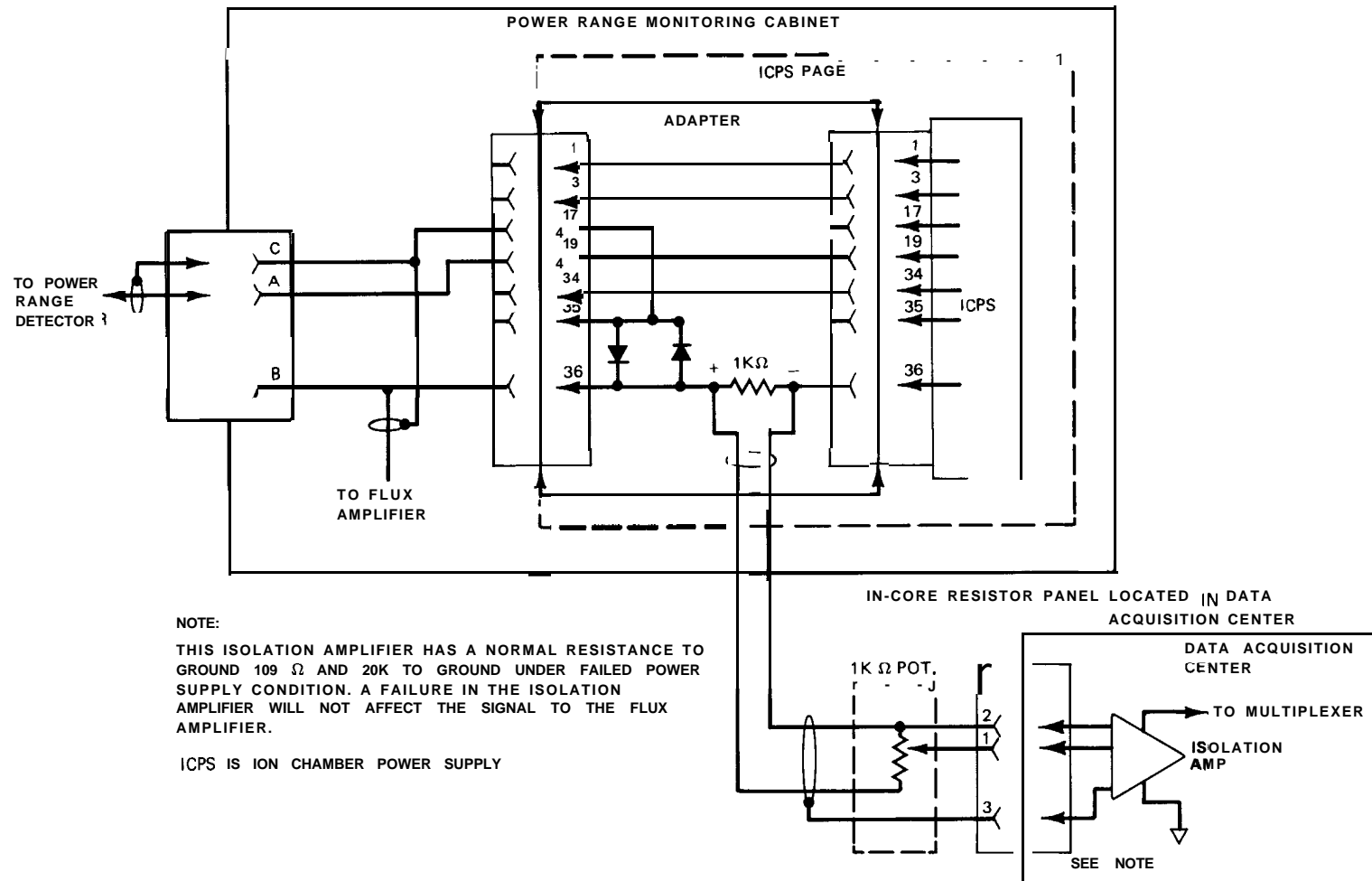


Figure 4-1. LPRM Power Supply Signal Tap

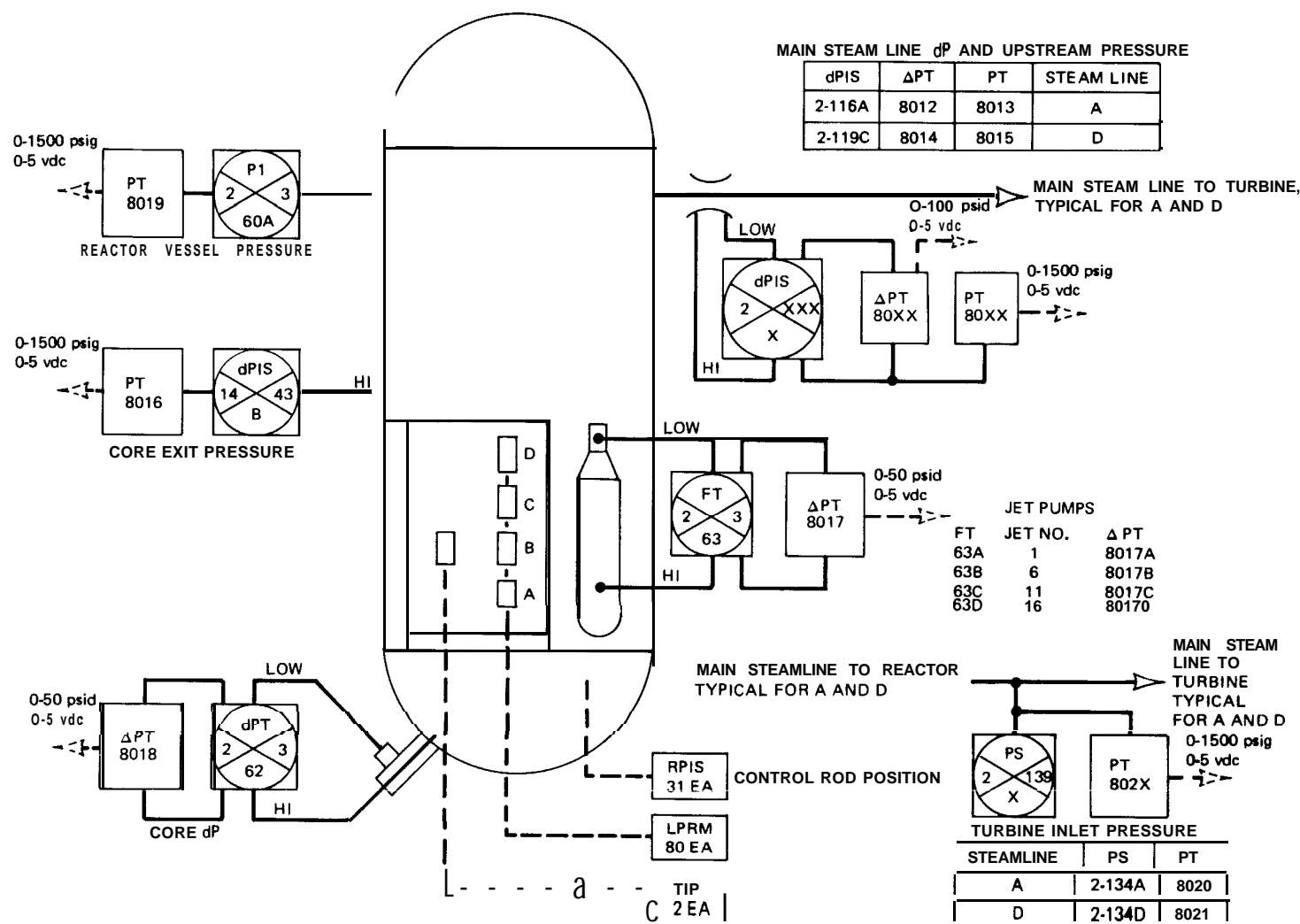
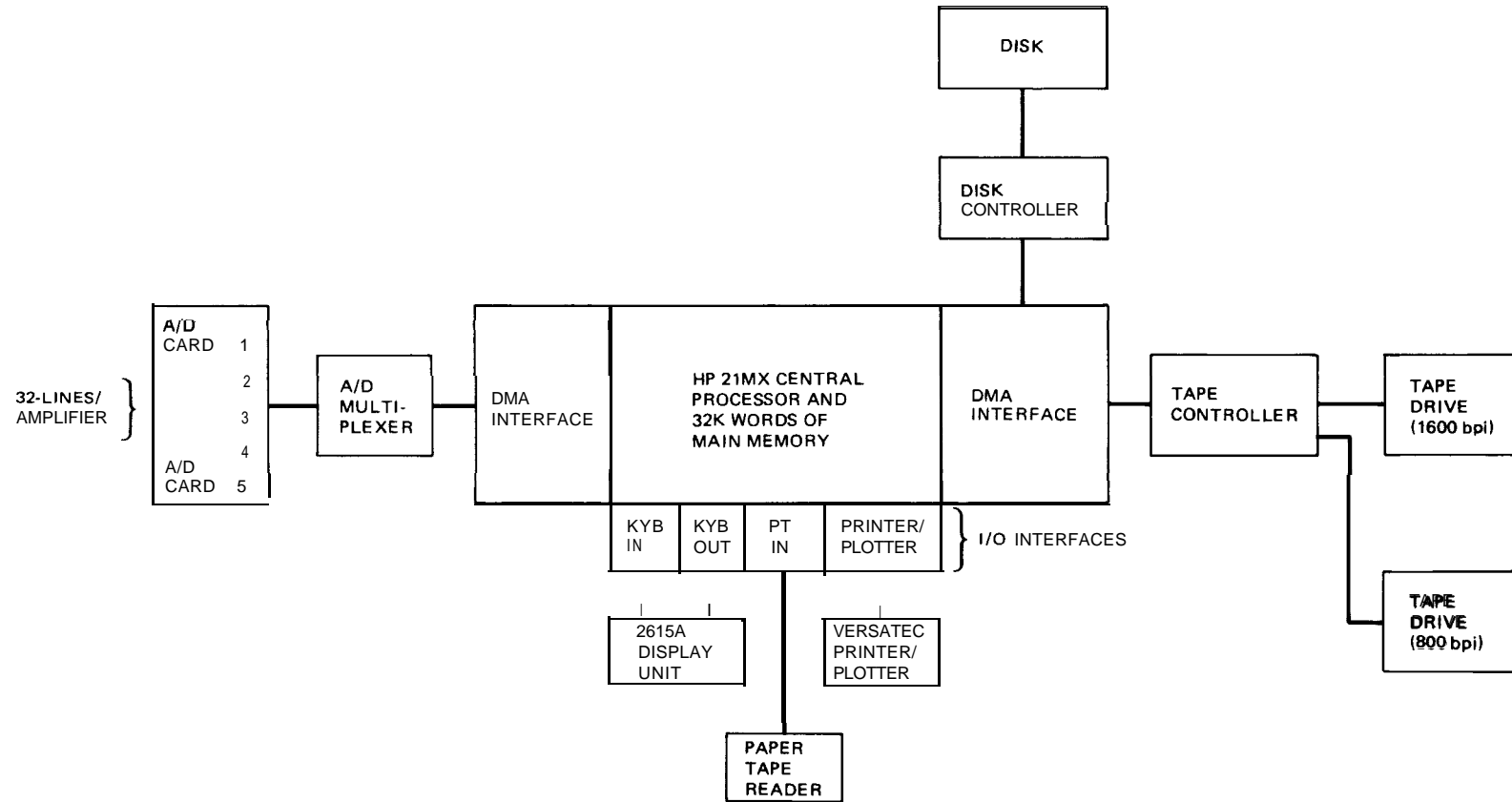


Figure 4-2. Special Pressure Transducer Installation



DMA: DIRECT MEMORY ACCESS

KYB: KEYBOARD

Figure 4-3. Digital Data Acquisition System Hardware Configuration

5. TEST PROCEDURES

5.1 TURBINE TRIP TRANSIENT TESTS

The turbine trip tests were preceded by small pressure perturbation testing so that the procedures in Section 5.2 were always followed first.

At the test condition the process computer program OD11 was run to determine the available fuel preconditioning envelope. The APRM Scram Clamp was then used to lower the high flux trip set point so that the expected transient fuel linear heat generation rate should not exceed the preconditioning envelope by more than 0.1 kW/ft. It was verified from OD6 that the operating MCPR for the 7x7 or 8x8 bundles was greater than the 1.4 required by the special plant Technical Specification limit for the test. The unit's auxiliary busses were transferred to the offsite source to prevent automatic recirculation pump trip.* The anticipatory turbine trip scram was changed to delay the scram signal from this source by approximately 1 second. Operating reactor water level was increased to the high level alarm point to prevent low reactor water level isolation. If the TIPs had been withdrawn for the period between the random pressure stepping sequence and the transient test, they were reinserted at 5 minutes before recording started.

At 5 minutes before the trip, the reactor operator started a countdown at which time the data acquisition system was started. The turbine was tripped manually at the end of the countdown, and data recording was continued for 5 minutes following the turbine trip. Offgas data was taken for 24 hours.

The system was restored to normal operation by:

1. Withdrawing TIP's
2. Returning APRM Scram setting to normal at end of last test
3. Notifying PECO of test completion
4. Removing LPRM ICPS adapters
5. Returning LPRM power supply voltages to pretest settings
6. Returning EHC cabinet to normal

The transient test results were evaluated to verify that all criteria had been met. These criteria were:

1. The ACPR for each test condition was used to correct the "best estimate" design basis transient by the process described in Reference 9. The corrected "best estimate" ACPR had to be less than the design basis safety limits established for the turbine trip transient tests in Table 3-4 of the special NRC licensing submittal in order to proceed to the next transient test.
2. The measured peak pressure during the turbine trip transient tests had to be less than the maximum peak pressure of the design basis transient in Table 3-4 of the NRC submittal, in order to proceed to the next transient test.
3. The minimum measured reactor water level which occurred during a turbine trip transient test, when extrapolated to the next highest power test condition, had to be at least +12 inches above the L2 (low-low) reactor isolation trip setting before proceeding with the next turbine trip test. This was to prevent reactor isolation leading to relief valve operation following the turbine trip test.

*Except for the third turbine trip, TT3, during which the recirculation pumps were manually tripped at 3 seconds to prevent low-level isolation following scram.

5.2 SMALL PRESSURE PERTURBATION TESTS

Prior to any testing, all signal calibrations were completed and NRC approval for the required Technical Specification changes pertaining to the low-flow test conditions had been received. Completion of the calibration required that LPRM ion chamber power supply (ICPS) adapters be installed. The LPRM connections were determined to have no effect on the LPRM readings by taking process computer edits (OD8) before and after insertion of the ICPS adapters. The installation of the special pressure regulator test board (A73) and the operability of the manual override switch were verified. Jumper logs of the EHC and safety systems were reviewed for status verification.

The reactor was then maneuvered to the test conditions by setting the desired fixed control rod pattern and by using flow control. With the test condition flow set, PI or OD8 outputs were obtained periodically during the xenon soak. Small power changes ($\pm 5\%$) during the pretest xenon soaks were made generally by flow control. When the xenon concentration had reached a local maximum or minimum (about 4-6 hours after initial maneuvering), the test data were collected.

The Data Acquisition System (DAS) was verified to be operational by making a noise recording and by manually recording plant signals simultaneously. The mean values of the recorded signals were computer calculated and compared with the manually recorded signals to verify the DAS operation and the instrument operability and calibration. This check was usually run during the xenon soak period.

The tests consisted of three sequences:

1. noise recording
2. periodic pressure step recordings*
3. pseudorandom pressure step recording

For the noise data, three reels of recordings of 10 or more minutes each were taken. Process computer edits OD1 (LPRM Calibration and Base Data) and PI (periodic log with heat balance data, calibrated LPRM readings, control rod positions, and a file of LPRM and sensor list) were obtained. A process computer drum dump (classes 4-20) was taken.

In preparation for the pressure perturbation tests, an OD6 process computer edit was obtained. Two TIP's were then set at symmetric locations in the core,[†] the first at 46 ± 1 inches and the second at 70 ± 1 inches above the bottom. For the low-flow test conditions the APRM scram and rod block slopes and intercepts were recalibrated to the settings specified in the temporary technical specification change [Scram: original $0.66W + 54\%$, modified to $0.58W + 62\%$; with scram clamp (limiter) set at 85%; Rod Block Monitor: originally $0.66W + 42\%$, modified to $0.58W + 50\%$].

The pressure perturbation data recordings were preceded by preliminary trial pressure steps. The manual override switch was activated by the reactor operator and the potentiometer on the EHC relay test board was set to give a 5 psi step. A single pressure step was run. The signal-to-noise level was examined and, if not adequate, the step size was increased in small increments of about 2-½ psi until the signal-to-noise level was satisfactory. Usually an 8 psi step was adequate. Then, with the reactor operator's concurrence, a sequence of pressure steps (down, then up) spaced uniformly 10 seconds apart was run for 10 to 12 minutes (tape limit). This test was repeated two additional times. Offgas readings were taken before and after each stepping sequence.

*Periodic step recordings were NOT taken at the last two test conditions PT3 and PT4.

**Plant equipment limitations resulted in setting the scram slope at 0.58 rather than the proposed 0.45

[†]Reactor coordinate locations 32-41 and 40-33 as shown in Figure 3-3.

The pseudorandom stepping sequence followed after a ten minute wait to allow the reactor system to stabilize. Stabilization usually occurred within 2 minutes. The pseudorandom stepping procedure was the same as for the uniformly spaced test except for the timing of the steps. The minimum step period was 1 second and three reels of 10 to 12 minutes of data were taken. After a few tests, the pseudorandom pressure stepping procedure had yielded such excellent results that the uniformly spaced pressure stepping tests were abandoned.

At the completion of the recordings, the manual override switch was deactivated to prevent accidental operation of the pressure stepping system, the reactor instrumentation was observed to assure return to the pre-test condition, offgas data were taken and the TIP's were withdrawn. The perturbation data were evaluated to verify that the following criteria had been met.

1. Maximum APRM response for pressure set point steps was less than $\pm 20\%$ of rated (checked prior to start of stepping sequence).
2. The decay ratio was less than 1.0 for each process variable that exhibits oscillatory response to pressure set point changes.
3. The daily offgas increase did not exceed 50%* of the unit's release rate prior to beginning testing. (Release rate 1 hour after test had to be less than 150% of release rate prior to start of test). When the tests requiring modification of the scram and rod block lines were completed, the systems were restored to pre-test settings. If there were no tests scheduled within a period of about 2 days, the LPRM plugs at the back of the data acquisition system were disconnected to prevent accidental scram in case of power failure to the signal amplifiers. The amplifiers had been wired to the power line so that they could not be shut off except by a failure of the vital a-c bus, which would also cause a reactor shutdown.

*Limits for test required by PECO

6. EXPERIMENTAL RESULTS

6.1 TURBINE TRIP TRANSIENT TESTS

6.1.1 Principal Observations from the Test Data

Manual trips of the Peach Bottom-2 turbine-generator were conducted at the test conditions shown in Table 3-5. The transient pressure responses measured in the main steam piping and reactor vessel, and the stop and bypass valve position measurements are plotted in Figures 6-1 through 6-3 for the three tests.* A comparison of the bypass valve opening responses for the three trips shows a 312 millisecond delay before valve motion in TT1, compared with 78 and 90 millisecond delays for TT2 and TT3, respectively. The increased delay before valve motion during the first test was found to be caused by a loss of initiating signal from stop valve position switches. The purpose of this signal is to trip the turbine load limit, causing an anticipatory full-open demand signal to the turbine bypass control valves.** During this test, the bypass control valves opened somewhat later as a result of pressure regulator control following the pressure rise at the turbine inlet. The stroking time for the turbine stop valves averaged approximately 95 milliseconds while the bypass valve stroking time, not including initial delay, averaged 770 milliseconds.^t

The time delays between the initiation of turbine stop valve motion and the pressure responses along the steam line and in the reactor vessel, which are compared for the three test conditions in Table 6-1, show that the propagation of the pressure wave in the main steam piping is essentially independent of the initial steam velocity prior to valve closure. This is an expected result since the initial steam velocity at all three test conditions is less than 5% of the velocity of sound in saturated steam at the test conditions. The effects of the convection terms on the wave propagation velocity in the main steam piping are, therefore, of little consequence for these test conditions. The high-frequency oscillations which appear in the pressure time response in Figures 6-1 through 6-3 are probably caused by the presence of acoustic oscillatory modes in the fairly long instrument sensor lines existing between the pressure measurement points on the main steam piping and reactor vessel, and the special pressure transducers which were temporarily mounted on the plant's instrument racks located in the reactor secondary containment. Theoretical calculations of the sensor line fundamental resonant frequencies based on idealized models of complex instrumentation sensor line arrangements and the many parallel terminating instruments have been calculated for each of the absolute pressure measurement points and are presented in Appendix B. These results generally compare reasonably well with the measured higher frequency resonances found in the data, which are also tabulated in Appendix B.^{††}

To determine the fundamental mode in the steam piping and vessel pressure responses the time response data were passed through a 2-pole digital Butterworth filter having a cutoff frequency of 5 Hz. The almost-square-wave character of the pressure response at the turbine inlet, following stop valve closure (Figures 6-4 through 6-6), compares rather well to the theoretically predicted response in a finite lossy electric transmission line following a step change in current. However, the response of the higher-frequency modes does not appear in the pressure measurements in the steam line upstream of the steam-flow-limiting nozzles close to the reactor vessel or in the reactor pressure measurements themselves. The theoretical acoustic frequency modes in a gas-filled resonating tube, closed at one end, are given by ^t*¹⁰

$$f_n = C(2n + 1)/4L \quad n = 0, 1, 2, \dots \quad (\text{Hz})$$

*The stop valve position signal failed during TT1. The time of initiation of stop valve closure can be precisely estimated from the pressure wave propagation delays measured in TT2 and TT3, which are given in Table 6-2.

**The cause of the signal malfunction was corrected prior to conducting the second and third turbine trip tests.

^tThe bypass valve stroking time is somewhat slower than expected. This has SINCE been traced to the failure to precharge the bypass valve hydraulic accumulators. Also one of the nine bypass valves was found to be partially seized, accounting for the decreased opening rate during the latter part of the time trace.

^{††}The large discrepancy between the measured oscillation frequency in the steam line D pressure sensor indicates either a large amount of air in the sensor line or a partially failed sensor.

^{†††}A detailed analysis of the acoustic modes in the Peach Bottom-2 main steam piping is actually more complex because of the 64-ft branch to the turbine bypass valves and the capacitance of the reactor vessel.¹¹

For the average length of the Peach Bottom-2 main steam piping between the turbine inlet and reactor vessel, 400 ft, a fundamental frequency mode of 0.9 Hz would be predicted for a 1480 ft/sec sound velocity in dry saturated steam.² The measured fundamental mode is approximately 0.8 Hz.

The response of pressure at the upstream pressure tap of steam line A flow nozzle does not exhibit the fundamental acoustical oscillation mode in the other pressure measurements. Its behavior is like a node with respect to the steam piping acoustic response modes.

Comparison of the reactor vessel and core exit pressure responses for the three tests demonstrates that the propagation of the fundamental acoustic mode in the steam piping occurs with essentially no attenuation and only a small time delay, approximately 70 milliseconds, through the steam dryers and separators. For all three tests, a strong -5 Hz mode is excited in the core exit pressure response: The time of its occurrence, approximately 900 milliseconds, corresponds closely to the time of initial control rod motion following the reactor scram.^{**}

The peak pressures measured during all three tests, and the time of their occurrence are presented in Table 6-2. The plant's relief valves did not open as a consequence of any of the three turbine trip tests.

The core neutron flux responses measured for the three tests are summarized in Figures 6-7 through 6-9. For purposes of comparison, the measured output of one of the plant electronic APRM amplifier outputs is plotted on the same scale as the computed and normalized average of the measured LPRM responses. The correspondence is, in fact, very good for tests TT1 and TT3. Following test TT2, it was discovered that if the plant control room recorders were switched in parallel with the Data Acquisition System input amplifier, the plant recorder low input impedance served to "load" the Data Acquisition System amplifier measurement.[†] The time of occurrence of the high flux trip of the plant's electronic APRM amplifiers can be detected from the electrical switching transient seen in the APRM amplifier recorder output. The APRM amplifier output, at the estimated time of occurrence of the high-neutron-flux trip, corresponds closely to the electrical set point programmed for the test conditions for tests TT1 and TT3.^{††} From the measured response of the backup scram relay output, the total electrical time delay prior to rod motion can be estimated. This is found to be approximately 150 milliseconds during all three tests. The difference in the responses for the three tests of the LPRMs, averaged in the radial plane at the four axial LPRM locations in the core, clearly demonstrates the effect of the initial core axial power distribution on the local neutron flux transient response. At the first test condition, TT1, the control rod pattern resulted in an average axial power distribution which was rather strongly peaked near the D level LPRM.^{†*} The measured transient neutron flux response is greatest from the average D level LPRM, decreasing in response uniformly down the core at the average lower level LPRM locations. In the second test, TT2, the average axial power distribution is peaked near mid-core, which results in the nearly equal large flux responses from the average B and C level LPRM's. The average D level response is reduced to only slightly greater than that from the average A level LPRM. In the third test, TT3, the average axial power distribution was flattened over the upper three quarters of the core axial length. The resulting transient responses of the average B and C level LPRM's are greatest and nearly identical, with the magnitude from the average D level LPRM response having increased significantly relative to that from the average A level LPRM. The peak neutron flux levels for the three test conditions are summarized in Table 6-2.

The effect of radial power distribution on the local flux transient responses is investigated in Figures 6-10A, B, and C, where LPRM responses are plotted in terms of percentage of the initial output.^{*†} These results offer a

^{*}This oscillatory mode could not be predicted by the idealized instrument line model.

^{**}See Figures 6-1 IA, B, C, and D for control rod motion measurements.

[†]The APRM recorder output signal used for the test measurements is isolated from the amplifier output for the reactor safety system, and loading of this signal has no effect on the plant's safety system response. This affected all but one of the APRM signals measured during tests TT1 and TT2; however, the information lost is of little consequence since the electronic APRM signals saturated during these tests.

^{††}In test TT2, the time of occurrence of the electrical transient from the trip corresponds closely to the calculated average flux level for the programmed APRM trip setpoint. The time of occurrence can also be determined from the process computer event log.

^{†*}See Figures 3-4, 3-6, and 3-8 for the initial average axial power distributions for the test conditions.

● Additional measurements from tests TT2 and TT3 are plotted in Appendix D.

convincing demonstration of the insignificance of the radial variation in the flux responses (radial shape function) relative to that taking place in the axial direction in the core for all three turbine trip tests.

The control rod drive scram speeds for the three turbine trip tests can be estimated from the measured plant Rod Position Information System (RPIS) drift relay output signals for a sample of 31 of the 185 control rod drives in the Peach Bottom-2 core. The rod position-time plots are presented in Figures 6-11 A, B, C, and D.* The RPIS inputs are magnetic relay contact closures indicating control rod position at one of 48 discrete positions. A drift relay output change indicates a rod motion from 1 of the 24 "even" notches.* The finite width of the logic signal on the time traces is caused by a finite $\pm\frac{1}{2}$ inch, pickup and dropout sensitivity of the magnetic relays which is equivalent to approximately ± 1 millisecond in control rod scram times. The initial control rod motion is indicated with the initial drop in the drift relay logic signal. The average and limits of variation in measured scram speeds for the three test conditions are summarized in Figure 6-12. If the times at which initial rod motion occurs are examined on the time plots of average neutron flux responses, very small initial rod movement is required to turn around the flux transient at any axial level in the core. This is the result of having both deep and shallow control rods in the patterns for all three test conditions.**

6.1.2 Secondary Observations from the Test Data

In Figures 6-13 through 6-21, the time response of other interesting process variables in the Nuclear Steam Supply System are presented. A comparison of the reactor water level plots for the three turbine trip tests indicates water level drops to its minimum between 5 and 7 seconds following reactor scram.† The magnitude of the water level drop was found to increase very rapidly with the initial operating power level. In Figure 6-13, the feedwater flow nozzle pressure drop traces indicate that the feedwater pumps responded erratically to an increased feedwater demand signal from the reactor feedwater control system following the drop in reactor water level during TT1.‡ This is probably caused by the existence of more than one possible stable operating point for the parallel operation of the two reactor steam turbine feedwater pumps at low-load conditions.

During the second turbine trip, TT2, both of the feedwater pumps initially pick up load approximately equally (see Figure 6-16); however, feedwater flow again drops off at approximately 8 seconds with reactor water level below the normal operating limits, indicating a trip of both feedwater pump drives occurred near maximum flow for the feedwater pumps.¶§ As a result of the feedwater pump trip, reactor water level again decreases, which causes the reactor to begin to isolate at approximately 24 seconds following a low-low reactor water level trip which occurred at approximately 23 seconds.†*

At the third test condition, TT3, three reactor feedwater pumps are initially in operation (see Figure 6-19). At approximately 3 seconds both of the reactor recirculation pumps are manually tripped in order to minimize the initial reactor water level drop following reactor scram. Between 7 and 8 seconds into the transient all three reactor feedwater pumps again trip. In this test, however, only a half-trip of the reactor water level safety system logic occurred, and no isolation resulted from the loss of feedwater pumps.

Following each of the three turbine trip tests, reactor feedwater temperature stays constant for at least the first 60 seconds following the loss of turbine extraction steam. This is expected from the large energy storage capability of the feedwater heater system and the piping transport delay between the feedwater heaters and the reactor vessel. (See Figures 6-13, 6-16, and 6-19.)

● Additional measurements from tests TT2 and TT3 are plotted in Appendix D.

*The RPISdrift relay outputs are essentially instantaneous from solid state parallel logic signals.

**See Figures 3-3, 3-5, and 3-7 for the initial control rod patterns corresponding to tests TT1, TT2, and TT3.

†The narrow range reactor water level signal becomes electrically saturated down scale due to the limited instrument range.

‡The feedwater control IS 3 element: i.e., the feedwater demand signal is based on a linear combination of reactor water level, feedwater flow, and steam flow.

¶§It has since been determined that the feedwater pump turbine trips occurring during TT2 and TT3 were a result of low feedwater pump suction pressure occurring at maximum flow.

†*Determined from the process computer event log.

During the first test, TT1, the measured diffuser differential pressures on the four calibrated jet pumps are seen to decrease at about 6 seconds following the turbine trip. Following the initial disturbance from the pressurization transient and scram,* the core support plate pressure drop also decreases. From the reduction in reactor recirculation loop flow, relative to feedwater flow following the reactor scram, in combination with decreasing reactor pressure, reactor recirculation loop temperatures are still falling slightly at 60 seconds following the turbine trip.

In the second test, TT2, the diffuser pressure drop on jet pumps 11 and 16 decreases at approximately 22 seconds following the turbine trip while jet pumps 1 and 6 are increasing slightly. The corresponding change in core support plate differential pressure drop decreases, indicating a reduction in reactor core flow. The recirculation loop flow nozzle measurements show a manual reduction of M-G set drive speed at the "A" recirculation loop occurred at approximately 20 seconds, followed by a speed reduction in "B" at approximately 48 seconds. Recirculation loop temperatures begin to increase slightly at 30 seconds due to the combination of the tripped reactor feedwater pumps and increasing reactor pressure, following isolation valve closure.**

During the third test, TT3, the diffuser pressure drops on all four measured jet pumps begin to decrease after approximately 3 seconds, with a corresponding decrease in core support plate differential pressure drop, following the manual trip of both M-G set drive motors. Recirculation loop temperatures increase slightly at approximately 21 seconds followed by a slight decrease at 30 seconds. Examination of the two-loop temperature measurements indicates slightly dissimilar time behavior beyond 20 seconds after the turbine trip.

6.2 LOW-F LOW STABILITY TESTS

The series of small pressure perturbation tests conducted at each of the low-flow stability test conditions were composed both of runs of periodic and pseudo-random binary switching (PRBS) of small step inputs to the pressure regulator reference set point. Typical reactor core and vessel pressure responses, and the average and local neutron flux signals, are plotted in Figures 6-22 and 6-23. The switching period of the periodic input command signal was 20 seconds, and the minimum switching time of the PRBS signal was 1 second. Since the set point change was non-zero mean, the mean reactor pressure is decreased slightly during the pressure perturbation tests.† The magnitude of the pressure set point steps was selected at approximately 8 psi which gave a good signal-to-noise ratio in the neutron flux response and did not cause operational difficulties during the testing. The rise time of the reactor pressure response to a pressure regulator step input command is approximately 1.5 seconds. The response of the pressure control feedback loop is very close to that of an ideal underdamped second-order system, for which normalized step response curves can be found in many standard control references.³ Using such a curve, it is possible to identify the natural frequency of the pressure control loop as being approximately 1/4 Hz. From the frequency response of a second-order system, the energy in the reactor pressure signal is expected to drop by at least 104 for each decade above the natural frequency. Because of the periodic nature of the signal, the greatest signal energy is expected at the odd harmonics of the fundamental frequency, 1/20 Hz, which is apparent in the calculated power spectral density (PSD) of the reactor pressure signal in Figure 6-24. The useful frequency bandwidth of the ideal 2047-bit PRBS input can be estimated by a rule-of-thumb^{††} to extend to 0.44 Hz, with a possible frequency resolution of 5×10^{-4} Hz.†^{†*} However, as Kerlin shows, the non-ideal actuator response, in this case that of the pressure control-loop, reduces the energy in the PRBS reactor pressure signal at frequencies above its natural frequency. The PSD for the PRBS input is shown in Figure 6-25.

The results of analysis of rod oscillator stability testing performed at other commercial boiling water reactors have shown that the resonant frequency of the reactor closed-loop neutron flux to reactivity transfer function lies between 0.2 and 0.6 Hz. At reduced reactor core flow, the resonance is expected to shift toward lower frequencies, due to the longer delay in the two-phase void transit time through the core. Examination of the neutron flux responses

*The high frequency oscillation in the core support plate differential pressure measurements in parallel with plant instrumentation, is caused by instrument line oscillations as shown in other experimental testing.

**Reactor pressure reaches a minimum at approximately 20 seconds (or 4 seconds prior to isolation valve closure) due to closure of the turbine bypass valves under pressure regulator control.

†This is a hardware limitation of the Peach Bottom-2 EHC pressure regulator test input card. The effect on the mean reactor power is very small due to the very low steady-state pressure coefficient of a boiling water reactor.

††See rule-of-thumb analysis by Kerlin (Reference 14).

†*Frequency resolution is sacrificed for statistical stability in PSD analysis.

shows a tendency to lead or overshoot the pressure response curve. This is because the neutron flux in a boiling water reactor core responds to the rate of change of pressure within a certain band of frequency, 0.1 to 0.5 Hz.

This has been confirmed in several earlier pressure oscillator experiments conducted in boiling water reactors which have shown the expected increasing magnitude^{**} and positive phase angle in the measured reactor pressure to neutron flux transfer function. The neutron flux signal energy is expected to be amplified somewhat in the frequency band in which the reactor pressure input signal energy is falling off. The PSD's of the reactor core pressure and APRM neutron flux signals, the magnitude and phase of the pressure to neutron flux transfer function, and the coherence between pressure and neutron flux signals are plotted in Figures 6-26 through 6-30 for the low-flow stability test condition (PT3).†† An examination of the average neutron flux PSD's does indicate that the pressure to neutron flux transfer function does tend to flatten the PSD in the frequency range of interest. The gain and phase plots do indeed show an almost ideal differentiator behavior from approximately 0.1 Hz to the occurrence of an easily identifiable resonant peak occurring at approximately 0.4 Hz. The superiority of the PRBS test signal is strongly demonstrated by comparison of the random scatter in the gain and phase plots, and the coherence between Cl.4 and 1 Hz for tests PT1 and PT2, and tests PT3 and PT4.†* The average neutron flux PSD's do not exhibit a noticeable resonance at 0.4 Hz, indicating the closed-loop transfer function measurement is a more sensitive technique for estimating the core stability margin, at least for the relatively high degree of stability exhibited by the Peach Bottom 2 EOC2 core at the test conditions.*†

The results of the non-linear least-squares curve fits of the two transfer function models described in Appendix A-I to the measured transfer function at test condition PT3 are shown in Figures 6-31 and 6-32. The parameters which were identified in the two models are tabulated in Table 6-3.*** It is seen from the results in the table that increasing the order of the denominator of the model beyond two causes an unstable root to be identified. The frequency at which the unstable root occurs (2.4 Hz), is in fact beyond the frequency range over which the frequency response measurement was taken. This is analogous to allowing too many degrees of freedom in the model for the number of independent measurements taken, i.e., too limited a frequency range to identify faster response modes in the system, a result which has been discussed by other investigators.^{15,16} It is reassuring, however, that the common parameters in both models which were identified, e.g., the natural frequency, ω_n , and relative damping, δ , are insensitive to the assumed order of the transfer function model.††† The second order denominator transfer function model was therefore chosen to best represent the measured reactor core closed-loop pressure to average neutron transfer function. The results of comparisons of the fitted second-order model to the data at the other test conditions are shown in Figures 6-33 to 6-35. The core relative stability margin estimates, in terms of decay ratio, are summarized in Table 6-4.

The effect of decreasing core flow on core stability margin is observed to be offset by the larger-than-expected decrease in core power, due to the tilting of the rated rod line from the transient xenon concentration change taking place between test conditions PT1 and PT2 (see Figure 6-36). The decay ratios for PT3 and PT4 show the expected trend of increasing core stability margin as power was decreased at minimum pump speed.

To examine the relative variation in the core transfer function in the axial core direction, the calculated gain and phase curves for four LPRM's in a central location in the reactor core, LPRM string 32-41, were determined.

*The delayed feedback path through the fuel thermal time constant results in a lead term in the closed loop transfer function.

**A slope in the magnitude curve of a factor of 10 (20 decibels) per decade of frequency is characteristic of an ideal lead network.

†See Appendix A for a description of the numerical Fourier analysis algorithm.

††See Appendix E for additional frequency response plots for test conditions PT1, PT2, and PT4.

†*In order to gain sufficient statistical stability in the PSD estimates for PT1 and PT2, it was necessary to combine a 15-minute PRBS run with four 6-minute periodic runs in the Fourier analysis. During tests PT3 and PT4, three 10-minute PRBS runs were available for analysis.

*†If the core stability margin is very small, the resonant peak is expected to be easily identified in the APRM noise power spectrum.

***See Figures 6-33 and 6-34 and E-1 through E-18, also Tables E-1 through E-3 in Appendix E for results at other test conditions.

†††The uncertainty in the decay ratio estimate is increased significantly, however, because of the larger sensitivity of this parameter to variations in the coefficients.

The results for tests PT3 and PT4 are replotted in Figures 6-37 and 6-38 for direct comparisons.* The effect of the shift in the power distribution from strongly peaked near mid-core in PT3 to relatively flat over the upper two-thirds of the core in PT4 is seen to be as much as 12 dB, a factor of 4, between the high-power-level LPRM's and that of A level. However, the variation in gain with frequency is very similar at all levels in the core, and the phase curves are very similar between 0.02 and 1 Hz.

*The PSD's and coherence functions are essentially the same as those calculated for the APRM signal

Table 6-1
PEACH BOTTOM-Z EOC-2
TURBINE TRIP TRANSIENT TESTS EVENT TIMING

Measured Variable	Test TT1	Time Delay (msec)	Test TT3
I. Turbine Stop Valve Closed	-	90	102
2. Begin Bypass Opening	312	78	90
3. Bypass Full Open	1080	840	876
4. Turbine Pressure Initial Response			
A. Steam Line	102 ^a	102	114
B. Steam Line	114	126	138
5. Steam Line Pressure initial Response			
A. Steam Line	342	348	342
D. Steam Line	360	378	372
6. Vessel Pressure Initial Response	408	432	408
7. Core Exit Pressure Initial Response	480	486	480

^aTT1 turbine pressure response is synchronized to TT2 to establish this value.

Table 6-2
PEACH BOTTOM-2
TURBINE TRIP TRANSIENT TEST
PEAK MEASURED RESPONSES

Variable	Test No.		
	TT1	TT2	TT3
1. Average Neutron Flux (% Rated) ^a	239	280	339
2. Core Exit Pressure (psia) ^b	1036	1034	1072
3. Reactor Vessel Pressure (psia) ^b	1031	1038	1061

^aAverage of 80 LPRM signals.

^bCorrected for sensor elevation head difference per Table B-1

Table 6-3
LOW-FLOW STABILITY TEST PT3
RESULTS OF EMPIRICAL TRANSFER FUNCTION MODEL
PARAMETER IDENTIFICATION

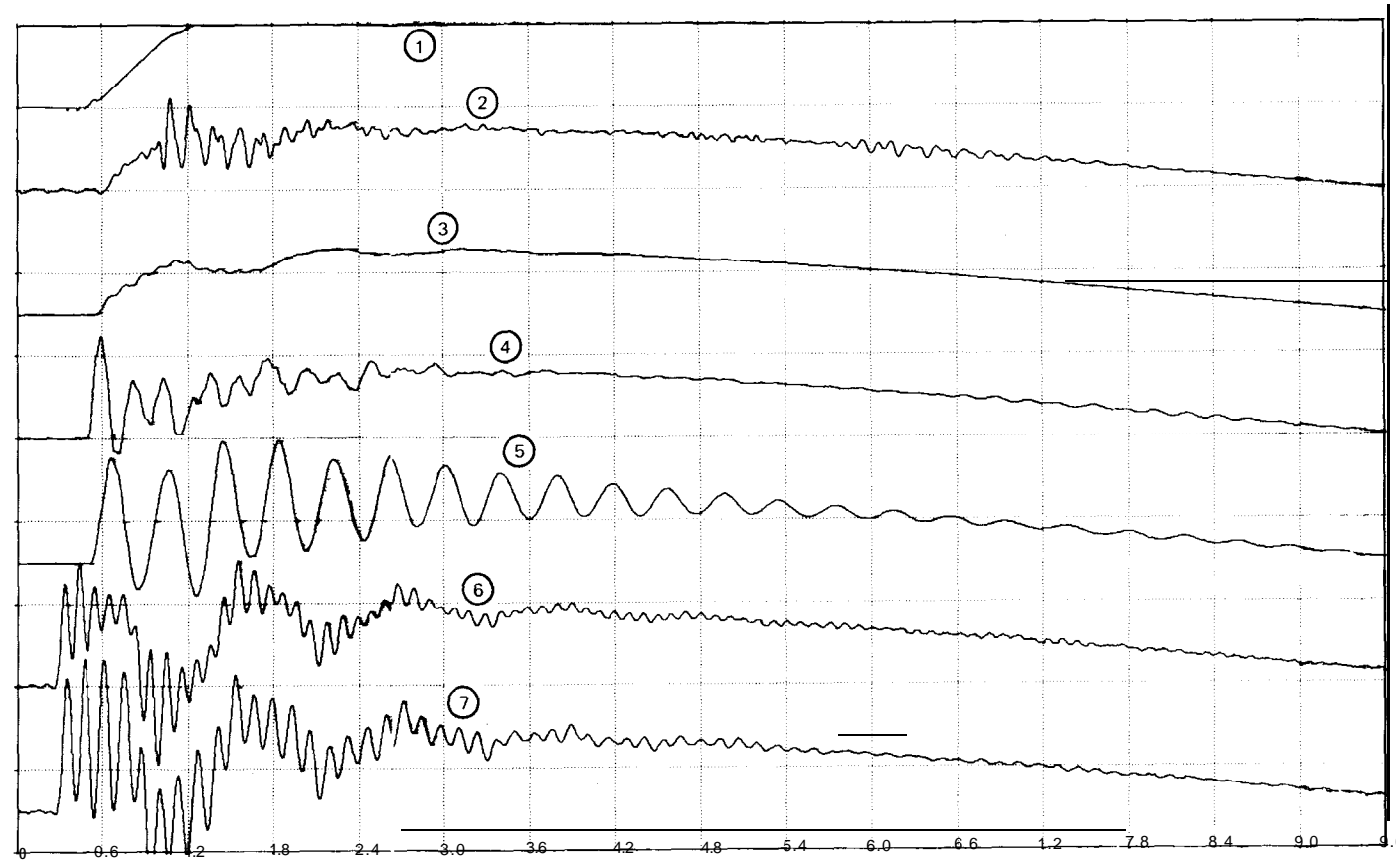
Model Order	1 Zero 2 Poles	1 Zero 3 Poles
a_0	0.3247 ± 0.056	0.3355 ± 0.057
a_1	0.9830 ± 0.050	1.0494 ± 0.062
b_1	0.1222 ± 0.015	0.06194 ± 0.023
b_2	0.1331 ± 0.004	0.1324 ± 0.003
b_3	-	$-9.184 \times 10^{-3} \pm 0.0037$
Gain, K_p (%/psi)	0.3247	0.3355
τ_1 (sec)	3.027	3.128
δ_1 (Dimensionless)	0.168	0.170
ω_1 (Rad/sec)	2.747	2.648
τ_2 (sec)		-6.531×10^{-2}
Decay Ratio (Dimensionless)	$0.3441 \pm 4.5 \times 10^{-4}$	0.3393 ± 0.108
$S(\bar{\alpha})$	0.02408	0.02004

Table 6-4
LOW-FLOW STABILITY TESTS
CORE STABILITY MARGIN ESTIMATES^a

Test Number	Closed-Loop Resonant Frequency (Hz)	Damping Coefficient	Decay Ratio
PT1	0.441	0.318	0.1206 ± 0.00044
PT2	0.471	0.319	0.1205 ± 0.00042
PT3	0.437	0.168	0.3441 ± 0.00045
PT4	0.402	0.190	0.2958 ± 0.00042

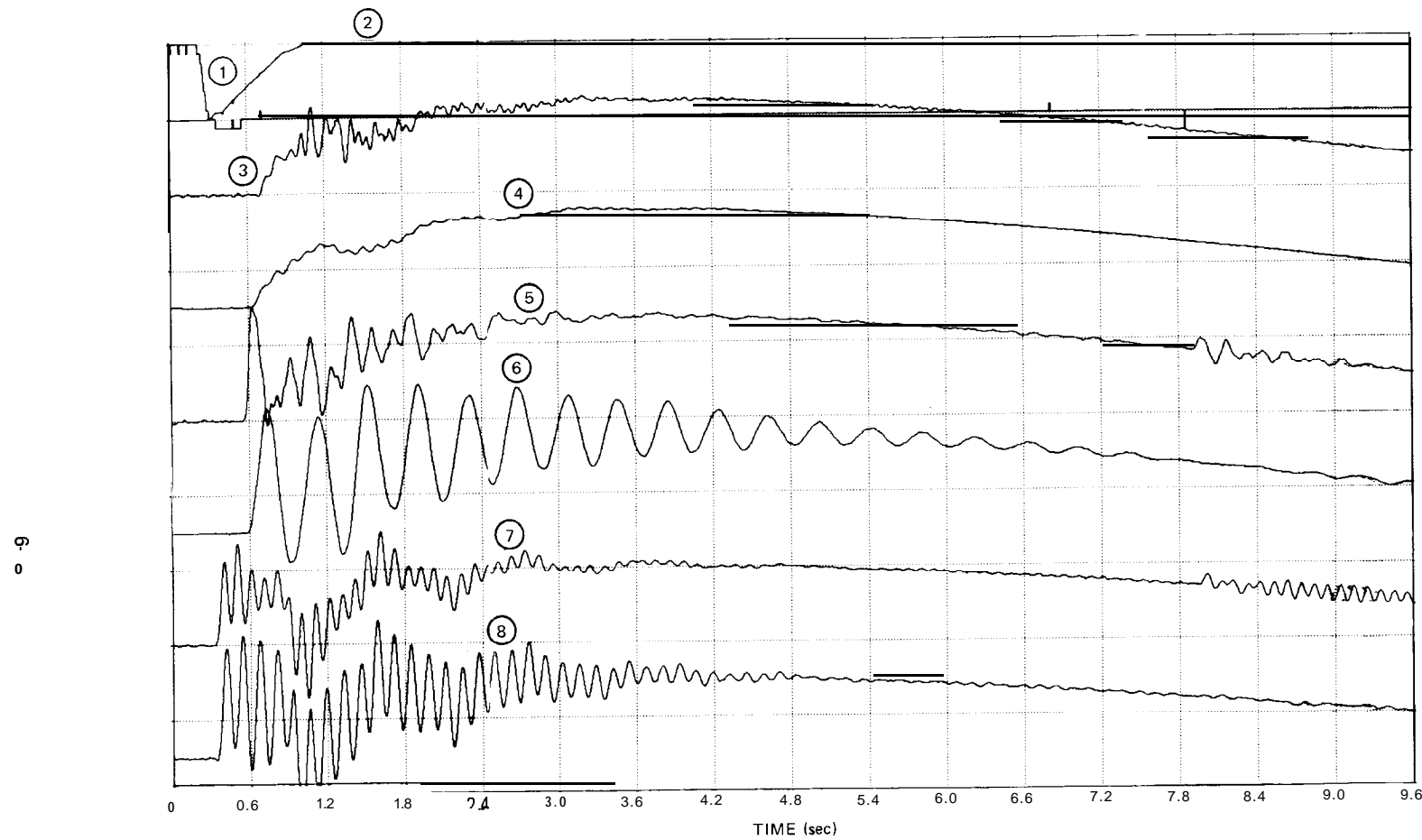
^aCore Dominant oscillatory response mode

6-9



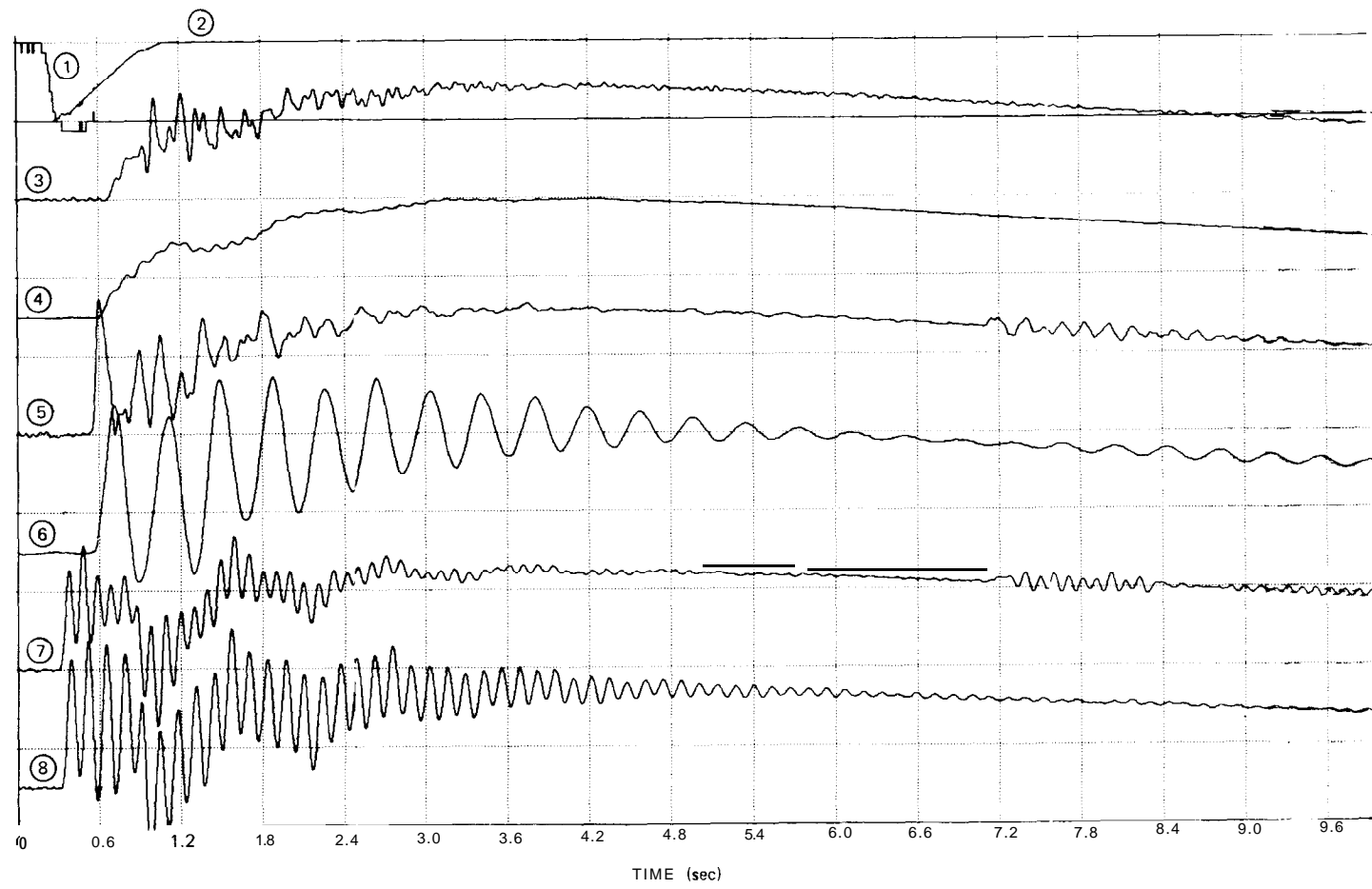
CURVE NO.	MEASURED VARIABLE	PLOT SCALE (UNITS/DIV)	INITIAL VALUE
1	TOTAL BYPASS POSITION	100%	0%
2	CORE EXIT PRESSURE	50 psi	998.7 psia
3	REACTOR VESSEL PRESSURE	50 psi	991.3 psia
4	STEAM LINE A PRESSURE	50 psi	985.5 psia
5	STEAM LINE D PRESSURE	50 psi	994.4 psia
6	TURBINE INLET PRESSURE A	50 psi	985.3 psia
7	TURBINE INLET PRESSURE D	50 psi	986.2 psia

figure 6-7. Peach Bottom-2 EOC2 Test Turbine Trip Test TT1 Transient Pressure Measurements



CURVE NO	MEASURED VARIABLE	PLOT SCALE (UNITS/DIV)	INITIAL VALUE
2	TURBINE STOP VALVE POSITION	100%	100%
2	TOTAL BYPASS POSITION	100%	0%
3	CORE EXIT PRESSURE	50 psi	980.8
4	REACTOR VESSEL PRESSURE	50 psi	976.3
5	STEAM LINE A PRESSURE	50 psi	968.1
6	STEAM LINE D PRESSURE	50 psi	974.4
7	TURBINE INLET PRESSURE A	50 psi	965.6
8	TURBINE INLET PRESSURE D	50 psi	960.9

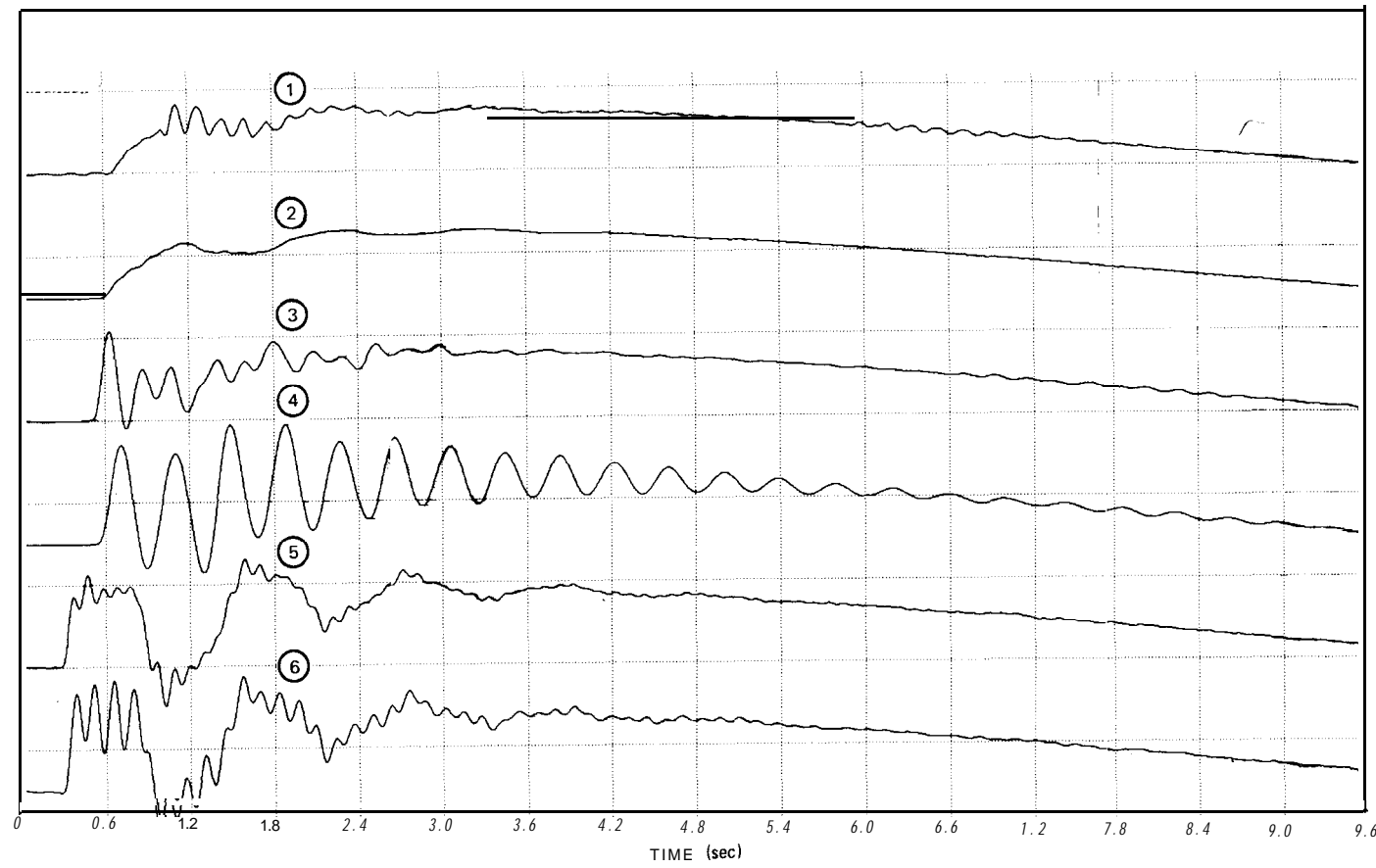
Figure 6-2. Peach Bottom-2 EOC2 Test Turbine Trip Test TT2 Transient Pressure Measurements



<u>CURVE NO.</u>	<u>MEASURED VARIABLE</u>	<u>PLOT SCALE (UNITS/DIV)</u>	<u>INITIAL VALUE</u>
2	TURBINE STOP VALVE POSITION	100%	100%
2	TOTAL BYPASS POSITION	100%	0%
3	CORE EXIT PRESSURE	50 psi	993.0 psia
4	REACTOR VESSEL PRESSURE	50 psi	986.6 psia
5	STEAM LINE A PRESSURE	50 psi	977.0 psia
6	STEAM LINE D PRESSURE	50 psi	983.8 psia
8	TURBINE INLET PRESSURE A	50 psi	970.0 psia
8	TURBINE INLET PRESSURE D	50 psi	966.4 psia

Figure 6-3. Peach Bottom-2 EOC2 Test Turbine Trip Test TT3 Transient Pressure Measurements

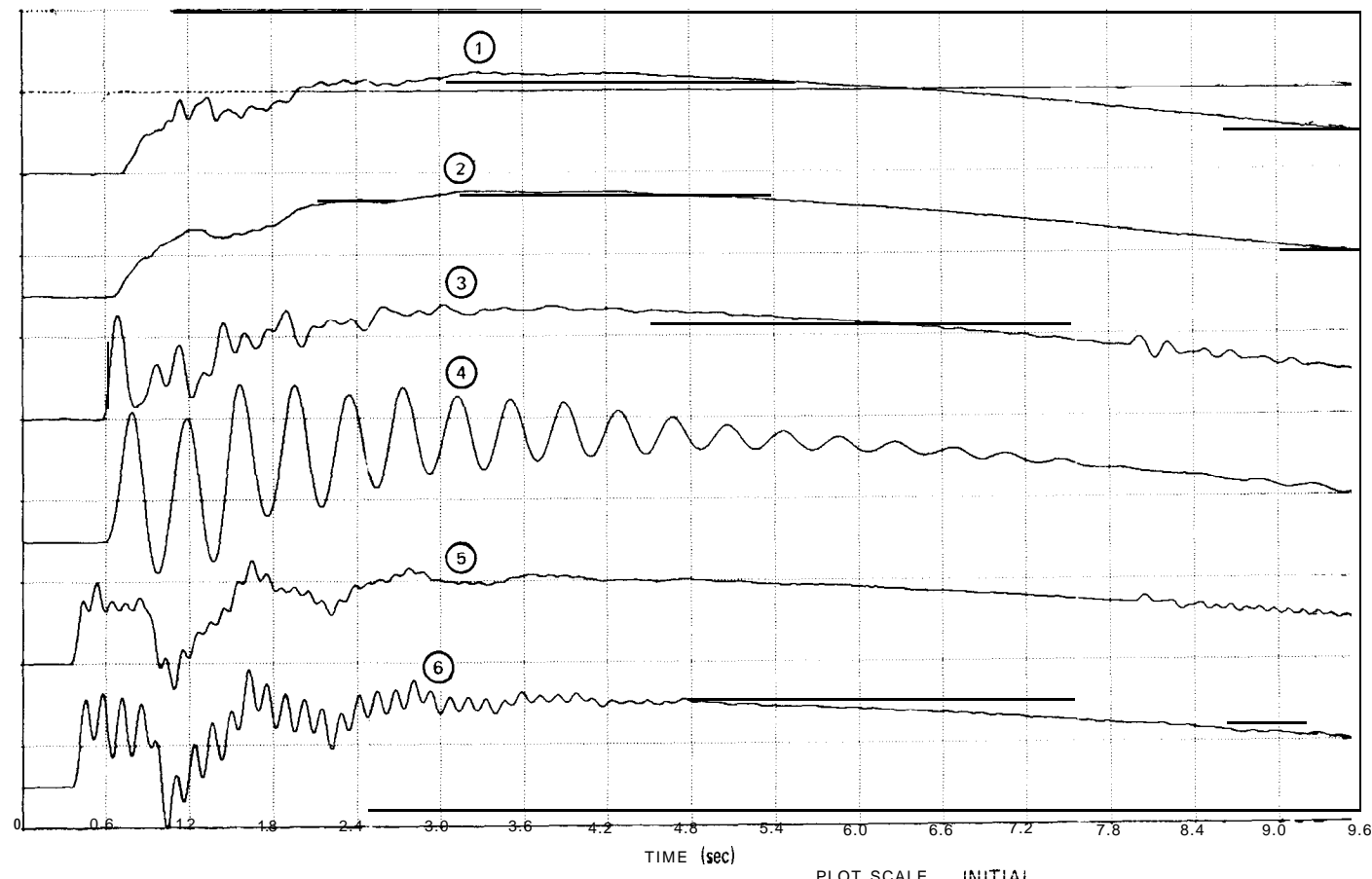
6-12



CURVE NO.	MEASURED VARIABLE	PLOT SCALE (UNITS/DIV)	INITIAL VALUE
1	CORE EXIT PRESSURE	50 psi	998.7 psia
2	REACTOR VESSEL PRESSURE	50 psi	991.3 psia
3	STEAM LINE A PRESSURE	50 psi	985.5 psia
4	STEAM LINE D PRESSURE	50 psi	994.4 psia
5	TURBINE INLET PRESSURE A	50 psi	985.3 psia
6	TURBINE INLET PRESSURE D	50 psi	986.2 psia

Figure 6-4. Peach Bottom-2 EOC2 Test Turbine Trip Test TT1 Filtered Pressure Measurements (5 Hz Lowpass Filter)

6.13



CURVE NO.	MEASURED VARIABLE	PLOT SCALE (UNITS/DIV)	INITIAL VALUE
1	CORE EXIT PRESSURE	50 psi	980.8 psia
2	REACTOR VESSEL PRESSURE	50 psi	976.3 psia
3	STEAM LINE A PRESSURE	50 psi	968.1 psia
4	STEAM LINE D PRESSURE	50 psi	974.4 psia
5	TURBINE INLET PRESSURE A	50 psi	965.6 psia
6	TURBINE INLET PRESSURE D	50 psi	960.9 psia

Figure 6-5. Peach Bottom-2 EOC2 Test Turbine Trip Test TT2 Filtered Pressure Measurements (5 Hz Lowpass Filter)

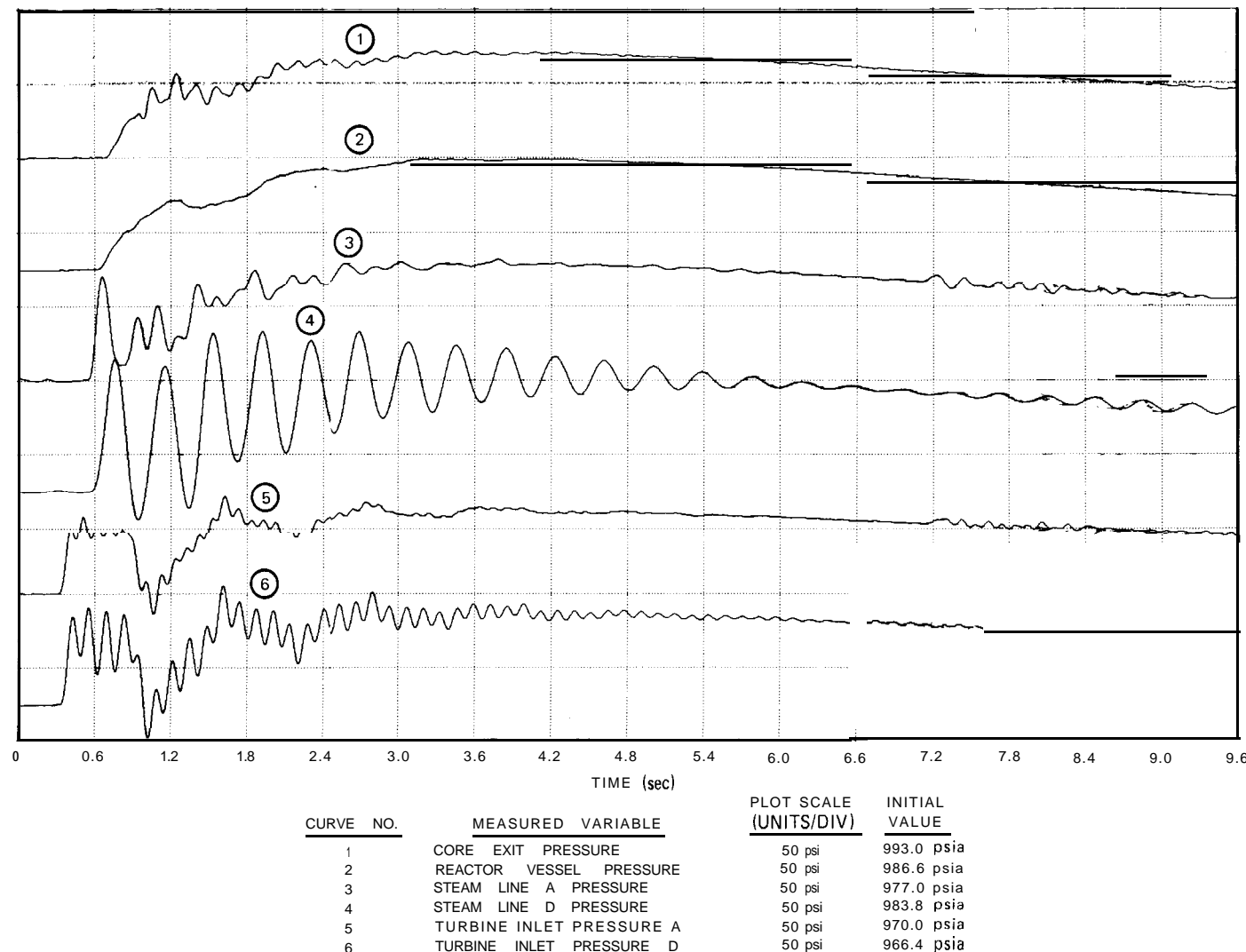


Figure 6-6. Peach Bottom-2 EOC2 Test Turbine Trip Test TT3 Filtered Pressure Measurements (5 Hz Lowpass Filter)

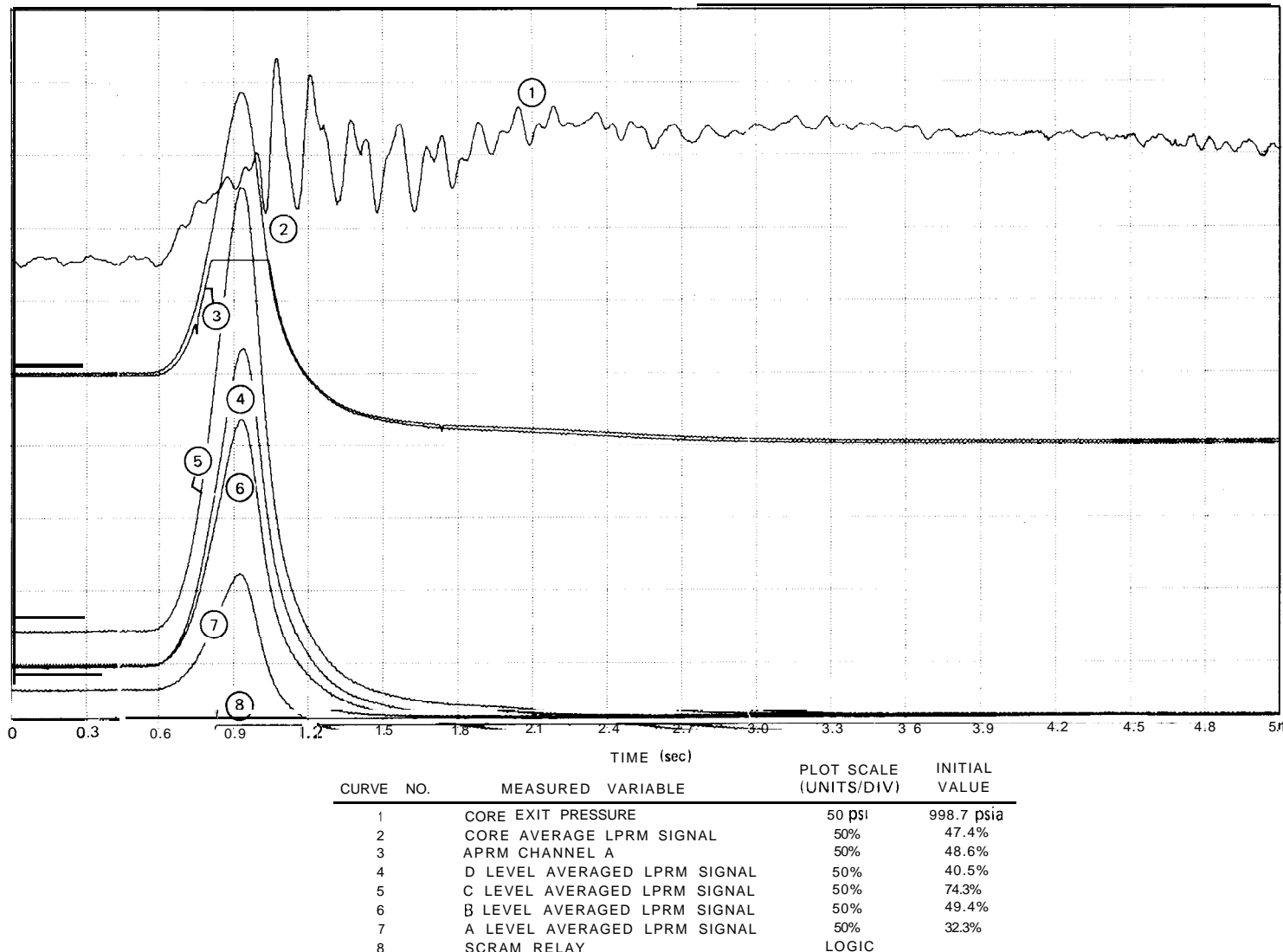


Figure 6-7. Peach Bottom-2 EOC2 Test Turbine Trip Test TT1 Reactor Core Response

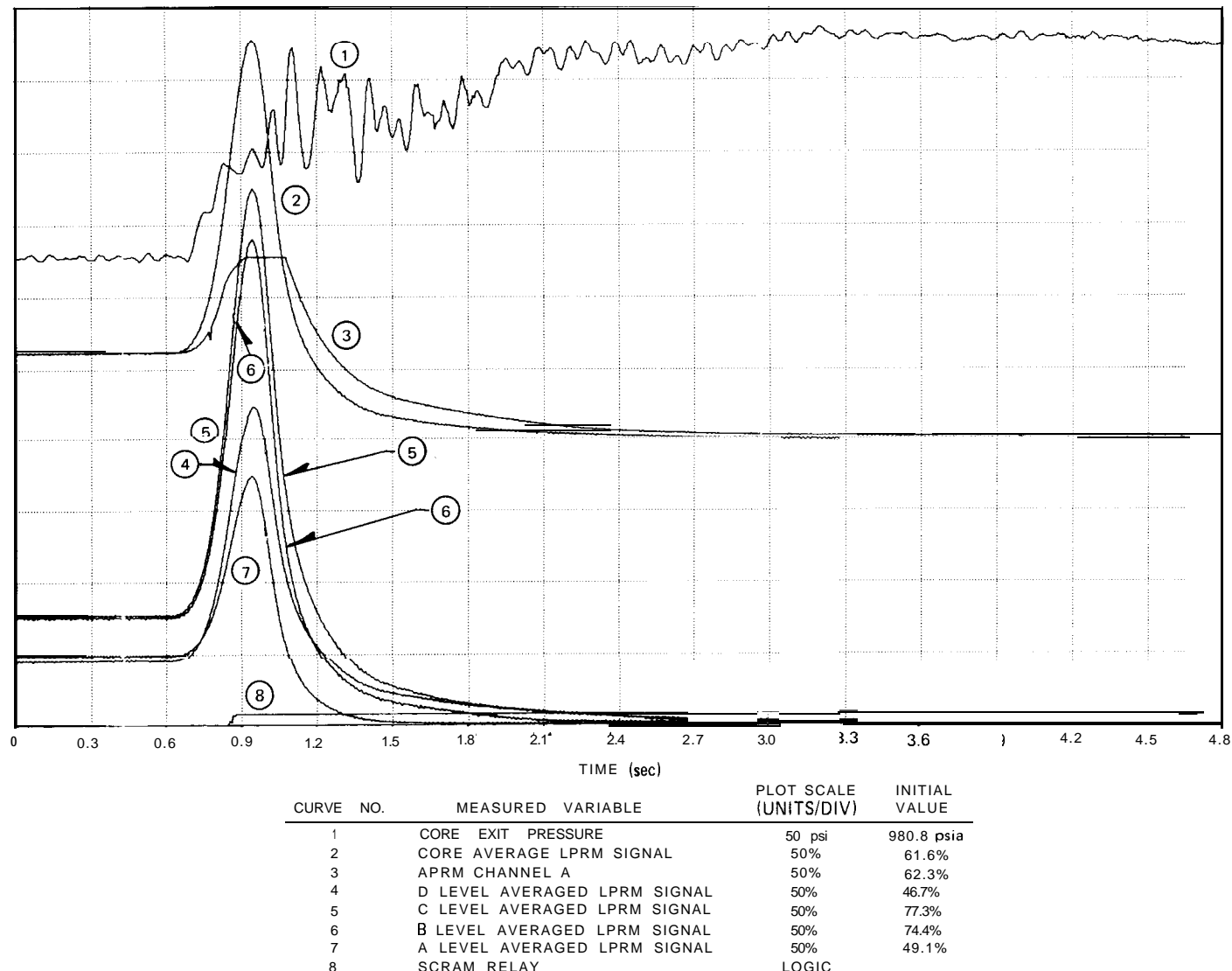


Figure 6-8. Peach Bottom-2 EOC2 Test Turbine Trip Test TT2 Reactor Core Response

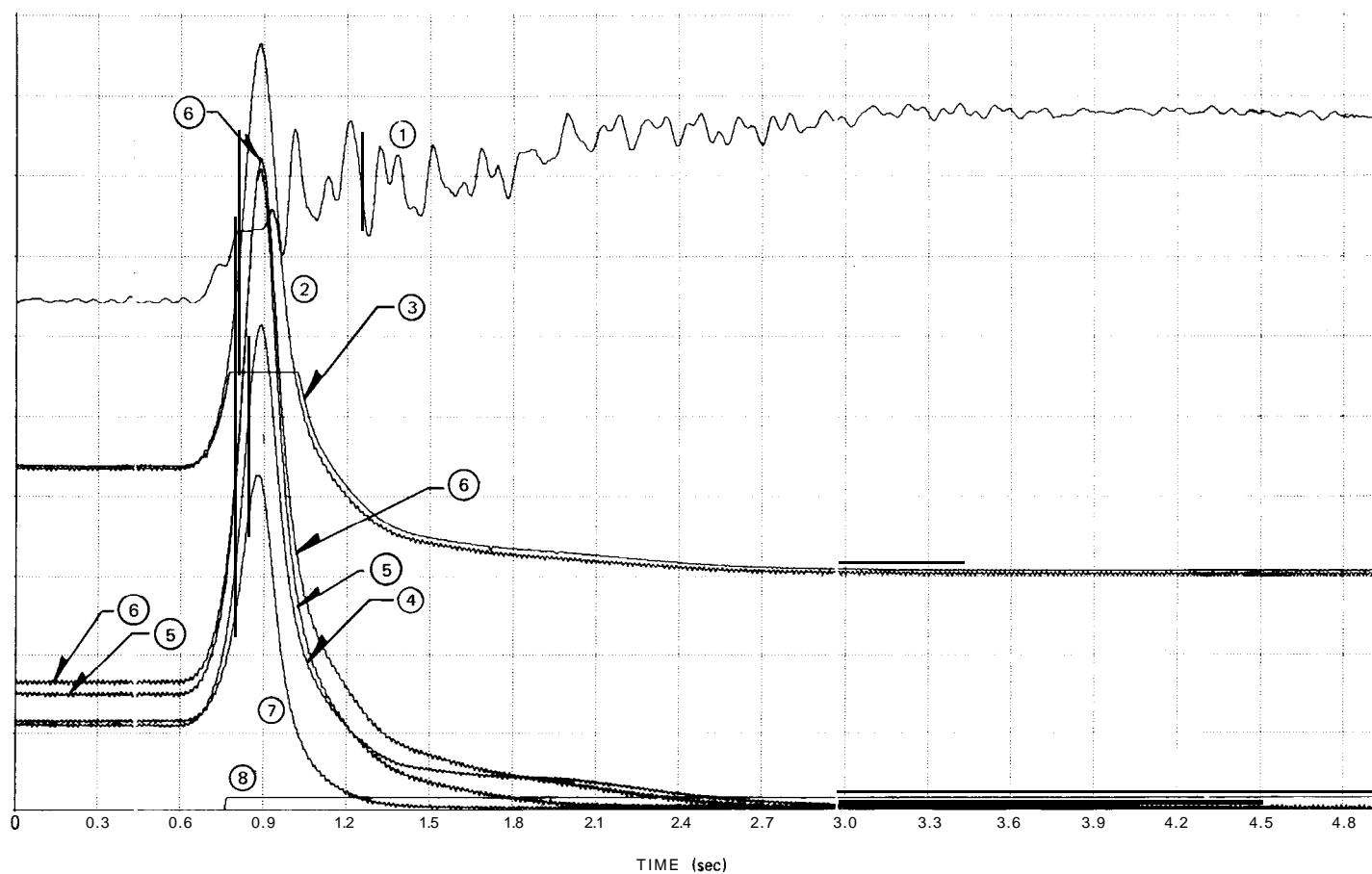


Figure 6-9. Peach Bottom-2 EOC2 Test Turbine Trip Test TT3 Reactor Core Response

CURVE NO.	MEASURED VARIABLE	PLOT SCALE (UNITS/DIV)	INITIAL VALUE
1	CORE EXIT PRESSURE	50 psi	993.0 psia
2	CORE AVERAGE LPRM SIGNAL	50%	69.1%
3	APRM CHANNEL A	50%	68.9%
4	D LEVEL AVERAGED LPRM SIGNAL	50%	55.8%
5	C LEVEL AVERAGED LPRM SIGNAL	50%	74.7%
6	B LEVEL AVERAGED LPRM SIGNAL	50%	80.7%
7	A LEVEL AVERAGED LPRM SIGNAL	50%	53.0%
8	SCRAM RELAY	LOGIC	

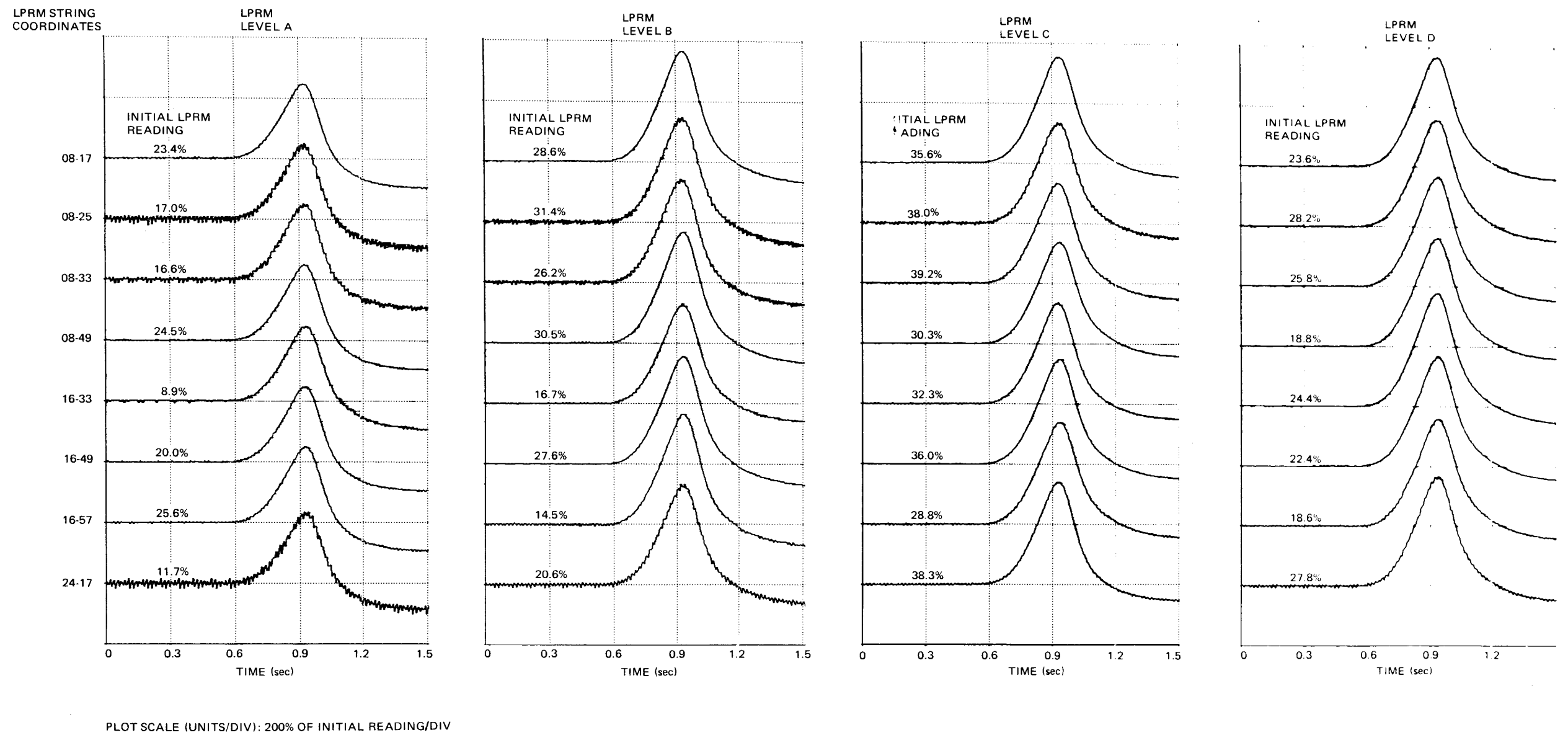


Figure 6-10A. Peach Bottom-2 EOC2 Test Turbine Trip Test TT1 Core Local Power Monitor Response

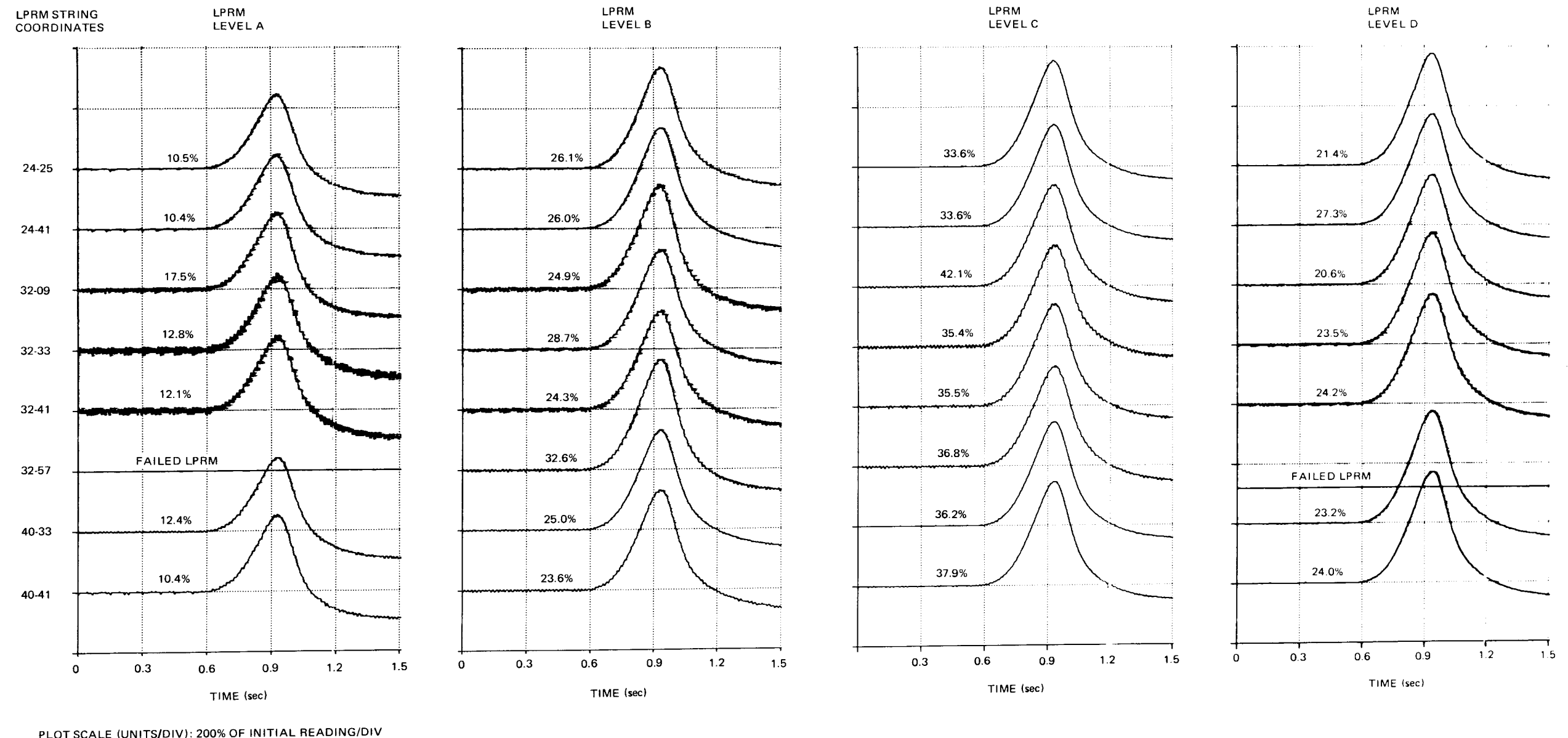
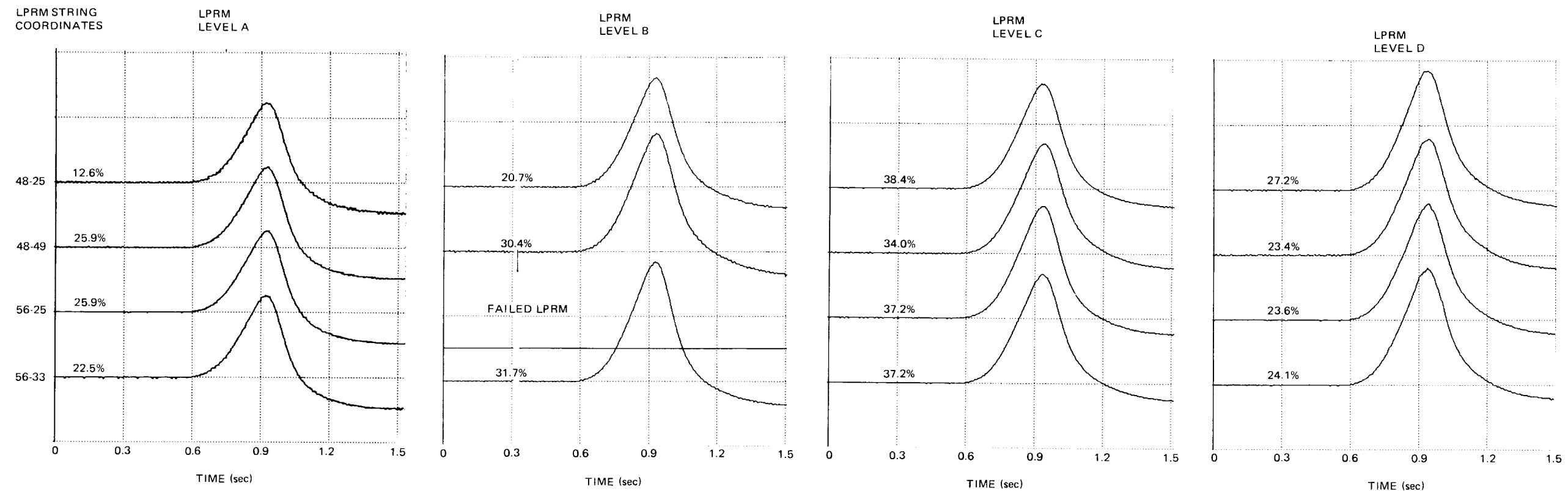


Figure 6-10B. Peach Bottom-2 EOC2 Test Turbine Trip Test TT1 Core Local Power Monitor Response



PLOT SCALE (UNITS/DIV): 200% OF INITIAL READING/DIV

Figure 6-10C. Peach Bottom-2 EOC2 Test Turbine Trip Test TT1 Core Local Power Monitor Response

6-25

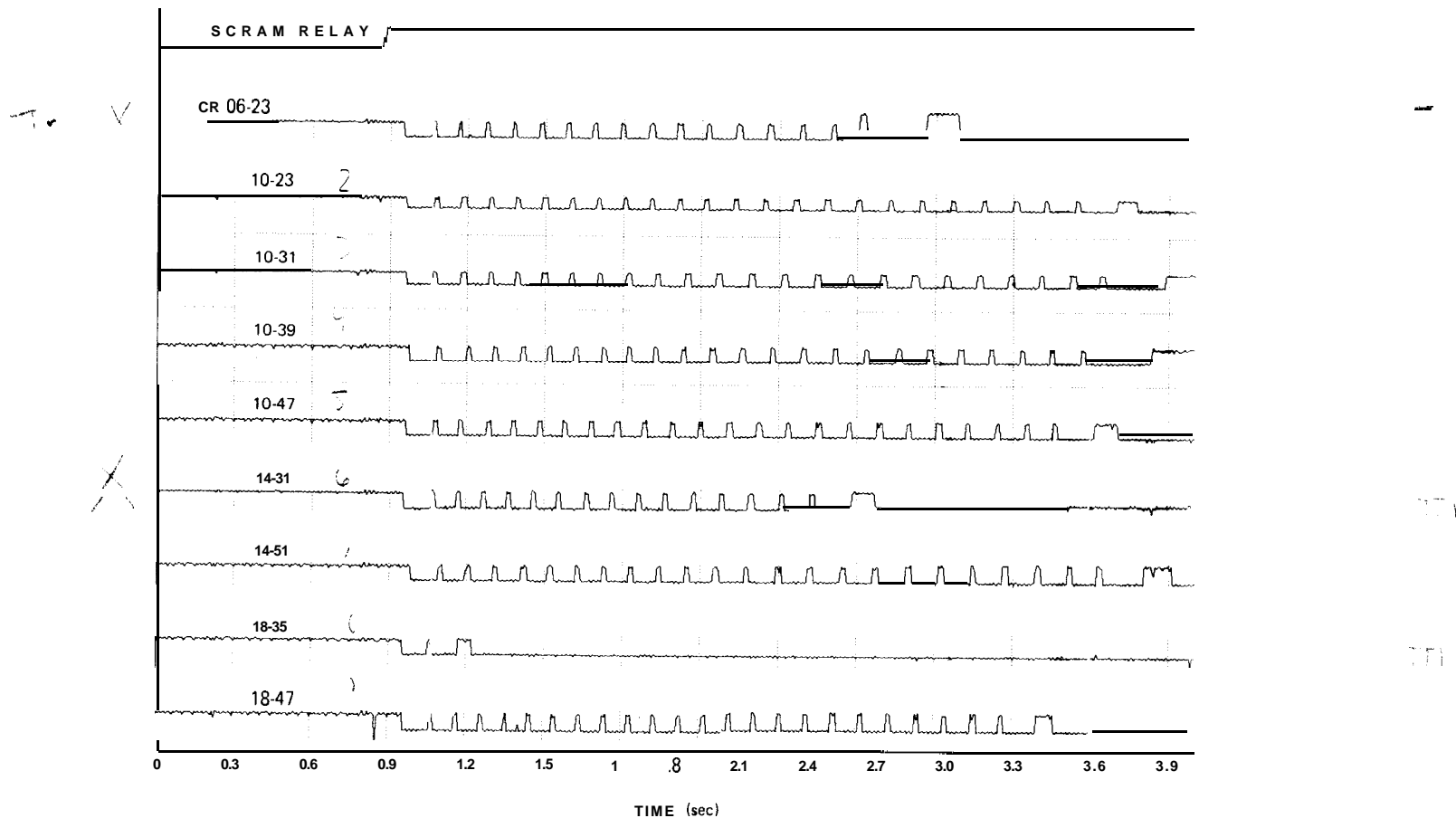


Figure 6-11A. Peach Bottom-2 EOC2 Test Turbine Trip Test TT1 Control Rod Drive Response

6-26

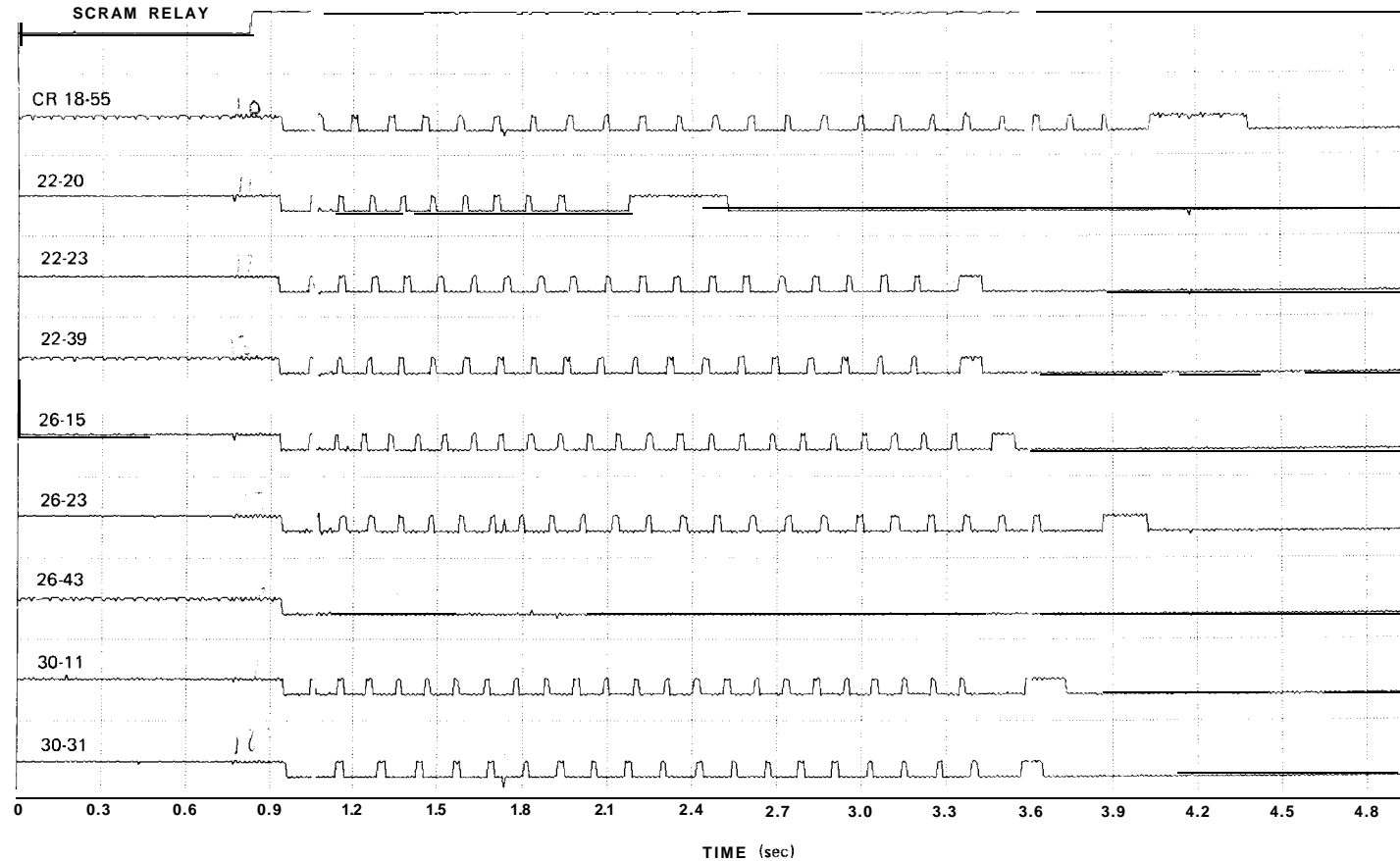


Figure 6-11B, Peach Bottom-2 EOC2 Test Turbine Trip Test TT1 Control Rod Drive Response

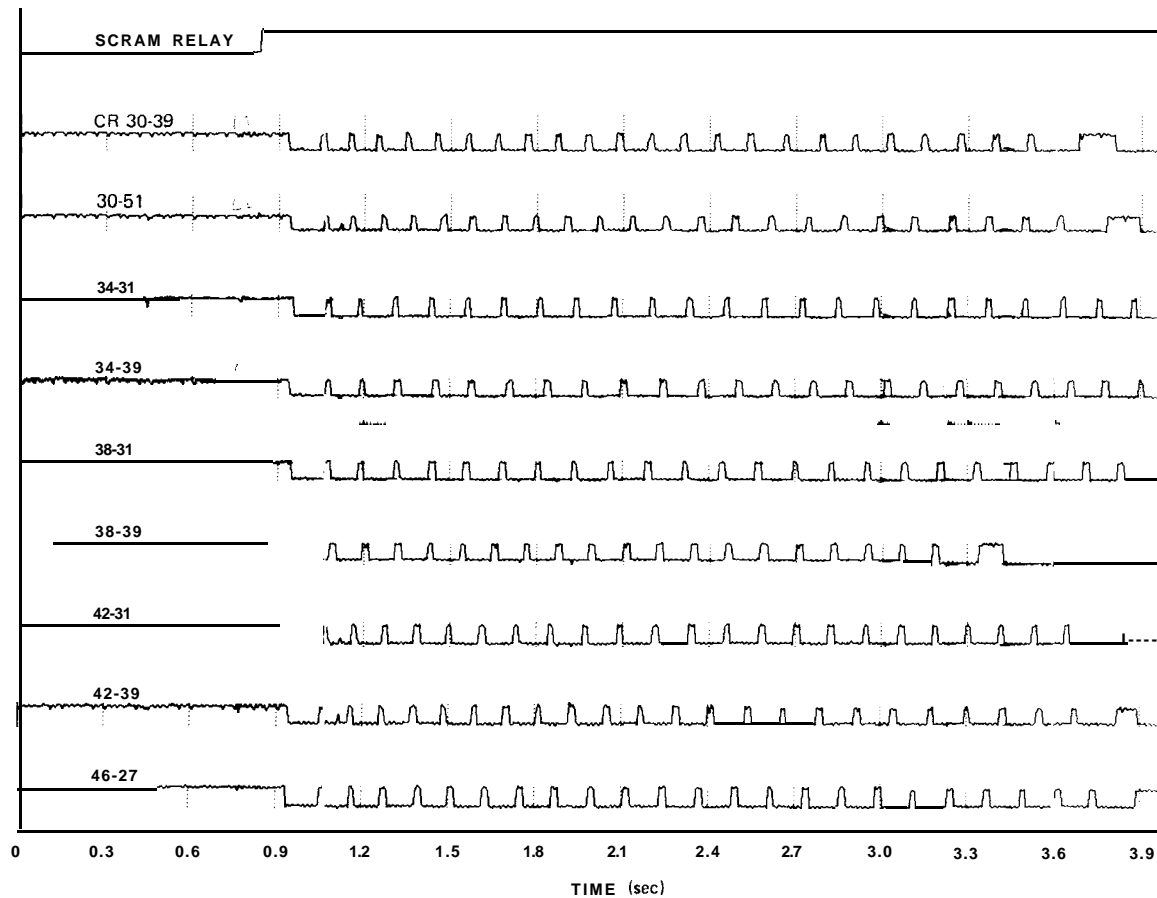


Figure 6-11C. Peach Bottom EOC2 Test Turbine Trip Test TT1 Control Rod Drive Response

6-28

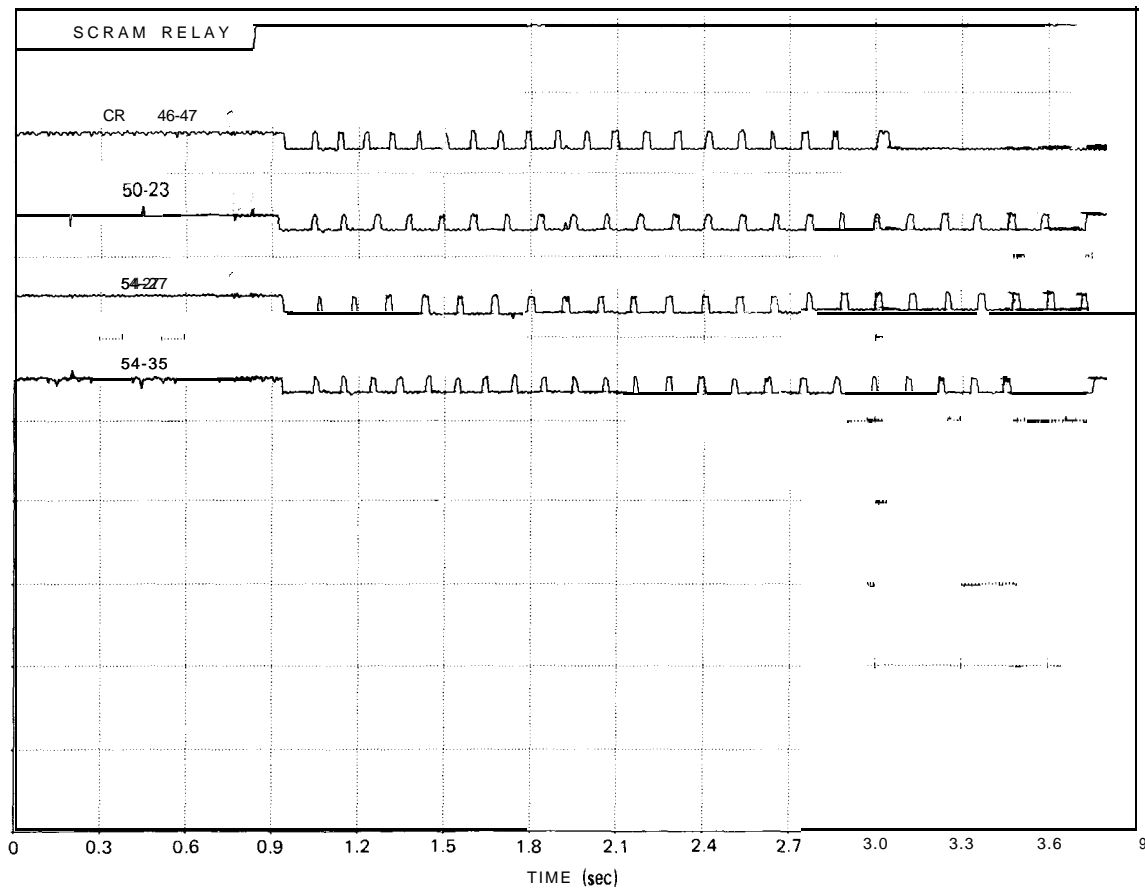


Figure 6-1 ID. Peach Bottom-2 EOC2 Test Turbine Trip Test TT1 Control Rod Drive Response

6Z9

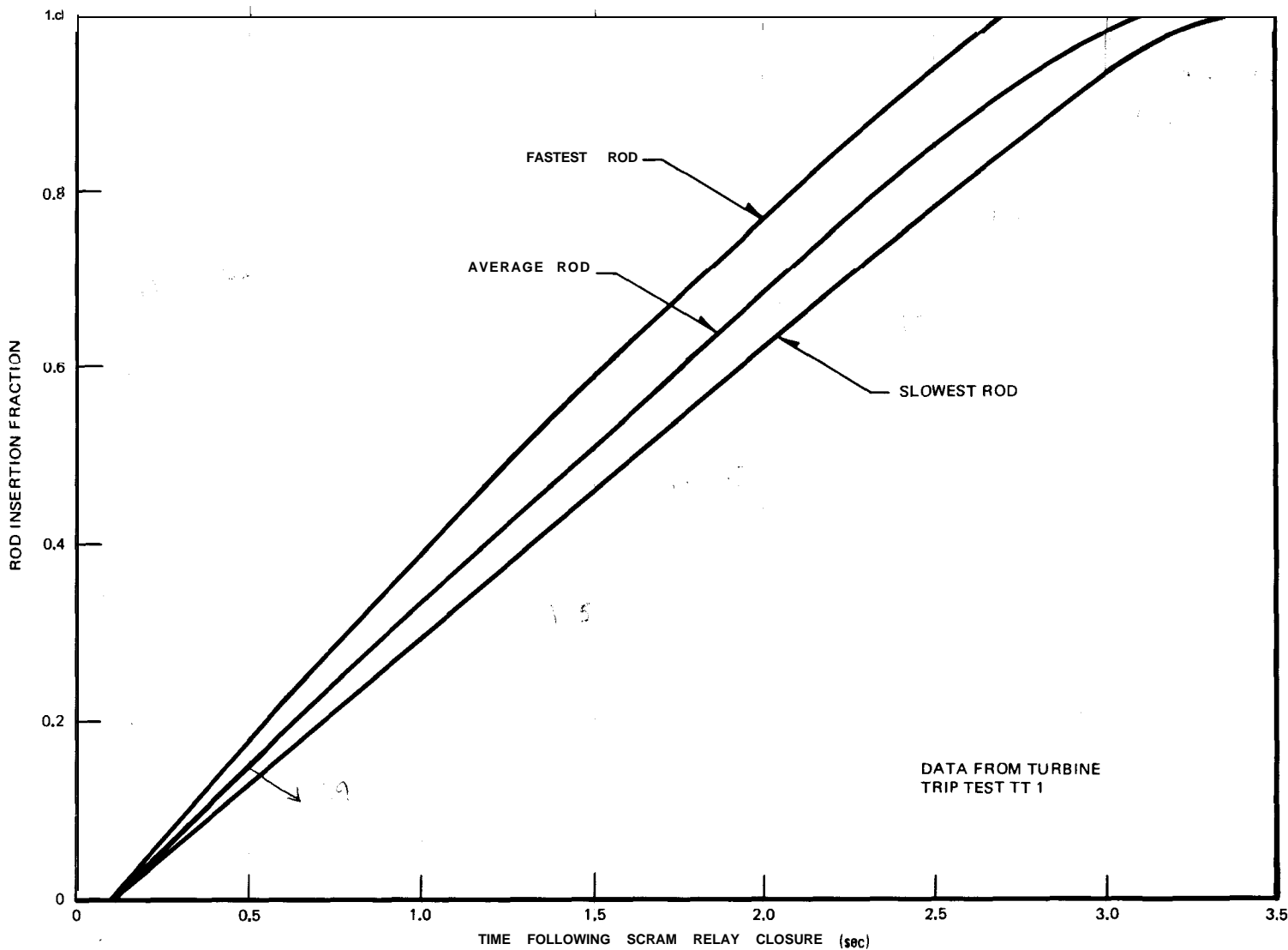
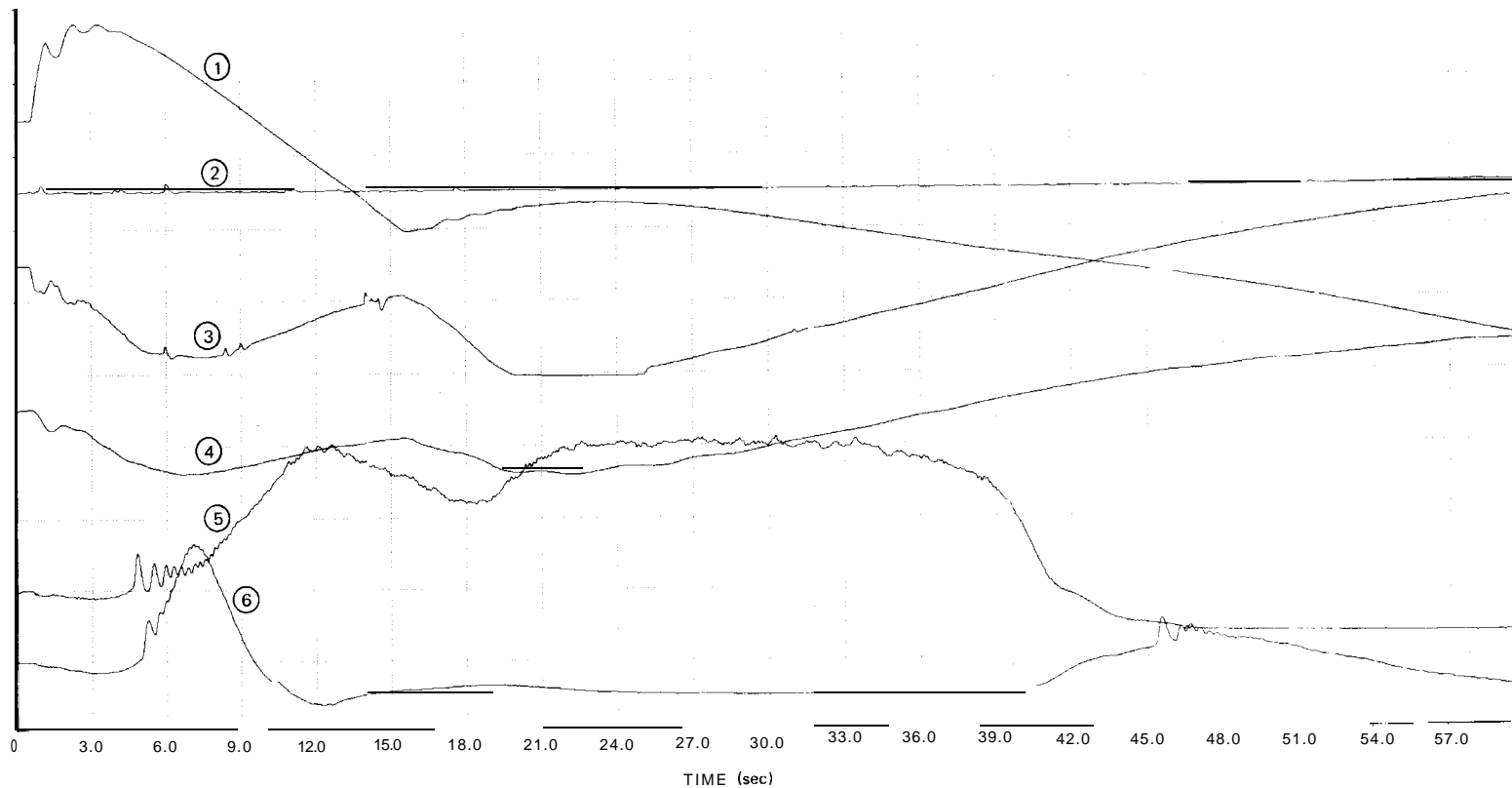


Figure 6-12. Peach Bottom-2 EOC2 Test Control Rod Scram Speed Summary

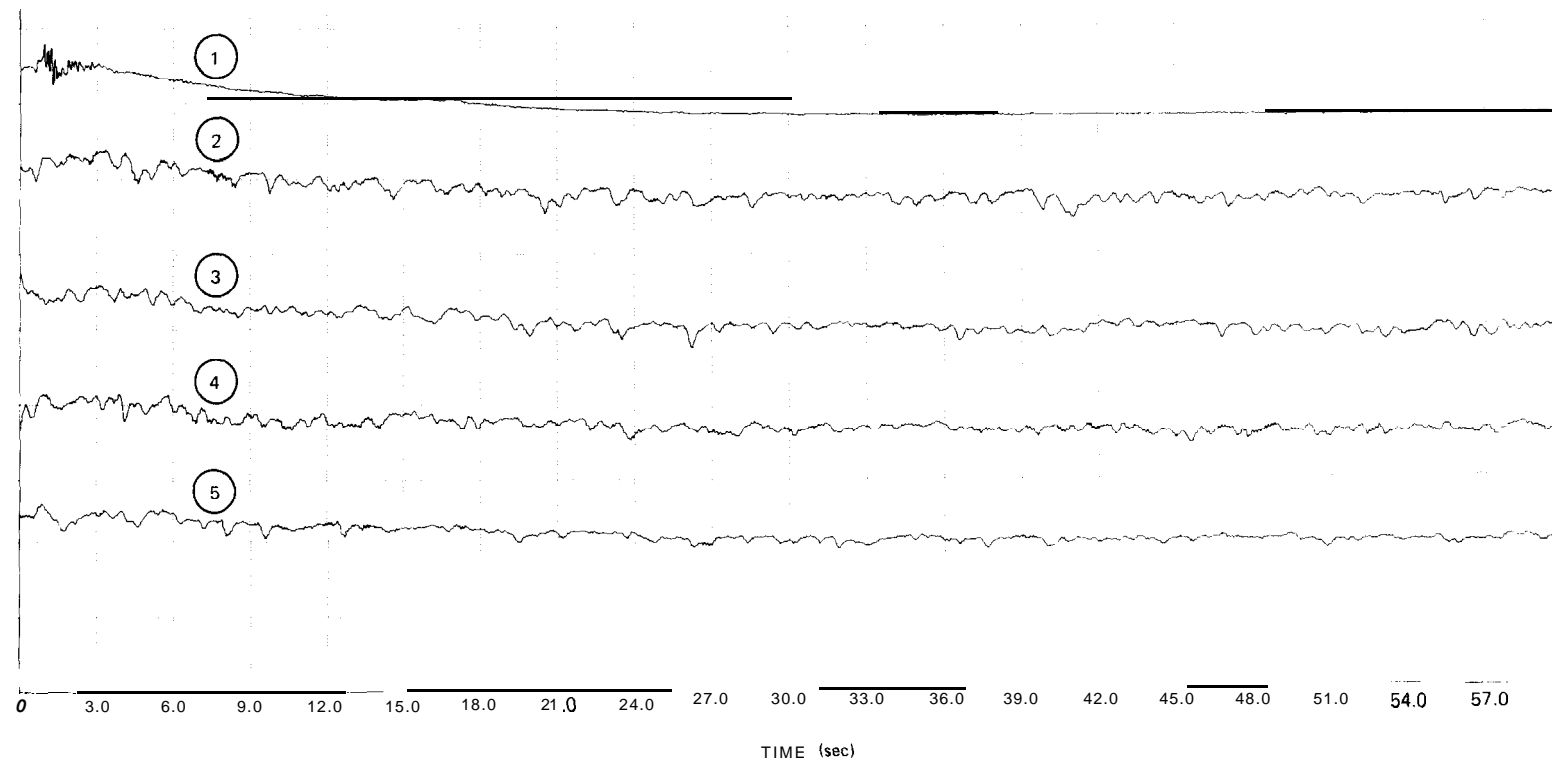
6-30



CURVE NO.	MEASURED VARIABLE	PLOT SCALE (UNITS/DIV)	INITIAL VALUE
2	REACTOR VESSEL PRESSURE FEEDWATER TEMPERATURE	50 psi 1°F	991.3 psia 283.5°F
3	REACTOR WATER LEVEL (INR)	20 inches	23.0 inches
4	REACTOR WATER LEVEL (WR)	20 inches	23.0"
5	FEEDWATER NOZZLE A DELTA P	5 psid	3.2 psid
6	FEEDWATER NOZZLE B DELTA P	5 psid	2.9 psid

*BIASED TO READ SAME AS NR LEVEL INSTRUMENT

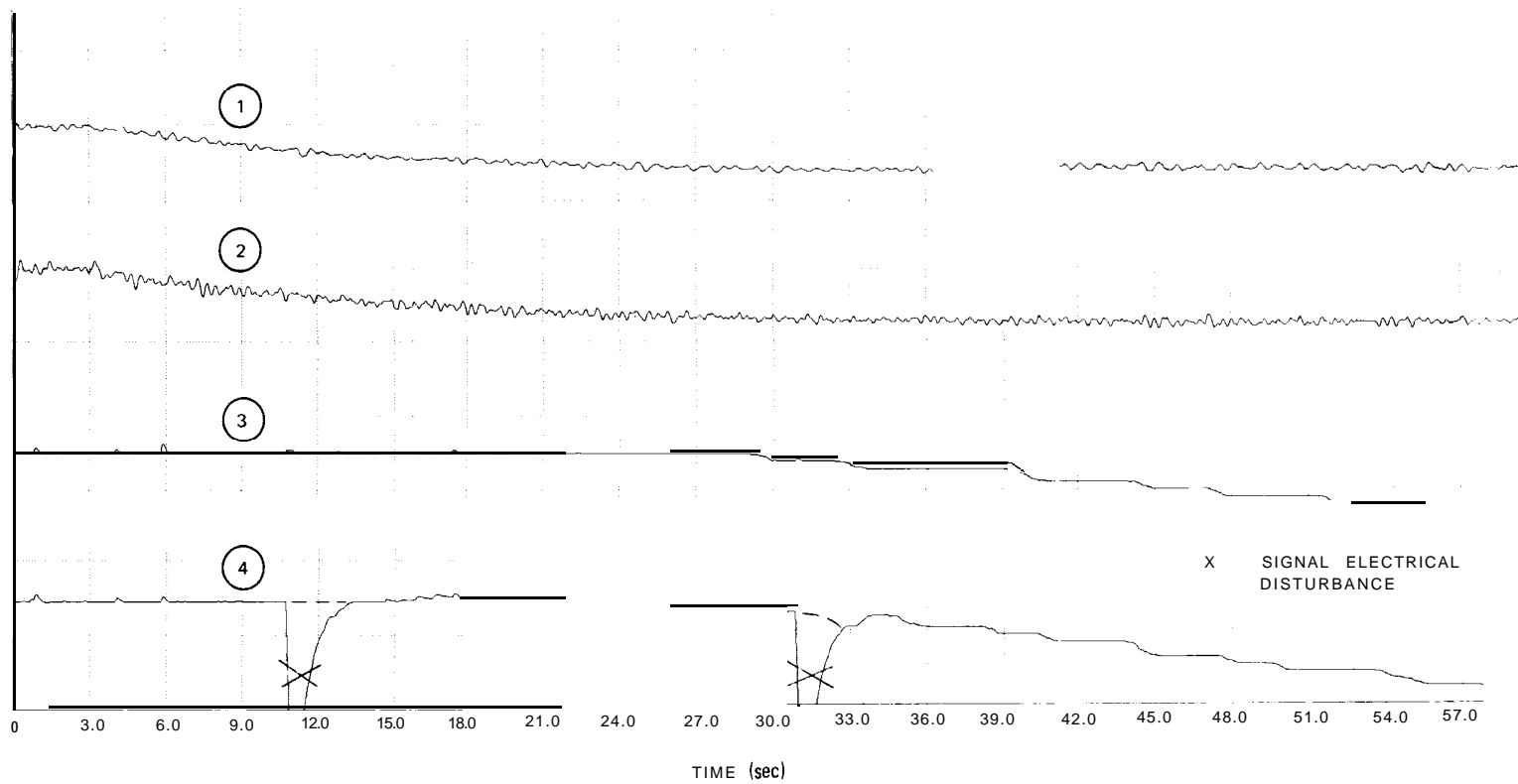
Figure 6-13. Peach Bottom-2 EOC2 Test Turbine Trip Test (TT1) Reactor Feedwater and Level Response



CURVE NO.	MEASURED VARIABLE	PLOT SCALE (UNITS/DIV)	INITIAL VALUE
1	CORE PRESSURE DROP	10 psid	8.0 psid
2	JET PUMP NO. 1 DELTA P	10 psid	11.4 psid
3	JET PUMP NO. 6 DELTA P	10 psid	13.1 psid
4	JET PUMP NO. 11 DELTA P	10 psid	9.4 psid
5	JET PUMP NO. 16 DELTA P	10 psid	12.4 psid

Figure 6-14. Peach Bottom-2 EOC2 Test Turbine Trip Test (TT1) Reactor Jet Pump and Core Pressure Drop Response

632



CURVE NO.	MEASURED VARIABLE	PLOT SCALE (UNITS/DIV)	INITIAL VALUE
1	RECIRCULATION FLOW NOZZLE A DELTA P	5 psid	8.7 psid
2	RECIRCULATION FLOW NOZZLE B DELTA P	5 psid	10.0 psid
3	RECIRCULATION LOOP A TEMPERATURE	5°F	531.0°F
4	RECIRCULATION LOOP B TEMPERATURE	5°F	530.9°F

Figure 6-15. Peach Bottom-2 EOC2 Test Turbine Trip Test (TT1) Reactor Recirculation Loop Response

633

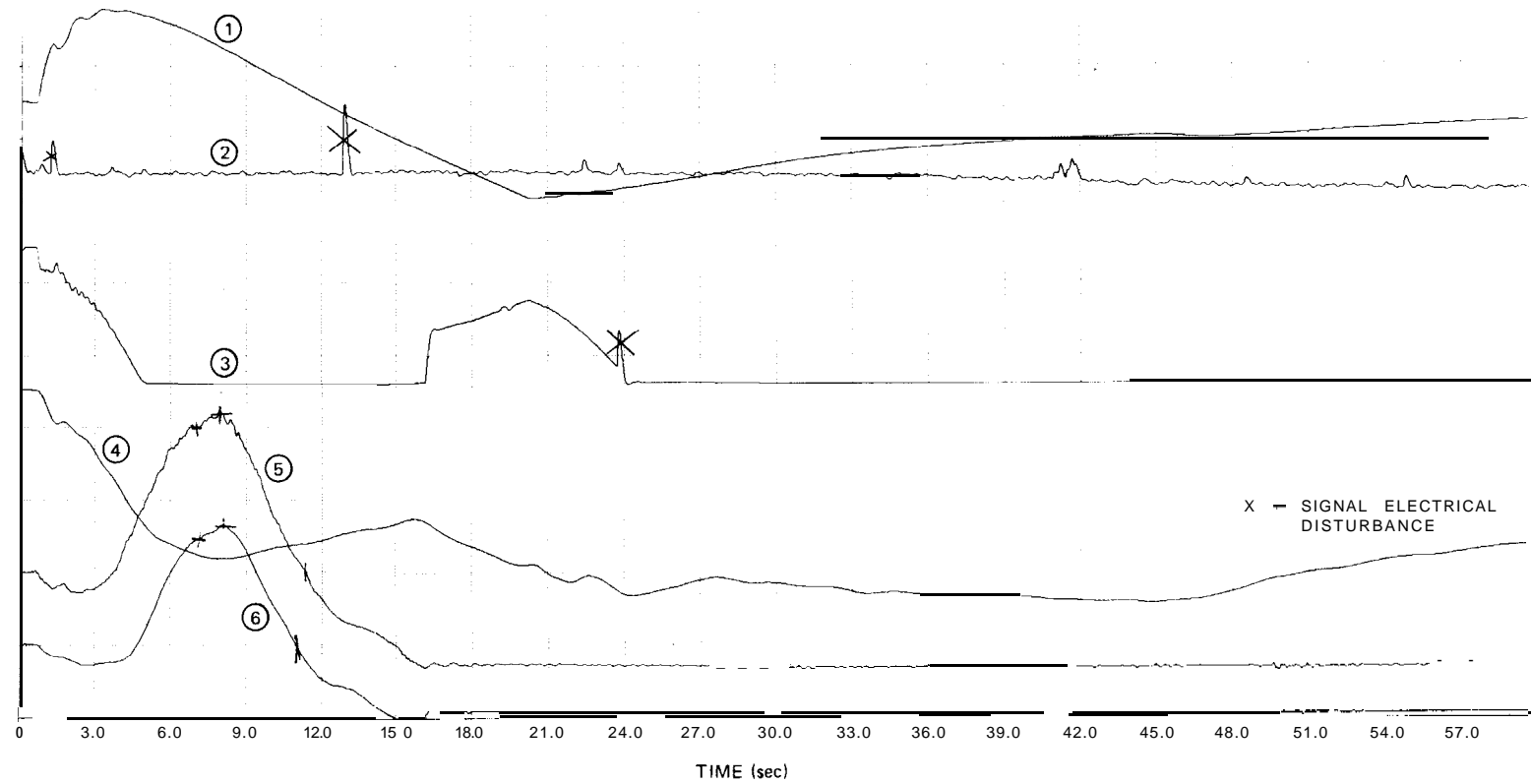
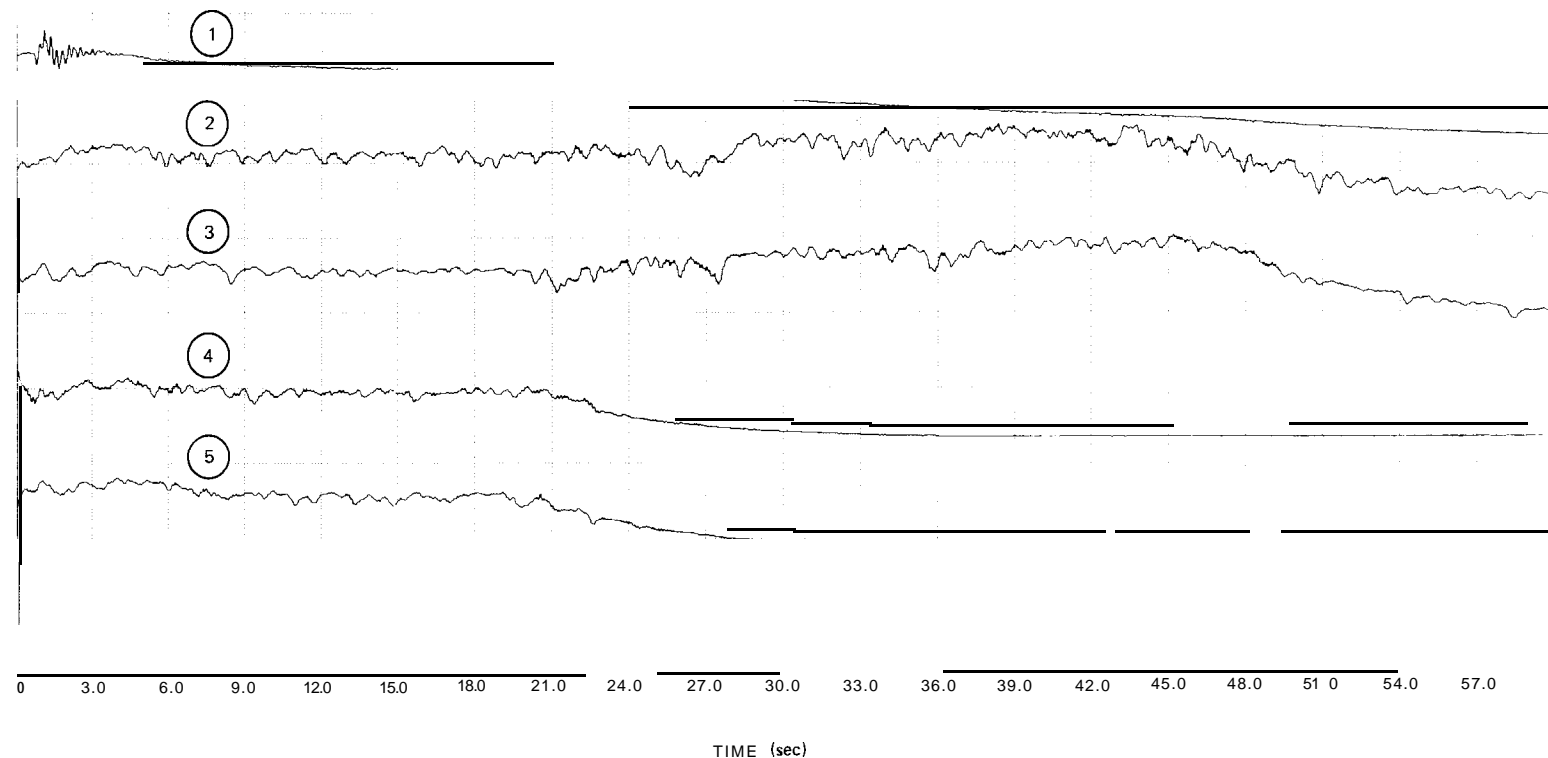


Figure 6- 16. Peach Bottom-2 EOC2 Test Turbine Trip Test TT2 Reactor Feedwater and Level Response

CURVE NO.	MEASURED VARIABLE	PLOT SCALE (UNITS/DIV)	INITIAL VALUE
1	REACTOR VESSEL PRESSURE	50 psi	976.3
2	FEEDWATER TEMPERATURE	2°F	335.6°F
3	REACTOR WATER LEVEL (NR)	20 inches	29.2 inches
4	REACTOR WATER LEVEL (WR)	20 inches	20.9 inches
5	FEEDWATER NOZZLE A DELTA P	5 psid	6.2 psid
6	FEEDWATER NOZZLE B DELTA P	5 psid	4.8 psid

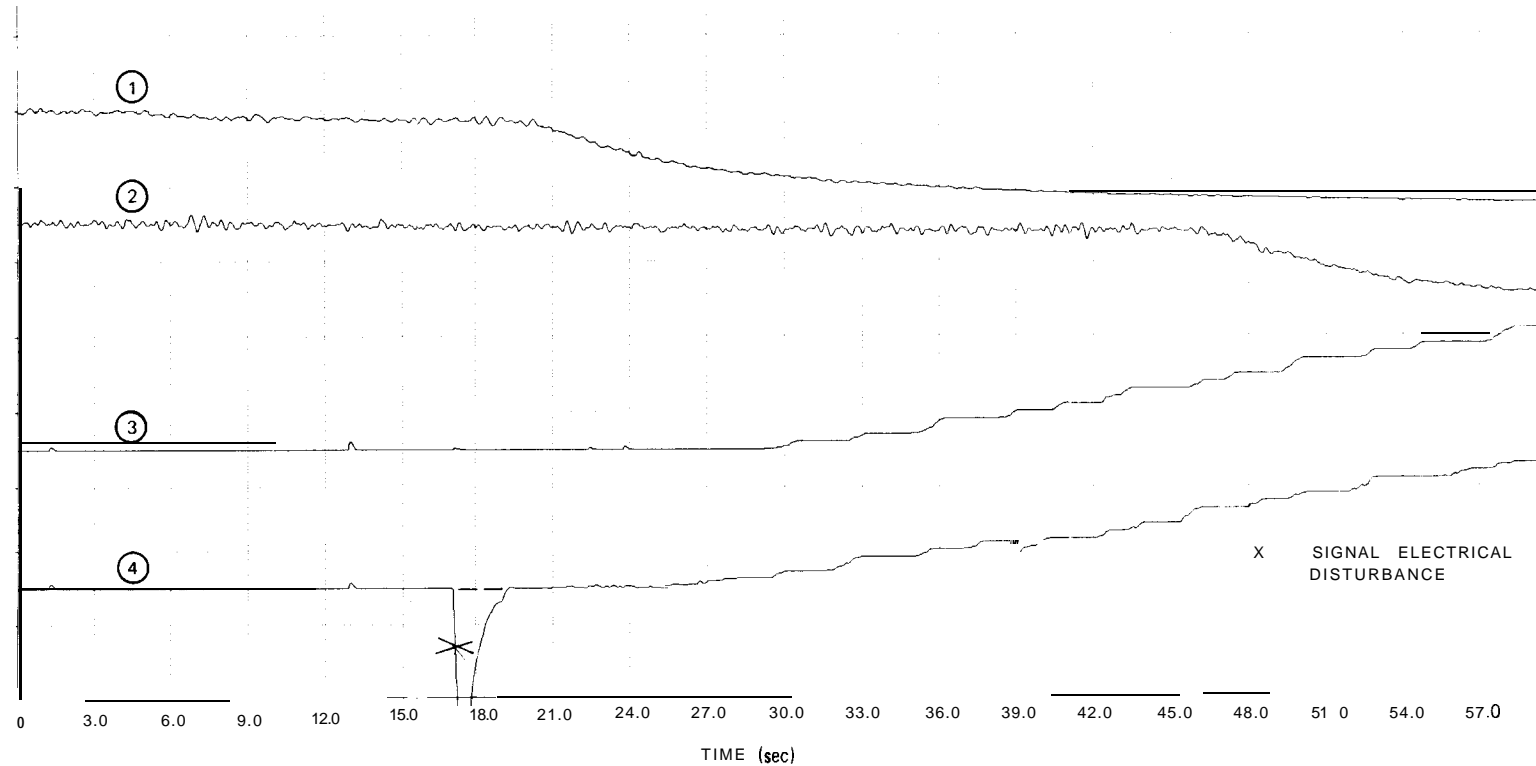
6-34



CURVE NO.	MEASURED VARIABLE	PLOT SCALE (UNITS/DIV)	INITIAL VALUE
1	CORE PRESSURE DROP	10 psid	12.2 psid
2	JET PUMP NO. 1 DELTA P	10 psid	7.3 psid
3	JET PUMP NO. 6 DELTA P	10 psid	9.0 psid
4	JET PUMP NO. 11 DELTA P	10 psid	6.4 psid
5	JET PUMP NO. 16 DELTA P	10 psid	7.2 psid

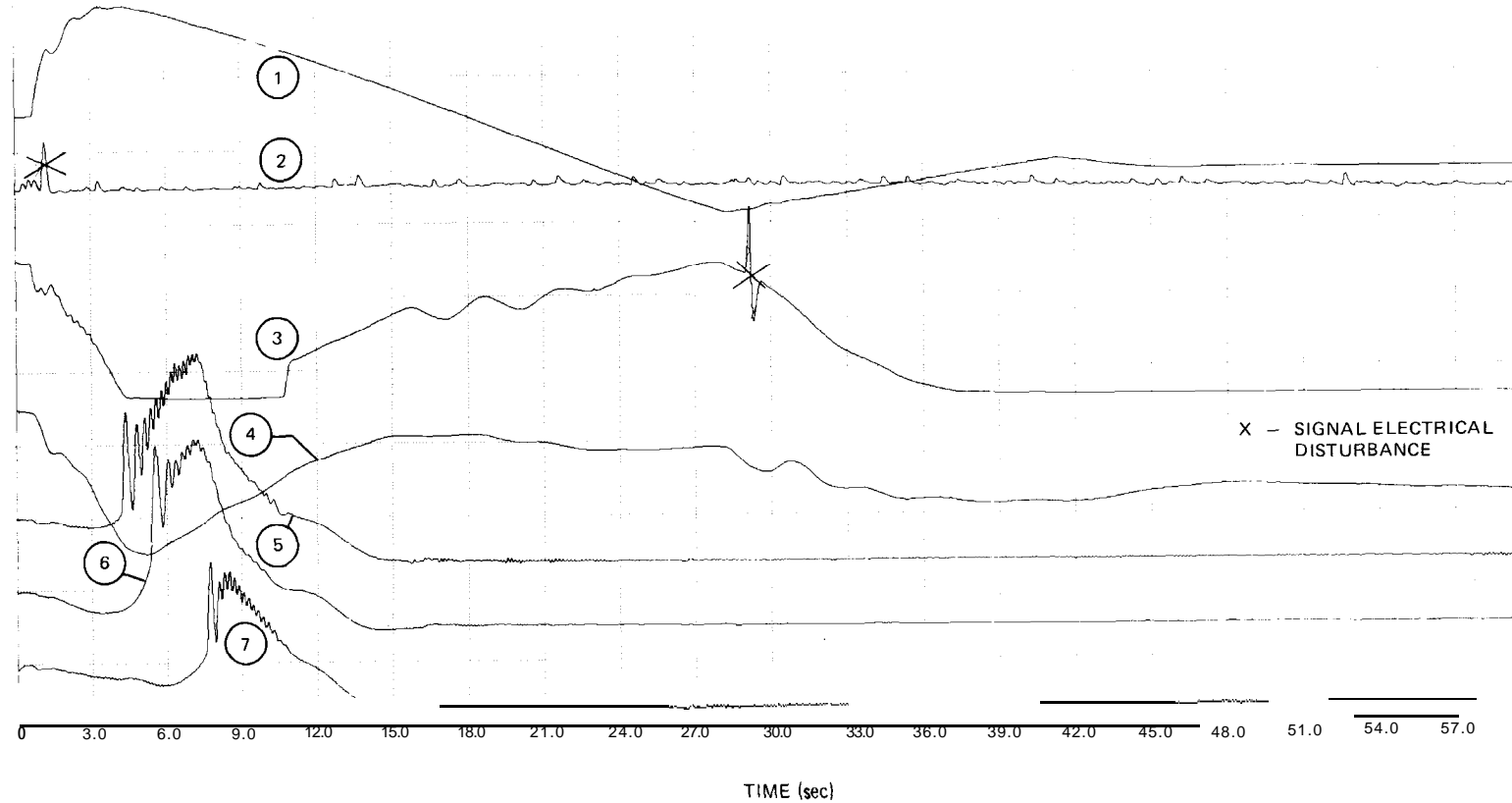
Figure 6-17. Peach Bottom-2 EOC2 Test Turbine Trip Test TT2 Reactor Jet Pump and Core Pressure Drop Response

635



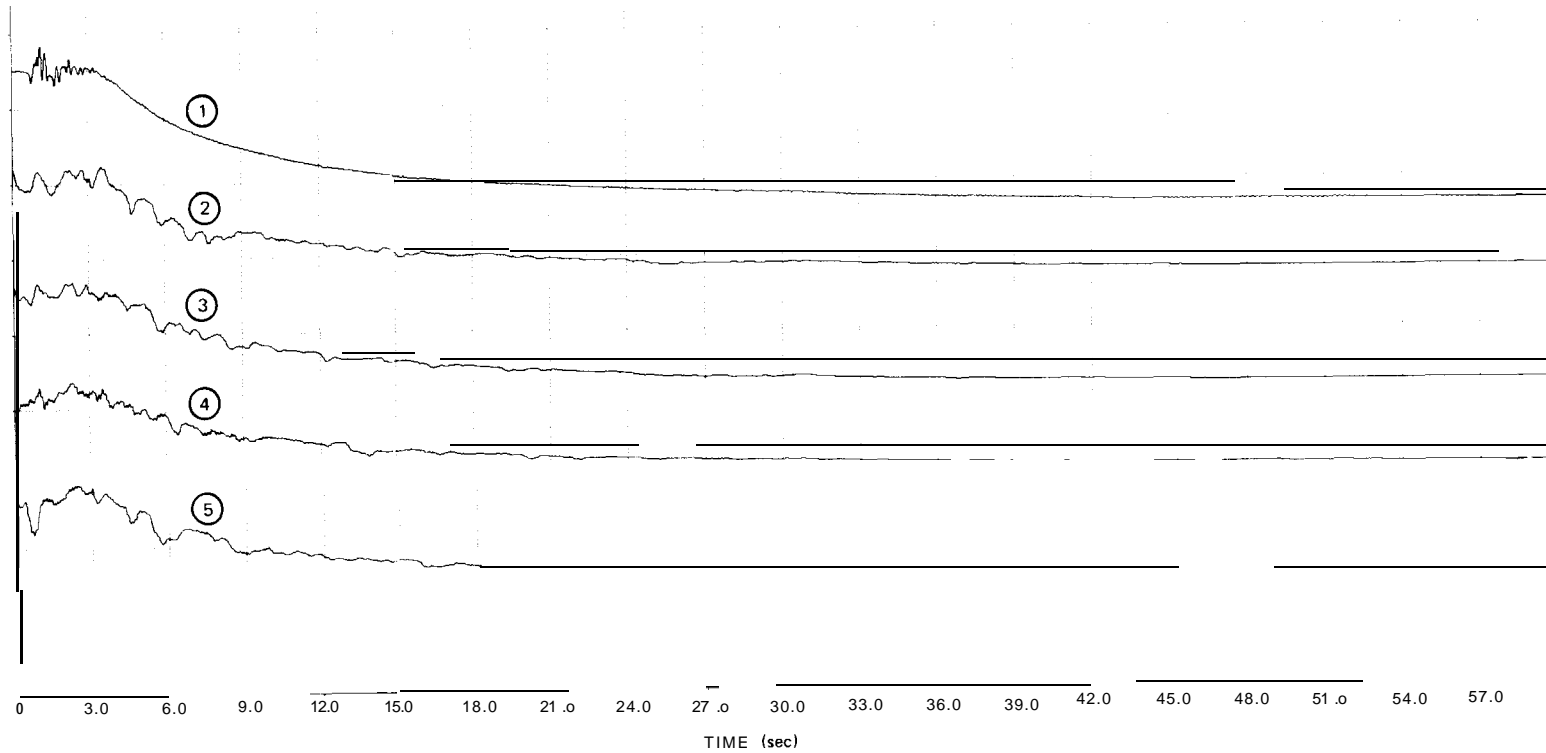
CURVE NO.	MEASURED VARIABLE	PLOT SCALE (UNITS/DIV)	INITIAL VALUE
1	RECIRCULATION FLOW NOZZLE A DELTA P	5 psid	6.4 psid
2	RECIRCULATION FLOW NOZZLE B DELTA P	5 psid	6.7 psid
3	RECIRCULATION LOOP A TEMPERATURE	5°F	522.0°F
4	RECIRCULATION LOOP B TEMPERATURE	5°F	522.7°F

Figure 6-18. Peach Bottom-2 EOC2 Test Turbine Trip Test TT2 Reactor Recirculation Loop Pressure



CURVE NO.	MEASURED VARIABLE	PLOT SCALE (UNITS/DIV)	INITIAL VALUE
1	REACTOR VESSEL PRESSURE	50 psi 10F	986.6 psia 346.40F
2	FEEDWATER TEMPERATURE		
3	REACTOR WATER LEVEL (NR)	20 inches	29.8 inches
4	REACTOR WATER LEVEL (WR)	20 inches	15.8 inches
5	FEEDWATER NOZZLE A DELTA P	5 psid	3.1 psid
6	FEEDWATER NOZZLE B DELTA P	5 psid	2.6 psid
7	FEEDWATER NOZZLE C DELTA P	5 psid	3.8 psid

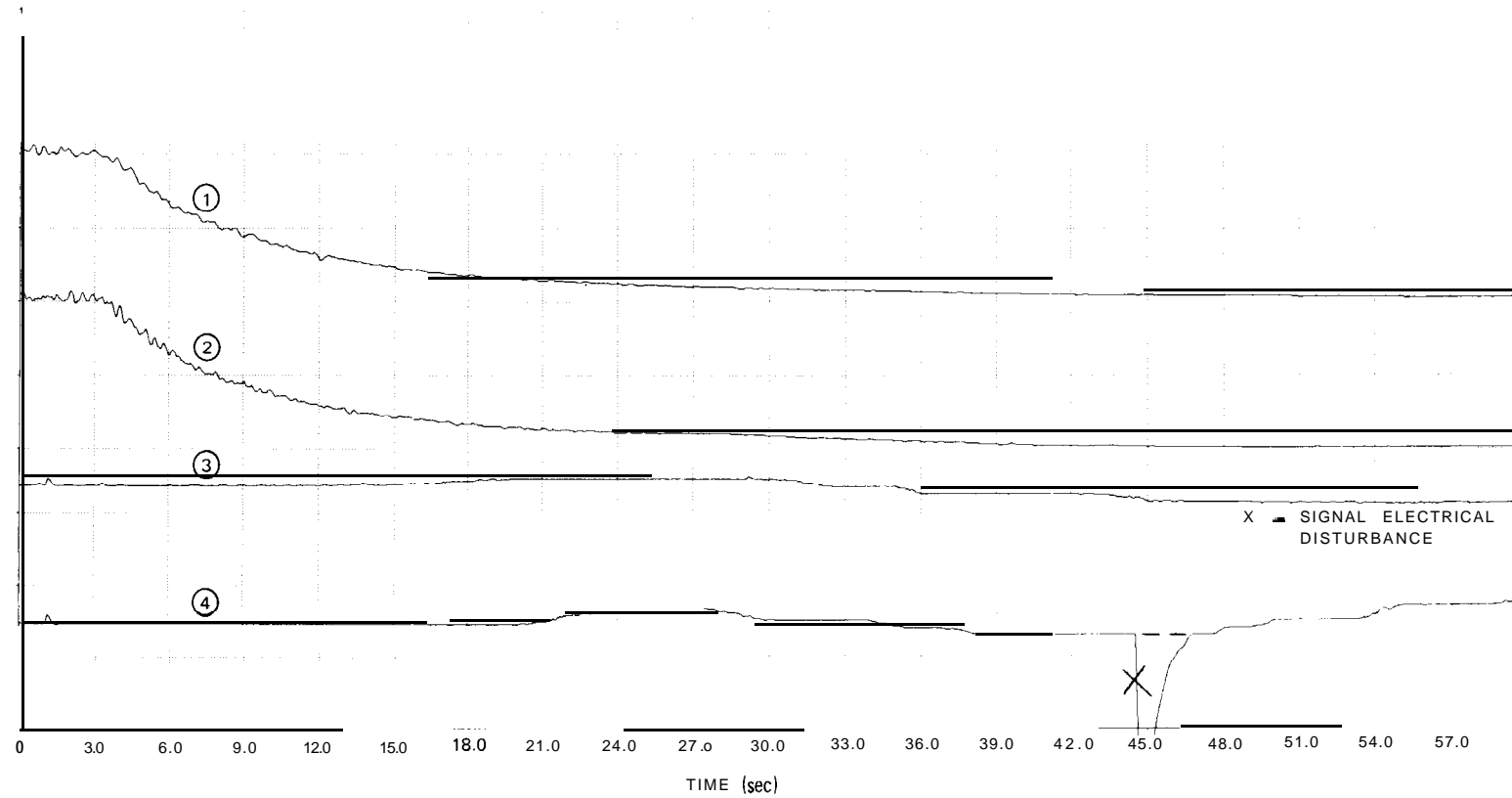
Figure 6-19. Peach Bottom-2 EOC2 Test Turbine Trip Test TT3 Reactor Feedwater and Level Response



CURVE NO.	MEASURED VARIABLE	PLOT SCALE (UNITS/DIV)	INITIAL VALUE
1	CORE PRESSURE DROP	10 psid	18.1 psid
2	JET PUMP NO. 1 DELTA P	10 psid	10.6 psid
3	JET PUMP NO. 6 DELTA P	10 psid	17.4 psid
4	JET PUMP NO. 11 DELTA P	10 psid	9.7 psid
5	JET PUMP NO. 16 DELTA P	10 psid	10.9 psid

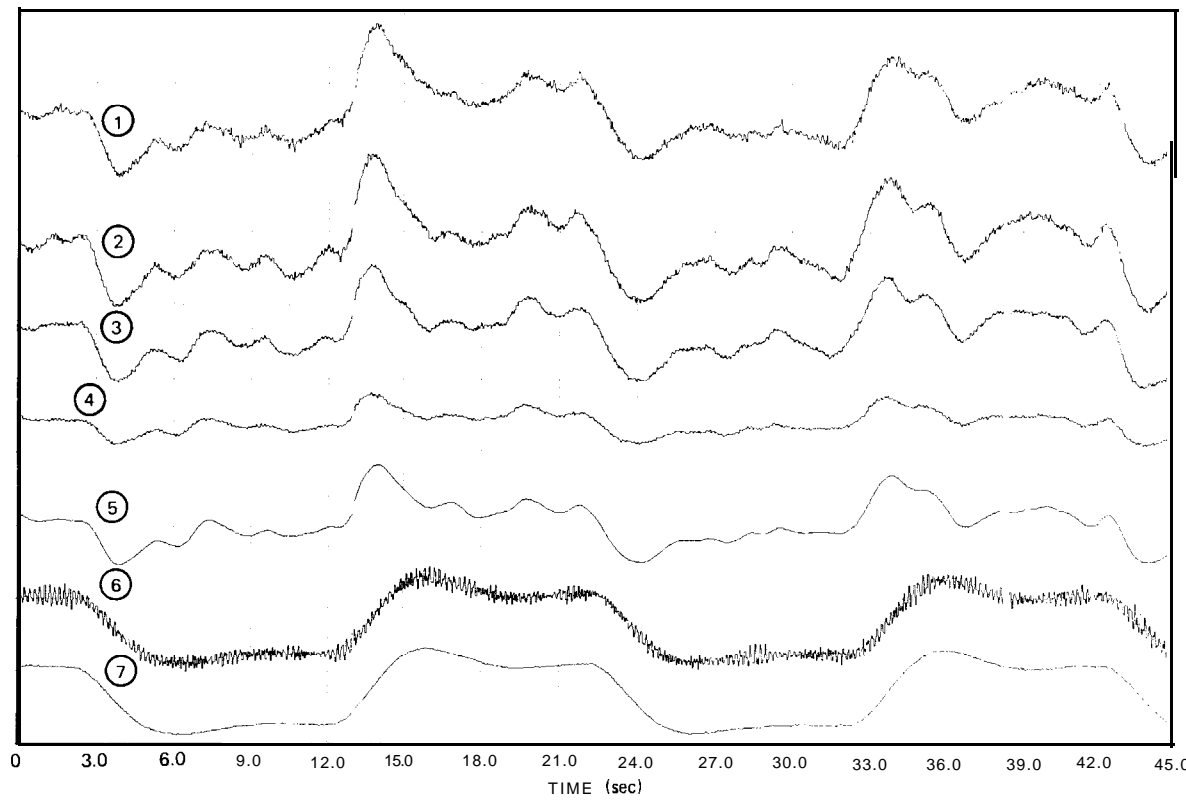
Figure B-20. Peach Bottom-2 EOC2 Test Turbine Trip Test TT3 Reactor Jet Pump and Core Pressure Drop Response

638



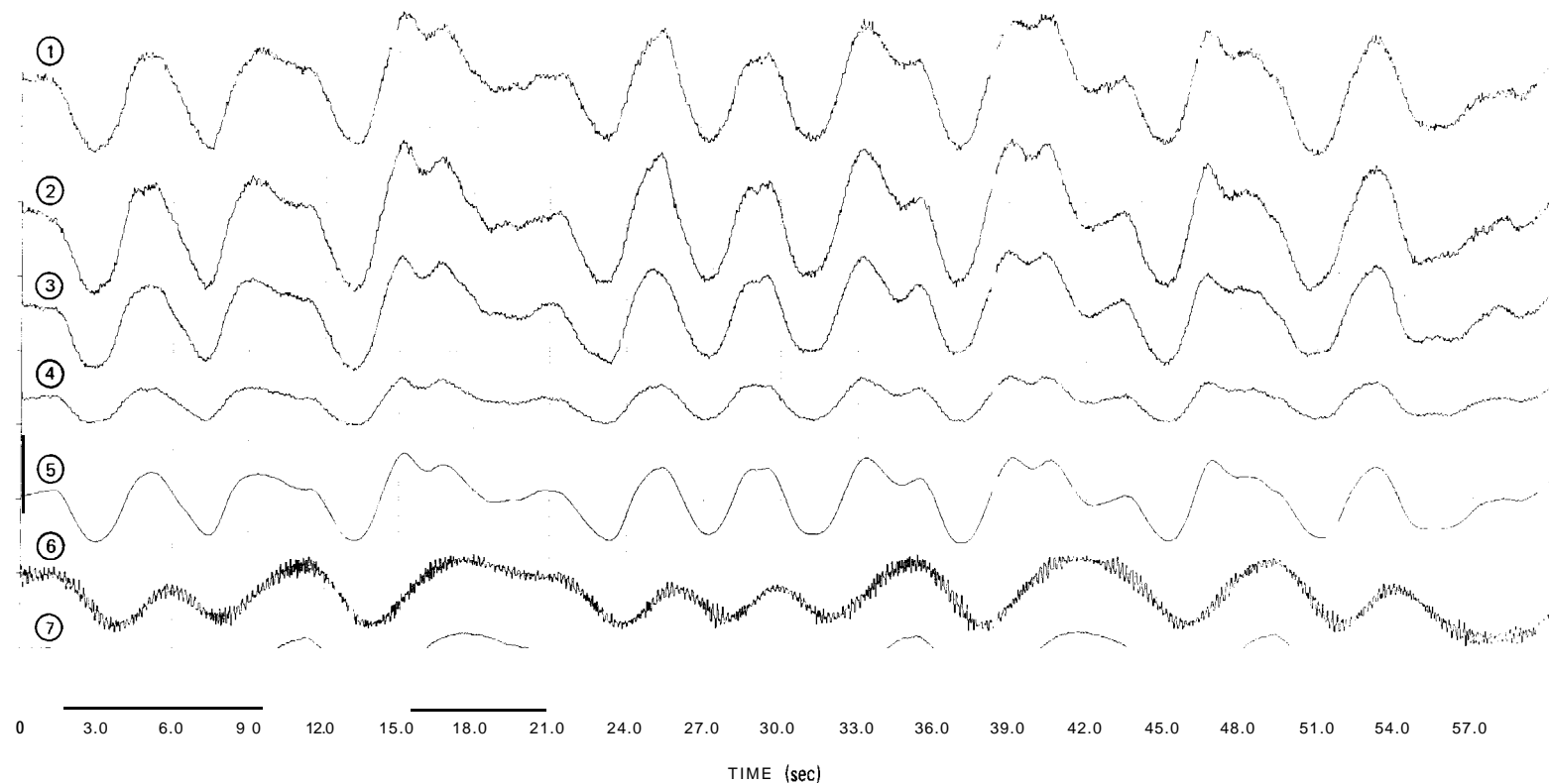
CURVE NO.	MEASURED VARIABLE	PLOT SCALE (UNITS/DIV)	INITIAL VALUE
2	RECIRCULATION FLOW NOZZLE A DELTA P	5 psid	9.8 psid
3	RECIRCULATION FLOW NOZZLE B DELTA P	5 psid	10.0 psid
4	RECIRCULATION LOOP A TEMPERATURE	50F	526.50F
	RECIRCULATION LOOP B TEMPERATURE	50F	527.70F

Figure 6-2 1. Peach Bottom 9 EOC2 Test Turbine Trip Test TT3 Reactor Recirculation Loop Response



CURVE NO.	MEASURED VARIABLE	PLOT SCALE (UNITS/DIV)	INITIAL VALUE
1	LPRM 32-41 D	5 W/cm ²	30 W/cm ²
2	LPRM 32-41 C	5 W/cm ²	40 W/cm ²
3	LPRM 32-41 B	5 W/cm ²	36 W/cm ²
4	LPRM 32-41 A	5 W/cm ²	22 W/cm ²
5	APRM CHANNEL A	10%	58%
6	REACTOR VESSEL PRESSURE	10 psi	986 psia
7	CORE EXIT PRESSURE	10 psi	997 psia

Figure B-22. Peach Bottom-2 EOC2 Test Low-Flow Stability Tests Periodic Pressure Regulator Setpoint Steps



CURVE NO.	MEASURED VARIABLE	PLOT SCALE (UNITS/DIV)	INITIAL VALUE
1	LPRM 32-41 D	W/cm ²	30 W/cm ²
2	LPRM 32-41 C	W/cm ²	40 w/cm*
3	LPRM 32-41 B	W/cm ²	36 W/cm ²
4	LPRM 32-41 A	W/cm ²	22 W/cm ²
5	APRM CHANNEL A	10%	58%
6	REACTOR VESSEL PRESSURE	10 psi	986 psia
7	CORE EXIT PRESSURE	10 psi	997 psia

Figure 6-23. Peach Bottom-2 EOC2 Test Low-Flow Stability Test PRBS Pressure Regulator Setpoint Steps

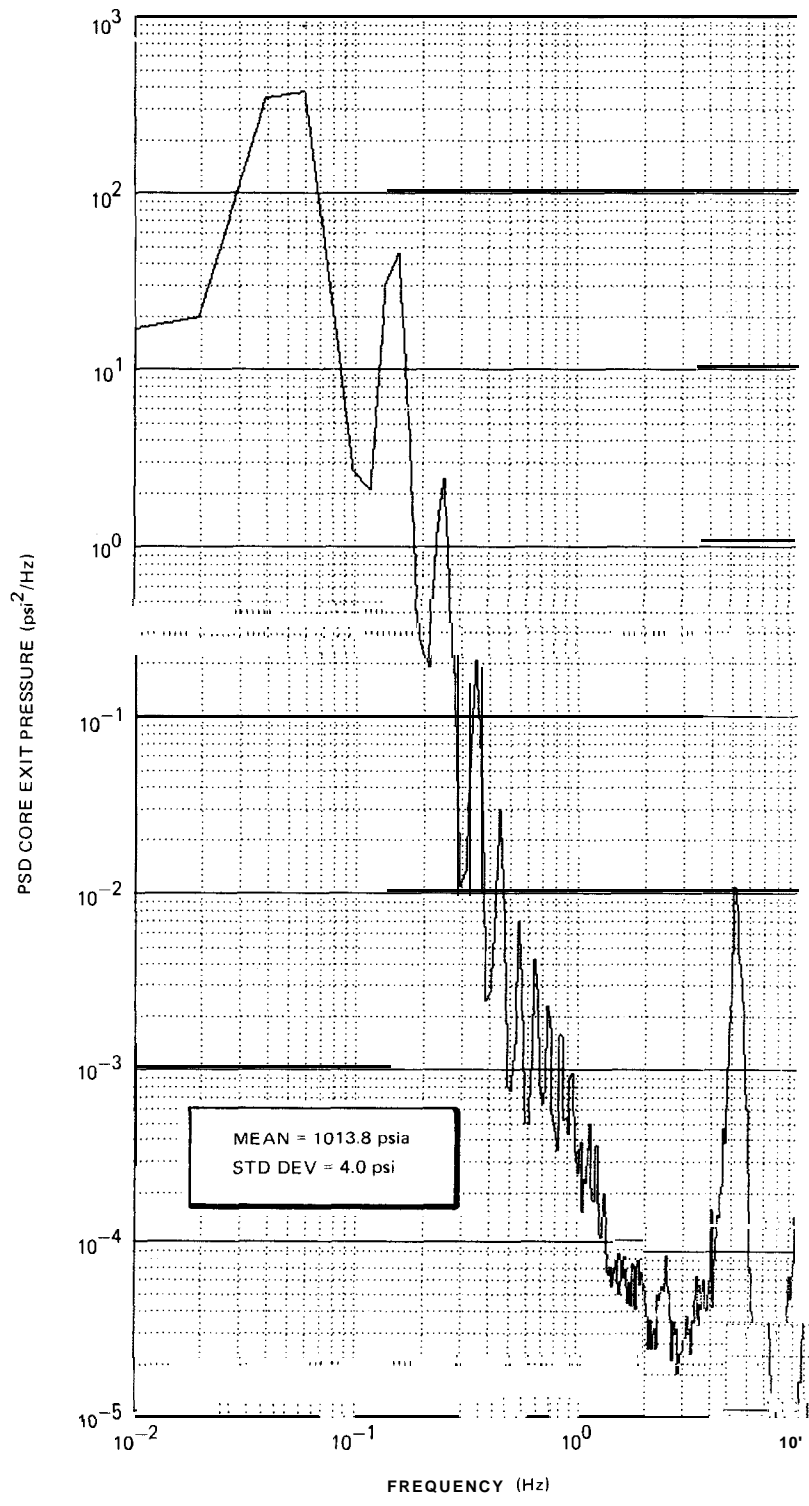


Figure 6-24. Power Spectrum Core Exit Pressure Periodic *Setpoint* Input

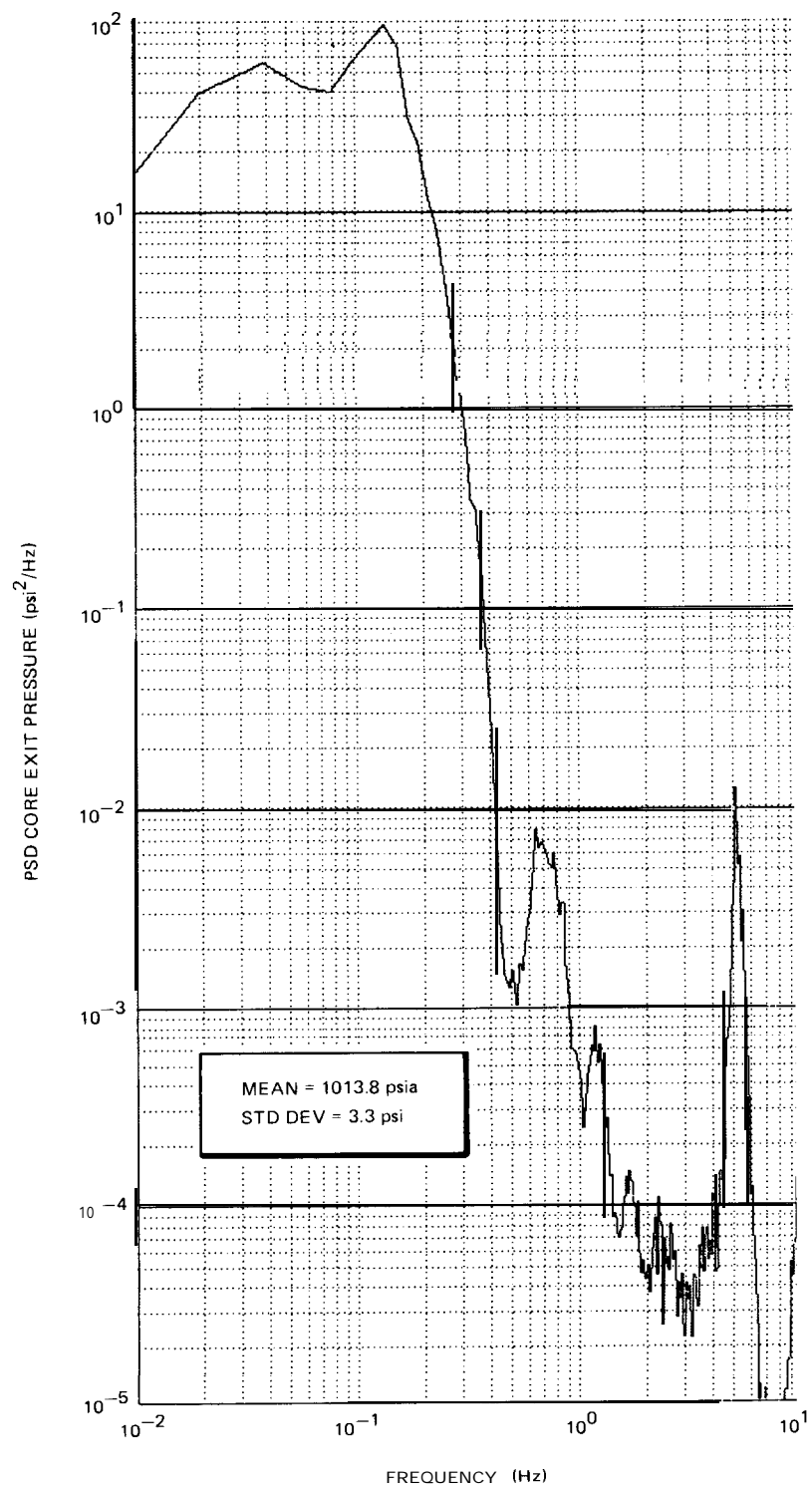


Figure 6-25. Power Spectrum Core Exit Pressure PRBS Setpoint Input

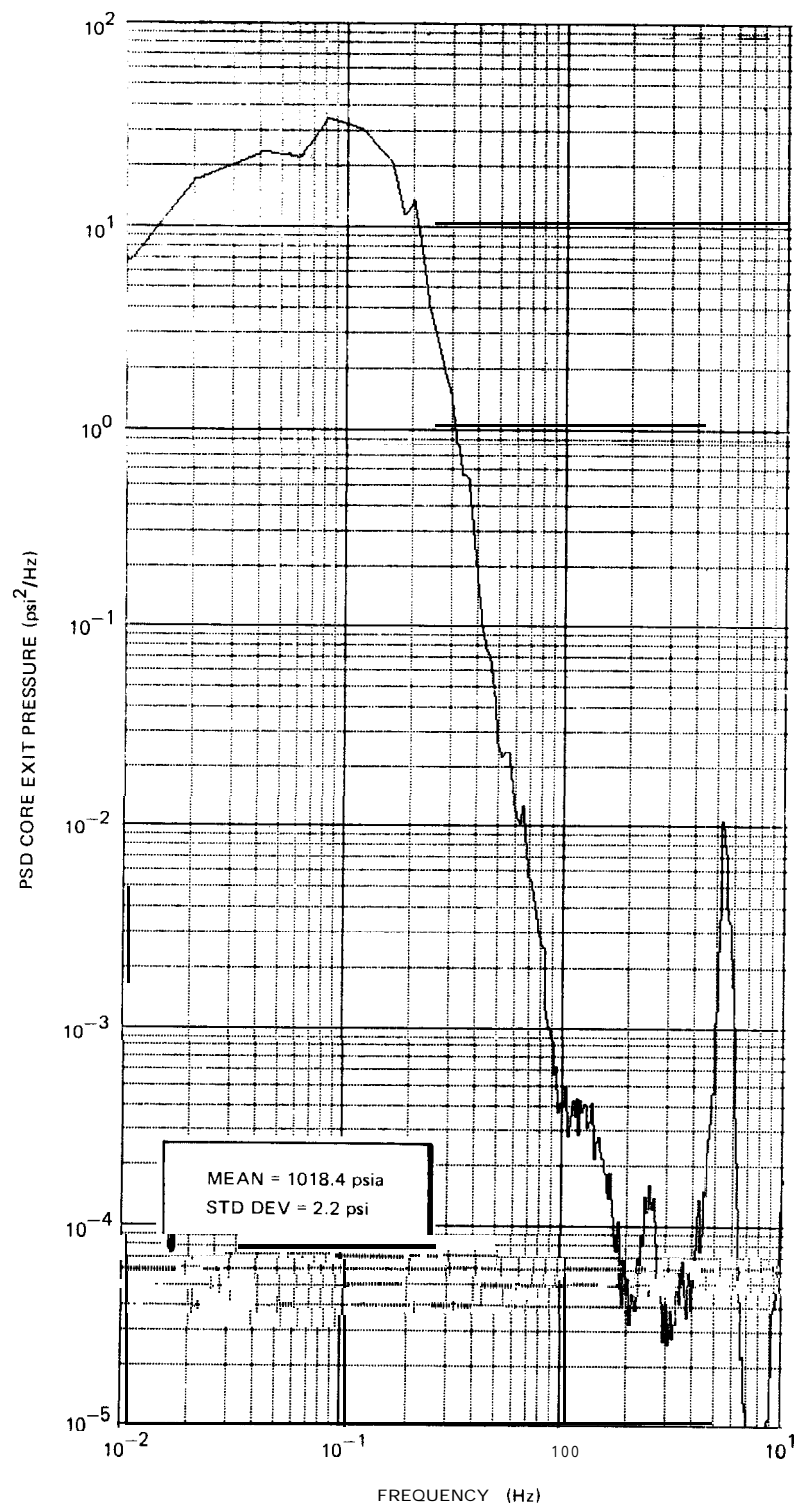


Figure 6-26. Peach Bottom-2 EOC2 Low-Flow Stability Test (PT3) Power Spectrum Core Exit Pressure

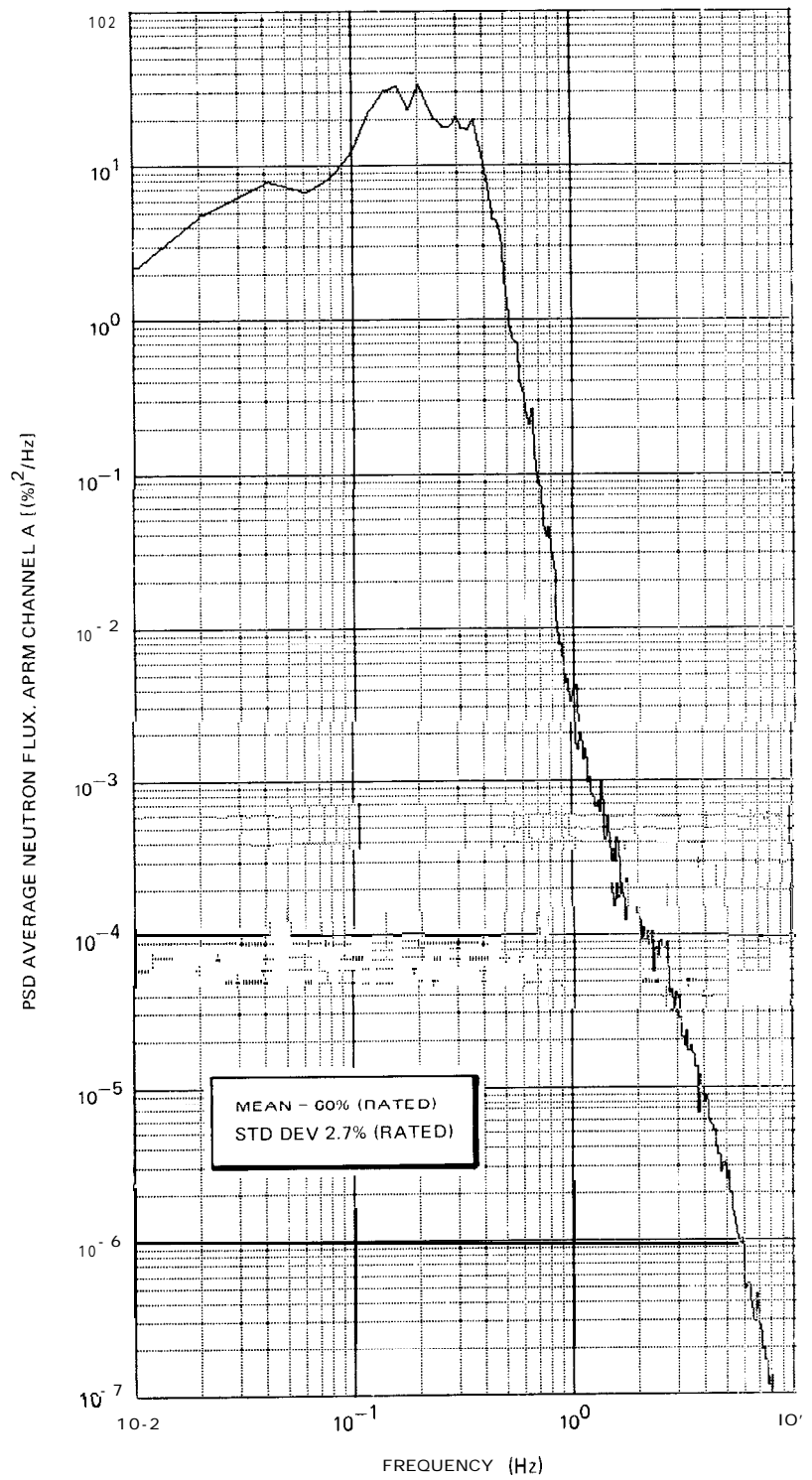


Figure 6-27. Peach Bottom-2 EOC2 Low-Flow Stability Test (PT3) Power Spectrum Average Neutron Flux (APRM A)

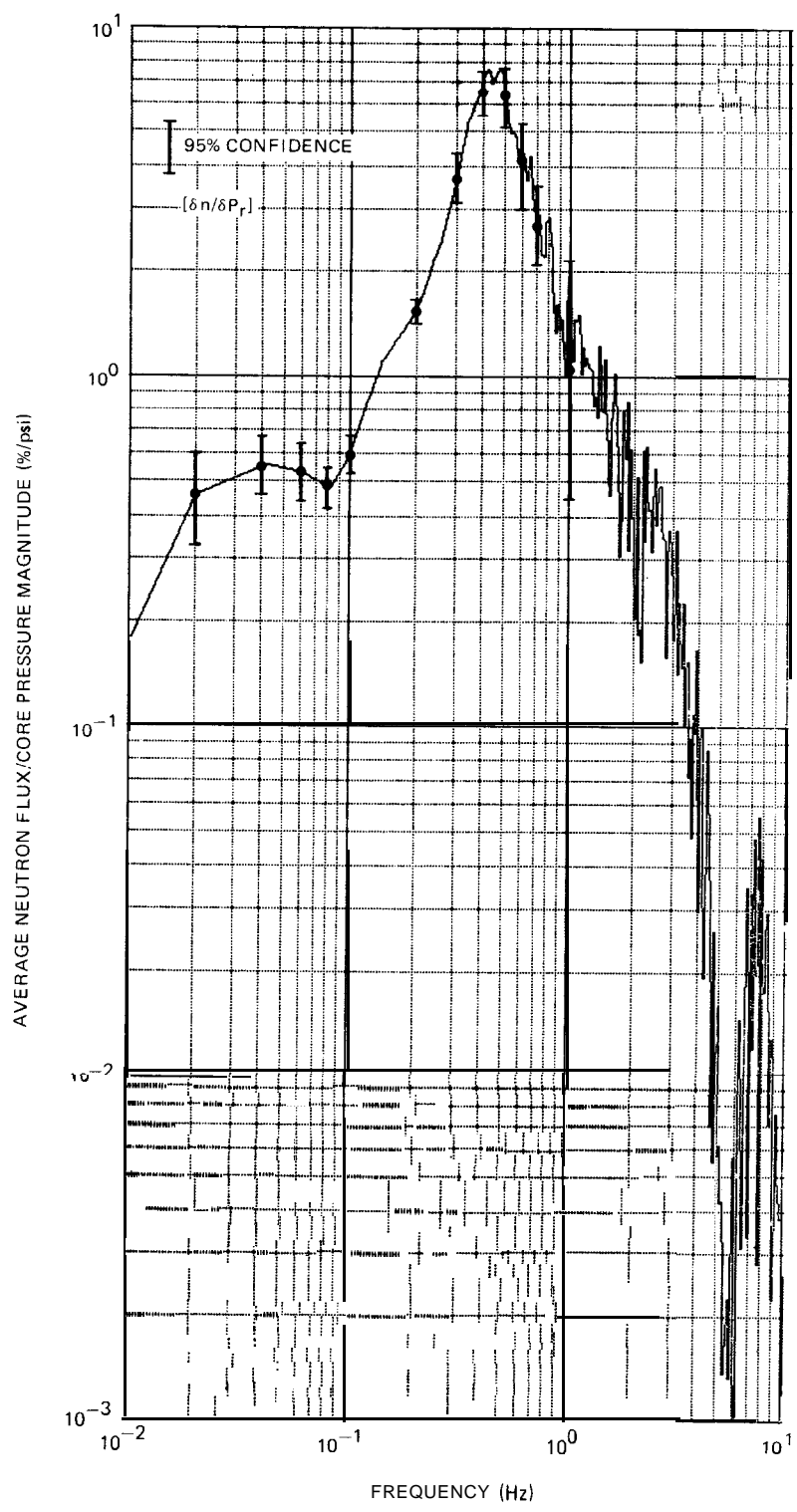


Figure 6-28. Peach Bottom-2 EOC2 Low-Flow Stability Test PT3 Measured Transfer Function Magnitude Average Neutron Flux (APRM A)/Core Pressure

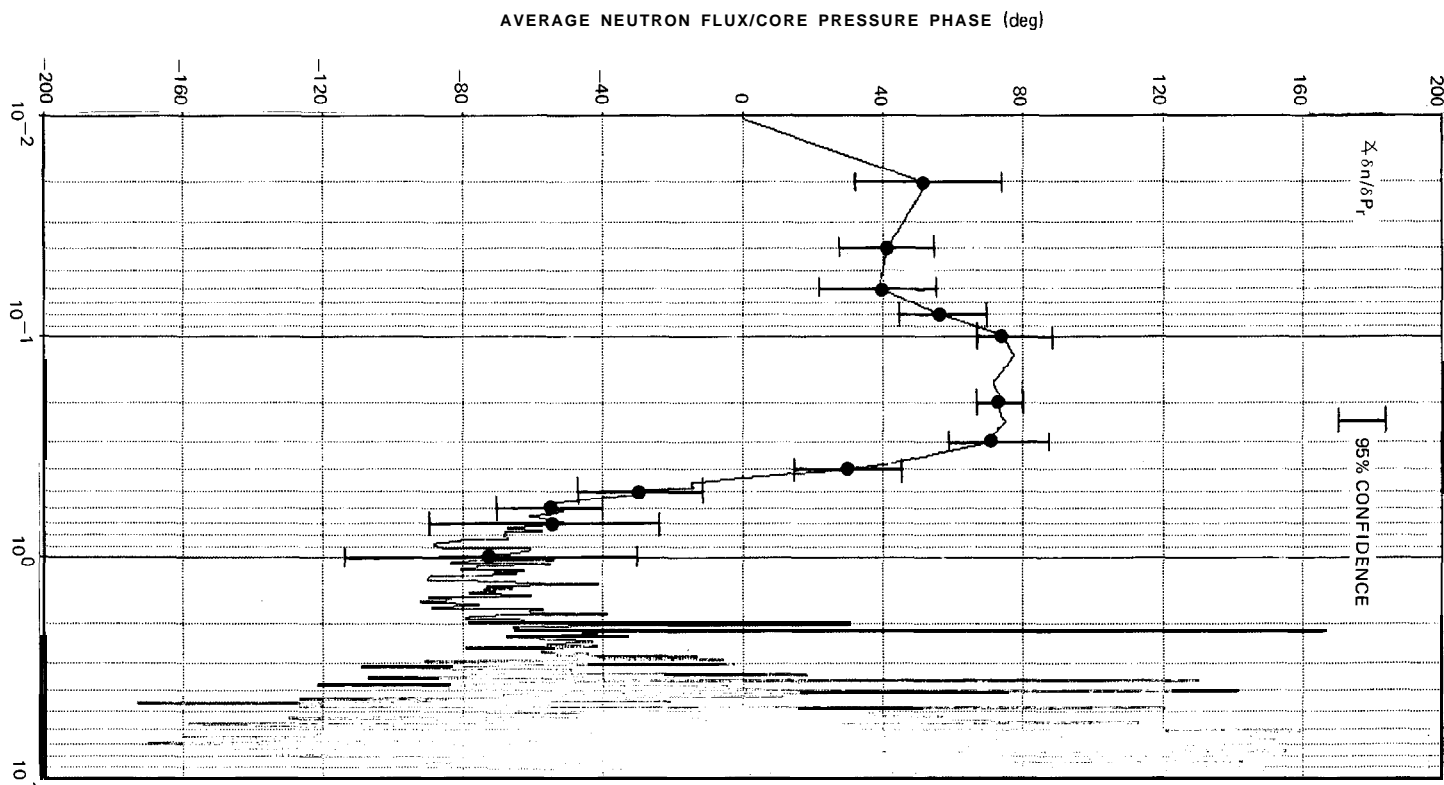


Figure 6-29. Peach Bottom-2 EOC2 Low-Flow Stability Test PT3 Measured Transfer Function Phase Average Neutron Flux (APRMA)/Core Pressure

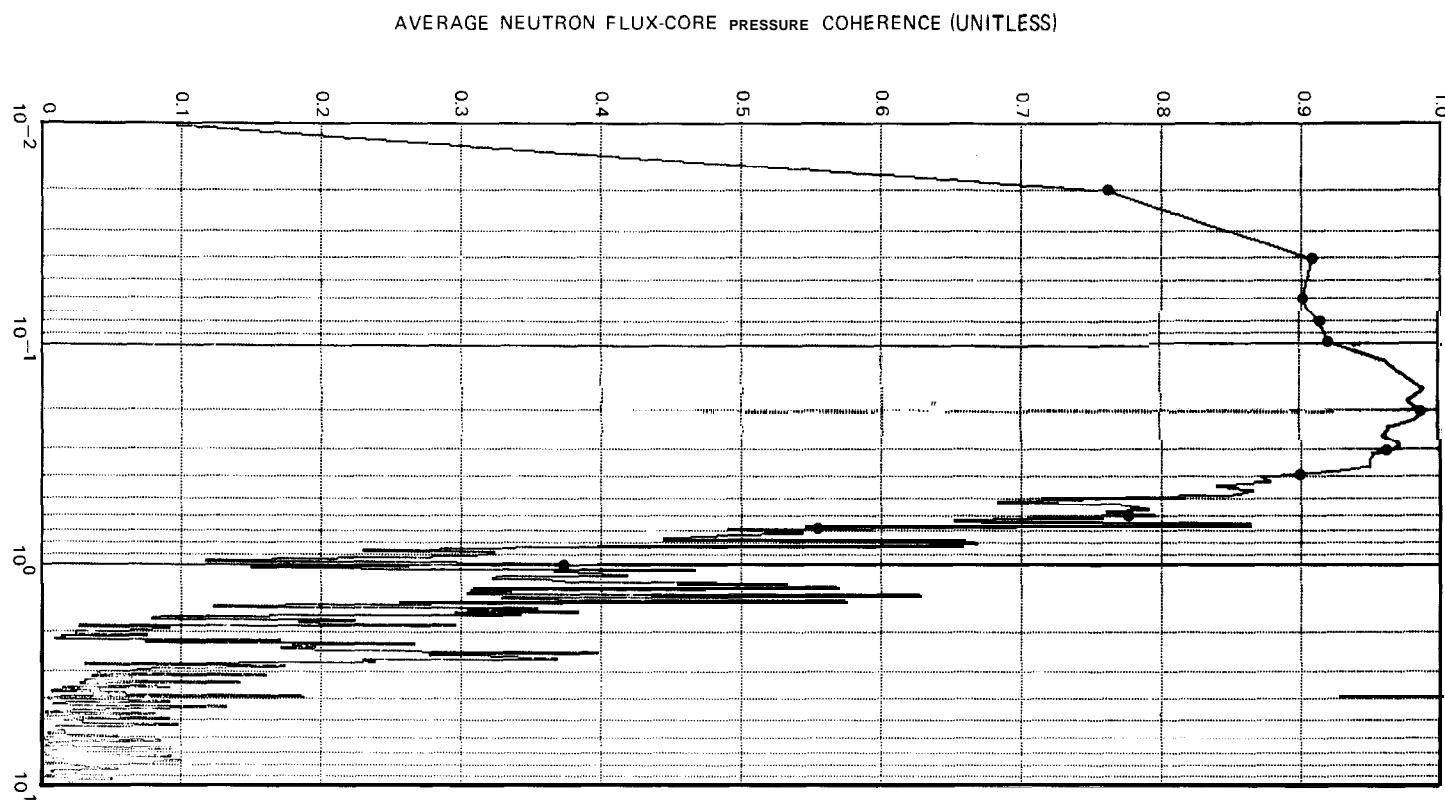


Figure 6-30. Peach Bottom-2 EOC2 Low Flow Stability Test (PT3) Coherence Between Average Neutron (APRM A) and Core Pressure Response

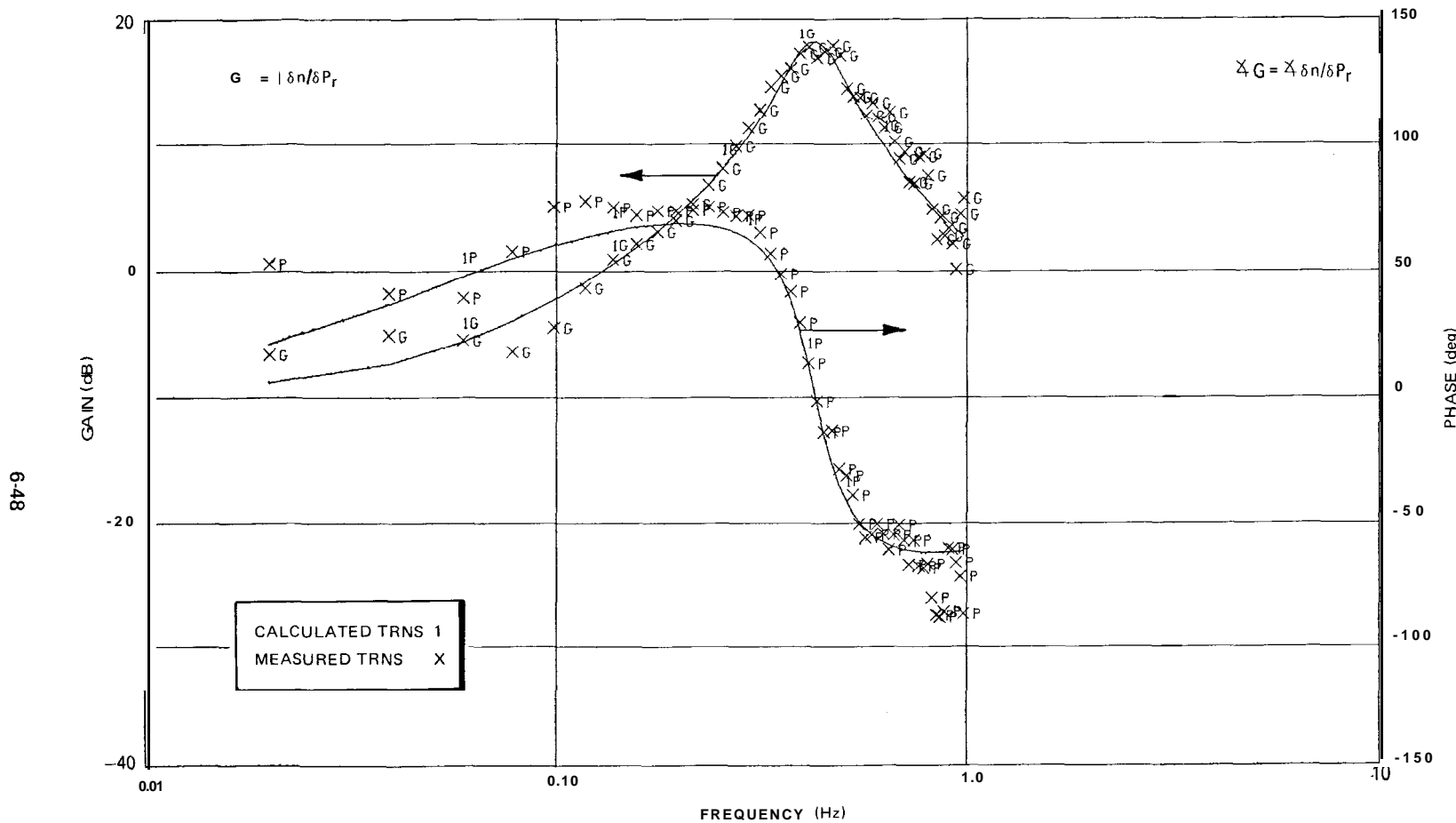


Figure 6-31. Peach Bottom-2 EOC2 Stability Test PT3 Transfer Function Model Comparison (1 Zero/2 Pole Model)

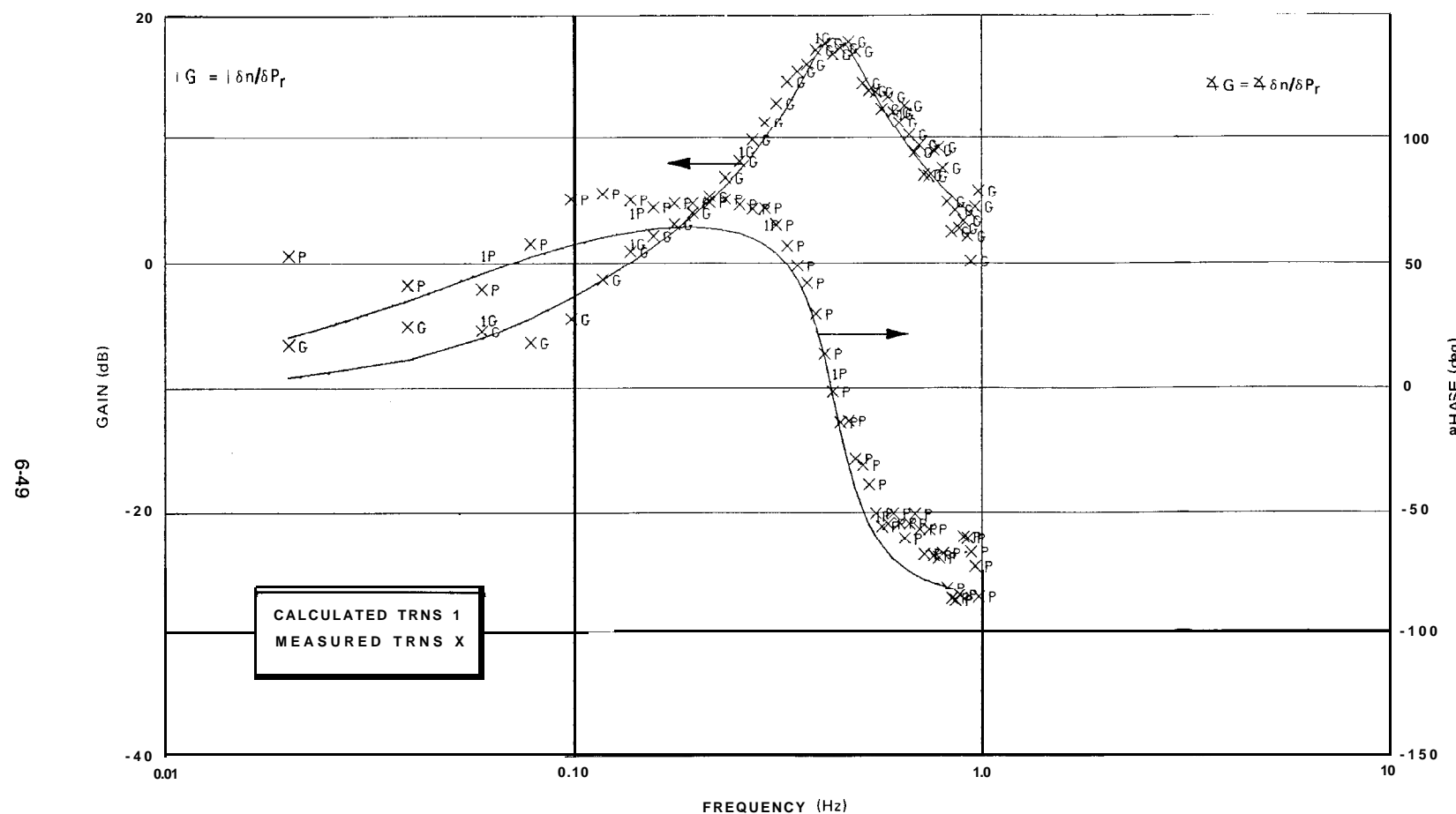


Figure 6-32. Peach Bottom-2 EOC2 Stability Test PT3 Transfer Function Model Comparison (1 Zero/3 Pole Model)

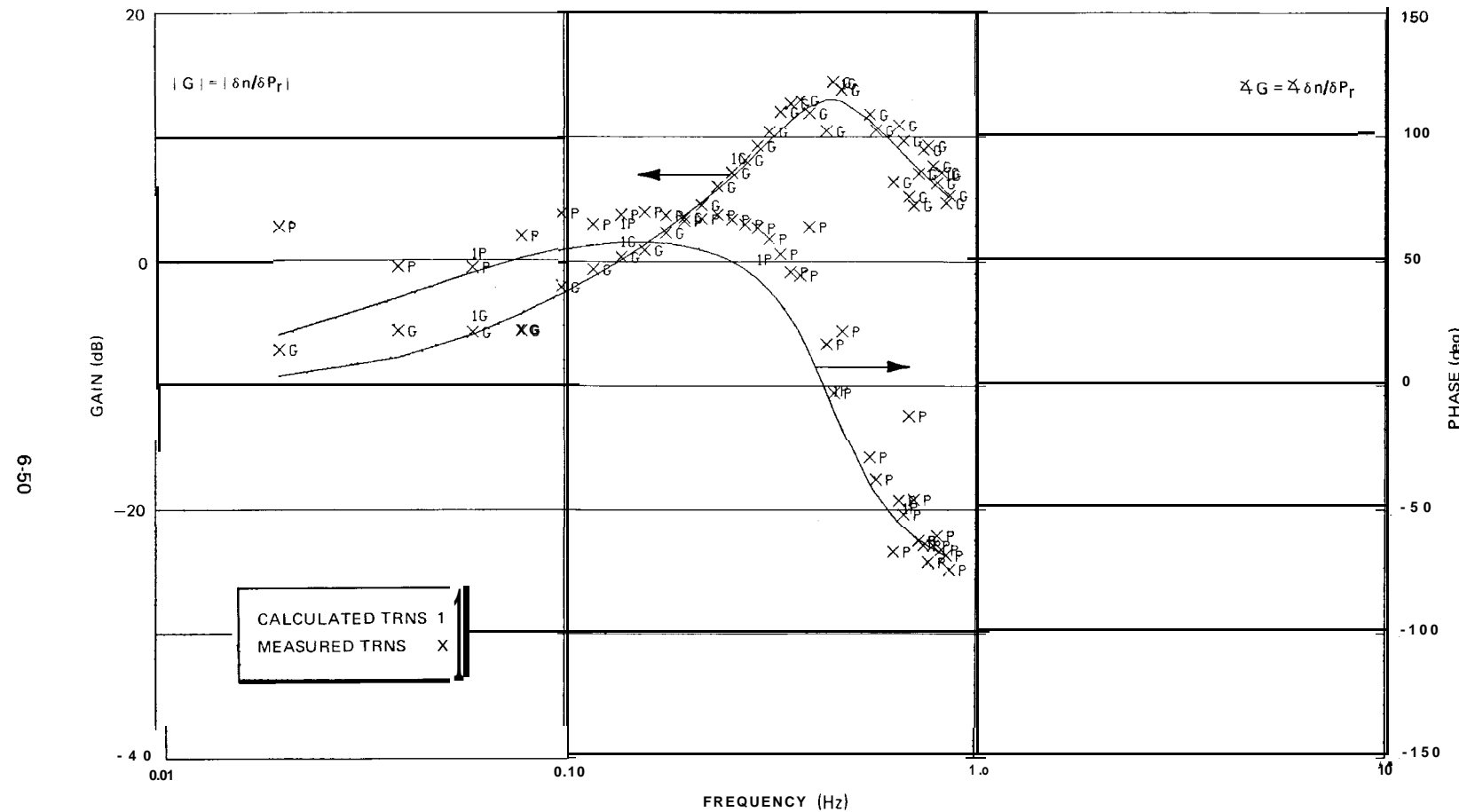


Figure 6-33. Peach Bottom-2 EOC2 Stability Test PT1 Transfer Function Model Comparison (1 Zero/2 Pole Model)

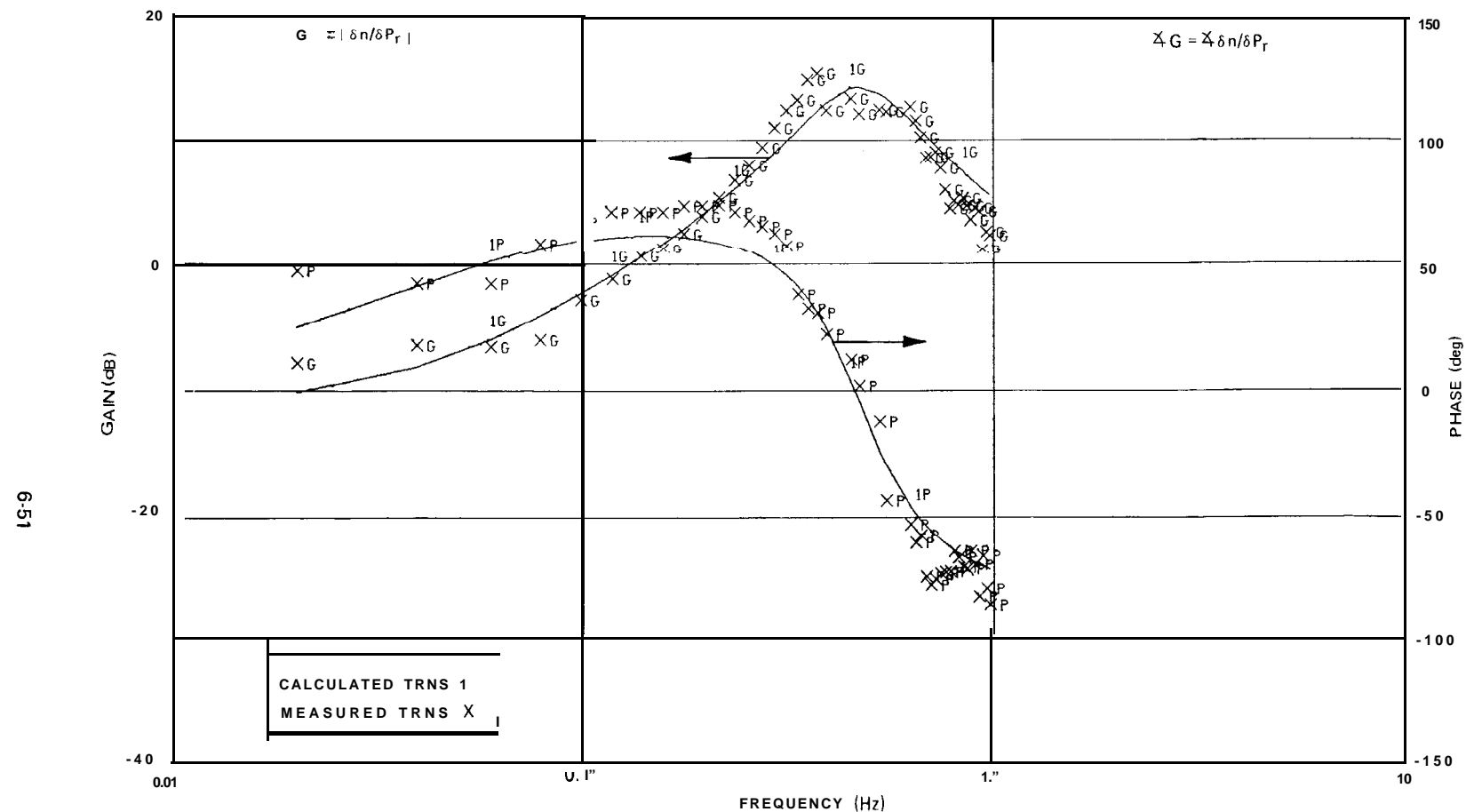


Figure 6-34. Peach Bottom-2 EOC2 Stability Test PT2 Transfer Function Model Comparison (1 Zero/2 Pole Model)

6-52

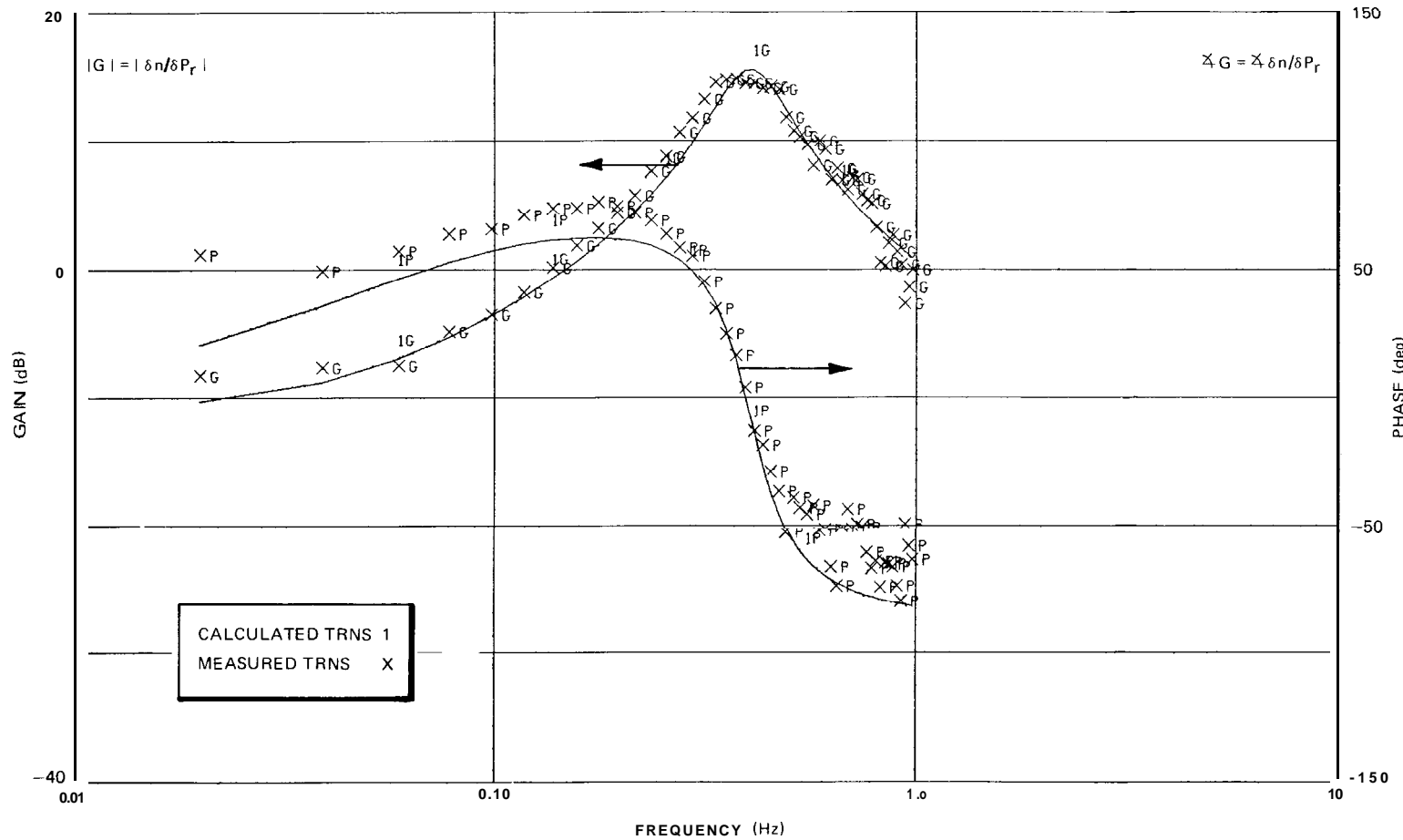


Figure 6-35. Peach Bottom EOC2 Low Flow Stability Test PT4 Transfer Function Model Comparison
(1 Zero/2 Pole Model)

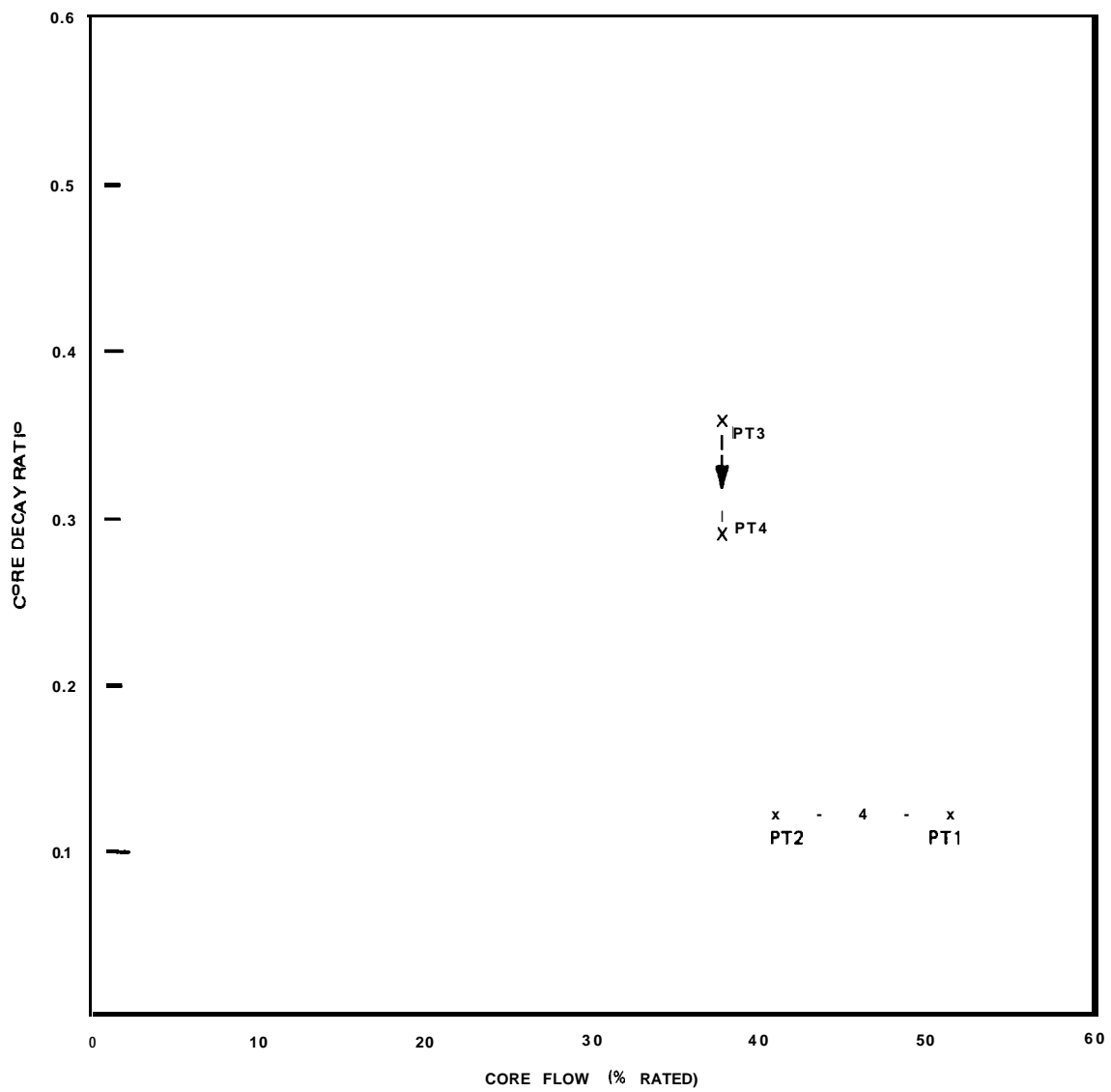


Figure 6-36. Peach Bottom-2 EOC2 Test Low Flow Stability Tests Core Stability Margin Versus Core Flow

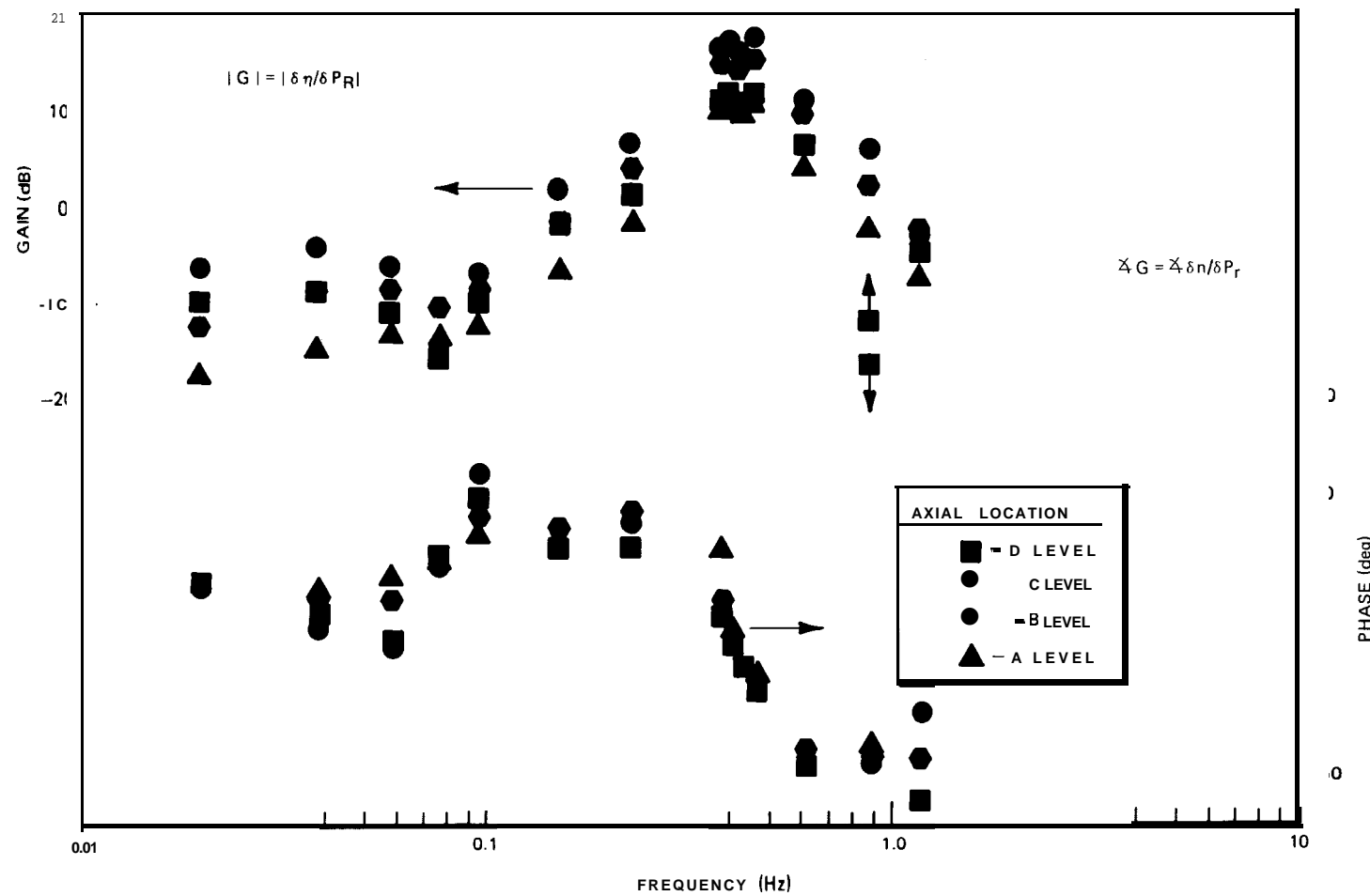


Figure 6-37. Peach Bottom-2 Low-Flow Stability Test PT3 Axial Local Flux Response (LPRM String 32-41)

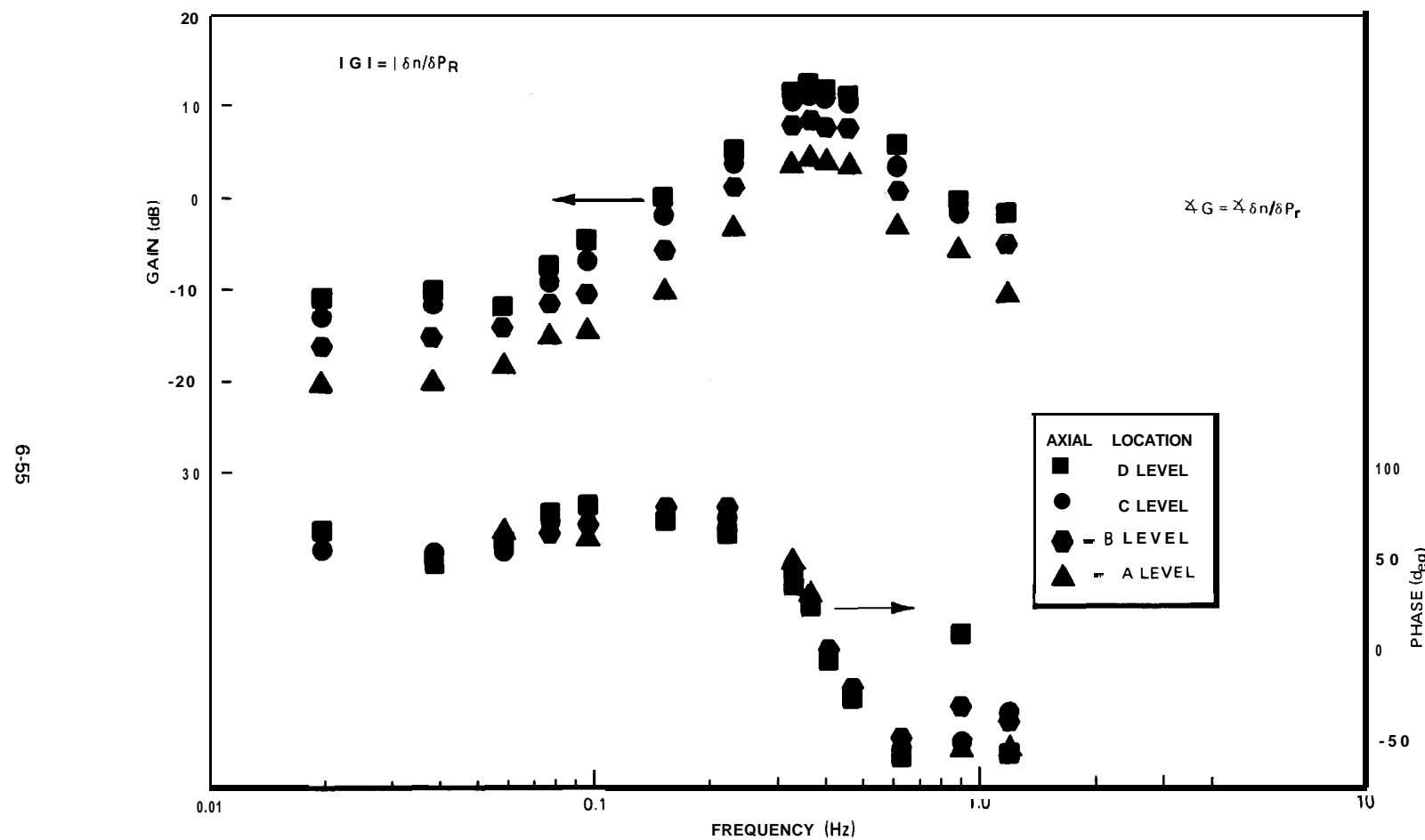


Figure 6-38. Peach Bottom-2 Low-Flow Stability Test PT4 Axial Local Flux Response (LPRM String 32-41)

7. REFERENCES

1. J. A. DeShong Jr., and W. C. Lipinski, *Analysis of Experimental Power-Reactivity Feedback Transfer Functions for a Natural Circulation Boiling Water Reactor*, Argonne National Laboratory, ANL-5850 (1958).
2. R. T. Lahey, Jr., C. L. Howard, M. J. Calcagno, E. Vincenti, and G. L. Santarossa, *Control Rod Oscillator Tests, Garigliano Nuclear Reactor*, General Electric Co., GEAP-5534 (1967).
3. R. O. Niemi, *Dresden-3 Rod Oscillator Tests*, General Electric Co., NEDM-13381 (1973).
4. *Proposed Peach Bottom Atomic Power Station Unit 2 Stability and Transient Test Program*. General Electric Licensing Report, NEDO-24003 (1977).
5. *General Electric Boiling Water Reactor Reload No. 1 License Amendment Submittal for Peach Bottom Atomic Power Station Unit2* NEDO-21172 (1976).
6. L. A. Carmichael and G. J. Scatena, *Stability and Dynamic Performance of the General Electric Boiling Water Reactor*, General Electric Co., APED-5652 (1969).
7. *Peach Bottom Atomic Power Station Units 2 and 3 Final Safety Analysis Report*, Philadelphia Electric Co
8. N. H. Larsen, *Core Design and Operating Data for Cycles 1 and 2 of Peach Bottom-Z*, Electric Power Research Institute, NP-563 (1978).
9. *Response to NRC Questions on G.E. Licensing Report, Proposed Peach Bottom Atomic Power Station Unit 2 Stability and Transient Test Program*, General Electric Co., NEDO-24003 (March 1977).
10. A. G. Webster, "Partial Differential Equations of Mathematical Physics," Dover Publications Inc. (1966).
11. H. G. Kwatny and L. H. Fink, "Acoustics, Stability, and Compensation in Boiling Water Reactor Pressure Control Systems," *IEEE Trans.* AC-20, No. 6 (December 1975).
12. ASME Steam Tables, "Thermodynamic and Transport Properties of Steam," (1967).
13. D'AZZO and Houpis, "Feedback Control System Analysis and Synthesis," McGraw-Hill (1960)
14. T. W. Kerlin, "Frequency Response Testing in Nuclear Reactors," Academic Press (1974)
15. P. A. Payne, "Automatic Control," *IEEE Trans.*, 15, 480
16. C. K. Sanathanan and Hideo Tsuke, "Int. J. Systems Science," 5, No. 4, pp 41-54 (1974)

APPENDIX A DATA REDUCTION METHODS

A.1 REACTOR TRANSFER FUNCTION IDENTIFICATION

The results of rod oscillator experimental stability measurements in a reactor core are usually reported in terms of a calculated open-loop transfer function.^{A-1, A-2} The block diagram representation of the reactor core reactivity feedback loops is shown in Figure A-1. If the forward-loop transfer function, $G_f(s)$, is assumed to be adequately modeled by the zero-power point kinetics transfer function,

$$G_f(s) = \left[\frac{\delta n/n_0}{\delta K_N} \right] = \frac{1}{s\Lambda + \beta - \sum_{i=1}^6 \frac{\lambda_i \beta_i}{s + \lambda_i}} \quad (A-1)$$

and since for a single-input, single-output system, the closed-loop response is given by,

$$G_c(s) = \left[\frac{\delta n/n_0}{\delta R_p} \right] = \frac{K_{cr} G_f(s)}{1 + G_f(s) H_{fb}(s)} \quad (A-2)$$

the reactivity feedback transfer function $H_{fb}(s)$ can be obtained from,

$$H_{fb}(s) = \left[\frac{1}{G_c(s)} - \frac{1}{G_f(s)} \right] \quad (A-3)$$

In the case of the boiling water reactor, $H_{fb}(s)$ is a parallel combination of the Doppler and void reactivity feedback paths, $[H_{fb1}(s) + H_{fb2}(s)]$. Since K_{cr} , the experimental rod reactivity to position calibration, is usually not well known, the results of rod oscillator experiments are normalized to high-frequency measurements. The approximation

$$G_c(s) \approx G_f(s) \quad (A-4)$$

when

$$\left| \frac{1}{G_f(s)} \right| \gg \left| H_{fb}(s) \right| \quad (A-5)$$

is used to find K_{cr} . For a boiling water reactor, this approximation is typically valid for frequencies greater than 2 Hz.

The reactor pressure to neutron flux closed-loop transfer function measurements must, however, be analyzed in a somewhat different manner. The original block diagram is modified in Figure A-2 to represent pressure disturbance input to the reactor power-to-reactivity feedback loop.* The closed-loop transfer function is now given by

$$G_c(s) = \left[\frac{\delta n/n_0}{\delta P_r} \right] = \frac{G_{fp}(s) G_f(s)}{1 + G_f(s) H_{fb}(s)} \quad (A-6)$$

*A potential feedback path between neutron flux and reactor pressure has been neglected. Its effect on the transfer function measurement is discussed later.

In this case, the gain between the reactor core pressure changes and the resulting void reactivity change, $G_{fp}(s)$, is itself an unknown transfer function. Therefore, a different technique for the determination of the BWR core stability margin must be found.

An accepted method for the identification of stable linear systems is one in which an empirical transfer function, $G_{CE}(s)$, is fitted to the magnitude and phase measurements of the system frequency response. As Grupe^{A-3} points out, the limitation to stable systems is not just a theoretical one, since no practical frequency response of unstable systems can be measured. The general empirical model described by Grupe is as follows:

$$G_{CE}(s) = \frac{a_m s^m + a_{m-1} s^{m-1} + \dots + a_0}{b_n s^n + b_{n-1} s^{n-1} + \dots + b_0} \quad (A-7)$$

or

$$G_{CE}(s) = \frac{K \prod_{i=1}^p (\tau_i s + 1) \cdot \prod_{j=1}^q (s^2/\omega_j^2 + 2\delta_j s/\omega_j + 1)}{s^r \cdot \prod_{k=1}^t (\tau_k s + 1) \cdot \prod_{\ell=1}^u (s^2/\omega_\ell^2 + 2\delta_\ell s/\omega_\ell + 1)} \quad (A-8)$$

where:

$p + 2q = m$ = order of the polynomial in numerator

$r + t + 2u = n$ = order of the polynomial in denominator

It is well known that the transfer function measurement of a linear system contains only information about the observable and controllable modes of a linear system, i.e., the modes of response that are excited by the input, e.g., core pressure, and those that are observable in the average neutron flux response. In the case of the boiling water reactor, analytical model investigations have shown that the fundamental underdamped mode of the reactor core reactivity feedback loop response is both observable in the average neutron flux measurement and excited by the input pressure disturbance.^{A-4} The results of the low-flow stability test transfer function measurements, which exhibit a well-defined resonant peak in the expected frequency range, 0.3-0.5 Hz, offer experimental verification of the analytical predictions.

Two empirical transfer function models were considered in the identification of the reactor transfer function. After observing the data, it was postulated that a transfer function having one real zero and two complex poles should adequately fit the measured transfer function between 0.02 and 1.0 Hz,

$$G_{CEI}(s) = \frac{K_p(\tau_1 s + 1)}{s^2/\omega_1^2 + 2\delta_1 s/\omega_1 + 1} \quad (A-9)$$

A higher order model,

$$G_{CEII}(s) = \frac{K_p(\tau_1 s + 1)}{(\tau_2 s + 1)(s^2/\omega_1^2 + 2\delta_1 s/\omega_1 + 1)} \quad (A-10)$$

was also tried to examine the effect of model order on the parameters which were identified.

The empirical models were fitted to the data by minimizing the sum of the phase and gain errors weighted by the uncertainty in their measurement (Reference A-5):

$$S(\bar{\alpha}) = \sum_{k=1}^N \left(\frac{M_{CM}^k - M_{CE}^k(\bar{\alpha})}{\sigma_M^k M_{CM}^k} \right)^2 + \sum_{k=1}^N \left(\frac{\theta_{CM}^k - \theta_{CE}^k(\bar{\alpha})}{\sigma_\theta^k \theta_{CM}^k} \right)^2 \quad (A-I 1)$$

where

N	=	the total number of frequency data points
M_{CM}^k (or θ_{CM}^k)	=	the magnitude (or phase) of the measured closed-loop transfer function at the k th frequency
M_{CE}^k (or θ_{CE}^k)	=	the magnitude (or phase) of the calculated closed-loop transfer function at the k th frequency
σ_M^k (or σ_θ^k)	=	the standard deviation in the magnitude (or phase) measurement at the k th frequency
$\bar{\alpha}$	=	a vector of the unknown parameters to be identified in the transfer function model.

The least-squares curve fit was accomplished using Powell's method for minimizing the sum of squares of nonlinear functions without calculating the derivatives. A-6 The version of the computer program used for these calculations is described in Reference A-7.

If the noise vector, $\bar{n}_k^T = [n_M^k, n_\theta^k]^T$, in the gain and phase measurements is assumed to have a Gaussian distribution,* the probability distribution of the measured transfer function at a single frequency can be written as A-8

$$P[\bar{Z}_M^k | \bar{\alpha}] = \frac{1}{2\pi|R|^{1/2}} \exp \left[-\frac{1}{2} (\bar{Z}_M^k - \bar{Z}_C^k)^T R^{-1} (\bar{Z}_M^k - \bar{Z}_C^k) \right] \quad (A-12)$$

where

$R = E \left\{ \bar{n}_k \bar{n}_k^T \right\}$	= measurement error covariance matrix
\bar{Z}_M^k (or \bar{Z}_C^k)	= measured (or calculated) vector containing magnitude and phase at k th frequency,

*In the next section the gain and phase errors are shown to be distributed with a Fischer's F distribution. However, for a large number of samples averaged this assumption is approximately correct.

If the values of \bar{n}_k are taken as independent at each frequency, then the probability of the entire set of measured responses, \bar{Z}_M) can be written as,

$$P[\bar{Z}_M/\bar{\alpha}] = \frac{1}{(2\pi)^N |R|^{N/2}} \exp \left[-\frac{1}{2} \sum_{k=1}^N (\bar{Z}_M^k - \bar{Z}_C^k)^T R^{-1} (\bar{Z}_M^k - \bar{Z}_C^k) \right] \quad (A-13)$$

Maximizing $P[\bar{Z}_M/\bar{\alpha}]$ is accomplished by minimizing the exponent for the unknown parameter set $\bar{\alpha}$. The value of $\bar{\alpha}$ which maximizes $P[\bar{Z}_M/\bar{\alpha}]$ also minimizes $S(\bar{\alpha})$ in Equation A-I 1. It can be shown that the error covariance matrix of the parameter estimates, $\bar{\alpha}^*$, can be estimated from A-9,

$$E \left[(\bar{\alpha}^* - \bar{\alpha}_{\text{true}})(\bar{\alpha}^* - \bar{\alpha}_{\text{true}})^T \right] = \left[\sum_{k=1}^N \left(\frac{d\bar{Z}_C^k}{d\bar{\alpha}} \right)^T R^{-1} \left(\frac{d\bar{Z}_C^k}{d\bar{\alpha}} \right) \right]^{-1} \quad (A-14)$$

The decay ratio of the dominant complex poles of the reactor closed-loop transfer function can be calculated from the roots of the quadratic term in the denominator of the fitted transfer function model. The complex roots are

$$s_{1,2} = -\alpha \pm j\beta \quad (A-15)$$

or

$$s_{1,2} = -\omega_1 \pm j\omega_1 \sqrt{1 - \delta_1^2} \quad (A-I 6)$$

from which the decay ratio is calculated

$$\delta_1 = \left[\frac{(\alpha/\beta)^2}{1 + (\alpha/\beta)^2} \right]^{1/2} \quad \text{for } \beta > 0 \quad (A-I 7)$$

and the natural logarithm of the decay ratio by,

$$\ln DR = -2\pi\delta_1 \sqrt{1 - \delta_1^2} \quad (A-18)$$

for $\delta_1 < 1$.

The uncertainty in the decay ratio estimate is related to the error covariance in the transfer function model parameter estimates by considering a Taylor series expansion of $DR(\alpha_1^*, \alpha_2^*, \dots, \alpha_M^*)$ about the point $(\alpha_1, \alpha_2, \dots, \alpha_M)_{\text{true}}$. To first order,

$$DR(\alpha_1^*, \alpha_2^*, \dots, \alpha_M^*) \approx DR(\alpha_1, \alpha_2, \dots, \alpha_M)_{\text{true}} + \sum_{i=1}^M \left(\frac{\partial DR}{\partial \alpha_i} \right)_{\bar{\alpha}_{\text{true}}} (\alpha_i^* - \alpha_{\text{true},i}) \quad (A-19)$$

*In nonlinear regression analysis, it may be that the bias errors are considerably larger than the statistical error estimates from this analysis.^{A-9}

The variance of DR is related to the covariance of the α_i^* estimates by

$$E[(DR^* - DR_{\text{true}})^2] \approx \sum_{i=1}^M \sum_{j=1}^M \left(\frac{\partial DR}{\partial \alpha_i} \right) \left(\frac{\partial DR}{\partial \alpha_j} \right)_{\bar{\alpha}_{\text{true}}} E[(\alpha_i^* - \alpha_{i,\text{true}})(\alpha_j^* - \alpha_{j,\text{true}})] \quad (\text{A-20})$$

or, in matrix notation,

$$E[(DR^* - DR_{\text{true}})^2] = (\nabla_{\bar{\alpha}_{\text{true}}} DR)^T M_{\bar{\alpha}} (\nabla_{\bar{\alpha}_{\text{true}}} DR) \quad (\text{A-21})$$

where

$$M_{\bar{\alpha}} = E[(\bar{\alpha}^* - \bar{\alpha}_{\text{true}})(\bar{\alpha}^* - \bar{\alpha}_{\text{true}})^T] \quad (\text{A-22})$$

A.2 TRANSFER FUNCTION CALCULATION

The neutron flux to pressure transfer functions were estimated from the data using the Fast Fourier Transform (FFT) algorithm of Cooley and Tukey.^{A-10} A finite series of data (x_k and y_k ; $k = 0, 1, \dots, N - 1$) was constructed by sampling the pressure and neutron flux signals at a constant sampling frequency, ($f_s = 1/\Delta t$ Hz), consistent with the aliasing requirements of the data acquisition system input filtering.* The spectral functions of the time series were calculated as follows:

1. The mean is calculated and subtracted from each time sample,

$$\tilde{x}_k = x_k - \bar{x}_k \quad (\text{A-23})$$

$$\tilde{y}_k = y_k - \hat{y}_k$$

where

$$\hat{x}_k = \frac{1}{N} \sum_{k=0}^{N-1} x_k \quad (\text{A-24})$$

$$\hat{y}_k = \frac{1}{N} \sum_{k=0}^{N-1} y_k$$

*The data was taken at a 5 millisecond sampling rate. To improve the low frequency resolution in the transfer function calculation the digital data was decimated by a factor of 10 after multiple passes through a second-order Butterworth digital filter ($f_C = 5$ Hz) to prevent aliasing.

2. Both time series are then multiplied by a Taper function, g_k , to reduce side-lobe leakage.

$$g_k = \begin{cases} \frac{1}{2} \left[1 - \cos\left(\frac{2\pi k}{N}\right) \right], & 0 \leq k < N/2 \\ 1, & k = N/2 \\ \frac{1}{2} \left[1 - \cos\left(\frac{2\pi(N-k)}{N}\right) \right], & N/2 < k \leq N-1 \end{cases} \quad (A-25)$$

generating the new time series,

$$\bar{x}_k = g_k \cdot \tilde{x}_k \quad (A-26)$$

and

$$\bar{y}_k = g_k \cdot \tilde{y}_k$$

3. The finite discrete Fourier transforms,

$$X(f_\ell) = At \sum_{k=0}^{N-1} \bar{x}_k W^{\ell k} \quad \text{for } \ell = 0, 1, \dots, N-1 \quad (A-27)$$

and

$$Y(f_\ell) = At \sum_{k=0}^{N-1} \bar{y}_k W^{\ell k} \quad (A-28)$$

where,

$$W^{\ell k} = \exp \left[-j2\pi \frac{k}{N} \right] \quad (A-29)$$

and

$$f_\ell = \ell/N\Delta t \text{ Hz},$$

of the time series were calculated, with the particular version of the Cooley-Tukey FFT algorithm described in Reference A-I 1.

4. Estimates of the power and cross-power spectral density functions are obtained from

$$\tilde{S}_{xy}(f_\ell) = \frac{2C_B}{N\Delta t} X^*(f_\ell) Y(f_\ell) \quad (A-30)$$

^tC_B is a bias compensation factor, dependent on sum of g_k squared. For the full cosine Taper data window, C_B = 8/3.^{A-12}

and

$$\begin{aligned}\tilde{S}_{xx}(f_\ell) &= \frac{2C_B}{N\Delta t} |X(f_\ell)|^2 \\ (A-31)\end{aligned}$$

$$\tilde{S}_{yy}(f_\ell) = \frac{2C_B}{N\Delta t} |Y(f_\ell)|^2$$

5. The unsmoothed spectral estimates, defined above, are known to be inconsistent estimates of the power spectral functions since increasing the length of the data sequence has no effect on the random errors in the power spectrum estimates. The statistical stability in the power spectral density estimates is achieved through segmenting the data series into M segments of N samples each, and smoothing the estimates through ensemble averaging of the M raw estimates,^{A-13}

$$\hat{S}_{xy}(f_\ell) = \frac{1}{M} \sum_{k=1}^M \tilde{S}_{xy}^k(f_\ell) \quad (A-32)$$

and

$$\hat{S}_{xx}(f_\ell) = \frac{1}{M} \sum_{k=1}^M \tilde{S}_{xx}^k(f_\ell) \quad (A-33)$$

$$\hat{S}_{yy}(f_\ell) = \frac{1}{M} \sum_{k=1}^M \tilde{S}_{yy}^k(f_\ell)$$

6. An estimate of the pressure to neutron flux closed-loop transfer function, $\hat{G}_c(f_\ell)$, can be defined from the ratio of the smoothed cross-power and power spectral density functions,*

$$\hat{G}_c(f_\ell) = \frac{\hat{S}_{xy}(f_\ell)}{\hat{S}_{xx}(f_\ell)} \quad (A-34)$$

7. The estimate of the squared-ordinary coherence between the pressure and neutron flux signals can be defined as

$$\hat{\gamma}_{xy}^2(f_\ell) = \frac{|\hat{S}_{xy}(f_\ell)|^2}{\hat{S}_{xx}(f_\ell)\hat{S}_{yy}(f_\ell)} \quad (A-35)$$

*There are several other ways in which the transfer function can be defined. A-13 However, Equation A-34 can be shown to be the best least-squares estimate.

which implies that,

$$0 \leq \hat{\gamma}_{xy}^2(f_\ell) \leq 1 \quad (\text{A-36})$$

A coherence value less than unity indicates a lack of complete linear dependence of the output $y(t)$ on the input $x(t)$. This may be due to the presence of extraneous noise in $y(t)$, not related to $x(t)$, or due to the fact that the system behaves somewhat nonlinearly. Notice that if the coherence is calculated from the unsmoothed estimates, S_{xy} , \hat{S}_{xx} , and \hat{S}_{yy} , then the result can be shown always to be unity (see page 330 of Reference A-13), which is a highly biased estimator of $\gamma_{xy}^2(f_\ell)$.

Approximate confidence intervals for the transfer function, gain, and phase estimates can be derived, based on a Gaussian signal assumption* and unbiased estimates, from consideration of the frequency response measurements as a least-squares regression analysis at each frequency [see Jenkins and Watts, Section 10.3 (Reference A-14)]. The $(1 - \alpha)\%$ confidence regions for,

$$\hat{G}_c(f_\ell) = \hat{M}_c^\ell e^{-j\hat{\theta}_c^\ell} \quad (\text{A-37})$$

at a specified frequency f_ℓ , can be written,

$$\hat{M}_c^\ell - \Delta M_c^\ell \leq M_{c,\text{true}}^\ell \leq \hat{M}_c^\ell + \Delta M_c^\ell \quad (\text{A-38})$$

$$\hat{\theta}_c^\ell - \Delta \theta_c^\ell \leq \theta_{c,\text{true}}^\ell \leq \hat{\theta}_c^\ell + \Delta \theta_c^\ell$$

and

$$(AM_c^\ell)^2 = \left(\frac{2}{v_{DF} - 2} \right) (F_{2, v_{DF} - 2; \alpha}) \left(\frac{1 - \hat{\gamma}_{xy}^2(f_\ell)}{\hat{\gamma}_{xy}^2(f_\ell)} \right) \hat{M}_c^\ell \quad (\text{A-39})$$

$$\Delta \theta_c^\ell = \sin^{-1} \left(\frac{\Delta M_c^\ell}{\hat{M}_c^\ell} \right)$$

where

$$v_{DF} = \text{number of degrees of freedom in each spectral estimate}$$

$$F_{2, v_{DF} - 2; \alpha} = 100\alpha \text{ percentage points of Fischer's F distribution with } v_{DF} - 2 \text{ degrees of freedom.}$$

It can be shown that the individual spectral or cross-spectral estimates are approximately distributed as χ^2 random deviates with two degrees of freedom.^{A-13} Averaging M spectral estimates at each frequency gives approximately $2M$ degrees of freedom in the estimates. However, the full cosine tapering of the time series has the effect of reducing the effective length of the series by $1/2$.^{A-12} Hence, the combined effect of the cosine tapering and averaging of the raw spectral estimates is to leave approximately M degrees of freedom in each spectral estimate.^{**} Therefore,

$$v_{DF} - 2 = M - 2 \quad (\text{A-40})$$

*The Gaussian signal assumption is violated for the PRBS or square-wave test signal input, so uncertainty estimates are only qualitative.

**For the test conditions PT2, PT3, and PT4, $M = 29$ raw spectra were averaged. For test PT1, $M = 41$. See Figures 6-8 and 6-9, and Figures E-3, E-4, E-8, E-9, E-13, and E-14 for error estimates.

Bendat^{A-15} suggests possible sources of bias involved in the transfer function estimates. The most important are:

1. Bias in the power and cross-power spectral estimates used to calculate the transfer function.
2. Measurement noise in the input signal $x(t)$ (output signal measurement noise does not cause bias).
3. Additional input noise sources which are correlated with $x(t)$.

The spectral estimator derived by averaging M raw spectra can be shown to be equivalent to smoothing the raw spectrum by the Bartlett spectral window (see Jenkins and Watts, A-14, Section 6.3). The bias associated with this window is given by

$$B_B(f) \simeq \frac{1}{N\Delta t} \int_{-\infty}^{\infty} |u| C_{zz}(u) e^{-2\pi j f u} du \quad (A-41)$$

where

$C_{zz}(u)$ = the autocovariance function of the signal analyzed

Assuming that the autocovariance function of the core pressure and neutron flux signals* can be approximated by,

$$C_{zz}(u) = \sigma_{zz}^2 e^{-|u|/T} \quad (A-42)$$

which gives,

$$B_B(f) < \frac{2\sigma_{zz}^2 T^2}{N\Delta t} \quad (A-43)$$

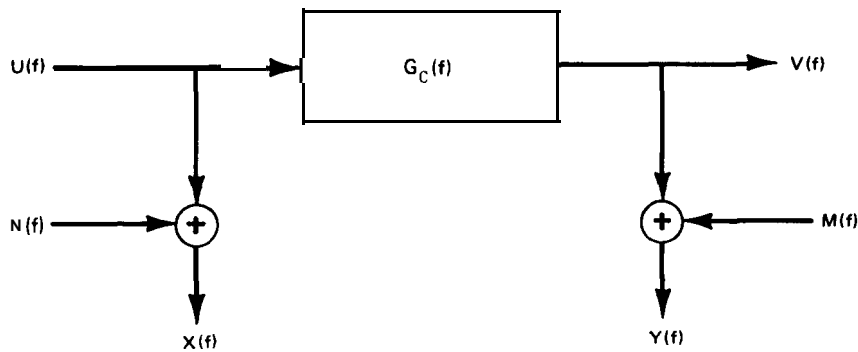
The time series data was decimated to give 50 seconds of data for each spectral estimate. The maximum bias in the pressure and neutron flux signals is estimated to be

Signal	σ_{zz}	$1/T$	Maximum Bias
Core Pressure	2.2 psi	2.5 sec^{-1}	-0.02 psi
Neutron Flux (APRM A)	2.5%	0.94	-0.15%

Either bias term contributes about 1% error to the transfer function gain near the resonant peak of the transfer function measurement. Since their polarity is the same, the total error in gain will be somewhat smaller. This error is therefore small relative to the random errors in the transfer function measurements.

*See Figures 6-26 and 6-27 for example

The effects of measurement noise have been shown by Bendat.^{A-15}



Since the measurement noise terms $n(t)$ and $m(t)$ are assumed to be uncorrelated with $u(t)$ and $v(t)$ respectively,

$$\begin{aligned} S_{xx}(f) &= S_{uu}(f) + S_{nn}(f) \\ S_{yy}(f) &= S_{vv}(f) + S_{mm}(f) \end{aligned} \quad (\text{A-44})$$

and

$$S_{xy}(f) = S_{uv}(f) \quad (\text{A-45})$$

The coherence, $\gamma_{xy}^2(f)$, can be shown to be

$$\gamma_{xy}^2(f) = \frac{1}{1 + (N_1/S_1) + (N_2/S_2) + (N_1/S_1)(N_2/S_2)} < 1 \quad (\text{A-46})$$

where

$$\begin{aligned} N_1 &= S_{nn}(f) & S_1 &= S_{uu}(f) \\ N_2 &= S_{mm}(f) & S_2 &= S_{vv}(f) \end{aligned} \quad (\text{A-47})$$

which is reduced by the noise in the input and output signals. The magnitude of the estimated transfer function, $|G_c(f)|$, is related to that of the true transfer function by,

$$|\hat{G}_c(f)| = \frac{|S_{xy}(f)|}{S_{xx}(f)} = \frac{|S_{uy}(f)|}{S_{nn}(f) + S_{nn}(f)} = \frac{|G_c(f)|}{|1 + S_{nn}(f)/S_{uu}(f)|} \quad (\text{A-48})$$

Hence the effect of the measurement noise in the input signal is to bias the magnitude of the estimated transfer function below that of the true transfer function.* To estimate the magnitude of the error caused by measurement noise,

*The measurement noise in the output signal has no effect on the transfer function measurement since $m(t)$ is assumed uncorrelated with $x(t)$.

the spectrum of the steady-state noise in the core exit pressure was measured for test condition PT3. The standard deviation in the steady-state pressure signal noise was found to be 0.113 psi. Assuming conservatively that the noise is band limited below 0.5 Hz,

$$S_{nn}(f) \simeq (0.113)^2 / 0.5 = 0.026 \text{ psi}^2/\text{Hz}. \quad (\text{A-49})$$

The standard deviation of the PRBS test input signal is 2.2 psi, and its spectrum is approximately the same shape as that of the steady-state noise between 0.1 and 0.5 Hz. Hence,

$$S_{nn}(f)/S_{uu}(f) \simeq 0.003 \quad (\text{A-50})$$

Thus, the bias in the transfer function magnitude estimate $\hat{G}_c(f)$, is approximately 0.003 due to the measurement noise in the input signal, $x(t)$, not correlated with the output $v(t)$.

Chatfield^{A-16} gives the expression for the bias in the transfer function measurement, caused by uncorrelated noise in the process output, $V(f)$, which affects the process input $U(f)$ through the feedback path, $F_p(f)$. For the reactor transfer function measurement, neutron flux disturbances caused by sources not correlated with the test input signal will cause disturbances in core pressure through the neutron flux to pressure feedback path, $F_p(f)$, which was neglected in Figure A-2. The bias in transfer function magnitude estimate is given by

$$\hat{G}_c(f) = \frac{S_{xy}(f)}{S_{xx}(f)} = \frac{G_c(f) + F_p(f)N_1}{1 + |F_p|^2 N_1} \quad (\text{A-51})$$

where

$$N_1 = \frac{S_{nn}(f)}{S_{uu}(f)} \quad (\text{A-52})$$

Thus, only if the ratio N_1 is zero or if the feedback transfer function $F_p(f)$ is equal to zero does $\hat{G}_c(f)$ equal the true transfer function $G_c(f)$. The steady-state average neutron flux noise in a BWR is approximately 5% of rated peak-to-peak. Assuming a Gaussian signal, the standard deviation^{A-17} is approximately

$$\sigma_N \simeq 5\% / 8 = 0.625\% \text{ Rated}$$

The feedback transfer function $F_p(f)$ can be approximated by the effective fuel time constant, $\tau_{f\ell}$, and an integrator representing the effective mass and energy storage in the reactor vessel. Hence,

$$F_p(f) \simeq \frac{K_p}{(2\pi f)(1 + 2\pi f\tau_{f\ell})} \text{ psi}/\% \quad (\text{A-53})$$

where

$$K_p \simeq 1.4 \text{ psi/sec-%} \quad (\text{A-54})$$

$$\tau_{f\ell} \simeq 7 \text{ seconds}$$

At the resonant peak frequency of the closed-loop transfer function, $G_c(f)$, 0.45 Hz,

$$|F_p| \simeq 0.025 \text{ psi}/\% \quad (\text{A-55})$$

and assuming the same bandwidth for the neutron flux noise and PRBS test input signal,

$$\frac{S_{nn}(f)}{S_{uu}(f)} \simeq \left(\frac{0.625\%}{2.2 \text{ psi}} \right)^2 = 0.08 \text{ (%/psi)}^2 \quad (\text{A-56})$$

The error in the transfer function estimate can be written,

$$\frac{\hat{G}_c(f) - G_c(f)}{G_c(f)} = \frac{F_p(f)N_1[1/G_c(f) - 1]}{(1 + |F_p|^2 N_1)} \quad (\text{A-57})$$

Near the resonant peak the measured transfer function magnitude is approximately,

$$|G_c(f)| \simeq 8\%/\text{psi} \quad (\text{A-58})$$

Assuming this is nearly the true value, the error due to feedback effects is approximately

$$\left| \frac{\hat{G}_c(f) - G_c(f)}{G_c(f)} \right| \simeq 0.002 \quad (\text{A-59})$$

which also is very small relative to the random errors in the transfer function estimates.

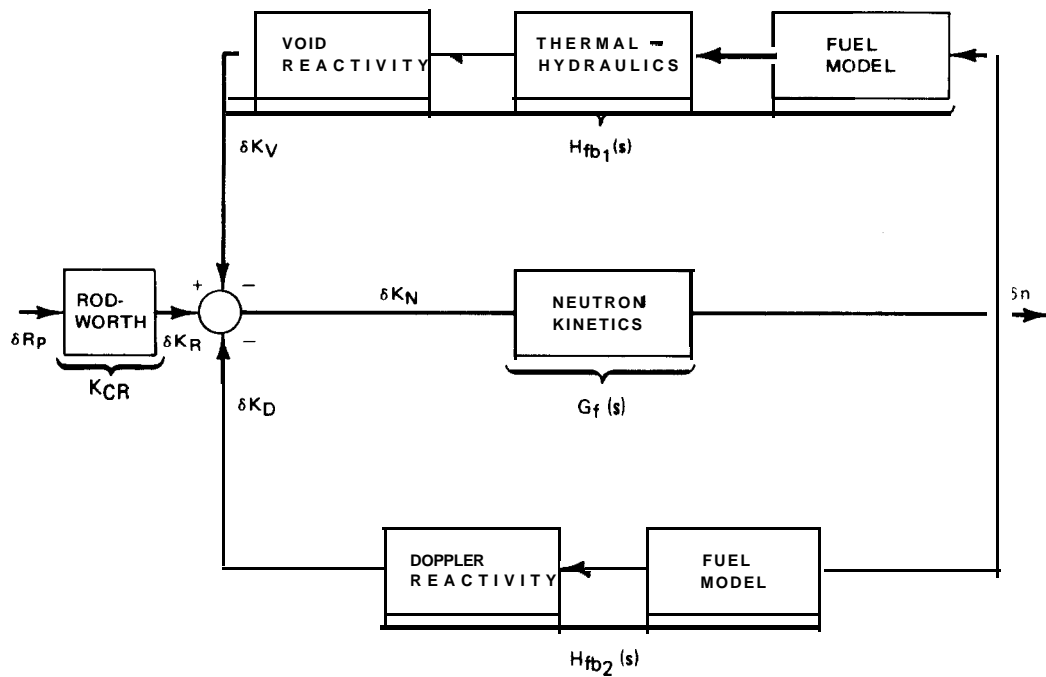


Figure A- 1. Boiling Water Reactor Reactivity Feedback Transfer Function Rod Oscillator Test

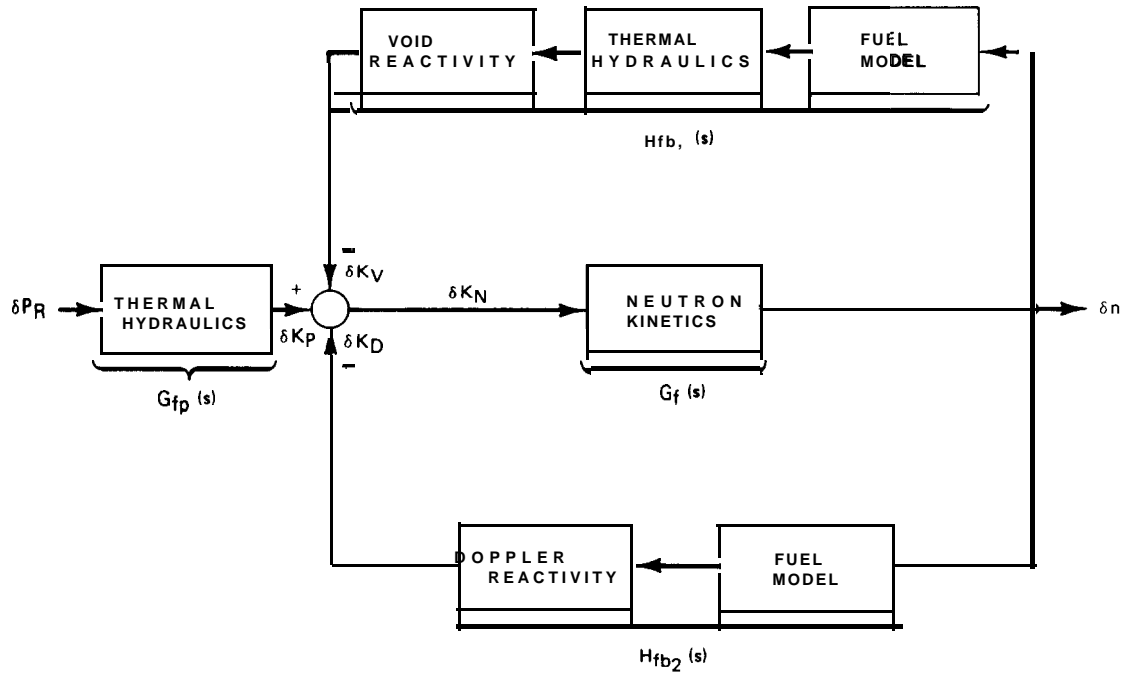


Figure A-2. Boiling Water Reactor Reactivity Feedback Transfer Function Pressure Perturbation Test

A.3 REFERENCES

- A-1. I. A. Engen, *A New Technique for Investigating Feedback and Stability of a Nuclear Reactor*, Argonne National Laboratory, ANL-7686 (1970).
- A-2. *Stability and Dynamic Performance of the General Electric Boiling Water Reactor*, General Electric Co. Licensing Topical Report, NEDO-21506 (1977).
- A-3. Daniel Graupe, "Identification of Systems," Van Nostrand Reinhold Co. (1972).
- A-4. L. A. Carmichael and G. J. Scatena, *Stability and Dynamic Performance of the General Electric Boiling Water Reactor*, General Electric Co., APED-5652 (1969).
- A-5. S. I. Chang and T. W. Kerlin, *A Method for Systematic Interpretation of Dynamic Measurements in a High Temperature Gas-Cooled Reactor*, University of Tennessee, UTGCR-2 (1976).
- A-6. M. J. D. Powell, "A Method for Minimizing a Sum of Squares of Nonlinear Functions Without Calculating Derivatives," *The Computer Journal*, 7, 303 (1965).
- A-7. B. S. Garbow, *Least Squares Functional Minimization Without Derivatives, System 360 Library Subroutine*. Argonne National Laboratory, ANL E250S (1968).
- A-8. L. W. Taylor, Jr., and K. W. Illiff, *Systems Identification Using a Modified Newton-Raphson Method — A Fortran Program*, National Aeronautics and Space Administration, TN D-6734 (1972).
- A-9. F. C. Schweppe, "Uncertain Dynamic Systems," Prentice Hall (1973).
- A-10. C. Bingham, M. D. Godfrey, and J. W. Tukey, "Modern Techniques of Power Spectrum Estimations," *IEEE Trans.*, AU-15, No. 2 (June 1967).
- A-11. R. P. Brumbach, *Digital Computer Routines for Power Spectral Analysis*. Contract Nonr-4298(00), AC Electronics, TR68-31 (1968).
- A-12. T. S. Durrani and J. M. Nightingale, "Data Windows for Digital Spectral Analysis," *Proc. IEEE*, 119, No. 3 (March 1972).
- A-13. R. K. Otnes and L. D. Enochson, "Digital Time Series Analysis," John Wiley (1972).
- A-14. G. Jenkins and D. Watts, "Spectral Analysis and Its Applications," Holden-Day Publishing Co. (1968).
- A-15. J. S. Bendat and A. G. Piersol, "Random Data: Analysis and Measurement Procedures," John Wiley (1971).
- A-16. C. Chatfield, "The Analysis of Time Series: Theory and Practice," Halsted Press.
- A-17. K. W. Goff, "Dynamics in Direct Digital Control-I, Estimating Characteristics and Effects of Noisy Signals," *ISA Journal*, pp 45-49 (November 1966).

APPENDIX B

MEASUREMENT ERROR ANALYSIS

B.I STATIC ERROR ESTIMATES

B.I.I Pressure Measurements

The potential error sources in the pressure measurements can be generated by the following components:

1. Pressure Calibration Equipment
2. Transducers
3. Signal Conditioning Amplifiers
4. Analog-to-Digital Converter

The error estimates for each component are as follows:

1. *Pressure Calibration Equipment*

Two Heise pressure gages were used as the primary calibration source for pressure transducer calibration during the Peach Bottom-2 tests. The accuracy of the Heise gages is 0.1% Full Scale (FS). Because the plant was in operation at the time of installation of the test equipment, no practical method was available to measure and suppress the bias on the absolute pressure measurements due to the elevation head difference between the pressure measurement point and the transducer locations. The elevations were scaled from plant layout drawings with an estimated uncertainty of ± 1 foot, and the fluid temperature can be estimated to within $\pm 25^\circ$ F. These contribute, respectively, 0.42 psi and $\pm 3 \times 10^{-3}$ psi/ft of elevation head. The calculated elevation head corrections and the combined statistical uncertainties are listed in Table B-I.

2. *Pressure Transducers*

Transducer errors are due to nonlinearity, temperature effects, hysteresis, and, for the differential pressure type, base pressure effects.

The errors for the various sources, obtained from manufacturer's specifications, are given in Table B-2 for the three types of pressure transducers used in Peach Bottom-2 EOC2 tests.

a. *Absolute Pressure Transducers*

Calibration was determined for a pressure range of 875 to 1150 psig. The linearity error is reduced to $(1150-875)/(1500-0) \times 0.4 = 0.08\%$ FS or 1.2 psi. The maximum nonlinearity observed during calibration was 0.5 psi. Hysteresis would be similarly reduced to 0.7 psi. The estimated error, calculated statistically, is 3.6 psi or 0.24% FS. A 10° F temperature drift, an average pressure of 1000 psig, and the largest elevation correction error were assumed.

b. **Differential Pressure Transducers**

The calibration range for the 100-psid transducers is the full 0 to 100 psi range. There is also a base pressure effect on the transducer zero. The error for the differential pressure transducers is 1.1 psi or 1.1% FS.

The calibration range for the 50-psid transducers is the full 0-50 psi range. The error for these differential pressure transducers is 0.56 psi or 1.1% FS.

3. **Amplifiers**

The NEFF amplifiers used were models 620050 (low level) and 620060 (high level). Errors are due to gain stability, linearity, zero stability, zero drift, and common mode rejection. Each error, total errors, and error sources are given in the Table B-3 for the two types of amplifiers. Error estimates assume a $\pm 3^\circ$ C temperature change, a voltage input ≈ 0.2 Vdc and a voltage output ≈ 10 Vdc.

4. **Analog-To-Digital Converter**

The Hewlett Packard analog-to-digital converter (ADC), converts analog input signals, in the voltage range of -10.240 to +10.235 volts, to digital form. The ADC contains a bipolar ADC circuit which uses the successive approximation methods to convert analog input signals into a 12-bit digital output, including a sign bit. Negative numbers are in 2's complement. The converter speed is 1 μ sec per bit. At this speed, the ADC will perform a conversion with an accuracy commensurate with 12-bit resolution. Least significant bit = 5 mV. Accuracy is ± 1 LSB or $\pm 0.049\%$ FS.

5. **Total System Pressure Errors**

The total system errors, including calibration, transducer, and readout, were calculated from the above data and are:

Pressure Range	Error	Nominal Value	Error (%)
1500 psig	4.8 psi	1000 psi	0.48
100 psi	1.2 psi	33.3 psi	3.6
50 psi	0.6 psi	16.7 psi	3.6

Since these values were calculated from specification limits, the expected errors are estimated conservatively to be one half of the above values or as shown in Table B-4.

B.1.2 Flux Signals

1. **LPRM Data (Local Power Radiation Monitor)**

The local power radiation monitor signals are subject to the following static error factors:

1. Plant Calibration Procedure
2. Amplifier Errors
3. Calibration Voltmeter Errors
4. Readout Errors (A/D Converter)

The amplifier and readout errors were previously reviewed in Section B.1. The voltmeter used for calibration was a Fluke model 8600 A digital voltmeter. The error for a signal of magnitude 25% of FS is $\pm 0.01\%$ FS. The principal error in the LPRM reading is due to the plant calibration procedure. This error lumps together all the uncertainties that are associated with the plant LPRM system, exclusive of the current test instrumentation. An estimate of the uncertainty in the local relative power as calculated by diffusion theory has been made and was found to be 3.0%.^{B-1} Since the test measurement system errors (items 2, 3, and 4) are negligible by comparison, the uncertainty in the LPRM measurement is 3.0% FS.

In terms of "percent of point" variations, LPRM measurements are expected to have less uncertainty than the quoted 3% FS. This is because some of the uncertainty in an absolute measurement is removed in a ratio calculation. For example, manufacturing uncertainties and uncertainties due to LPRM exposure are eliminated during the calibration based on TIP scan. The principal uncertainty in the LPRM calibration is due to the uncertainty in core thermal power, which has been estimated to be 1.76% (1σ).^{B-1} The effect of power distribution shift on the electronic APRM measurement (average of 20 LPRM signals) can be estimated from the calculated normalization constant in the "Pseudo" APRM calculation for the tests.

Turbine Trip	Normalization Constant, K
TT1	2.0049
TT2	1.8095
TT3	<u>1.8350</u>
	1.88 (Average)

The maximum deviation from the average is found to be $+0.125$ or 5.2% FS of the 0-125% electronic APRM output range. The plant electronic APRM specification quotes an overall accuracy of the averaging circuitry (including linearity and stability) of 2.4% FS, with a trip setting accuracy of 2% FS. Assuming that the power distribution and electronic errors are 2σ values, we estimate the overall statistical error in the electronic APRM measurement to be

	Error (1σ)
1. APRM Measurement	3.2% FS
2. APRM High Flux Trip Set Point	3.1% FS

The steady-state calculated "Pseudo" APRM signal is not subject to the power distribution uncertainty because it uses the initial process computer power determination to calculate the normalization factor, and it does make use of the plant's APRM electronics. Hence its estimated uncertainty is simply that of the process computer power determination, 1.76% of rated power (1σ).

B.1.3 Process Signal Uncertainties

The plant signal uncertainties (1σ) have been evaluated.^{B-1, B-2} The uncertainties for various signals are given in Table B-5. The dominant factor in the core flow uncertainty is the uncertainty of the calibration constant K_{calib} , of the four diffuser double-tapped jet pumps. The uncertainty in K_{calib} was determined to be 3%, which leads to individual jet pump flow uncertainties of 1.5%.

B.2 DYNAMIC ERROR ESTIMATES

B.2.1 Pressure Measurements

Errors in both timing and amplitude are also generated by the dynamic response characteristics of the various components in the pressure measurement systems:

1. Sensor Instrument Line Response
2. Transducer Response
3. Signal Conditioning Amplifier Response
4. Analog to Digital Converter Response

The dynamic response capability of the various components is described below.

B.2.1.1 Sensor Instrument Line

The special pressure transducers for the Peach Bottom-2 EOC2 transient testing were installed on the plant instrumentation racks in the secondary reactor containment building. This arrangement was dictated by the limited access to the reactor secondary containment for transducer calibration and the environment in the primary containment during power operation. This introduces the possibility of measurement errors caused by acoustic oscillations in the long runs of instrument piping between the pressure measurement locations in the drywell and the sensors located on the instrument racks in the secondary containment building. Also the sensor line response is affected by the hydraulic impedance of the existing plant instruments, which operate in parallel with the special test transducers. The schematic diagrams shown in Figures B-1 to B-3 illustrate the core exit pressure, the reactor vessel pressure, and the main steam line pressure measurement transducer installations.

The instrument line lengths and diameters are summarized in Table B-6. The dynamic response of each sensor line type was estimated by digitally simulating its response to pressure ramp inputs, approximating that encountered during the turbine trip testing. The digital simulation was carried out using a convolution method for simulating coupled distributed piping networks described in Reference B-3. The simulations for water-and-steam-filled lines were based on the impulse response kernel derived by Brown for compressible laminar transient flow in cylindrical conduits B-4,B-5

Simulated pressure responses of the transducer end of the instrument lines are shown in Figures B-4 to B-6 for the assumed 150 psi/sec ramp inputs at the reactor end of the instrument lines.* These results are summarized in Table B-7. The most probable estimates of instrument line natural frequencies were identified from power spectral density measurements of the pressure signals taken during the Low-Flow Stability Tests (see Figures B-7 to B-12). The principal resonances found in these signals, most probably related to the instrument line dynamic responses are also tabulated in Table B-7. From these comparisons, it is most likely that the instrument line simulation models overestimated the natural frequency of the real lines and hence underestimate the time delay inherent in their responses. This result may be due to the effect of air trapped in the lines, caused by incomplete bleeding, which would result in an effective reduction in the acoustic wave velocity. B-6 Also the loading effects on the hydraulic transmission lines due to the generally unknown input impedances of the parallel plant instruments.**

*Essentially the same magnitude of oscillation and time delay were observed for ramp rates of 50 to 200 psi/sec. The filtered responses are described later.

**While this data was available for the Viatran pressure transducers used for the test measurements, it is not readily obtained from manufacturers of process instruments.

B.2.1.2 Transducer Response

The specified response time, i.e., time to reach 90% of full scale, is less than 1 msec for the Model 218 Viatran Absolute pressure transducers. Hence their dynamic response is negligible relative to that of the instrument lines.

B.2.1.3 Signal Conditioning Amplifiers

The NEFF signal conditioning amplifiers for the absolute pressure signals incorporate a 2 pole Butterworth filter with a 10-Hz bandwidth (see Table 4-I). The effect of filtering the pressure signals is also plotted in Figures B-4 to B-6. They show that the filter causes a continuing time delay for a pressure ramp input forcing of the instrument lines. Since the natural frequency of the lines is generally overestimated in the digital simulation models, the Butterworth filter will probably not be as effective in reducing the oscillatory components of the pressure signals in the real system.

B.2.1.4 Analog-to-Digital Converter

The maximum conversion rate for the Hewlett Packard analog-to-digital converter with DMA is 45 kHz, including the response of the sample-and-hold amplifier. However, the limitations of the data throughput to the digital tape recorder reduce the sampling rate to approximately 36 μ sec per channel. The time resolution of the 160 channels recorded is, therefore, approximately 6 msec. This time response is negligible compared to that of the Butterworth input filters.

B.2.2 Flux Signals

The dynamic errors in the neutron flux measurements are generated in the following components of the Local Power Range Monitoring System.

1. Neutron Flux Detector Dynamic Response
2. Neutron Detector Cable Response
3. Signal Conditioning Amplifier Response
4. Analog-to-Digital Converter Response

The dynamic errors due to these components are described below:

B.2.2.1 Neutron Flux Detector

The LPRM fission chamber current is made up of both prompt and delayed components. The prompt component is from prompt neutrons and gamma rays from the reactor core. The delayed component comes from delayed neutrons and gammas from the core, as well as delayed betas from the detector coating and its structural materials. Since the LPRM measurements are intended to represent the total neutron flux, the sum of the components of detector current from prompt and delayed neutrons is the desired signal. However, the component caused by the prompt gammas from fissions in the core, is also approximately proportional to total neutron flux, and hence can be considered part of the desired signal. During a transient flux condition, the dynamic errors in the detector response are caused by the delayed gamma and beta detector current components. These currents are not proportional to total neutron flux, but are instead related to the past history of the time varying flux.^{B-7} The relative sensitivity of the detector to neutrons and gammas decreases with burnup. This sensitivity ratio is used as a criterion for determining the end-of-useful life of the detector. For a step change in prompt neutron flux, the time response of a GE fission detector was calculated for both beginning and end-of-life conditions. These calculations were based upon the gamma decay curve and the nominal detector parameters reported in References B-8, B-9, B-10. The results of the calculations show that a maximum time response error of -2% could be generated at the detector end-of-life condition and -0.6% at beginning of life. Since only a fraction of the detectors in the core (assume 25%) could have been at end-of-life conditions during the Peach Bottom-2 testing, the average dynamic error is expected to be no more than -1%.

Another source of error in the detector output current is due to a band-limited white noise source caused by the counting uncorrelated events.^{B-11} A typical value for the detector mean-square current/direct current ratio is^{B-12}

$$\frac{\langle I^2 \rangle}{\langle I \rangle} = 1.14 \times 10^{-13} \frac{\text{amp}^2}{\text{Hz} \cdot \text{amp}}$$

with a noise bandwidth of 1.7×10^5 Hz. Using the detector neutron sensitivity and the design neutron flux level from Reference B-8, the maximum error from the noise source is found to be less than 0.2% of the maximum detector current level.

B.2.2.2 Detector Cable Response

Stray currents produced in the detector cables cause dynamic errors in the transient neutron flux measurements. These currents are generated in the cables from the prompt and delayed gammas from the core, and the betas from the cable materials. Hence this dynamic error is made up of components which are proportional to the average neutron flux along the cable length and which are a function of the time history of the neutron flux. There is also a constant bias current produced in the detector cable by thermally induced ohmic conduction. The step response for a detector at the D level in the core was calculated for the cable parameters described in Reference B-13. The maximum error due to the induced currents ranged from 1.5% at beginning of detector life to 14% at end-of-life. For the average detector at the centerline of the core, the errors are expected to be less -0.8% to 7% since less cable is exposed to the core conditions. Again assuming 25% of the detectors were at the end of their useful life, the maximum dynamic error due to induced cable currents is -4%.

B.2.2.3 Signal Conditioning Amplifier

A Butterworth filter with a 100 Hz bandwidth was used to filter the LPRM signals. The time response of the filter is the same order as that of the sampling capability of the analog-to-digital converter, hence a time resolution of 6 milliseconds in the neutron flux signals is possible.

The combined maximum dynamic error (or bias) in the neutron flux measurements (from the LPRM and cable) is -6%. in addition to the random errors described above.

B.2.3 Process Signals

The errors introduced from the limited time response capability of the signals measured from plant instruments can only be roughly estimated because of the lack of information on their installed dynamic qualification testing. The estimated time response capability of each class of plant process signals measured is tabulated in Table B-8.

Table B-1
ELEVATION HEAD CORRECTION FOR
ABSOLUTE PRESSURE MEASUREMENTS

Plant Pressure Signal	Transducer Elevation Head (ft H ₂ O)	Transducer Pressure Correction (psi)	Error (psi)
Core Exit	6.4	27.5	0.5
Reactor	2.4	10.4	0.4
Steam Line	2.0	8.4	0.4
Turbine inlet	2.6	11.3	0.4

Table B-2
SPECIAL PRESSURE TRANSDUCER SPECIFICATIONS

Error Source	Model 218 (0-1500 psi) Viatran		Model 220 (0-100 psi) Viatran		Model 220 (0-50 psi) Viatran	
	Gage Pressure	Differential Pressure	Gage Pressure	Differential Pressure	Gage Pressure	Differential Pressure
Linearity	0.4% FS	6.0 psi	0.4% FS	0.4 psi	0.4% FS	0.2 psi
Hysteresis	0.25% FS	0.375 psi	0.2% FS	0.2 psi	0.2% FS	0.1 psi
Base Pressure	0	0	1% FS @ 1000 psi	1.0 psi	1% FS @ 1000 psi	0.5 psi
Temperature effect on Zero	2% FS for 100°F	3.0 psi for 10°F	2% FS for 100°F	0.2 psi for 10°F	2% FS for 100°F	0.1 psi for 10°F
Temperature effect on Span	1% FS for 100°F	1.5 psi for 10°F	1% FS for 100°F	0.1 psi for 10°F	1% FS for 100°F	0.05 psi for 10°F

Table B-3
SIGNAL CONDITIONING AMPLIFIER SPECIFICATIONS

Error Source	Model 620050	%	Model 620060	%
Gain Stability	$\pm 0.01\% \pm 0.002\%/\text{ }^{\circ}\text{C}$	0.016	$\pm 0.01\% \pm 0.002\%/\text{ }^{\circ}\text{C}$	0.016
Linearity	$\pm 0.01\% \text{ FS}$	0.01	$\pm 0.01\% \text{ FS}$	0.01
Zero Stability	$\pm 4 \mu\text{V R T I} \pm 15 \mu\text{V R T O}$	0.00415	$\pm 150 \mu\text{V R T O}$	0.0015
Zero Drift	$\pm 1 \mu\text{V R T I} \pm 15 \mu\text{V R T O}/\text{ }^{\circ}\text{C}$	0.00145	$\pm 25 \mu\text{V R T O}/\text{ }^{\circ}\text{C}$	0.00075
Common Mode Rejection	66 dB + Gain (in dB)	0.005	60 dB + Gain (in dB)	0.01
Total Bias Error		0.020		0.021

Table B-4
PRESSURE MEASUREMENT ERROR ESTIMATES

Pressure Range of Transducer (psi)	Nominal Signal Value (psi)	Estimated Expected Error (1 σ) (%)	Estimated Expected Error (1 σ) (psi)
1500	1000	0.24	2.4
100	33.3	1.80	0.6
50	16.7	1.80	0.3

Table B-5
PROCESS MEASUREMENT ERRORS

Signal	Instrument Error (1 σ)	Uncertainty (% FS)
Reactor Pressure ^a	7.5 psi	0.75
Core Flow ^a	$3 \times 10^6 \text{ lb/h}$	2.5
Feedwater Temperature	$0.7^{\circ}\text{F at } 350^{\circ}\text{F}$	0.2
Feedwater Flow	$8.2 \times 10^4 \text{ lb/h}$	1.76
Recirculation Suction Temperature	3°F	0.5

^aProcess computer measurements only

Table B-6
PLANT INSTRUMENT LINE DATA

Plant Pressure Signal	Line Diameter (Inches)	Line Length (ft)	
1. Core Exit Pressure	11.75 0.957	40. 111.	
2. Reactor Pressure	1.50 0.957	25. 82.	
3. Steamline Pressure	0.957	111. (135.) ^a	
4. Turbine Inlet Pressure	0.957	76. (90.) ^a	110

^a"A" Steam line ("D" Steam line).

Table B-7
**SIMULATED INSTRUMENT LINE DYNAMIC
ERROR ESTIMATES AND COMPARISON TO
EXPERIMENTAL RESULTS**

Plant Pressure Signal	Simulated Line Natural Frequency	Maximum Time Delay for Ramp Input ^a	Maximum Amplitude Error for Ramp Input ^a	Measured Natural Frequencies
1. Core Exit Pressure	-9.5 Hz	-30 millisec	-4 psi	5.2 Hz 10.0 Hz
2. Reactor Pressure	-10 Hz	-30 millisec	-3 psi	8.7 Hz
3. Steamline Pressure	-8.5 Hz	-30 millisec	-3 psi	5.8 A Steam line 2.5 D Steam line
4. Turbine Inlet Pressure	b	b	b	9.8 A Steam line 7.5 D Steam line

^aIncludes delay and attenuation due to 10 Hz Butterworth Signal Conditioning Filters.

bNot simulated.

Table B-8
PLANT PROCESS INSTRUMENTATION
ESTIMATED DYNAMIC RESPONSE

Plant Process Signal Type	Estimated Time Response (sec)
1. Flow Measurement	<0.25
2. Level Measurement	<0.25
3. Temperature Measurement	5 - 20

B-11

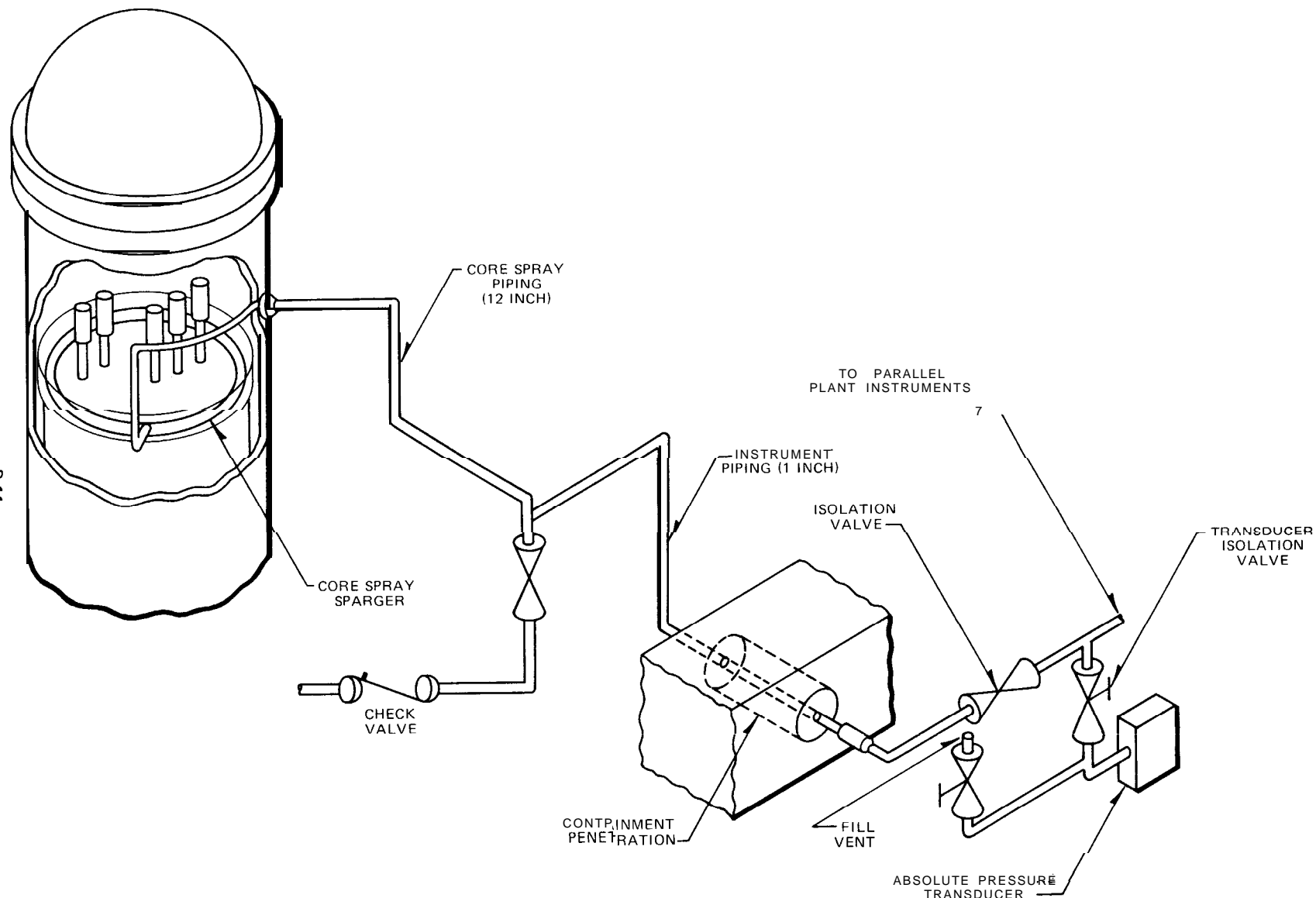


Figure B- 1. Core Pressure Measurement in EOC2 Test

B-12

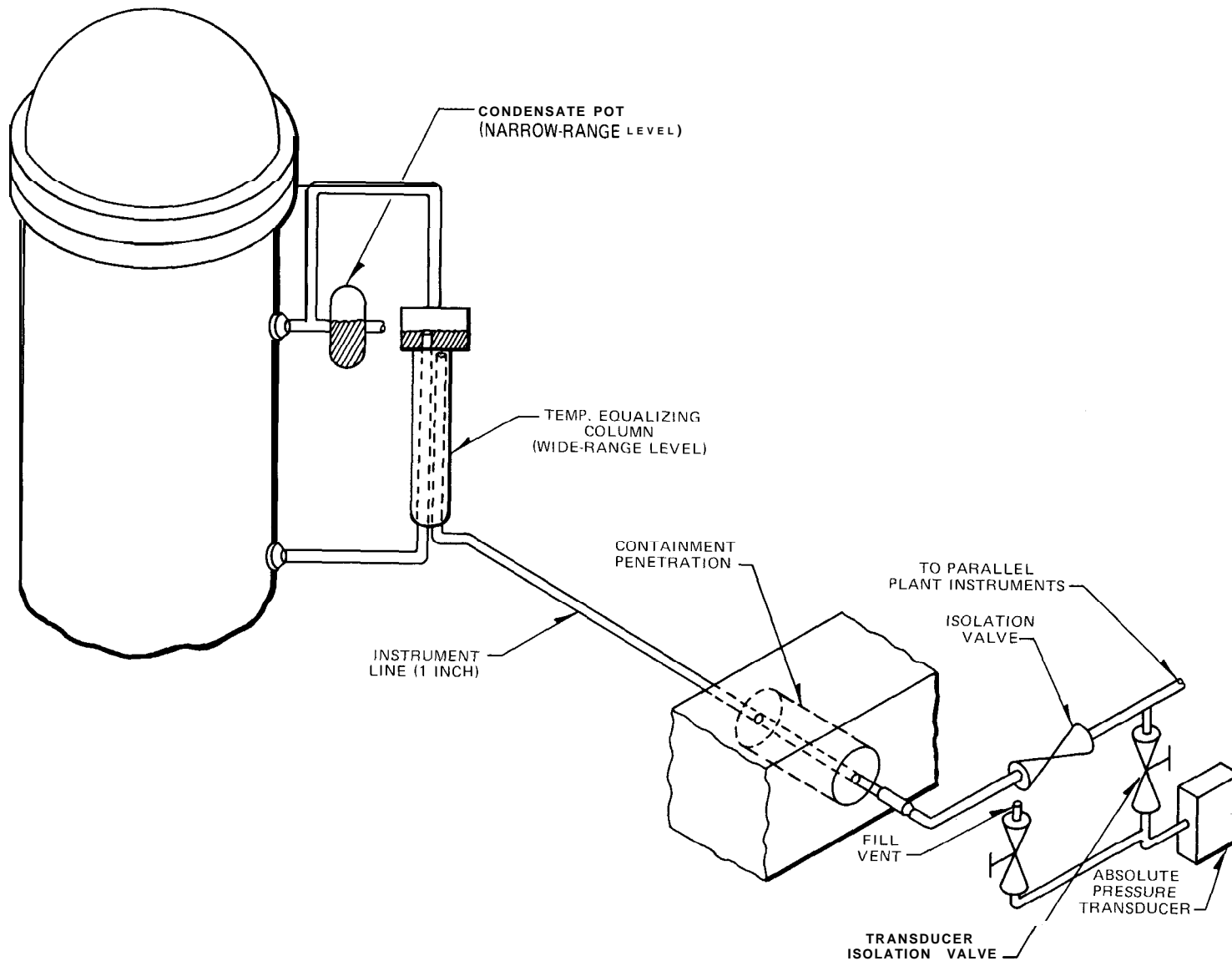


Figure B-2. Reactor Pressure Measurement in EOC2 Test

B-13

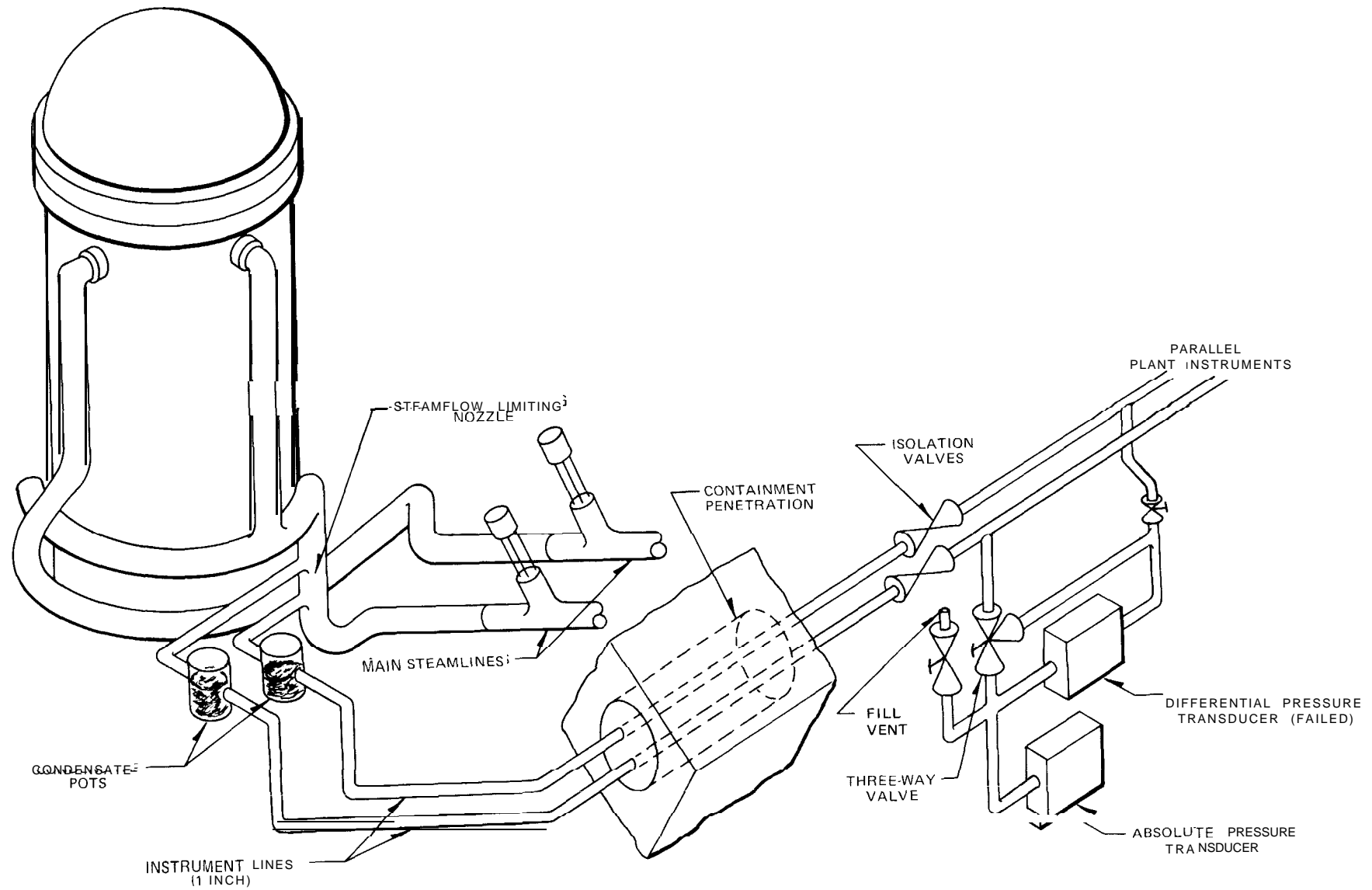


Figure B-3. Steam Line Pressure Measurement in EOC2 Test

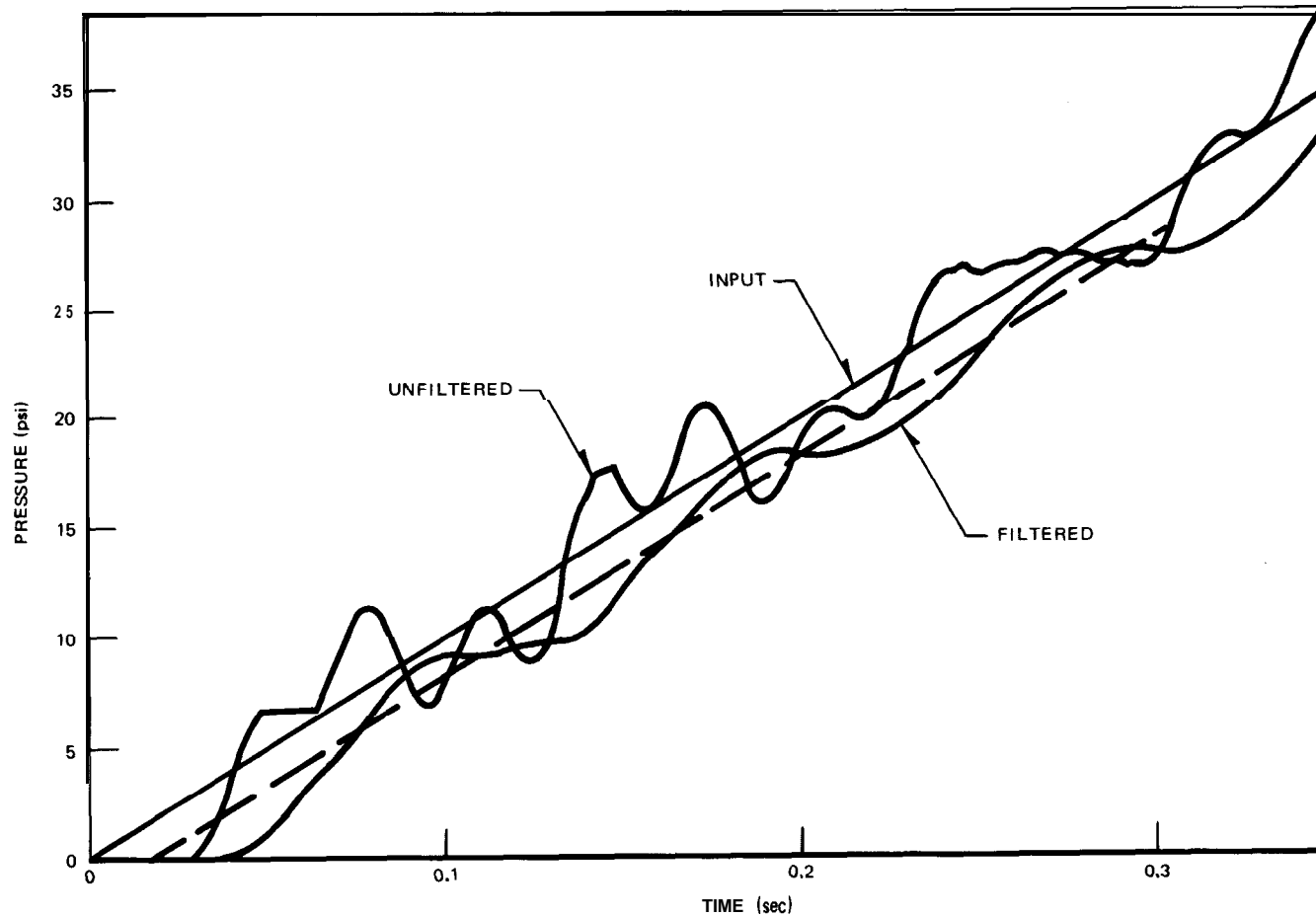


Figure B-4. Simulated Core Spray Sensor, Filtered and Unfiltered, 100 psi/sec Ramp Input

W15

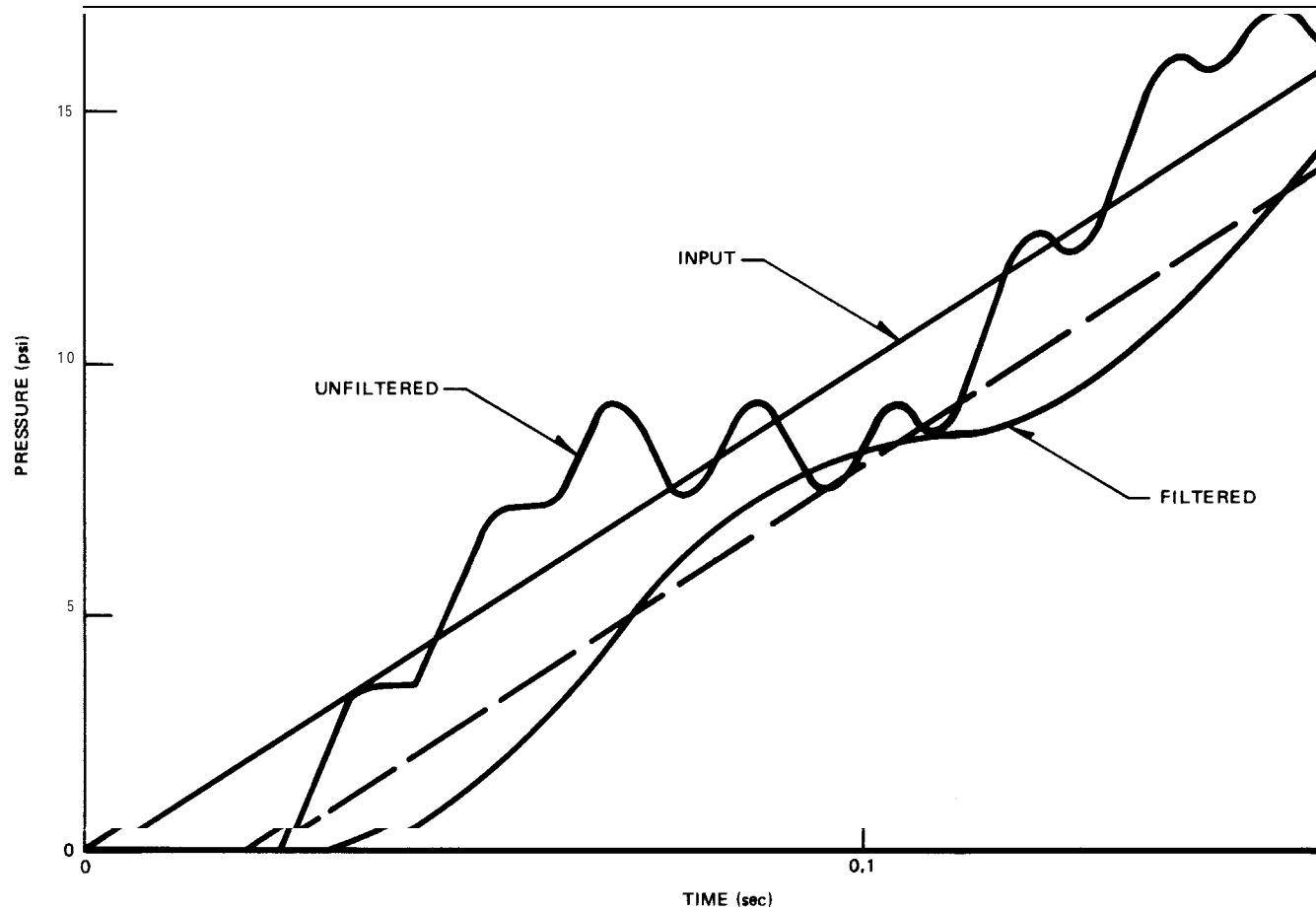


Figure g-5. Simulated Reactor Pressure, Filtered and Unfiltered, 100 psi/sec Ramp Input

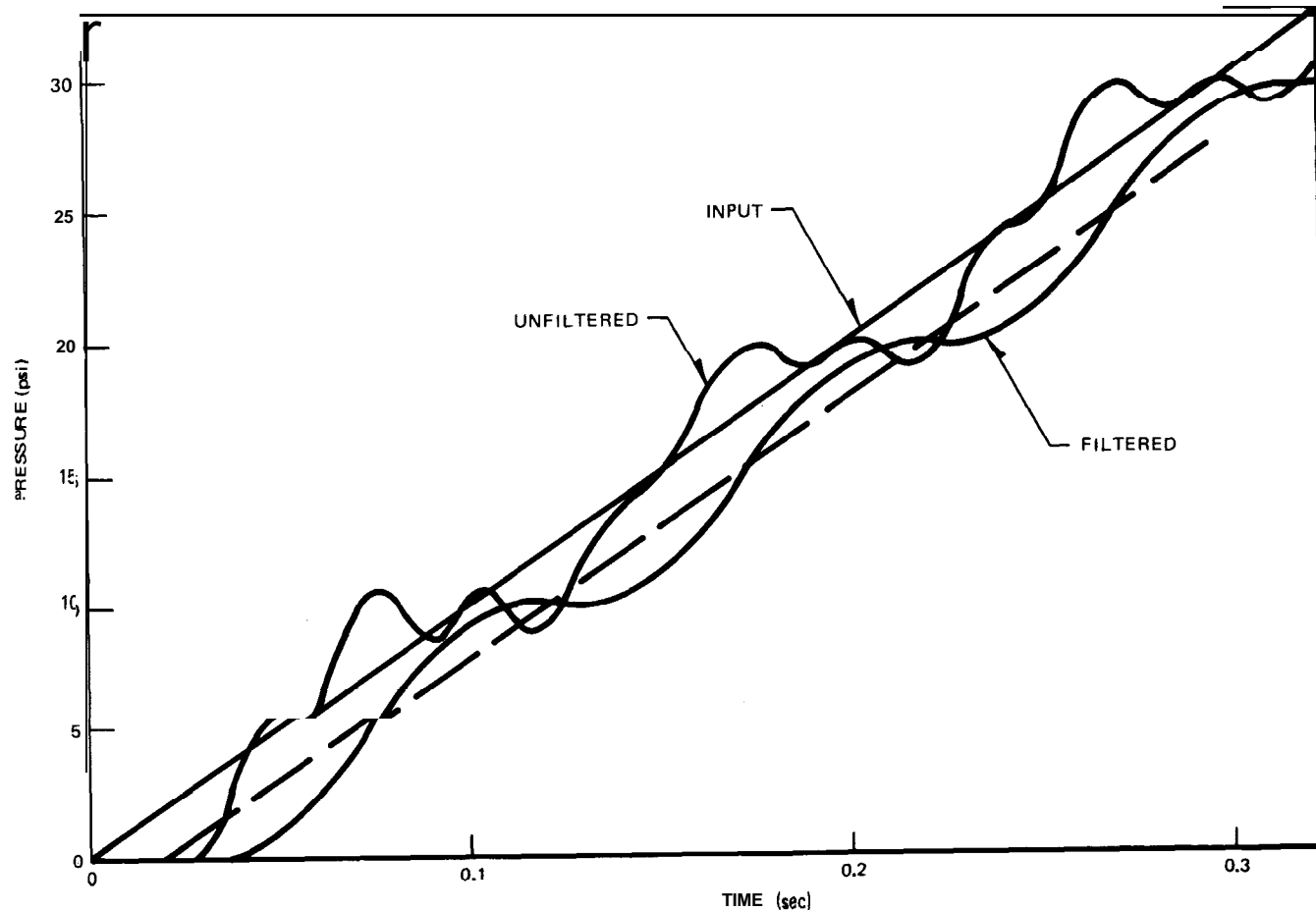


Figure B-6. Simulated Steamline Pressure, Filtered and Unfiltered, 100 psi/sec Ramp Input

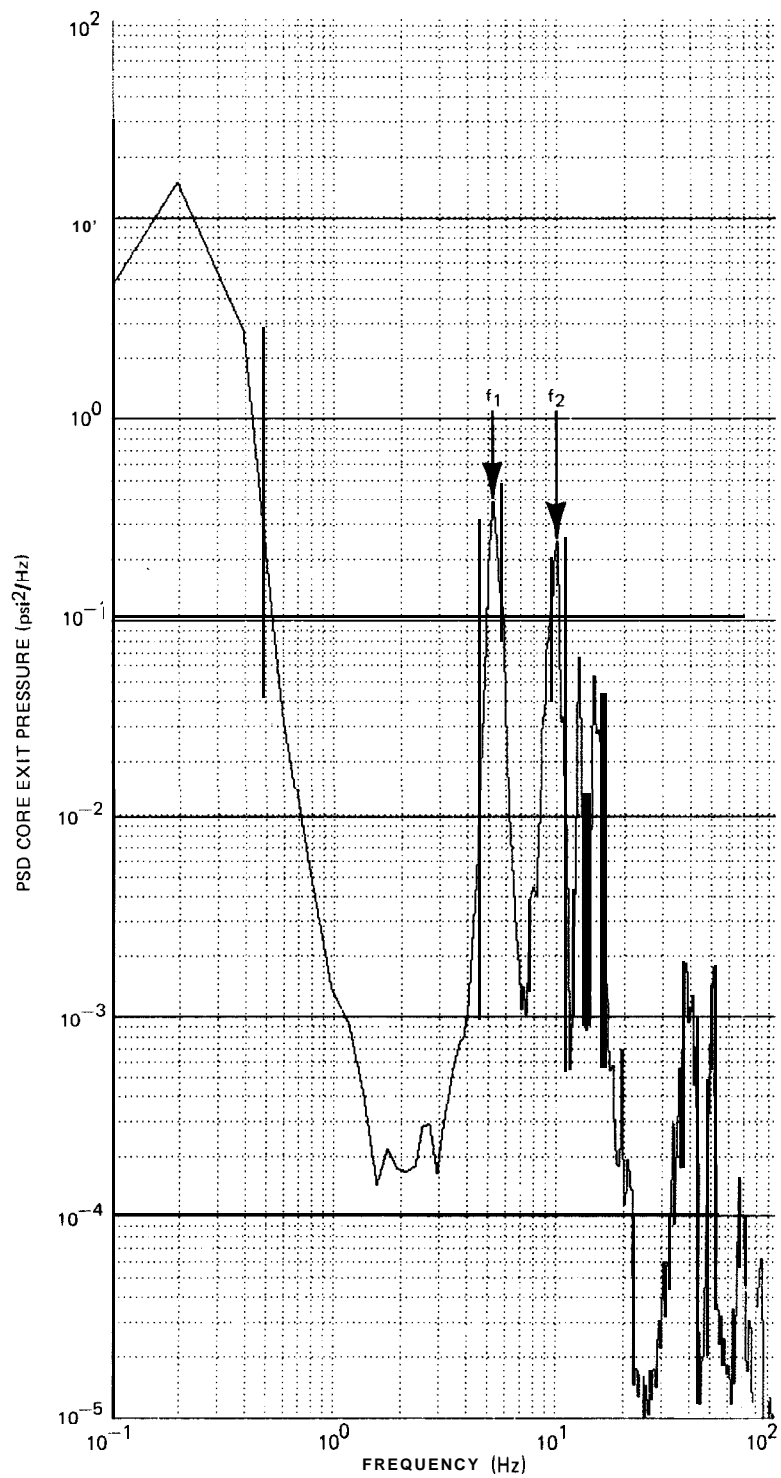


Figure B-7. Peach Bottom-2 EOC2 Test Low-Flow Stability Test (PT1) Power Spectrum of Core Exit Pressure

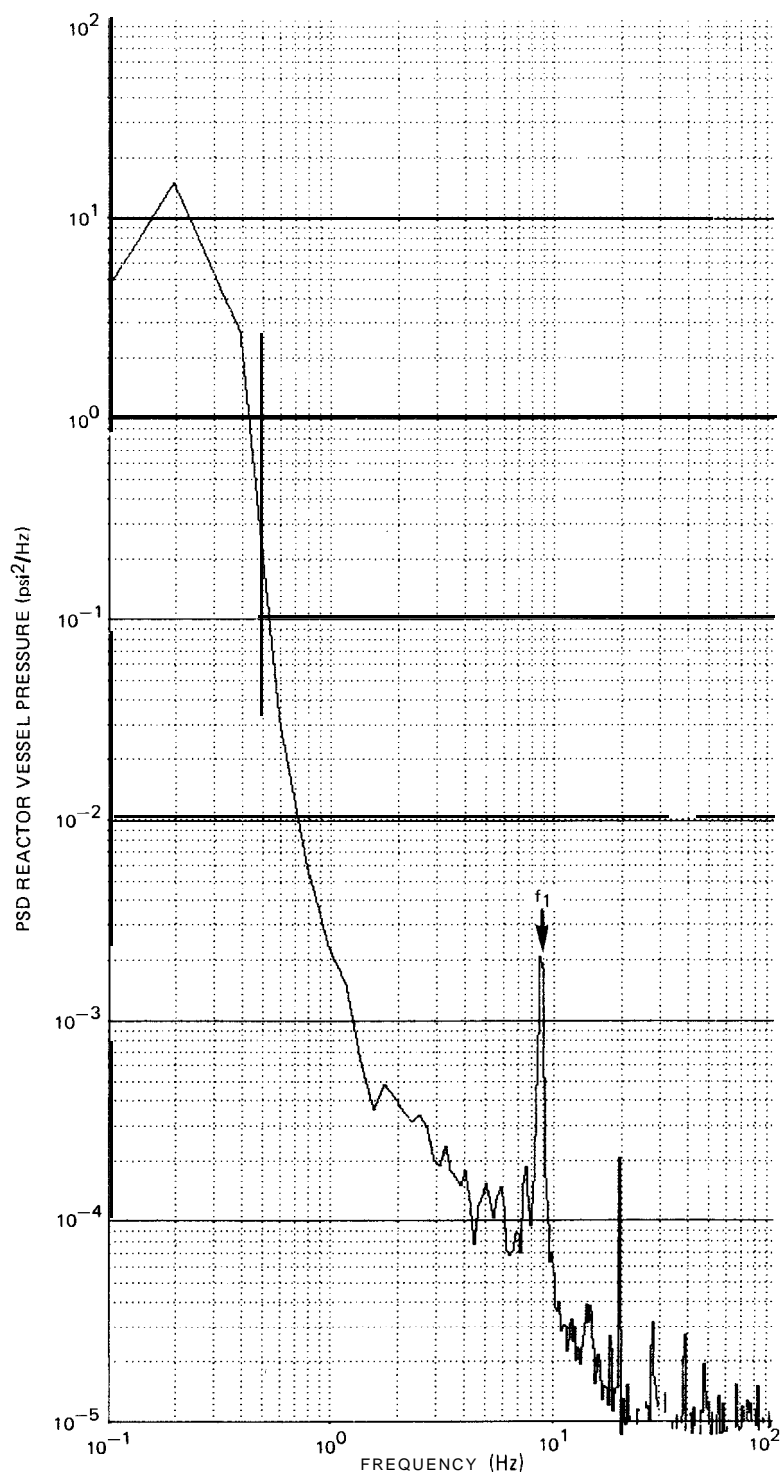


Figure B-8. Peach Bottom-2 EOC2 Test Low-Flow Stability Test (PT1) Power Spectrum of Reactor Pressure

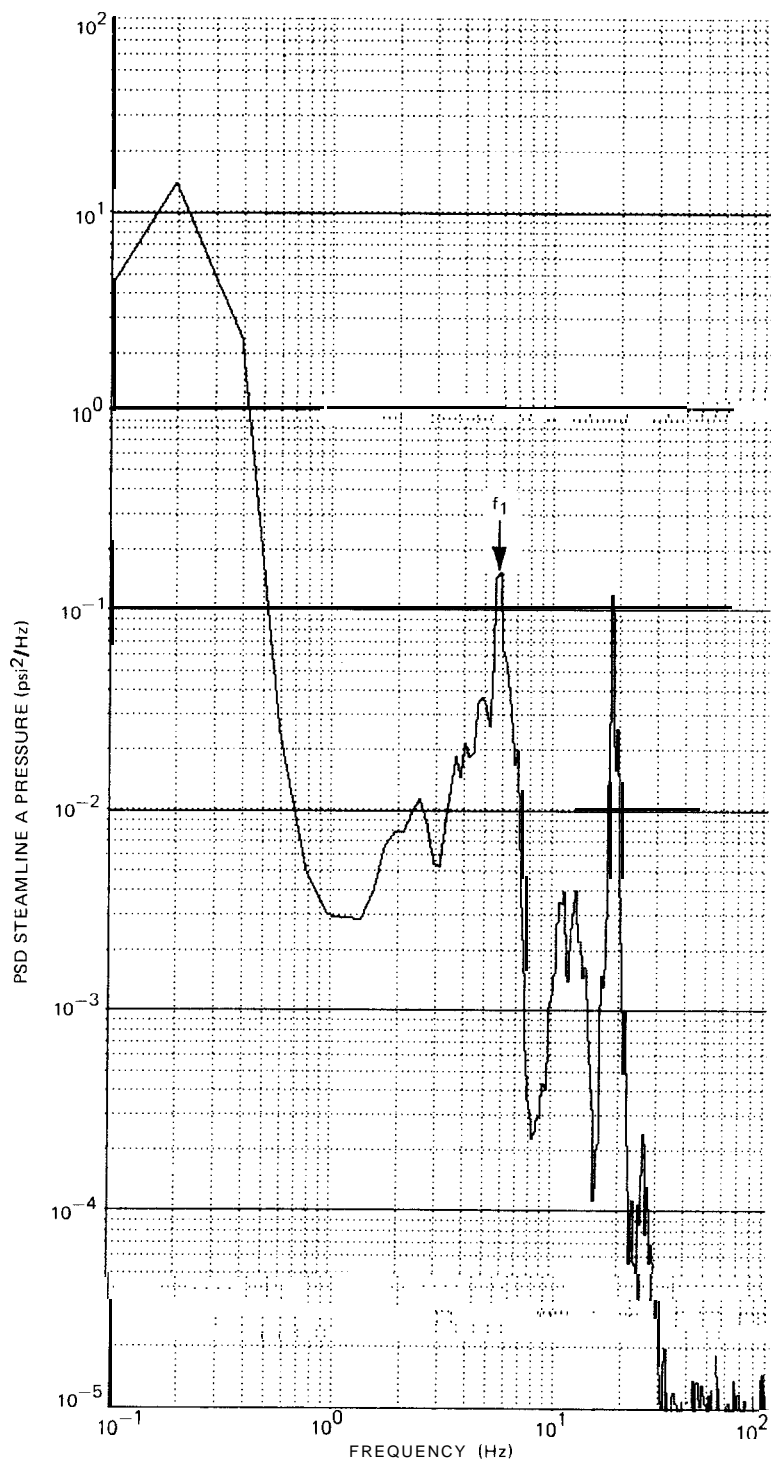


Figure B-9. Peach Bottom-2 EOC2 Test Low-Flow Stability Test (PT1) Power Spectrum of Stearline A Pressure

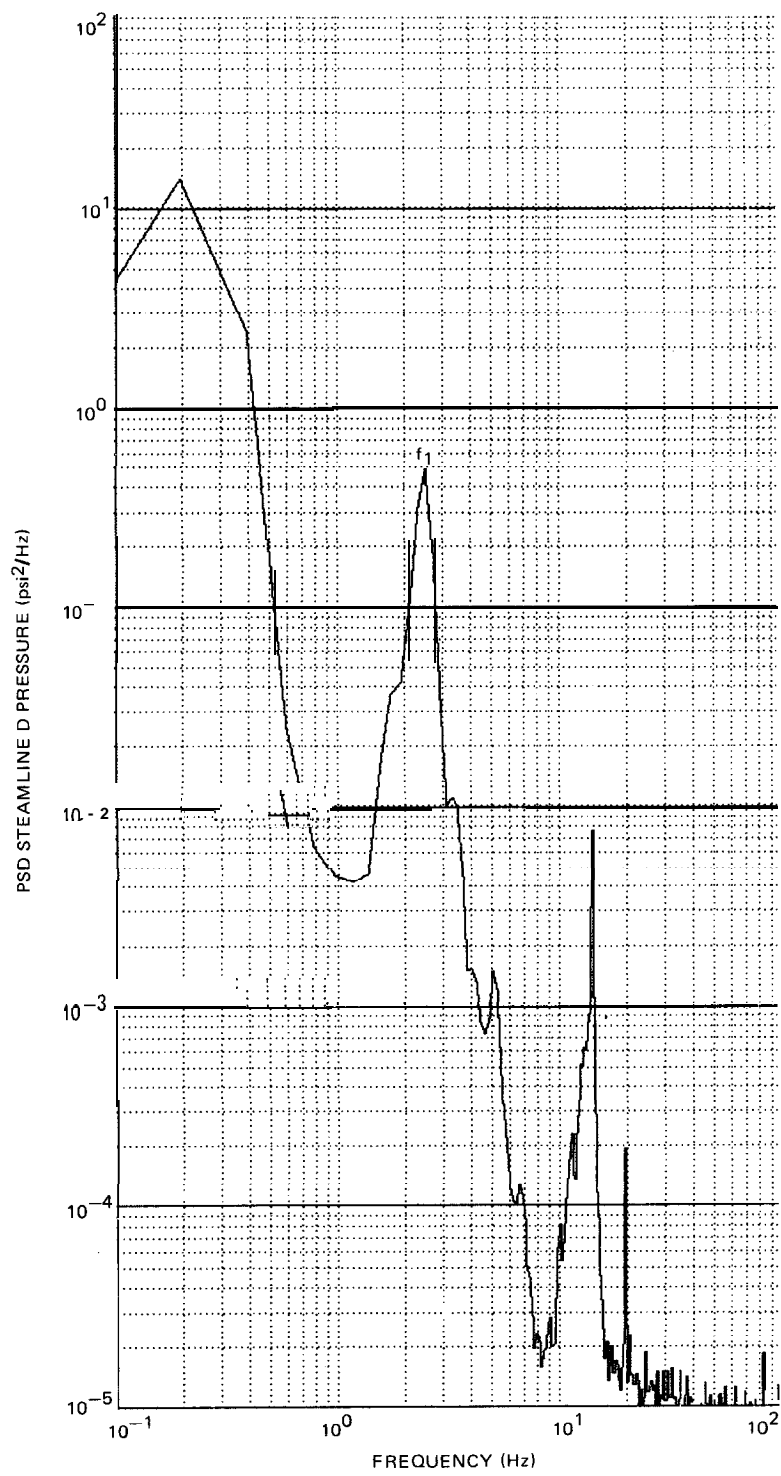


Figure B- 10. Peach Bottom9 EOC2 Test Low-Flow Stability Test (PT1) Power Spectrum of Steamline D Pressure

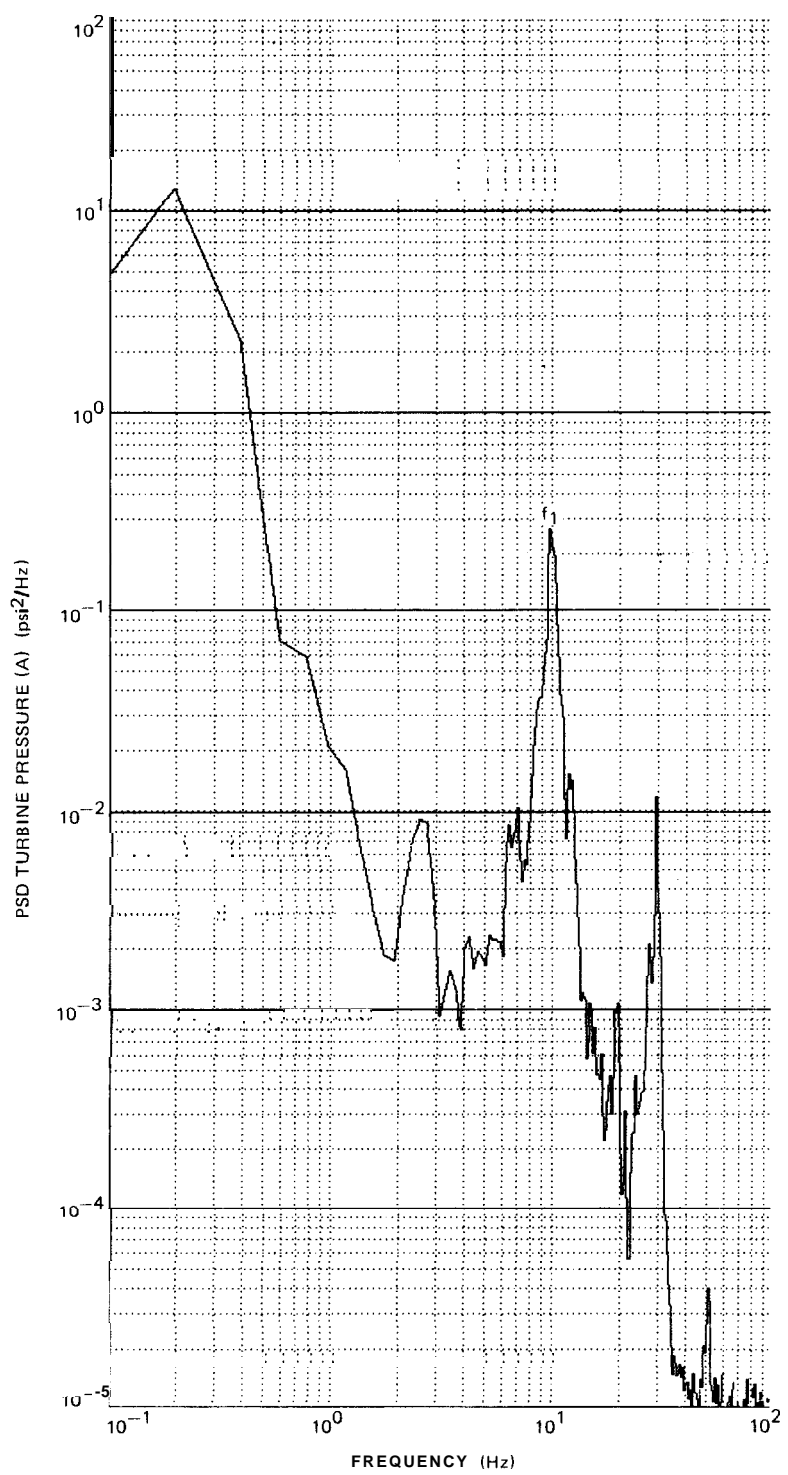


Figure B- 11. Peach Bottom-2 EOC2 Test Low-Flow Stability Test (PT1) Power Spectrum of Turbine Pressure (A)

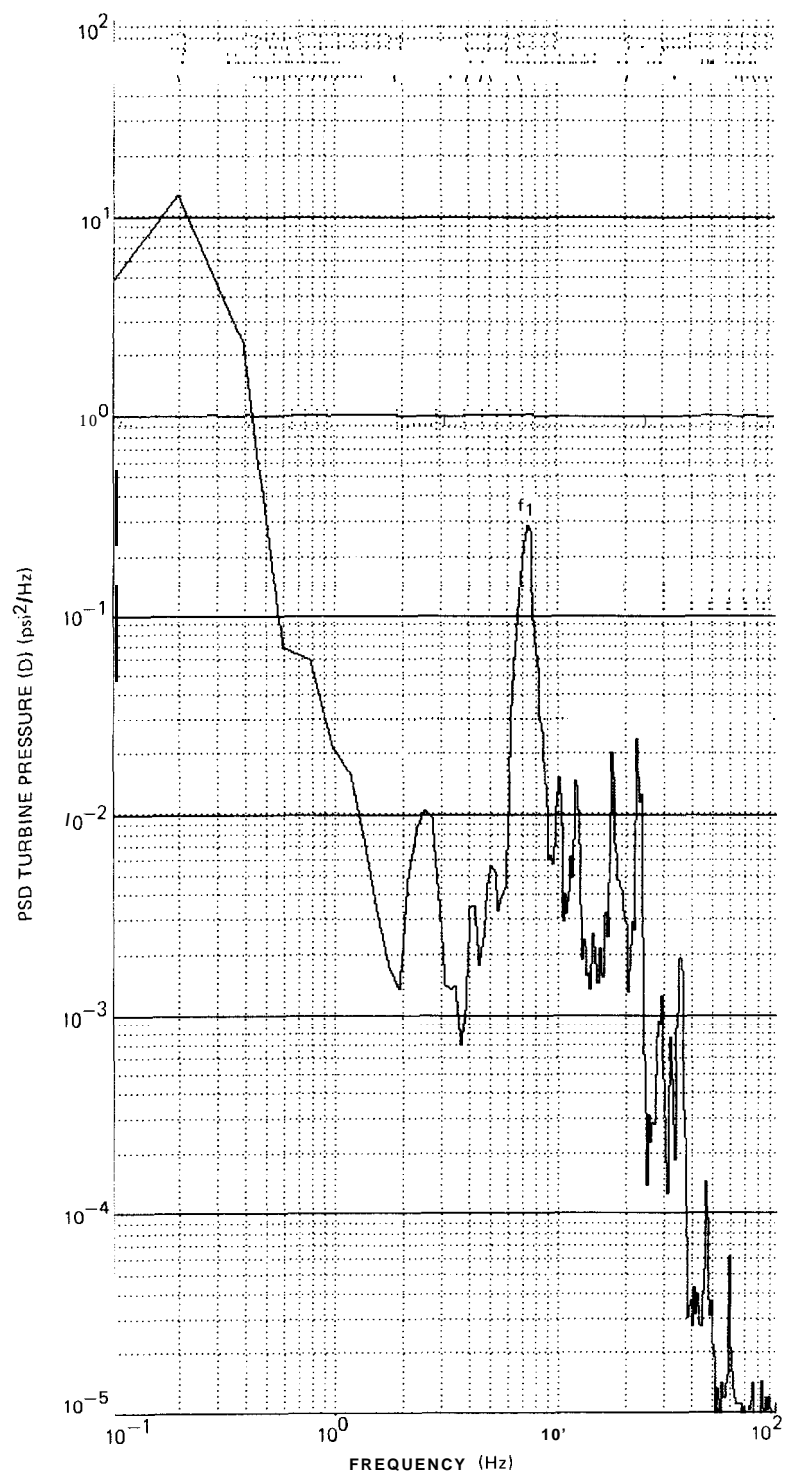


Figure B-12. Peach Bottom-2 EOC2 Test Low Flow Stability Test (PT1) Power Spectrum of Turbine Pressure (D)

B.3 REFERENCES

- B - I J. F. Carew, *Process Computer Performance Evaluation Accuracy*, General Electric Co., NEDO-20340 (1974).
- B-2. *General Electric Nuclear Boiler Design Specification*, General Electric Co., 22A1314AB, Rev. 13 (1973).
- B-3. R. S. Sidell and D. N. Wormley, "An Efficient Simulation Method for Distributed Lumped Fluid Networks," *Journal of Dynamics Systems, Measurements and Control, Trans. ASME, Series G*, 99 (March 1977).
- B-4. F. T. Brown, "The Transient Response of Fluid Lines," *Journal of Basic Engineering, Trans. ASME, Series D*, 84 (September 1962).
- B-5. J. T. Karan, Jr., and R. G. Leonard, "A Simple Yet Theoretically Based Time Domain Model for Fluid Transmission Lines," *Journal of Fluids Engineering, Trans. ASME, Series I*, No. 4, 95 (December 1973).
- B-6. R. E. Goodson and R. G. Leonard, "A Survey of Modeling Techniques for Fluid Line Transients," ASME Paper No. 71-WA/FE-9 (1971).
- B-7. J. P. Neissel, Personal Communication (1974).
- B-8. W. R. Morgan, *In-Core Neutron Monitoring System for General Electric Boiling Water Reactors*, General Electric Co., APED-5706 (1969).
- B-9. Tasako and Sasamoto, "Calculation of Decay Power of Fission Fragments," *Nucl. Sci. and Eng.*, 54, 177-189 (1974).
- B-10. Y. Dayal, B. F. Conroy, and J. P. Neissel, Personal Communication (1968)
- B-11. R. E. Uhrig, "Random Noise Techniques in Nuclear Reactor Systems," The Ronald Press Co. (1970)
- B-12. J. P. Neissel, Personal Communication (1974)
- B-13. J. P. Neissel, Personal Communication (1974)

APPENDIX C
PROCESS COMPUTER EDITS

Figure C-1.. Peach_Bottom-2 EOC2 Test Low-Flow Stability Test (PT1), Process Computer P1 Edit

2

Figure C-2. Peach Bottom-2 EOC2 Test Low-Flow Stability Test (PT2) Process Computer PI Edit

LOCATION	1	2	3	4	5	6	7	8	9	10	11	12	DATE	4157	PERIODIC LOG							
AXIAL REL PWR	0.83	0.86	0.96	1.07	1.23	1.32	1.31	1.24	1.13	1.00	0.79	0.49	TIME	1607	PEACHBOTTOM UNIT 2							
REGION REL PWR	0.96	1.02	0.96	1.02	1.15	1.01	0.96	1.01	0.96				SEQNO	12								
HING REL PWR	1.18	1.15	1.14	1.08	1.10	1.06	1.02	0.78														
APRM GAF	1.00	1.00	1.01	0.98	1.01	0.98																
FAILED LPRM LIST	1609.D.1	4809.C.1	3217.C.2	4817.C.2	5617.B.1	5617.D.1	3225.B.2															
	4025.D.1	4825.B.2	5625.B.1	2433.C.1	4833.C.2	0841.A.1	0841.D.1	5641.C.1														
	5641.D.1	3257.D.1	4057.B.1																			
BASE CHIT CODE																						
FAILED SENSORS	5	6	15	17	25	26							CALIBRATED LPRM READINGS									
REGION	1	2	3	4	5	6	7	8	9				57	14	16	17	19					
MCHFR	4.55	4.73	4.57	4.79	4.08	4.76	4.68	4.75	4.56					24	29	28	32					
LOC	21.22-19	25.14-19	39.22-19	13.36-19	25.30-19	47.26-19	21.40-19	35.48-19	39.40-19					31	39	37	44					
FLOW	0.0439	0.0445	0.0439	0.0445	0.0433	0.0445	0.0441	0.0445	0.0439					32	38	38	38					
PKFL	1.46	1.50	1.46	1.50	1.49	1.51	1.45	1.50	1.46					49	14	20	21	25	20	19		
MFLPD	0.528	0.528	0.525	0.530	0.483	0.530	0.529	0.528	0.524					28	36	41	44	37	28			
LOC	17.18-12	25.18-13	43.18-12	17.36-13	35.36-12	43.26-13	17.44-12	35.44-13	43.44-12					34	43	48	47	48	36			
PKFL	2.19	2.18	2.17	2.19	2.00	2.19	2.19	2.19	2.17					35	30	28	26	30	37			
MAXEQ	0.311	0.297	0.311	0.295	0.331	0.296	0.306	0.297	0.311					41	22	21	24	25	22	19		
LOC	21.22	25.14	39.22	13.36	25.30	47.26	21.40	35.48	39.40					38	41	44	46	43	40	30		
FLOW	0.0439	0.0445	0.0439	0.0445	0.0433	0.0445	0.0441	0.0445	0.0439					48	48	41	41	46	47	40		
PKF	1.27	1.24	1.27	1.23	1.31	1.23	1.26	1.23	1.27					29	28	31	31	33	27	34		
														33	22	22	22	24	24	21	17	
														38	40	41	47	48	39	29		
														46	40	45	50	44	46	39		
														27	26	33	35	32	25	34		
59		48	48	48	48	48	48	48	48					OPERATOR	NON SYM							
55		48	48	36	48	36	48	36	48					SUBS VAL	ROD LOC							
51		48	48	32	48	30	48	30	48					CR LOC	FIRST QUAD							
47		48	48	40	48	42	48	40	48					25	26	33	36	32	27	37		
43		48	48	32	48	30	48	24	48					17	20	22	23	24	23	14		
39		48	36	48	40	48	48	48	48					32	43	42	43	41	38	23		
35		48	48	30	48	24	48	32	48					39	51	46	41	47	47	30		
31		48	36	48	42	48	48	48	48					33	28	29	30	26	31	32		
27		48	48	30	48	24	48	32	48					33	28	29	30	26	31	32		
23		48	36	48	40	48	48	48	48					09D	18	20	23	23	17			
19		48	48	32	48	30	48	24	48					C	29	35	39	37	29			
15		48	48	40	48	40	48	42	48					B	38	45	48	46	35			
11		48	48	32	48	30	48	30	48					A	33	28	27	26	35			
07		48	48	36	48	36	48	36	48													
03																						
	02	06	10	14	18	22	26	30	34	38	42	46	50	54	58							

Figure C-3. Peach Bottom-2 EOC2 Test Low-Flow Stability Test (PT3) Process Computer P1 Edit

24

Figure C-4. Peach Bottom-2 EOC2 Test Low-Flow Stability Test (PT4) Process Computer P1 Edit

LOCATION	1	2	3	4	5	6	7	8	9	10	11	12	DATE	4 9 /7	PERIODIC LOG		
AХАІ REL PWH	0.47	0.69	0.81	0.91	1.03	1.20	1.20	1.40	1.39	1.28	1.00	0.52	TIME	0527	PEACHBOTTOM UNIT 2		
REGION REL PWR	1.04	0.98	1.04	0.98	0.90	0.98	1.04	0.98	1.04								
RING REL PWR	0.97	0.85	0.95	0.83	0.86	0.04	1.22	1.05									
APRM GAF	0.98	1.00	0.99	1.00	0.99	0.98											
FAILED LPRM LIST	1609,D,1	4809,C,1	3217,C,1	4817,C,1	5617,B,2	5617,D,1	3225,B,1						CMWT	1562	PR 094		
4025,D,1	4825,B,1	5625,B,2	2433,C,1	4833,C,1	0841,A,1	0841,D,1	5641,C,2						GMWE	471.4	DPC M 2 /2		
5641,D,1	3257,D,1	4057,B,2											CMCHFR	5.48	DPC C 20.44		
													CMFLPD	0.483	RWL 23.62		
													CMPF	2.401	DHS 13.31		
													CMEQ	0.132	WFW 5.86		
													CAEQ	0.060	WD 43.57		
													CAQA	0.075	WTSUB -1.00		
													CAVF	0.235	WTHB -1.00		
													CAPD	24.07	WT 101.30		
													CRD	0.239	WTFLAG 5.		
													CRSYM	1.	ITER 1		
													IREC	0			
													IFQL	0			
BASE CRIT CODE																	
FAILED SENSORS	5	6	10	15	17	21	25	28									
053114 VALP T055	99.4																
REGION	1	2	3	4	5	6	7	8	9						CALIBRATED LPRM READINGS		
MCHFR	5.48	5.86	5.49	5.89	7.37	5.89	5.49	5.87	5.50								
LOC	21.6 16	25.6 16	55.22 16	5.36 16	23.30 16	55.26 16	5.40 16	35.56 16	39.56 16								
FLOW	0.1129	0.1143	0.1129	0.1143	0.1299	0.1143	0.1130	0.1143	0.1130				57	19	21	22	25
PKFL	2.48	2.37	2.47	2.36	1.76	2.36	2.47	2.37	2.47				30	38	38	42	
MFLPD	0.483	0.459	0.482	0.457	0.364	0.457	0.481	0.459	0.481				29	40	35	43	
LOC	21.6 12	25.6 16	55.22 12	5.36 16	35.32 16	55.26 16	5.40 12	35.56 16	39.56 12				26	32	30	32	
PKFL	2.49	2.37	2.49	2.36	1.88	2.36	2.48	2.37	2.48				49	19	23	25	25
MAXEQ	0.132	0.131	0.132	0.130	0.077	0.131	0.132	0.130	0.132				33	36	40	36	34
LOC	21.6	23.2	55.22	1.38	25.30	59.24	5.40	37.60	39.56				31	29	23	20	32
FLOW	0.1129	0.0693	0.1129	0.0693	0.1217	0.0693	0.1130	0.0603	0.1130				27	20	13	11	28
PKF	1.64	1.00	1.64	0.99	1.13	1.00	1.64	0.99	1.63				41	25	25	26	24
													39	39	38	37	39
													34	23	27	25	22
													23	12	11	12	14
59		48	48	48	48	48	48	48	48								
55		48	48	38	48	28	48	38	48								
51		48	48	0	48	0	48	0	48				33	27	26	22	24
47		48	48	40	48	20	48	10	48				40	32	32	35	36
43	48	48	0	48	0	48	0	48	0				29	18	28	30	25
39	48	38	48	20	48	40	48	48	40				16	9	14	14	12
35	48	48	0	48	0	48	0	48	0				25	28	25	22	24
													38	39	36	36	40
													32	20	27	30	25
													17	10	12	15	13
31	48	28	48	16	48	48	40	48	48								
27	48	48	0	48	0	48	0	48	0								
23	48	38	48	20	48	40	48	48	40								
19	48	48	0	48	0	48	0	48	0								
15	48	48	40	48	20	48	16	48	20								
11	48	48	0	48	0	48	0	48	0								
07	48	48	38	48	28	48	38	48	48								
03	48	48	48	48	48	48	48	48	48								
02	06	10	14	18	22	26	30	34	38				09D	19	24	27	22
													C	32	37	42	37
													B	32	33	28	33
													A	27	20	17	18
													08	16	24	32	40
																	56

Figure C-5. Peach Bottom-2 EOC2 Test Turbine Trip Transient (TT1) Process Computer P1 Edit

Figure C-6. Peach Bottom-2 EOC2 Test Turbine Trip Transient Test (TT2) Process Computer P1 Edit

Figure C-7. Peach Bottom-2 EOC2 Test Turbine Trip Transient Test (TT3) Process Computer P1 Edit

APPENDIX D
ADDITIONAL TURBINE TRIP TEST MEASUREMENTS

Relay
4-27-77 Time 1636 (4³⁶PM) CMFLD = 59
CMWT 2266 57-30-12
CMWE 721
WT 102
CRO .143
DHS 17.8

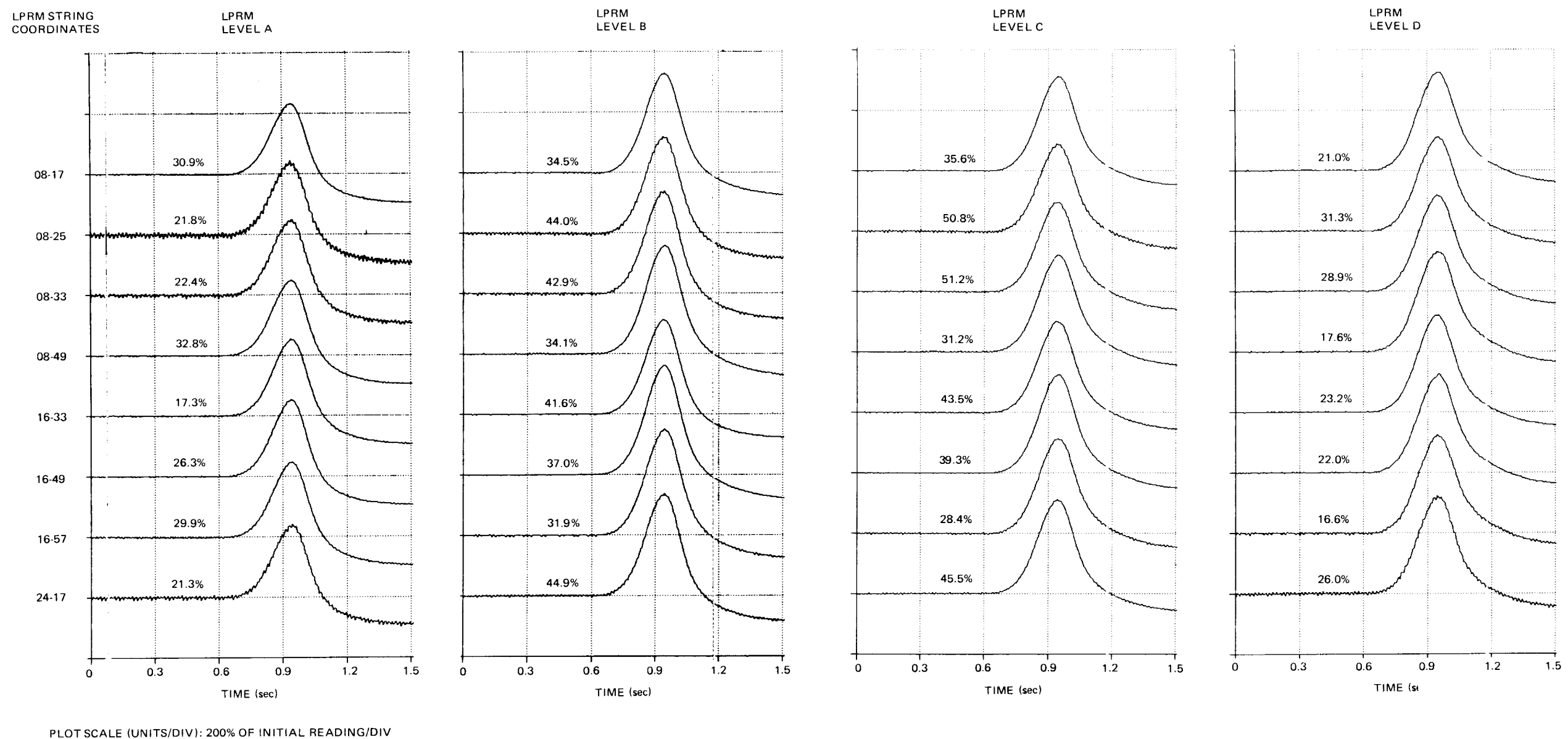
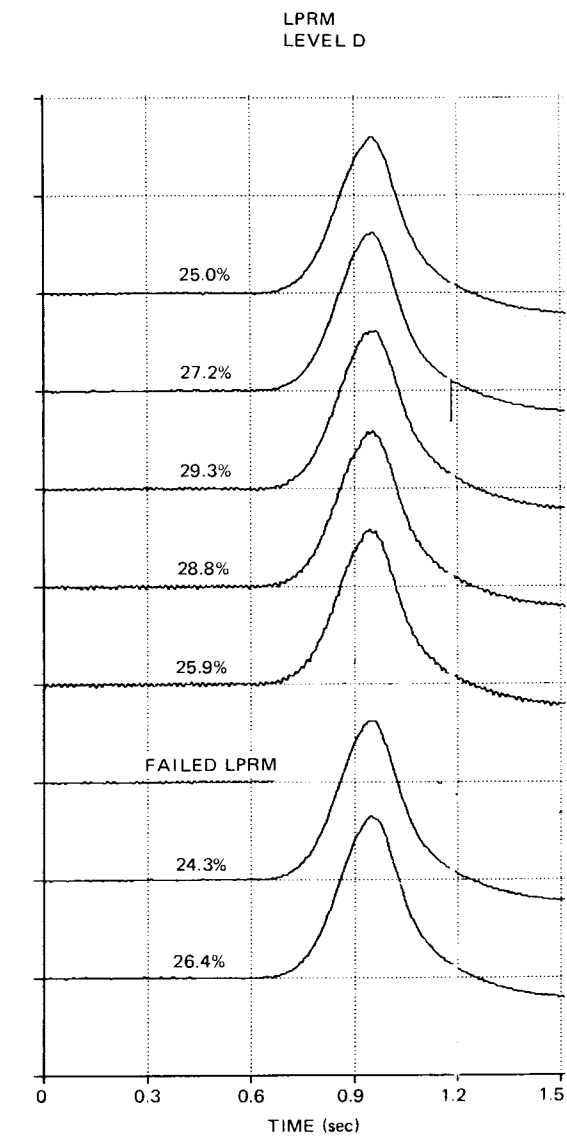
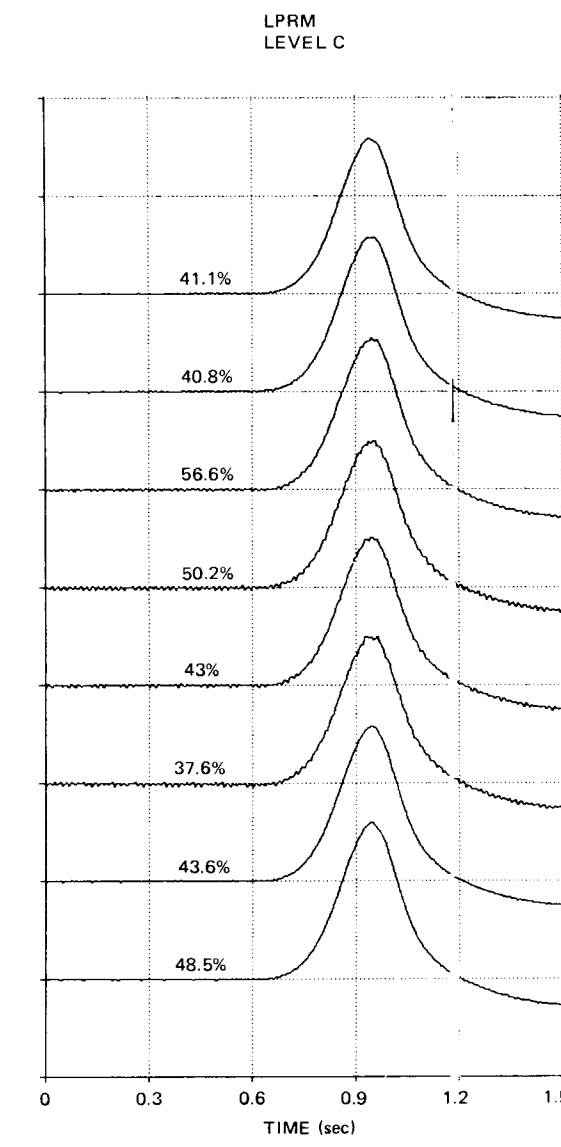
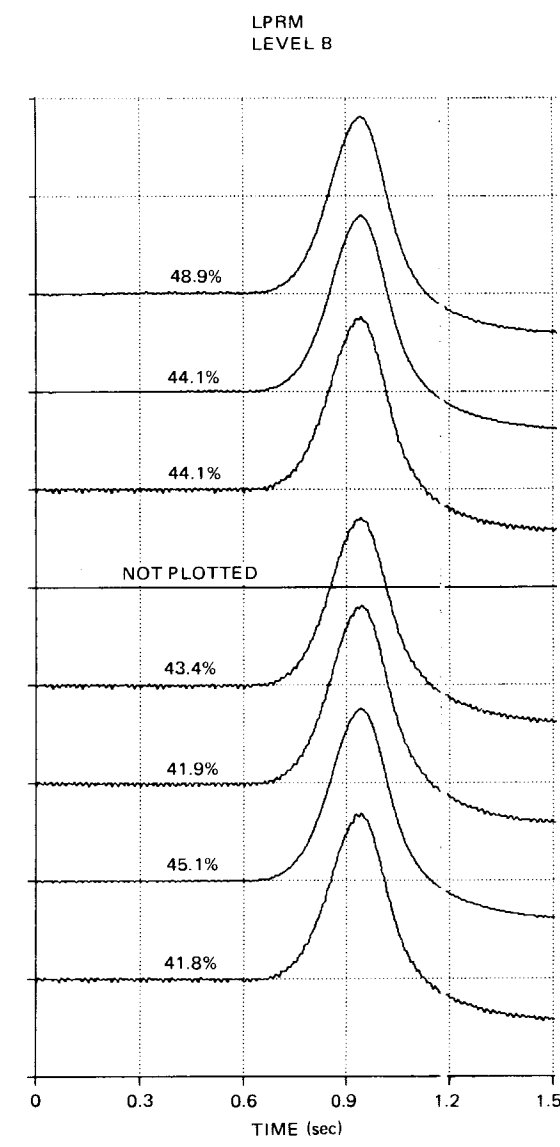
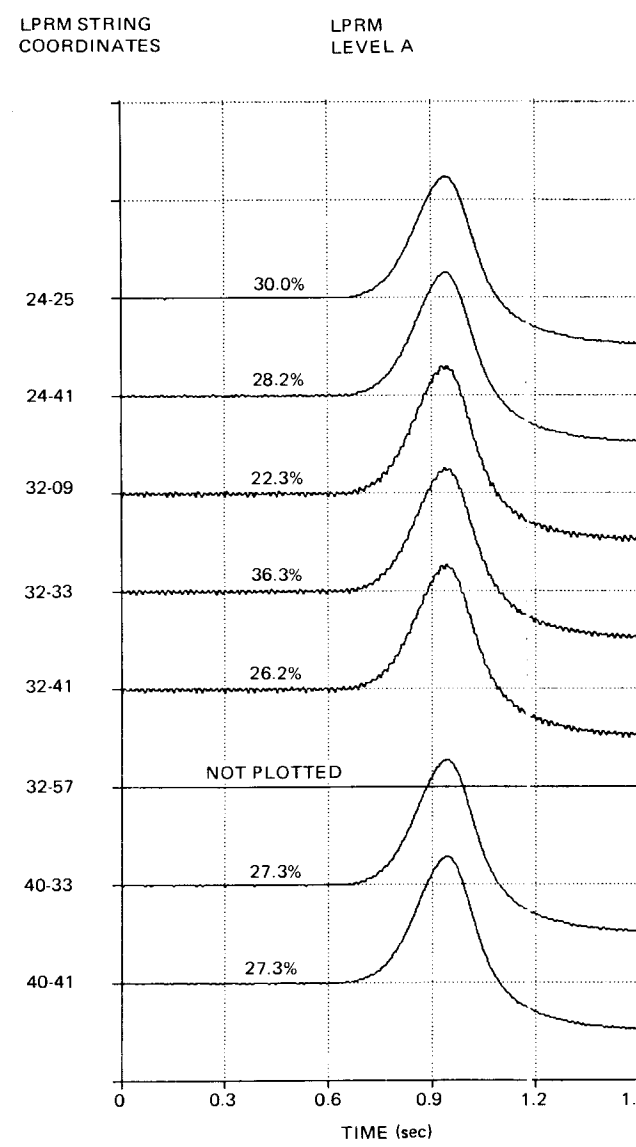
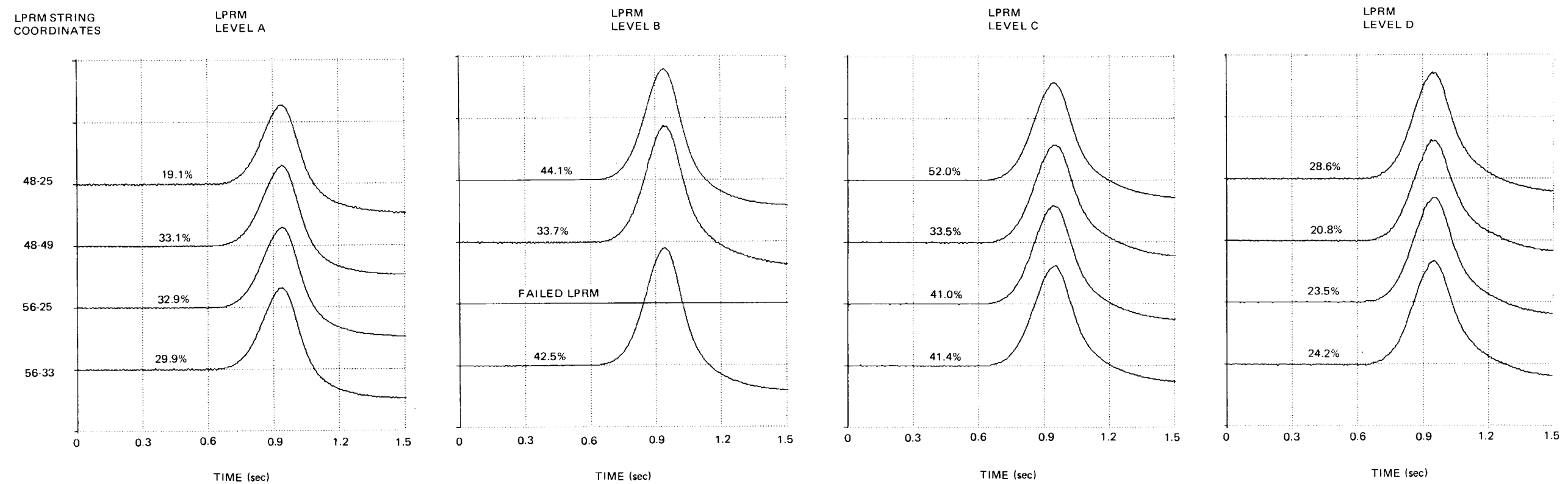


Figure D-1A. Peach Bottom-2 EOC2 Test Turbine Trip Test TT2 Core Local Power Monitor Response



PLOT SCALE (UNITS/DIV): 200% OF INITIAL READING/DIV

Figure D-1B. Peach Bottom-2 EOC2 Test Turbine Trip Test TT2 Core Local Power Monitor Response



PLOT SCALE (UNITS/DIV): 200% OF INITIAL READING/DIV

Figure D-1C. Peach Bottom-2 EOC2 Test Turbine Trip Test TT2 Core Local Power Monitor Response

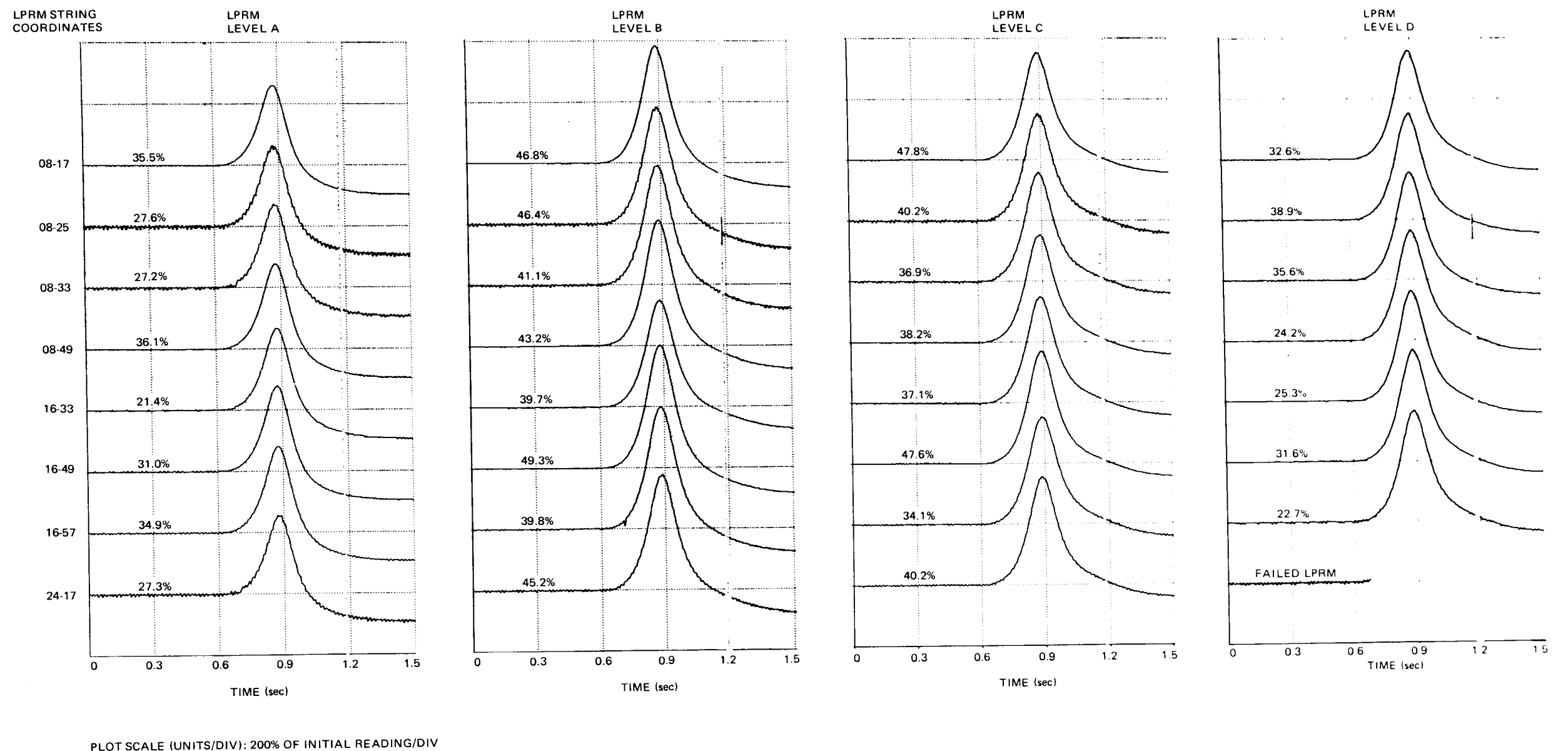


Figure D-2A. Peach Bottom-2 EOC2 Test Turbine Trip Test TT3 Core Local Power Monitor Response

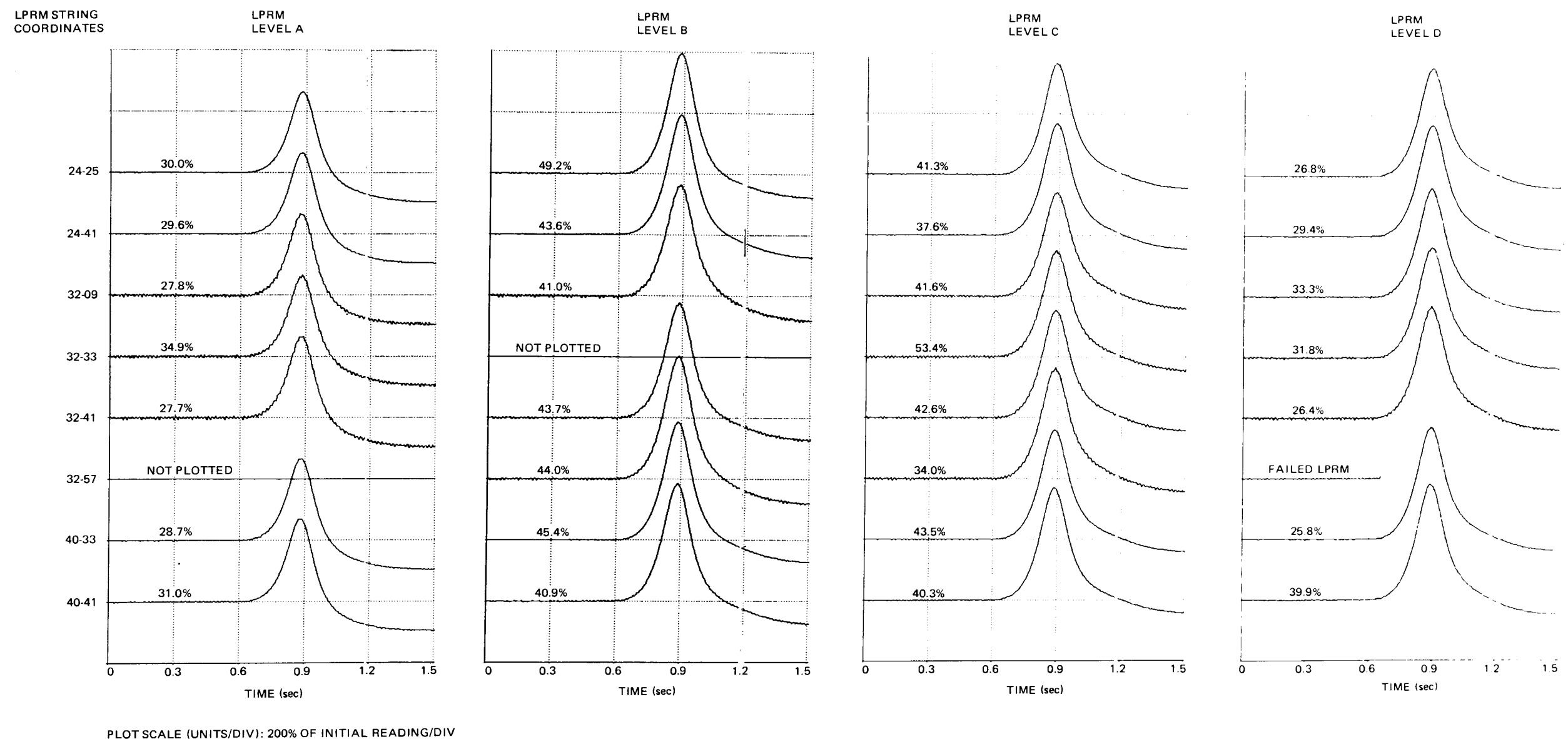
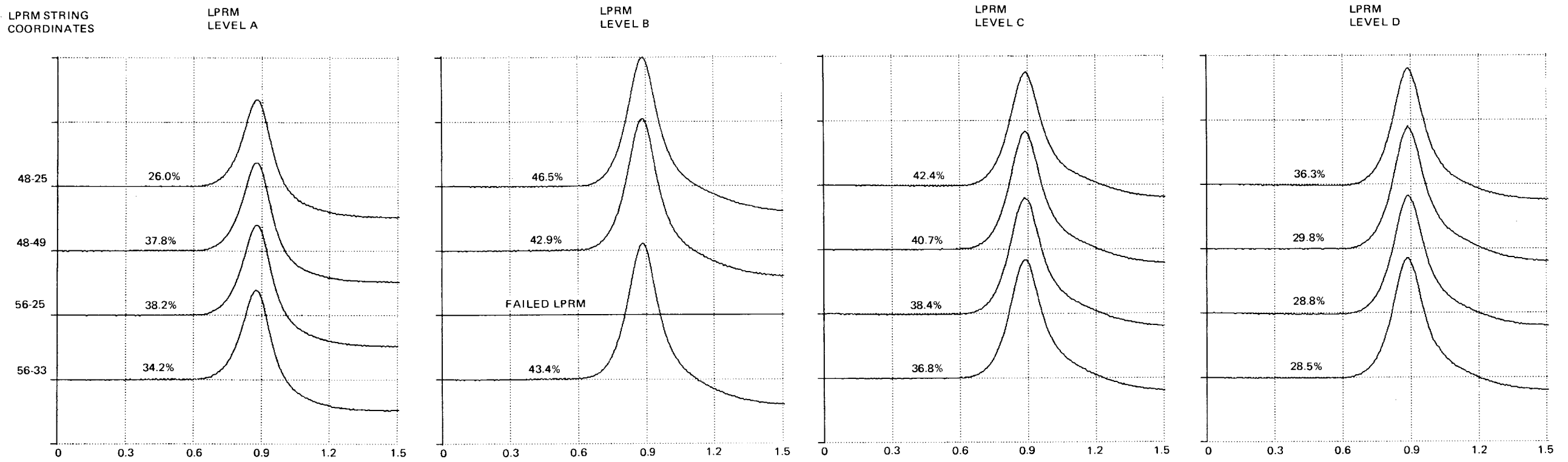


Figure D-2B. Peach Bottom-2 EOC2 Test Turbine Trip Test TT3 Core Local Power Monitor Response



PLOT SCALE (UNITS/DIV): 200% OF INITIAL READING/DIV

Figure D-2C. Peach Bottom-2 EOC2 Test Turbine Trip Test TT3 Core Local Power Monitor Response

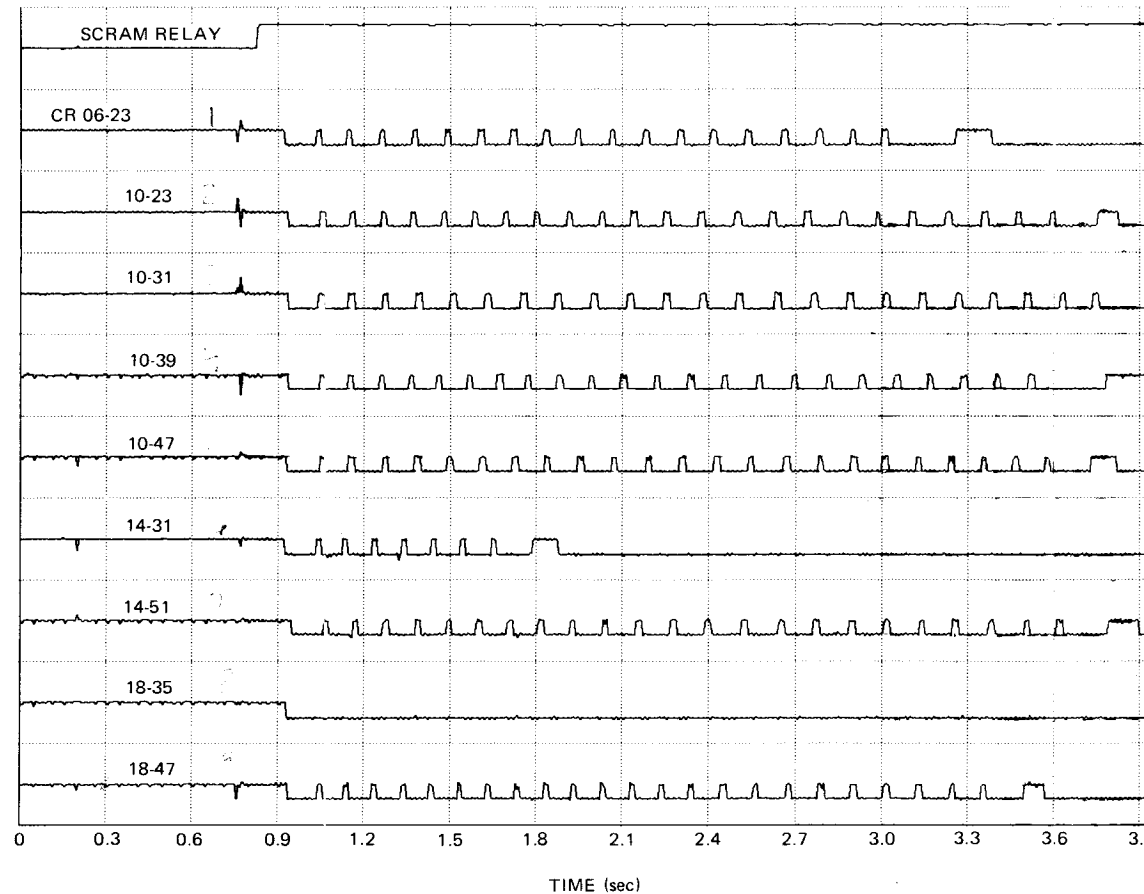


Figure D-3A. Peach Bottom-2 EOC2 Test Turbine
Trip Test TT2 Control Rod Drive
Response

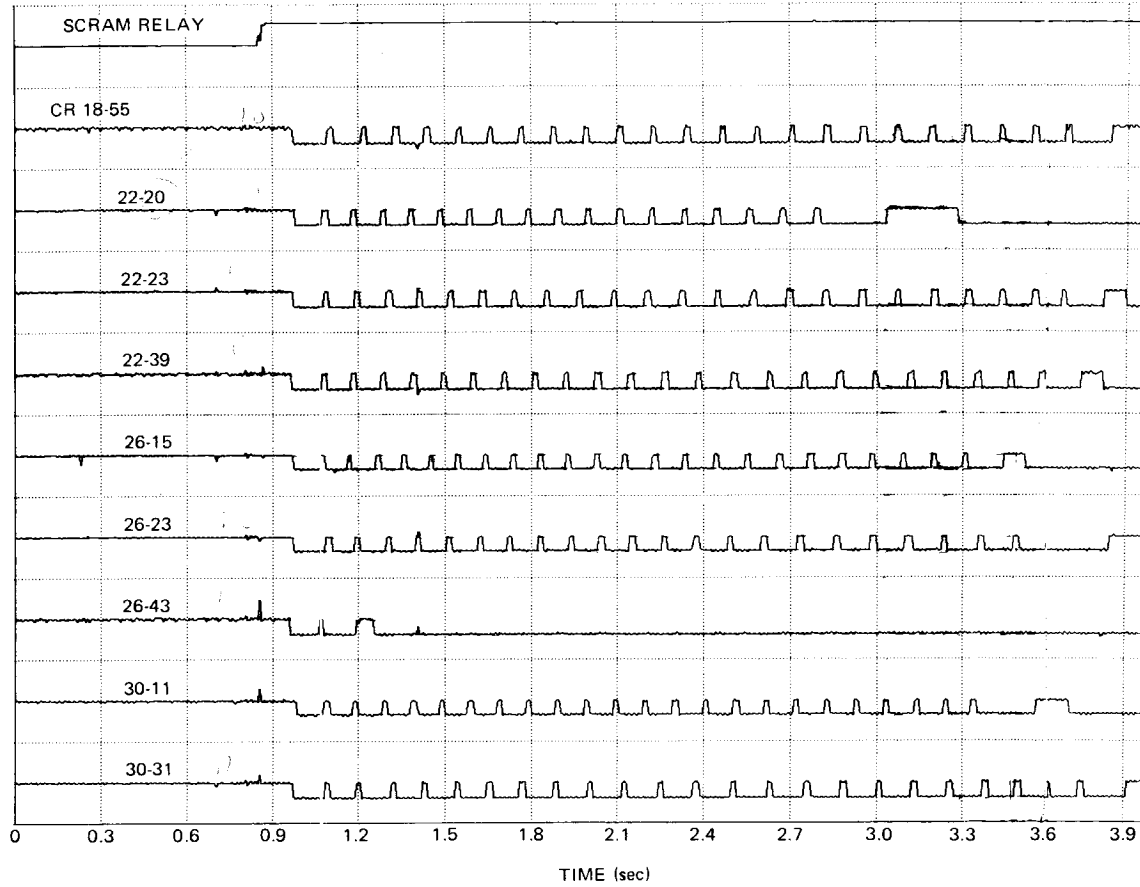


Figure D-3B. Peach Bottom-2 EOC2 Test Turbine
Trip Test TT2 Control Rod Drive
Response

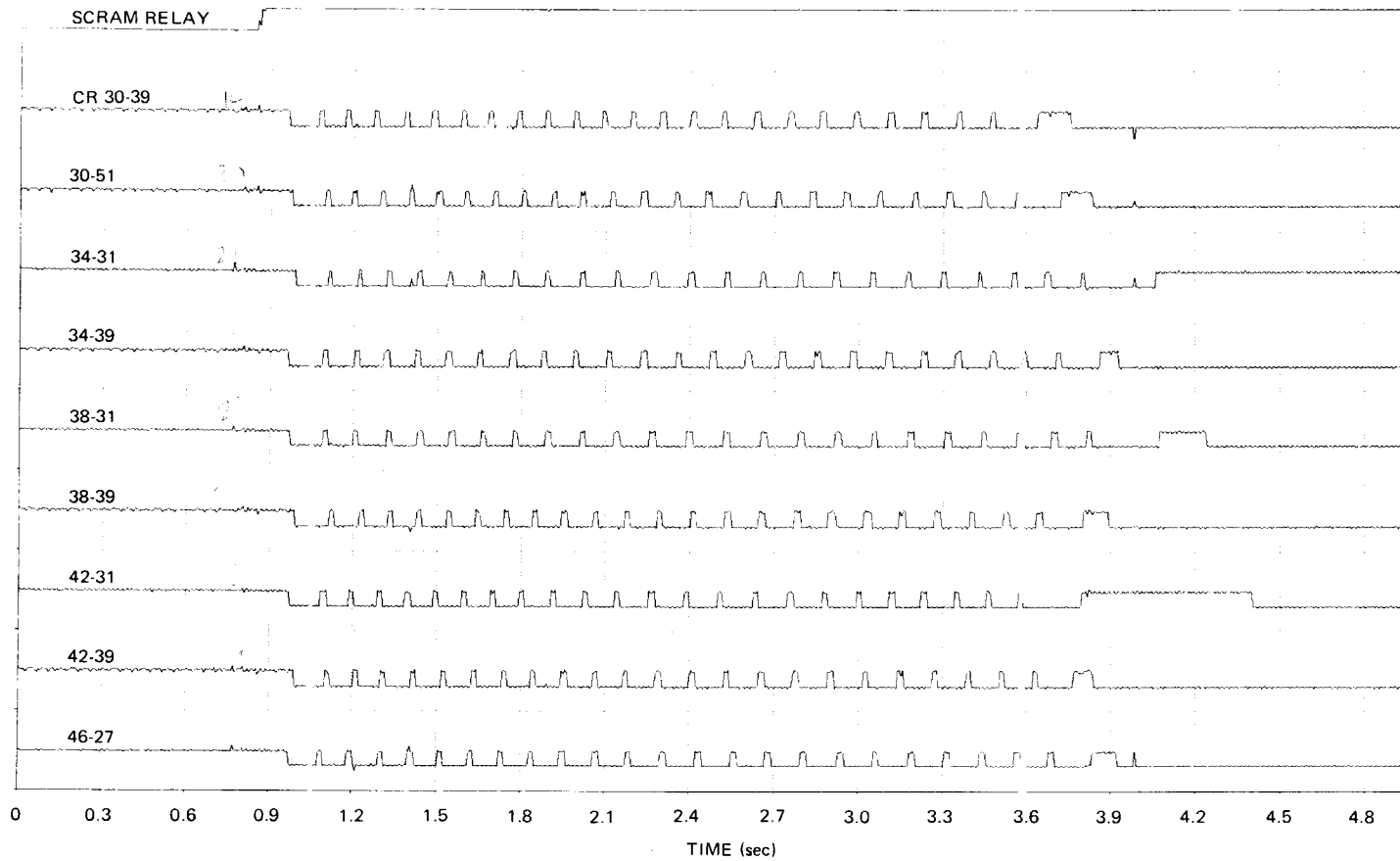


Figure D-3C. Peach Bottom-2 EOC2 Test Turbine
Trip Test TT2 Control Rod Drive
Response

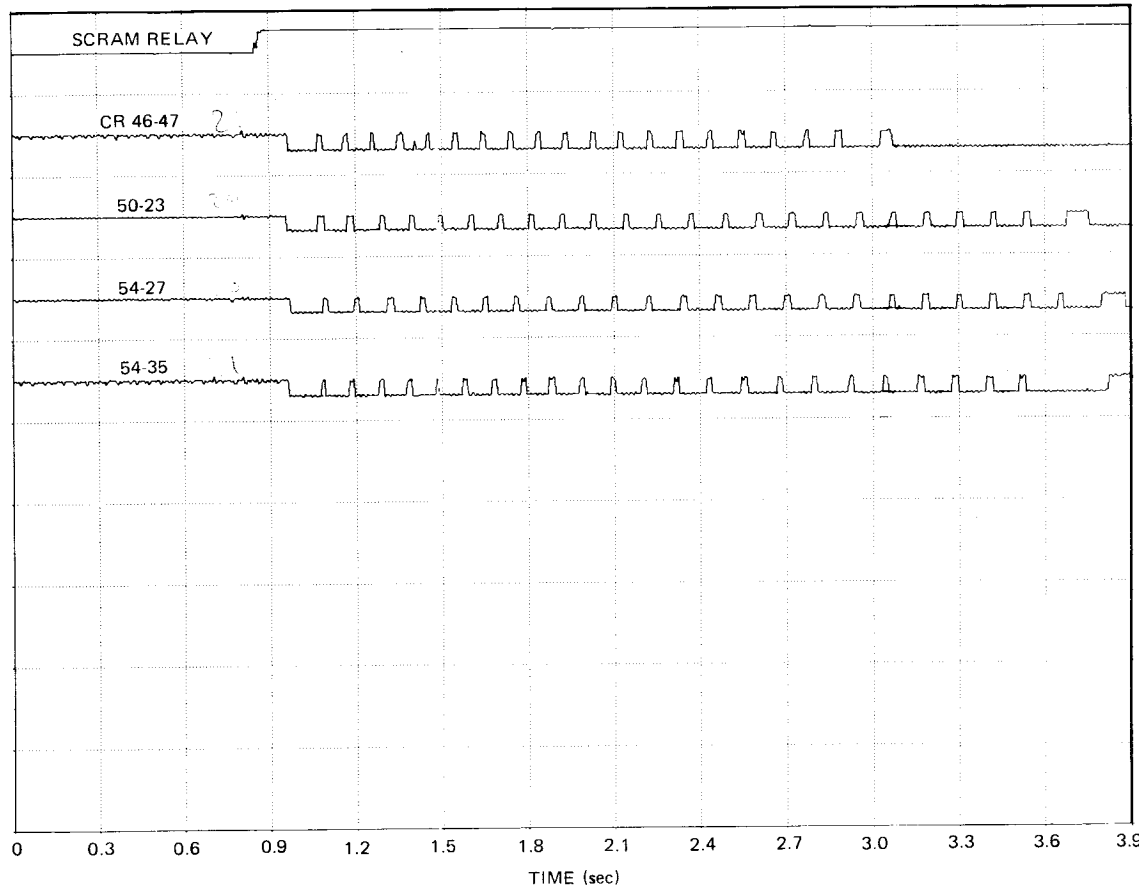


Figure D-3D. Peach Bottom-2 EOC2 Test Turbine
Trip Test TT2 Control Rod Drive
Response

D19

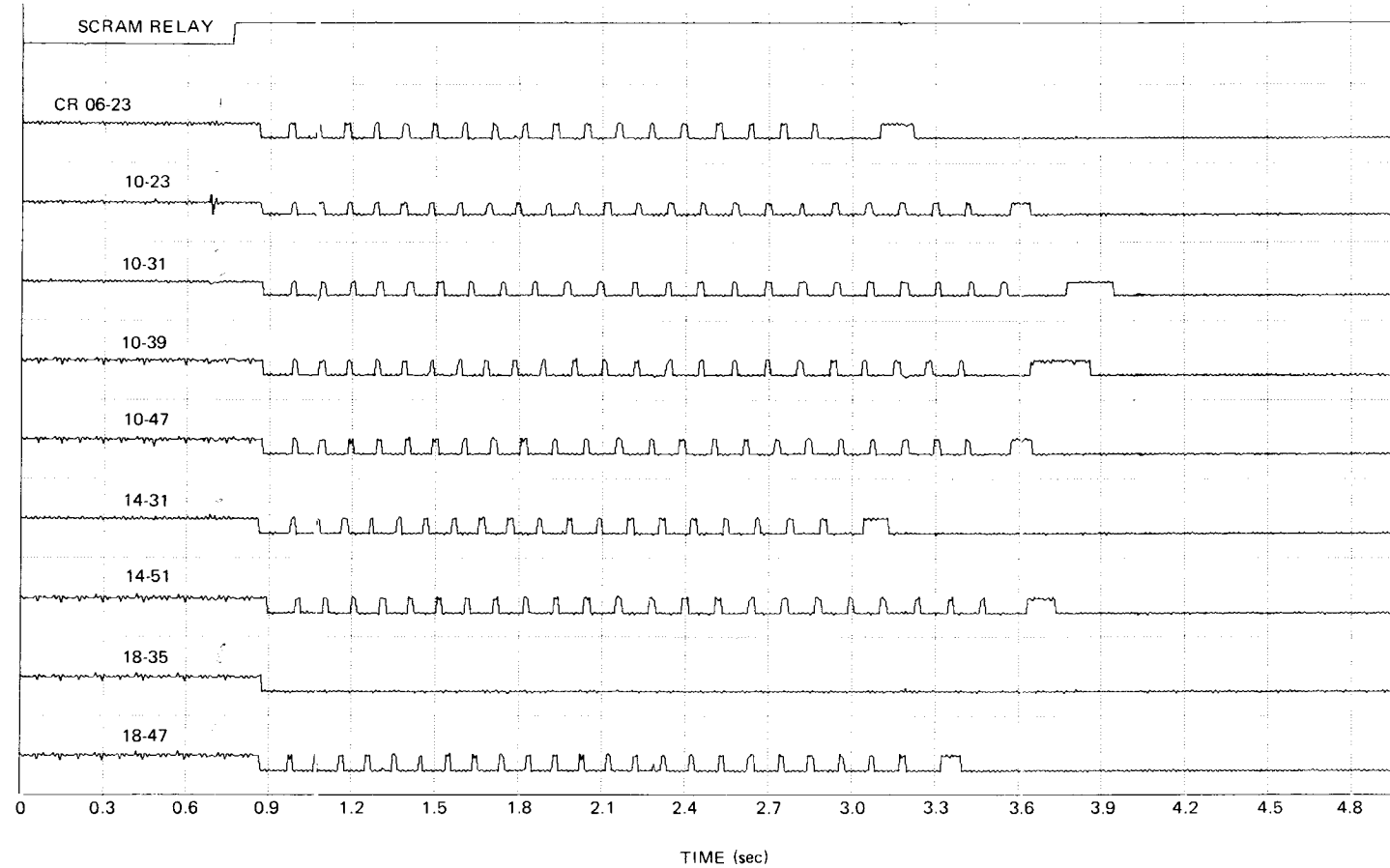


Figure D-4A. Peach Bottom-2 EOC2 Test Turbine
Trip Test TT3 Control Rod Drive
Response

D.20

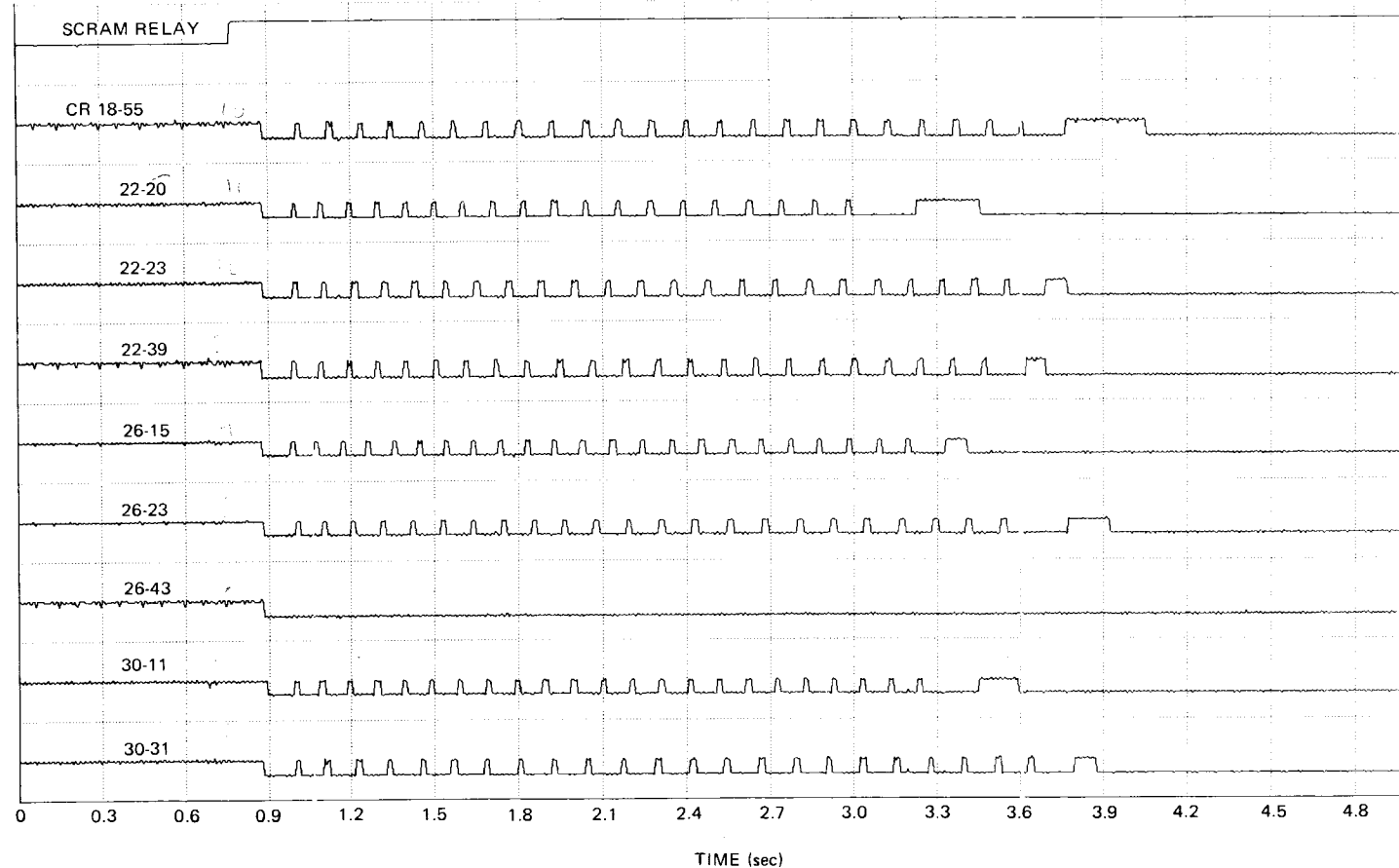


Figure D-4B. Peach Bottom-2 EOC2 Test Turbine
Trip Test TT3 Control Rod Drive
Response

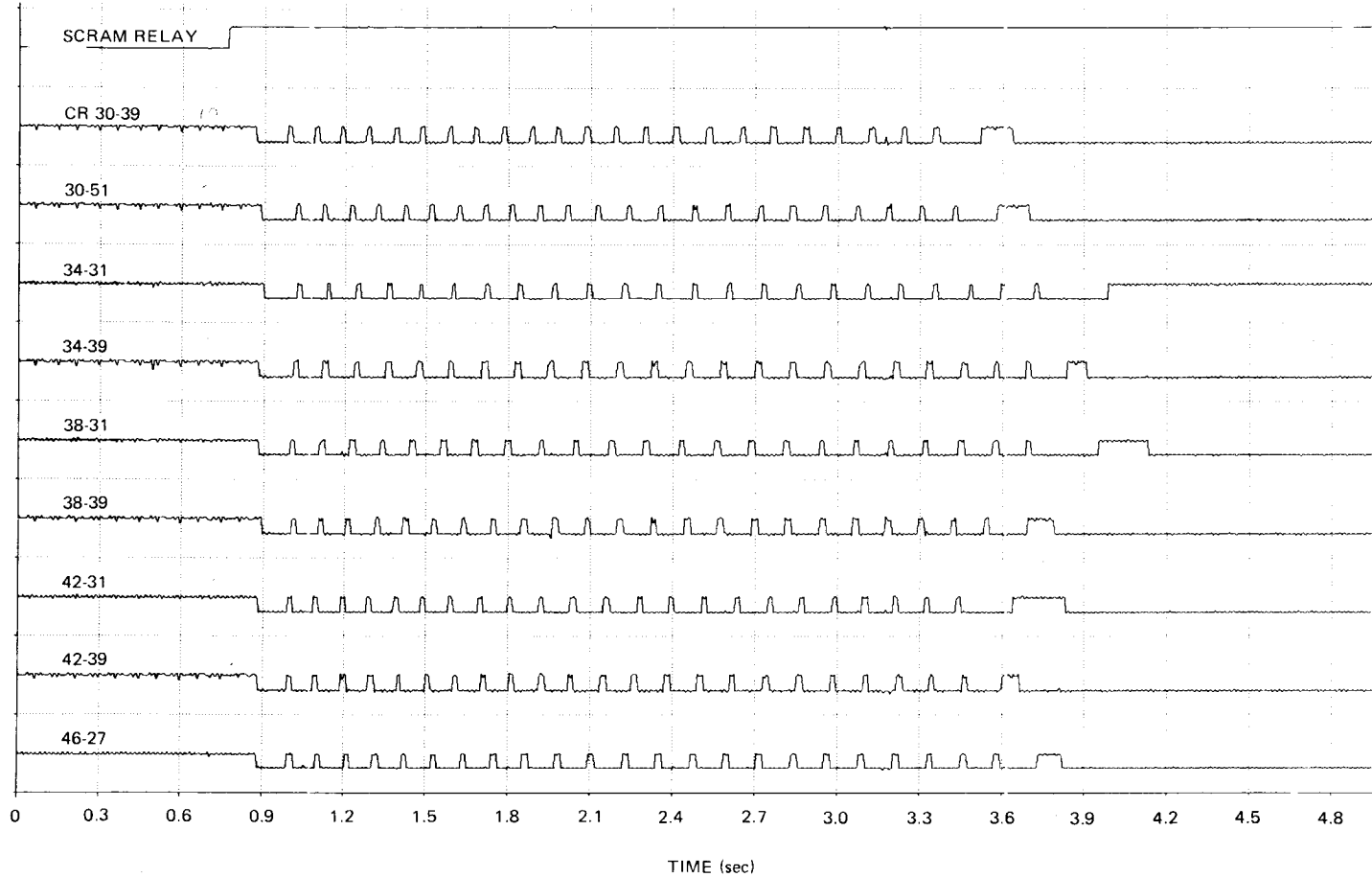


Figure D-4C. Peach Bottom-2 EOC2 Test Turbine
Trip Test TT3 Control Rod Drive
Response

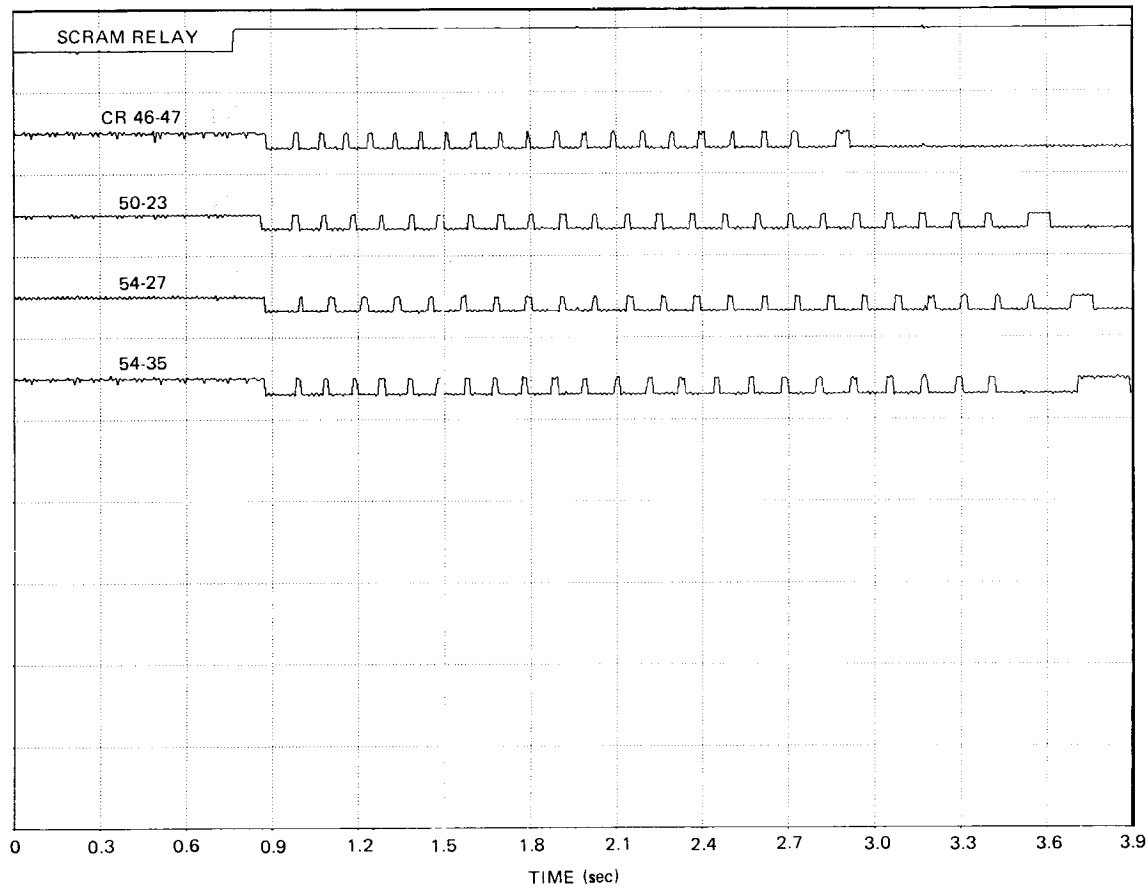


Figure D-4D. Peach Bottom-2 EOC2 Test Turbine Trip Test TT3 Control Rod Drive Response

APPENDIX E

ADDITIONAL LOW-FLOW STABILITY FREQUENCY RESPONSE MEASUREMENTS

Table E-I
LOW-FLOW STABILITY TEST PT1
RESULTS OF EMPIRICAL TRANSFER FUNCTION
MODEL PARAMETER IDENTIFICATION

Model Order	1 Zero 2 Poles	1 Zero 3 Poles
a_0	0.3201 ± 0.067	0.3442 ± 0.056
a_1	1.025 ± 0.030	1.0419 ± 0.063
b_1	0.2301 ± 0.036	0.1272 ± 0.049
b_2	0.1300 ± 0.008	0.1126 ± 0.012
b_3	—	-0.01288 ± 0.012
Gain, K_p (%/psi)	0.3201	0.3442
τ_1 (sec)	3.203	3.027
δ_1 (Dimensionless)	0.318	0.305
ω_1 (Rad/sec)	2.772	2.731
τ_2 (sec)	—	-0.0961 1
Decay Ratio (Dimensionless)	$0.1206 \pm 4.4 \times 10^{-4}$	0.1338 ± 0.046
$S(\bar{\alpha})$	0.02250	0.01668

Table E-2
LOW-FLOW STABILITY TEST PT2
RESULTS OF EMPIRICAL TRANSFER FUNCTION
MODEL PARAMETER IDENTIFICATION

Model Order	1 Zero 2 Poles	1 Zero 3 Poles
a_0	0.2335 ± 0.051	0.3019 ± 0.044
a_1	0.9153 ± 0.072	1.100 ± 0.038
b_1	0.2155 ± 0.032	0.0555 ± 0.049
b_2	0.1140 ± 0.006	0.1089 ± 0.007
b_3		-0.02049 ± 0.005
Gain, K_p (%/psi)	0.2335	0.3019
τ_1 (sec)	3.920	3.644
δ_1 (Dimensionless)	0.319	0.272
ω_1 (Rad/sec)	2.961	2.684
τ_2 (sec)		-0.1476
Decay Ratio (Dimensionless)	$0.1205 \pm 4.2 \times 10^{-4}$	0.1688 ± 0.136
$S(\bar{\alpha})$	0.01688	0.009710

Table E-3
LOW-FLOW STABILITY TEST PT4
RESULTS OF EMPIRICAL TRANSFER FUNCTION
MODEL PARAMETER IDENTIFICATION

Model Order	1 Zero 2 Poles	1 Zero 3 Poles
a_0	0.2836 ± 0.053	0.2833 ± 0.041
a_1	0.9006 ± 0.039	1.044 ± 0.065
b_1	0.1506 ± 0.017	0.07288 ± 0.029
b_2	0.1565 L0.002	0.1532 L0.01 1
b_3	-	-0.01683 ± 0.006
Gain, K_p (%/psi)	0.2836	0.2833
τ_1 (sec)	3.176	3.685
δ_1 (Dimensionless)	0.190	0.208
ω_1 (Rad/sec)	2.528	2.425
τ_2 (sec)		-9.885 x 1 0^-2
Decay Ratio (Dimensionless)	$0.2958 \pm 4.2 \times 10^{-4}$	0.2626 L0.0863
$S(\bar{\alpha})$	0.022853	0.01323

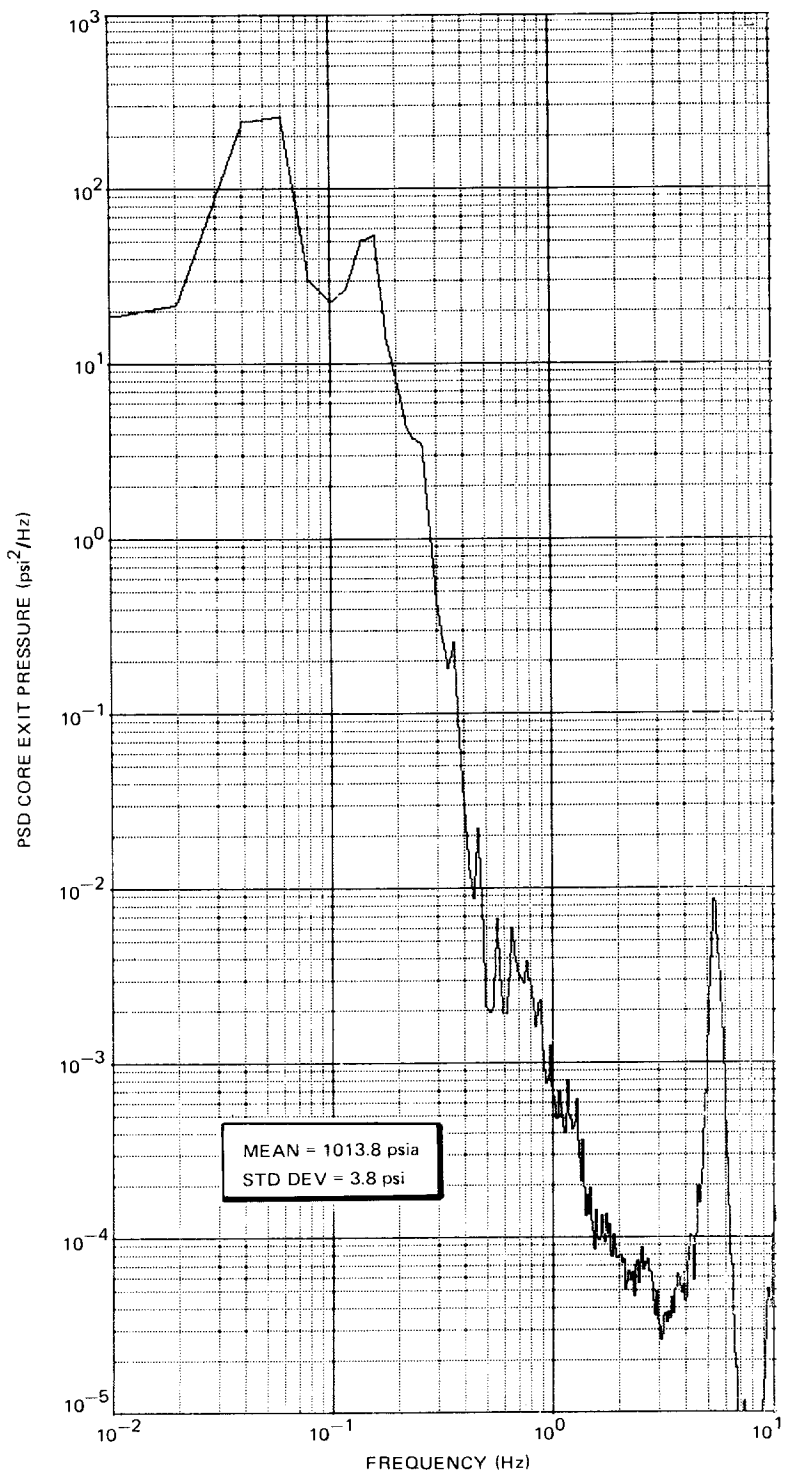


Figure E-1. Peach Bottom-2 EOC2 Low-Flow Stability Test (PT1) Power Spectrum Core Exit Pressure

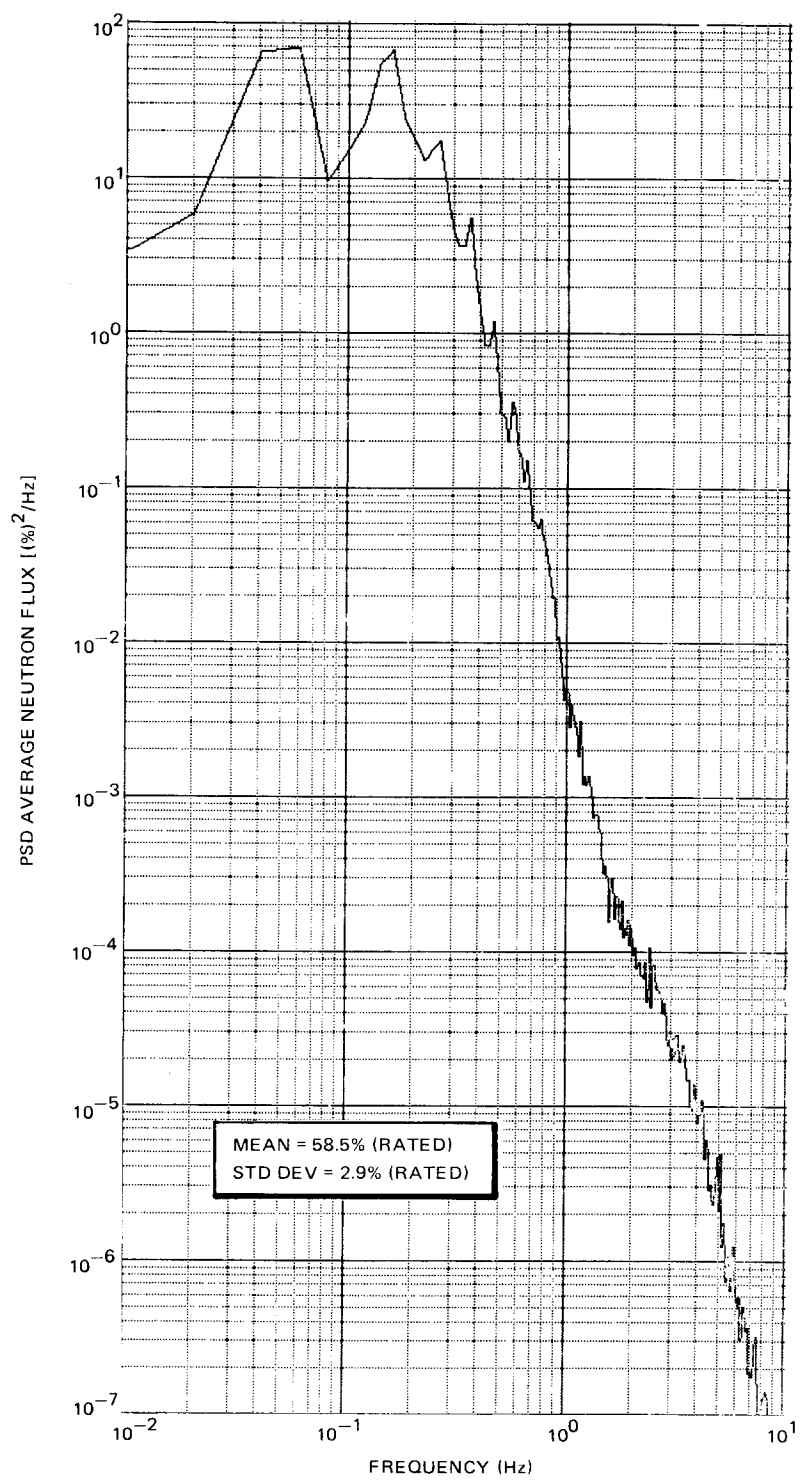


Figure E-2. Peach Bottom-2 EOC2 Low-Flow Stability Test (PT1) Power Spectrum Average Neutron Flux (APRM A)

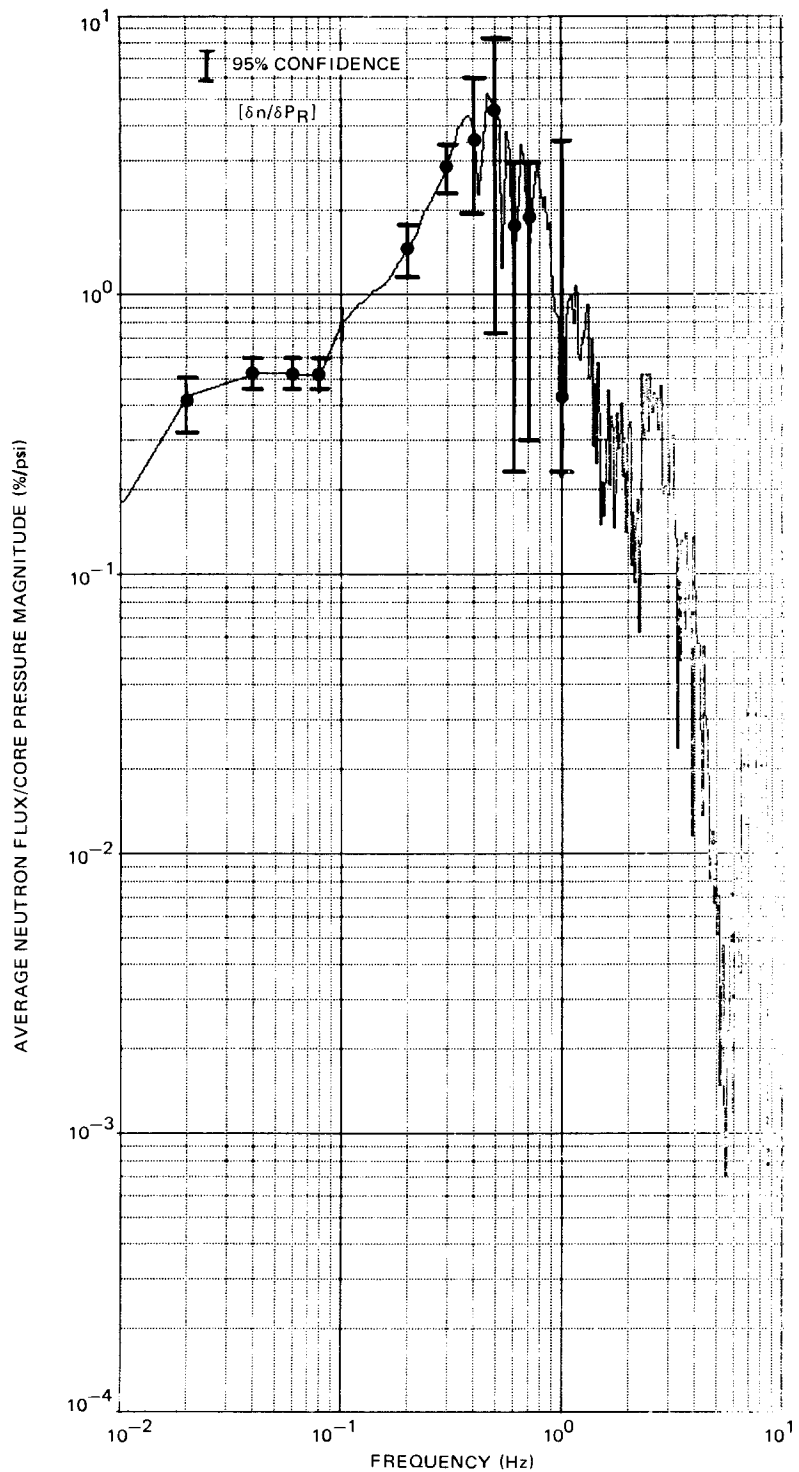


Figure E-3. Peach Bottom-2 EOC2 Low-Flow Stability Test (PT1) Measured Transfer Function Magnitude Average Neutron Flux (APRM A)/Core Pressure

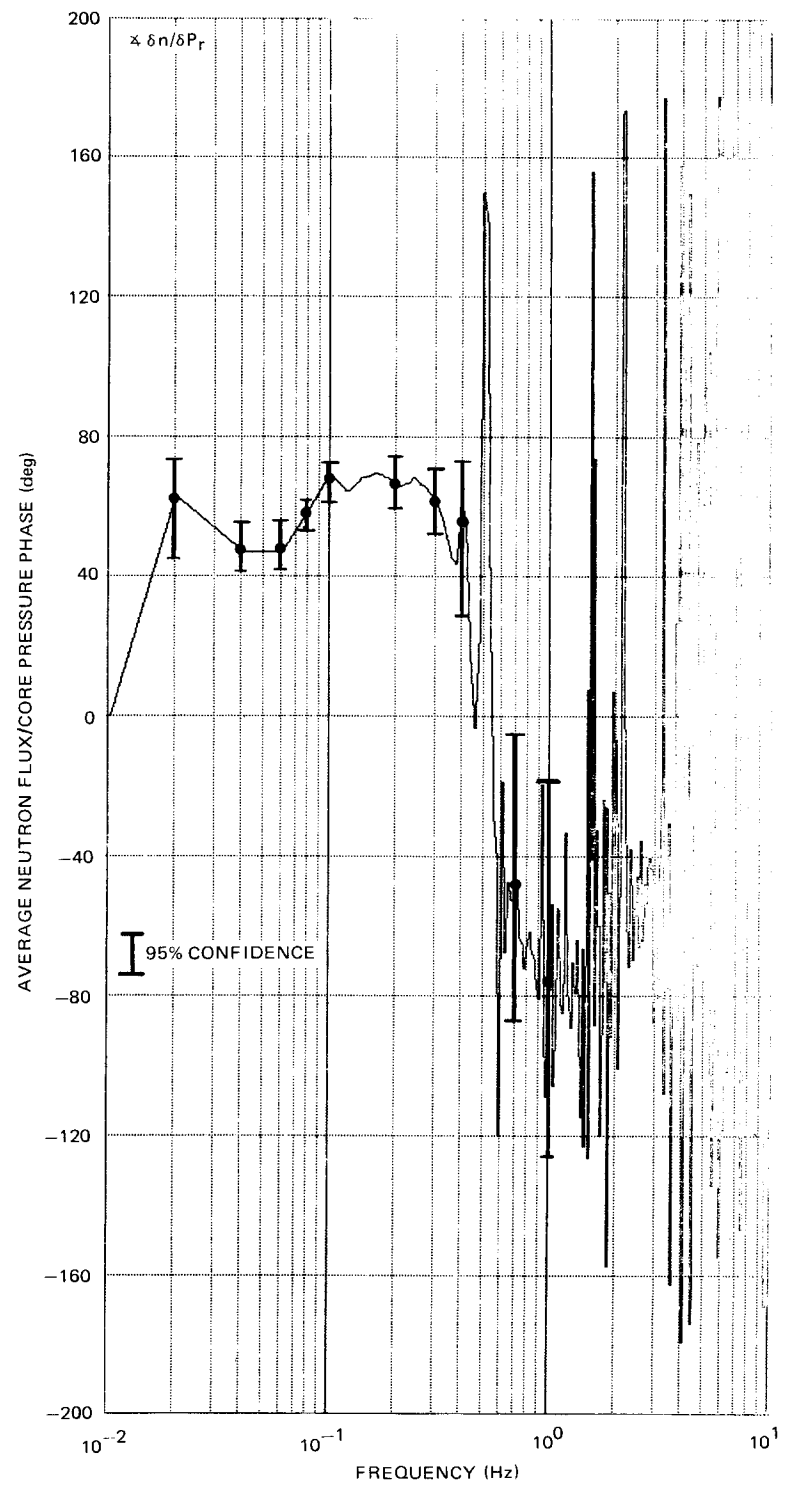


Figure E-4. Peach Bottom-2 EOC2 Low-Flow Stability Test (PT1) Measured Transfer Function Phase Average Neutron Flux (APRM A)/Core Pressure

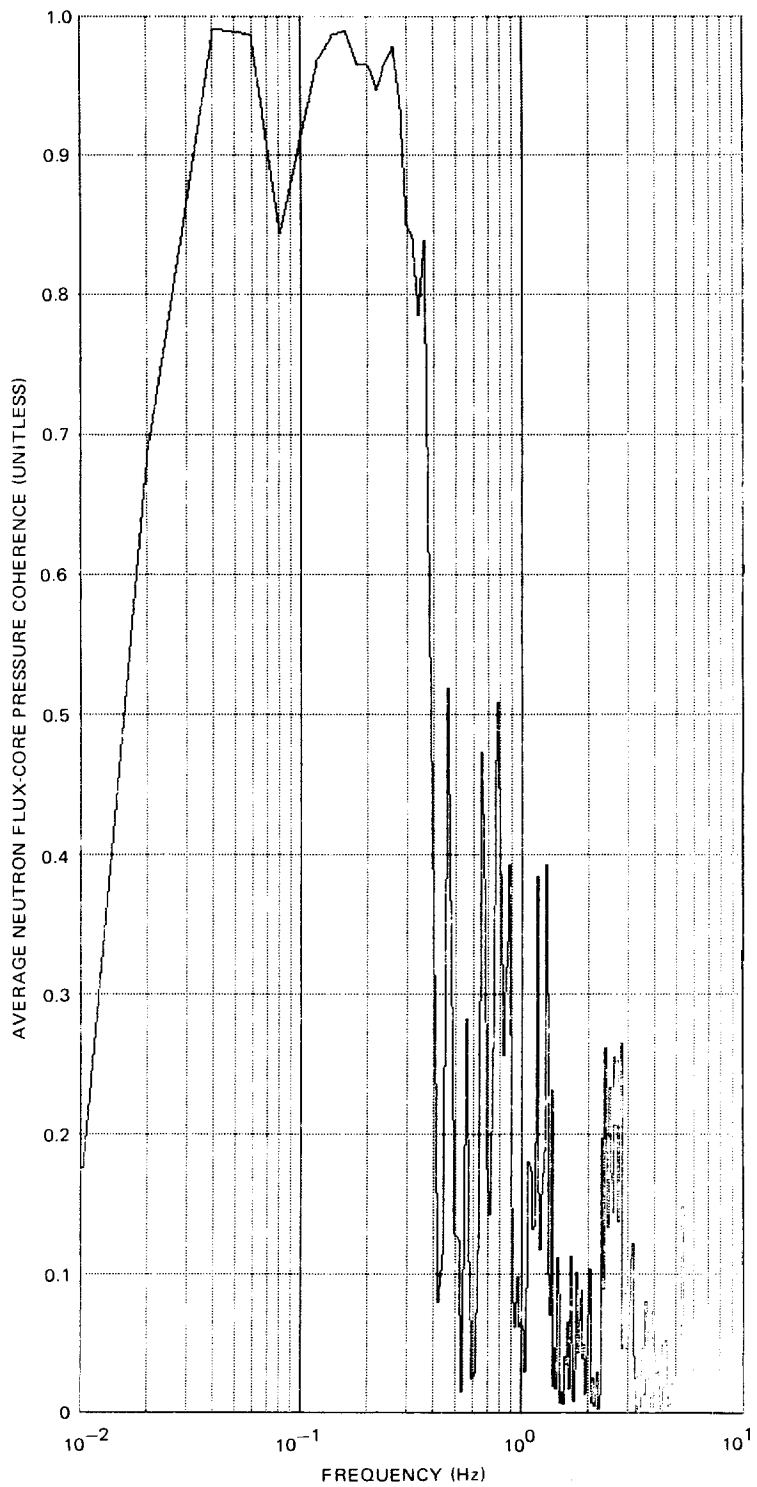


Figure E-5. Peach Bottom-2 EOC2 Low-Flow Stability Test (PT1) Coherence Between Average Neutron Flux (APRM A) and Core Pressure Response

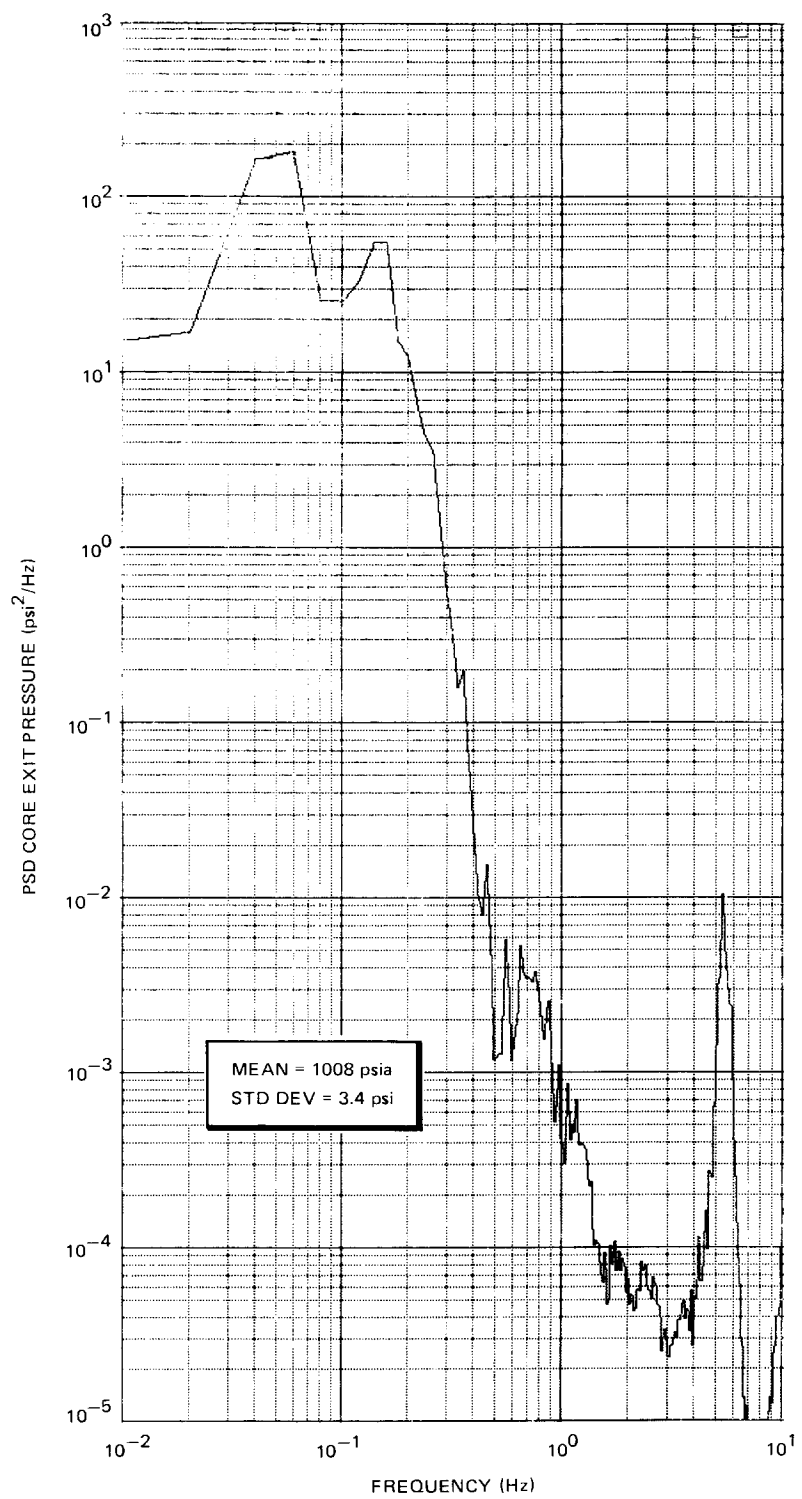


Figure E-6. Peach Bottom-2 EOC2 Low-Flow Stability Test (PT2) Power Spectrum Core Exit Pressure

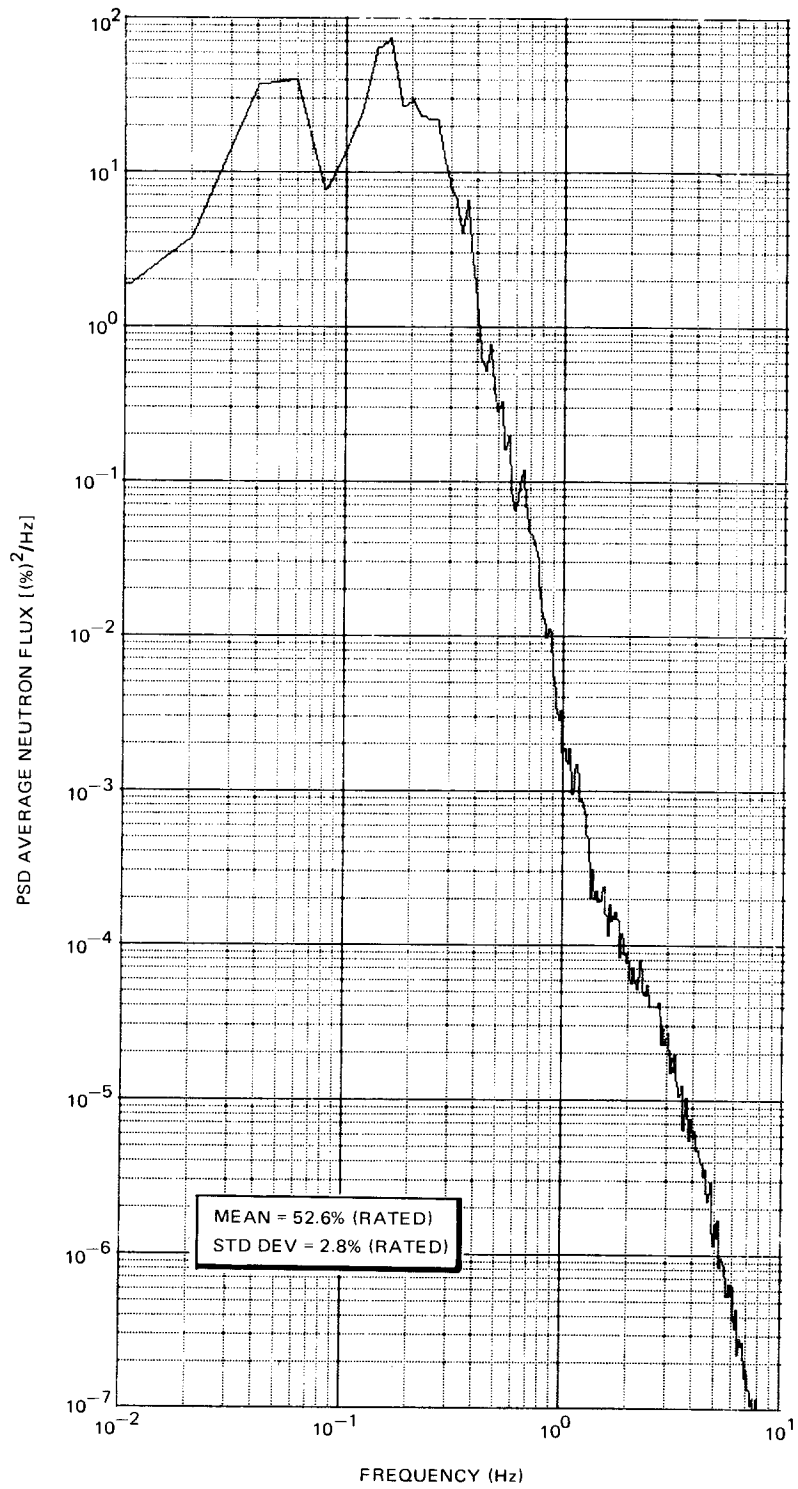


Figure E-7. Peach Bottom-2 EOC2 Low-Flow Stability Test (PT2) Power Spectrum Average Neutron Flux (APRM A)

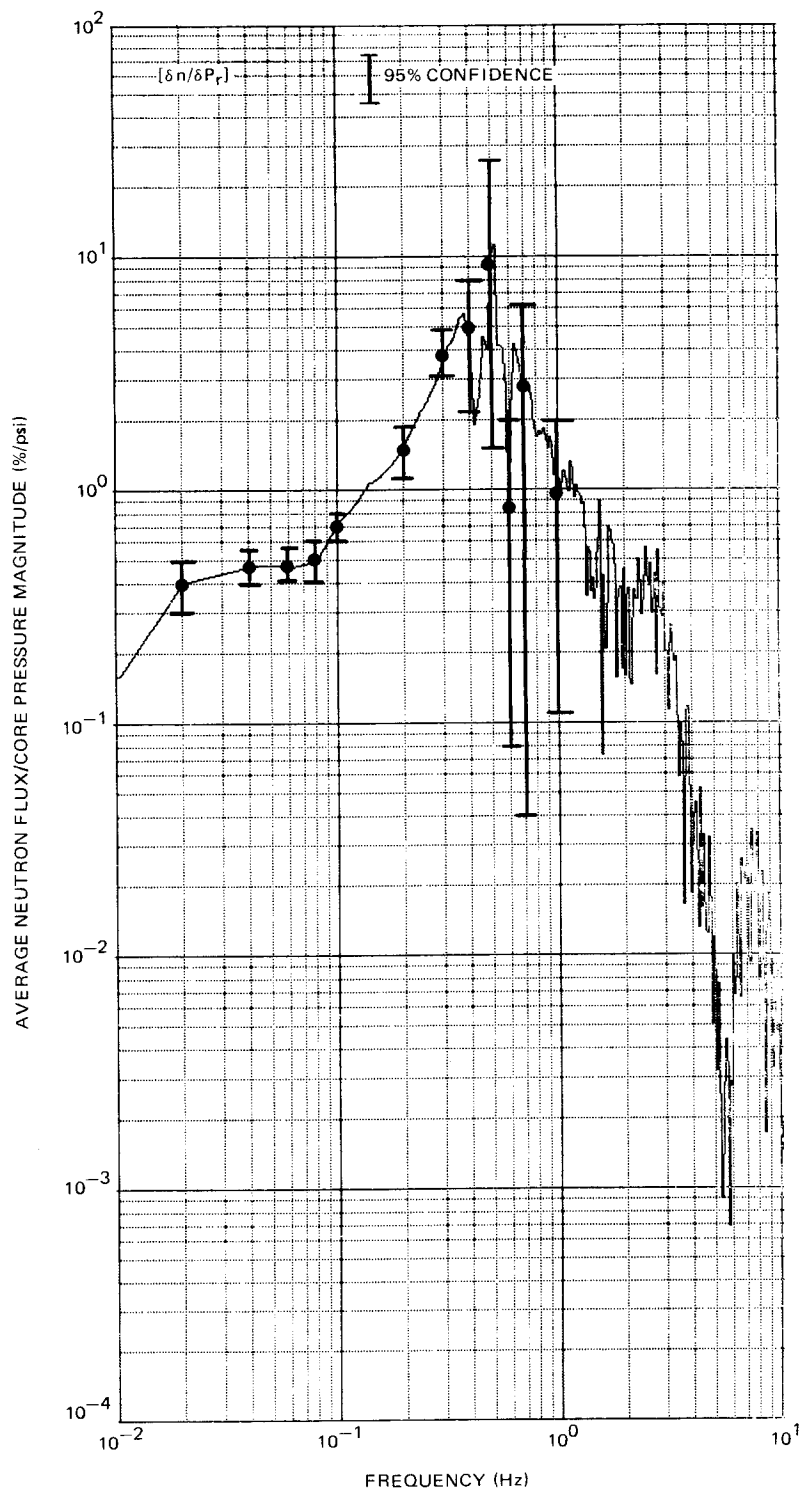


Figure E-8. Peach Bottom-2 EOC2 Low-Flow Stability Test (PT2) Measured Transfer Function Magnitude Average Neutron Flux (APRM A)/Core Pressure

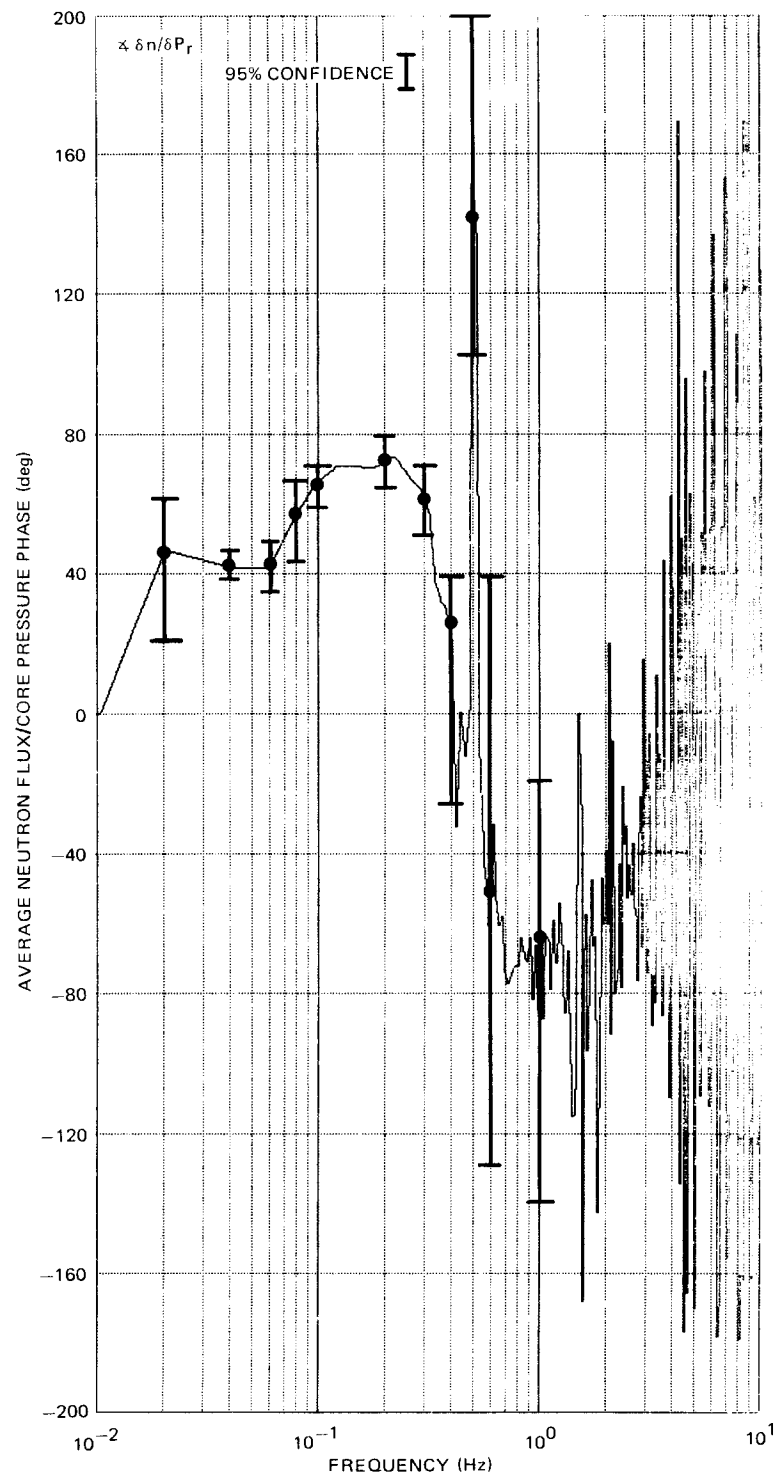


Figure E-9. Peach Bottom-2 EOC2 Low-Flow Stability Test (PT2) Measured Transfer Function Phase Average Neutron Flux (APRM A)/Core Pressure

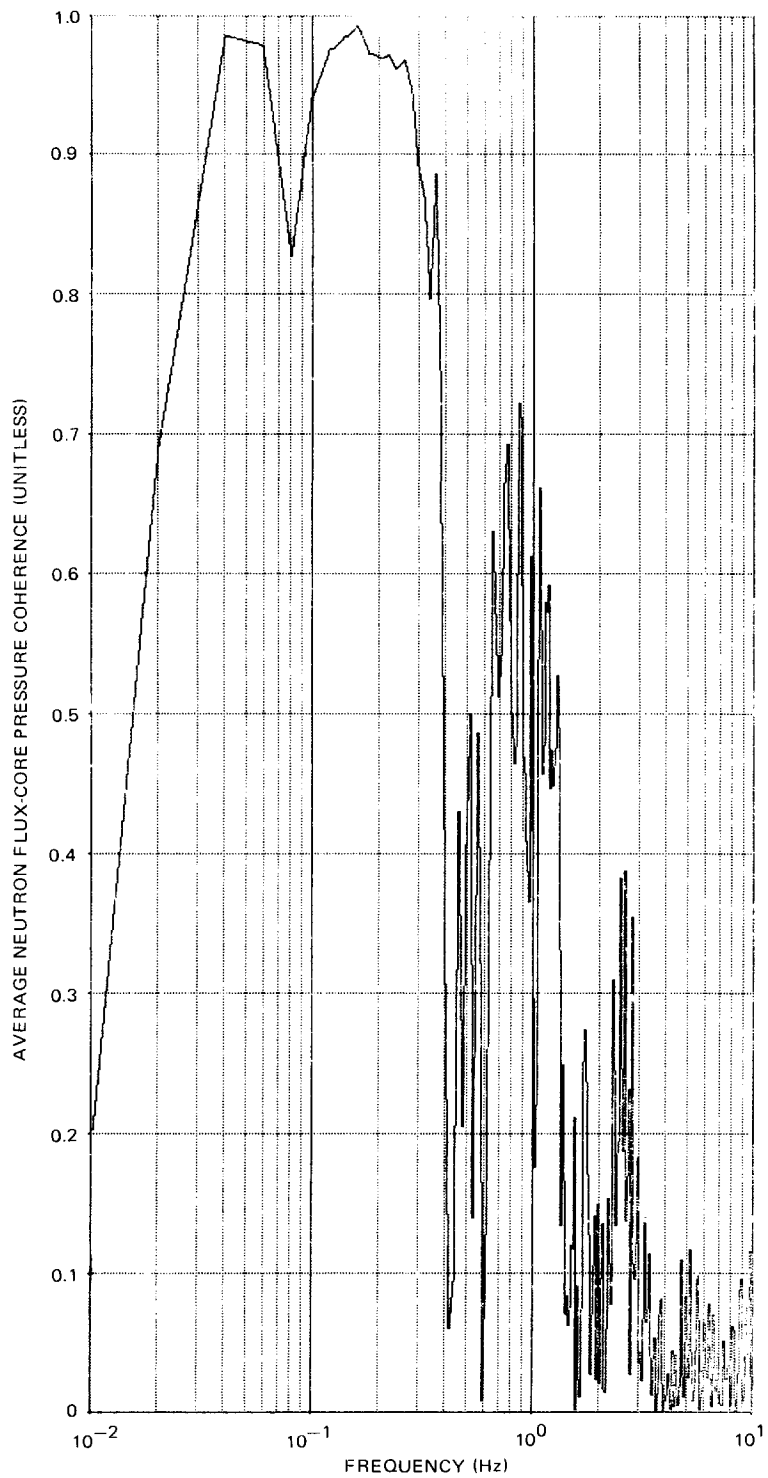


Figure E-10. Peach Bottom-2 EOC2 Low-Flow Stability Test (PT2) Coherence Between Average Neutron Flux (APRM A) and Core Pressure Response

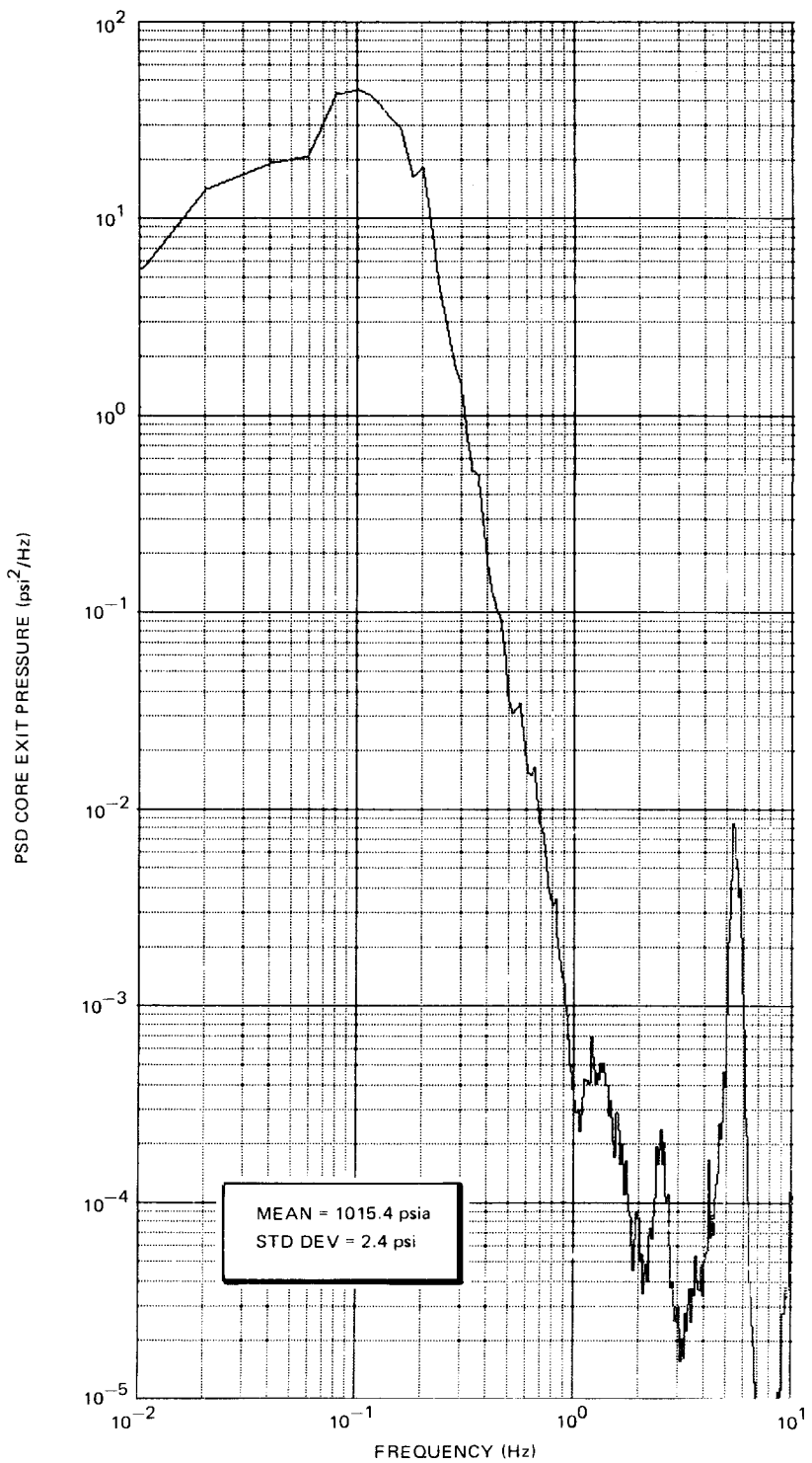


Figure E-11. Peach Bottom-2 EOC2 Low-Flow Stability Test (PT4) Power Spectrum Core Exit Pressure

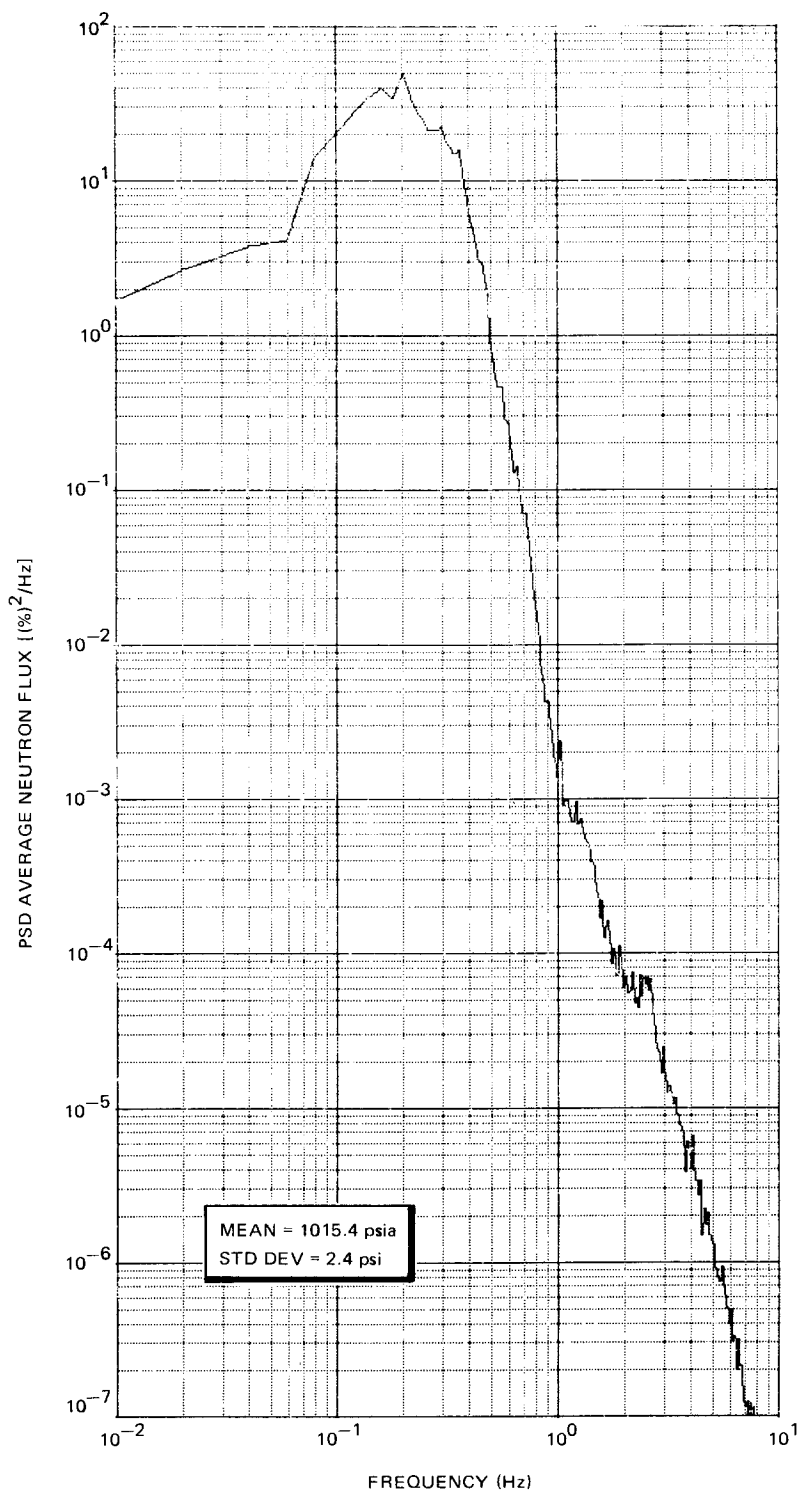


Figure E-12. Peach Bottom-2 EOC2 Low-Flow Stability Test (PT4) Power Spectrum Average Neutron Flux (APRM A)

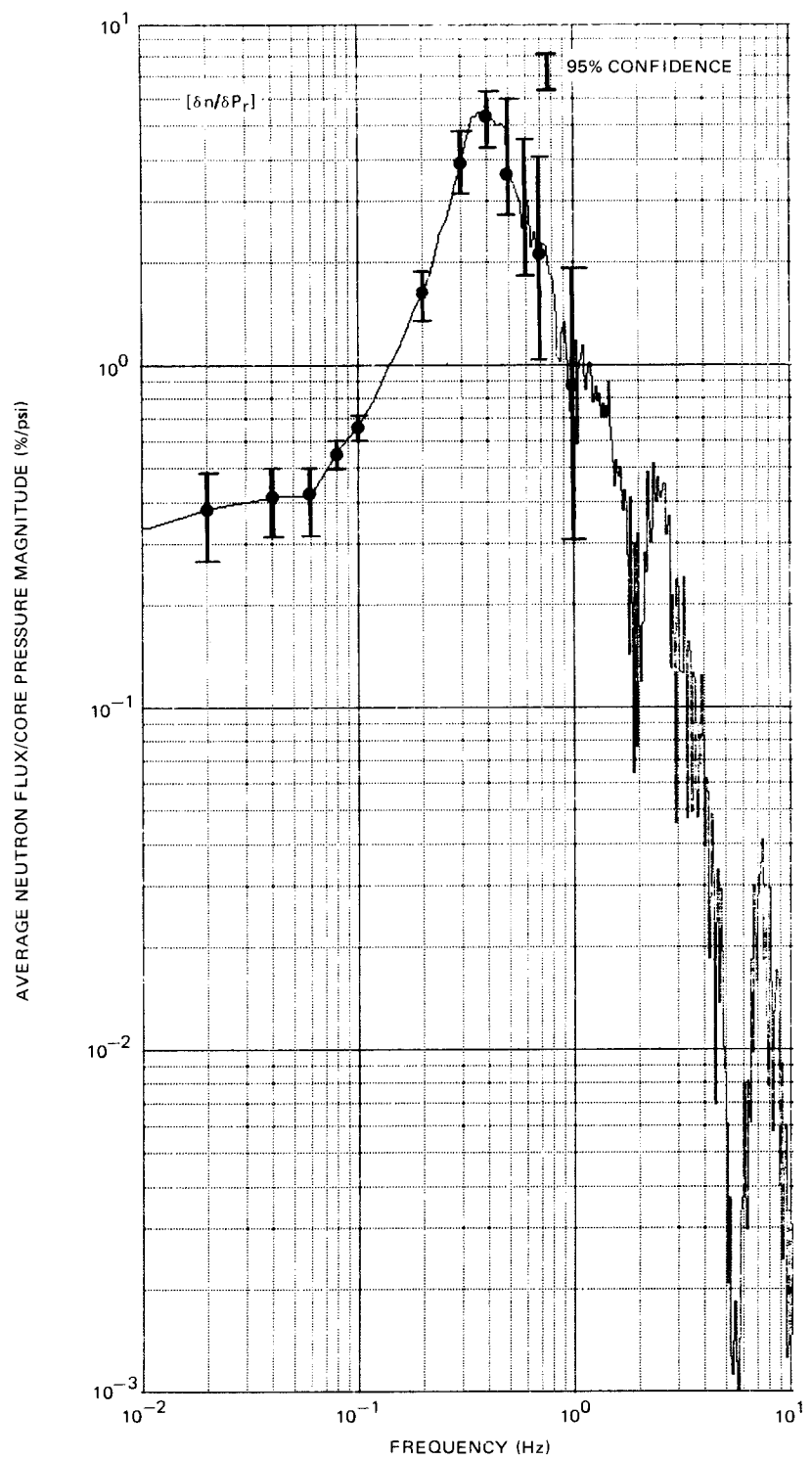


Figure E-13. Peach Bottom-2 EOC2 Low-Flow Stability Test (PT4) Measured Transfer Function Magnitude Average Neutron Flux (APRM A)/Core Pressure

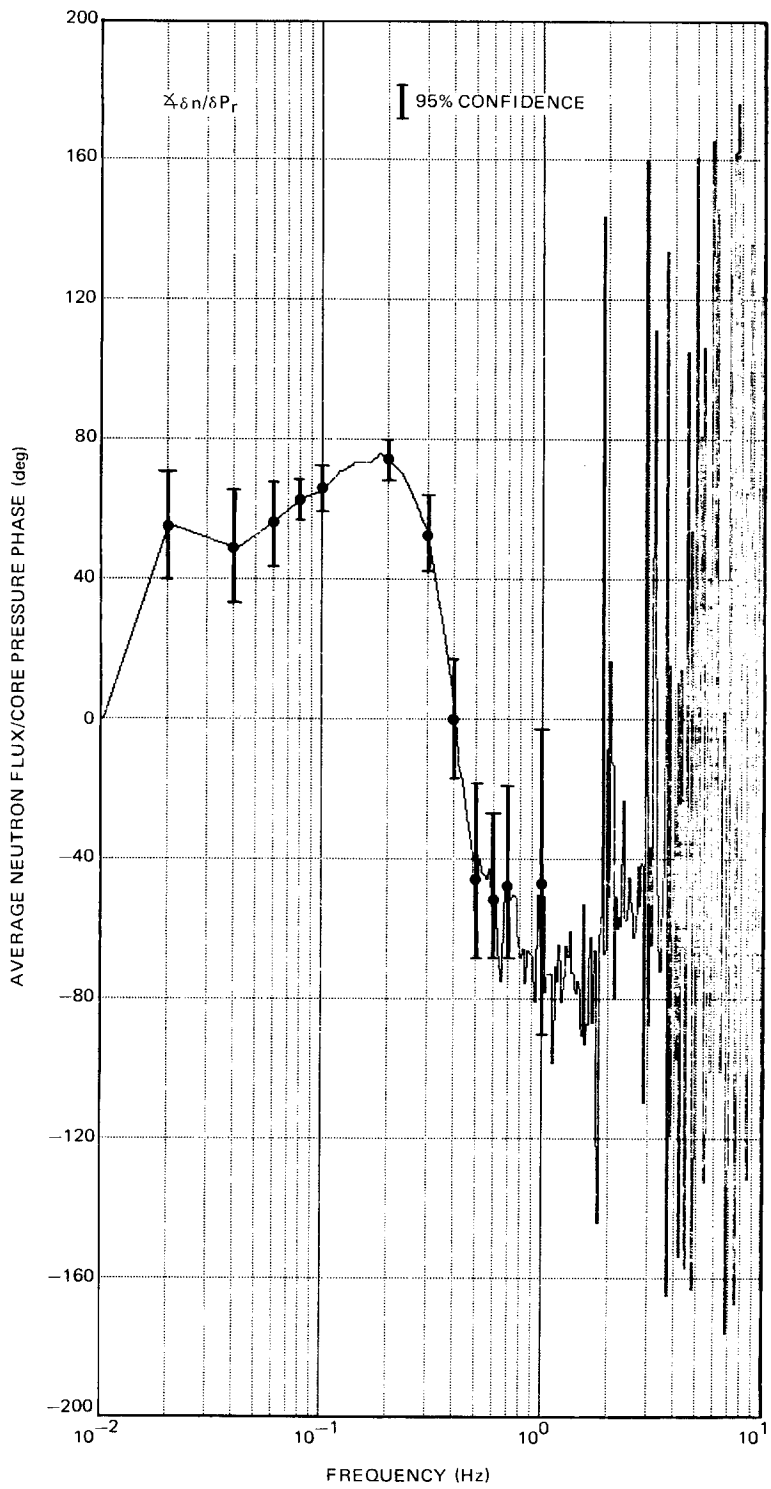


Figure E-14. Peach Bottom-2 EOC2 Low-Flow Stability Test (PT4) Measured Transfer Function Phase Average Neutron Flux (APRM A)/Core Pressure

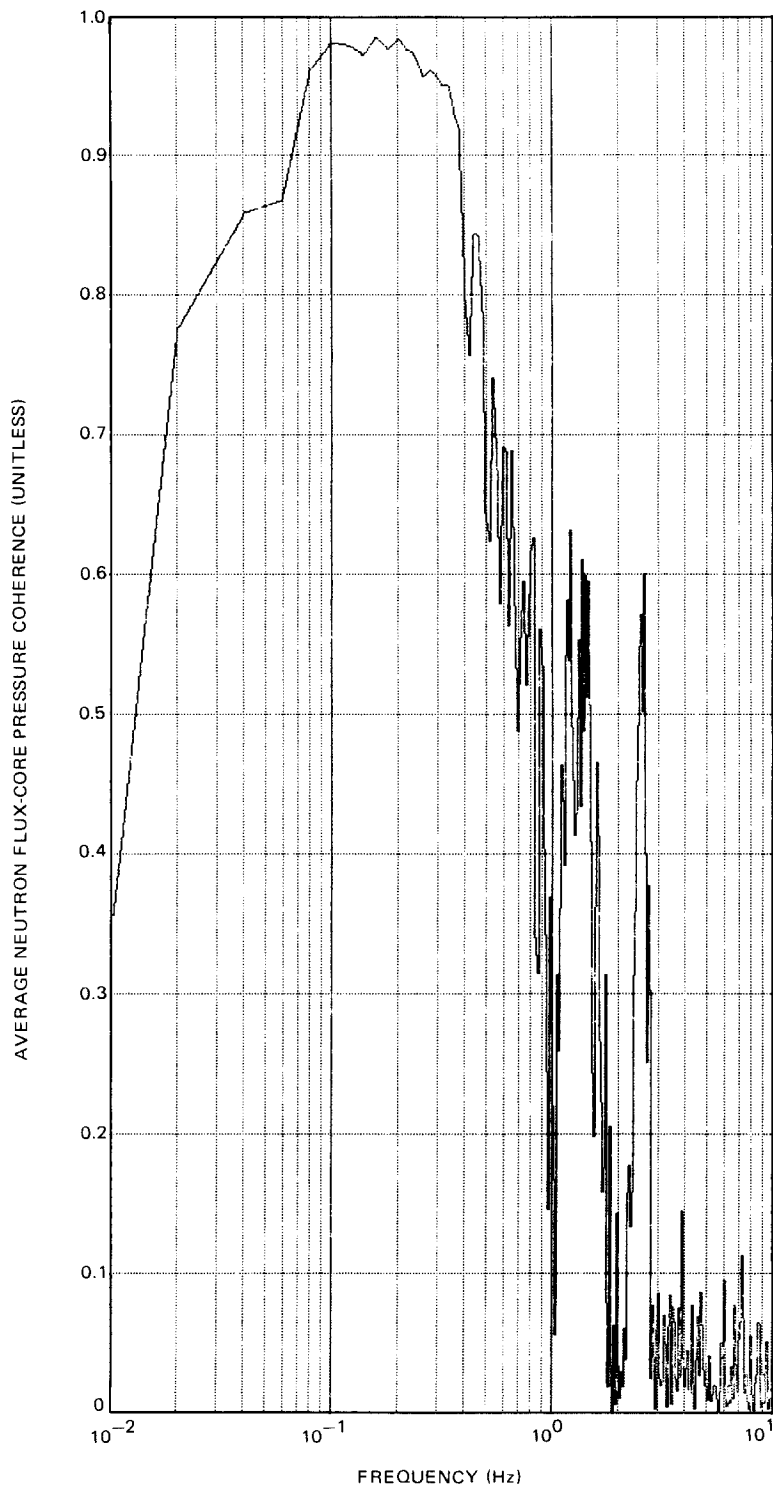


Figure E-15. Peach Bottom-2 EOC2 Low-Flow Stability Test (PT4) Coherence Between Average Neutron Flux (APRM A) and Core Pressure Response

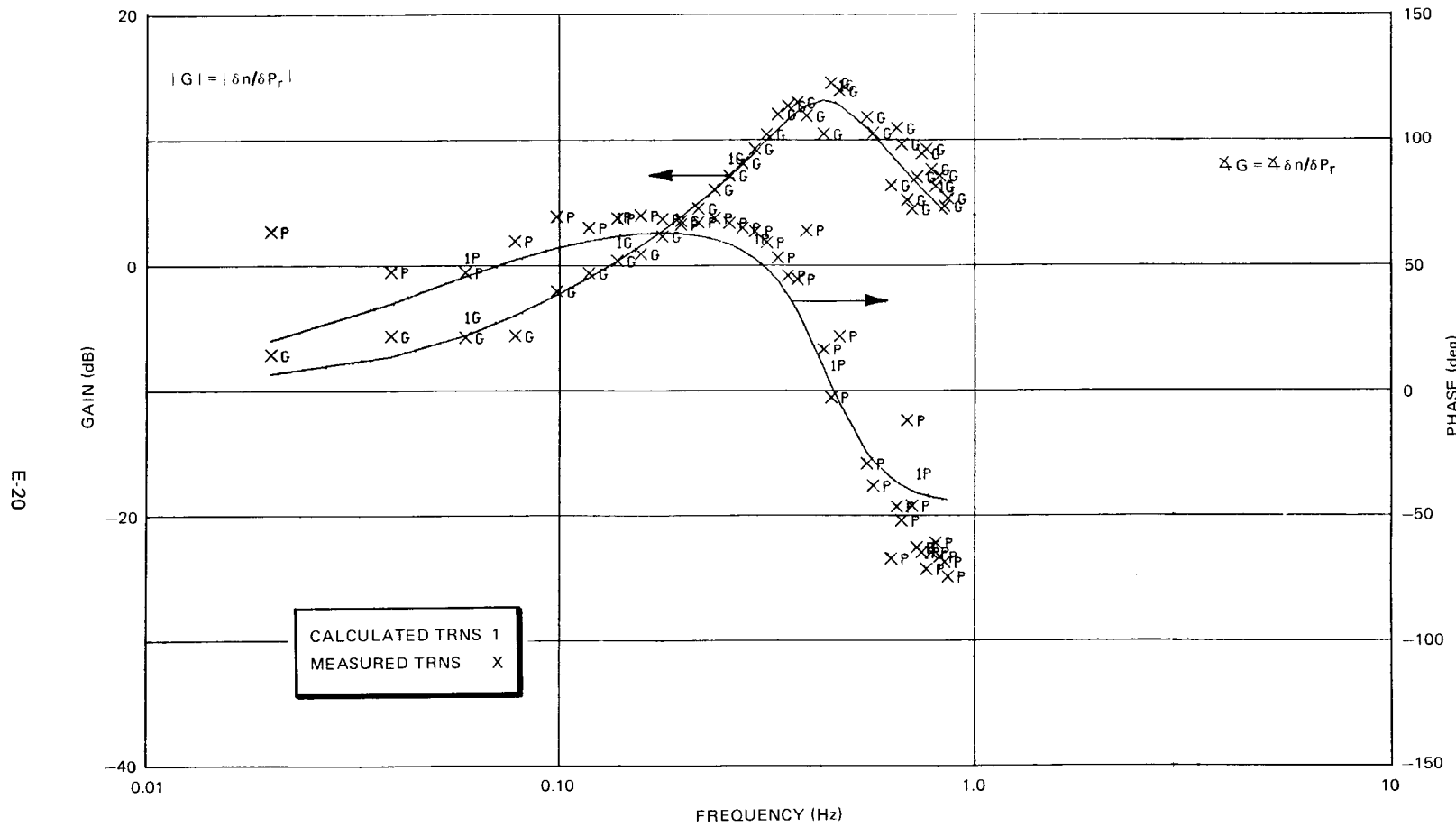


Figure E-16. Peach Bottom-2 EOC2 Low-Flow Stability Test PT1 Transfer Function Model Comparison
(1 Zero/3 Poles)

E21

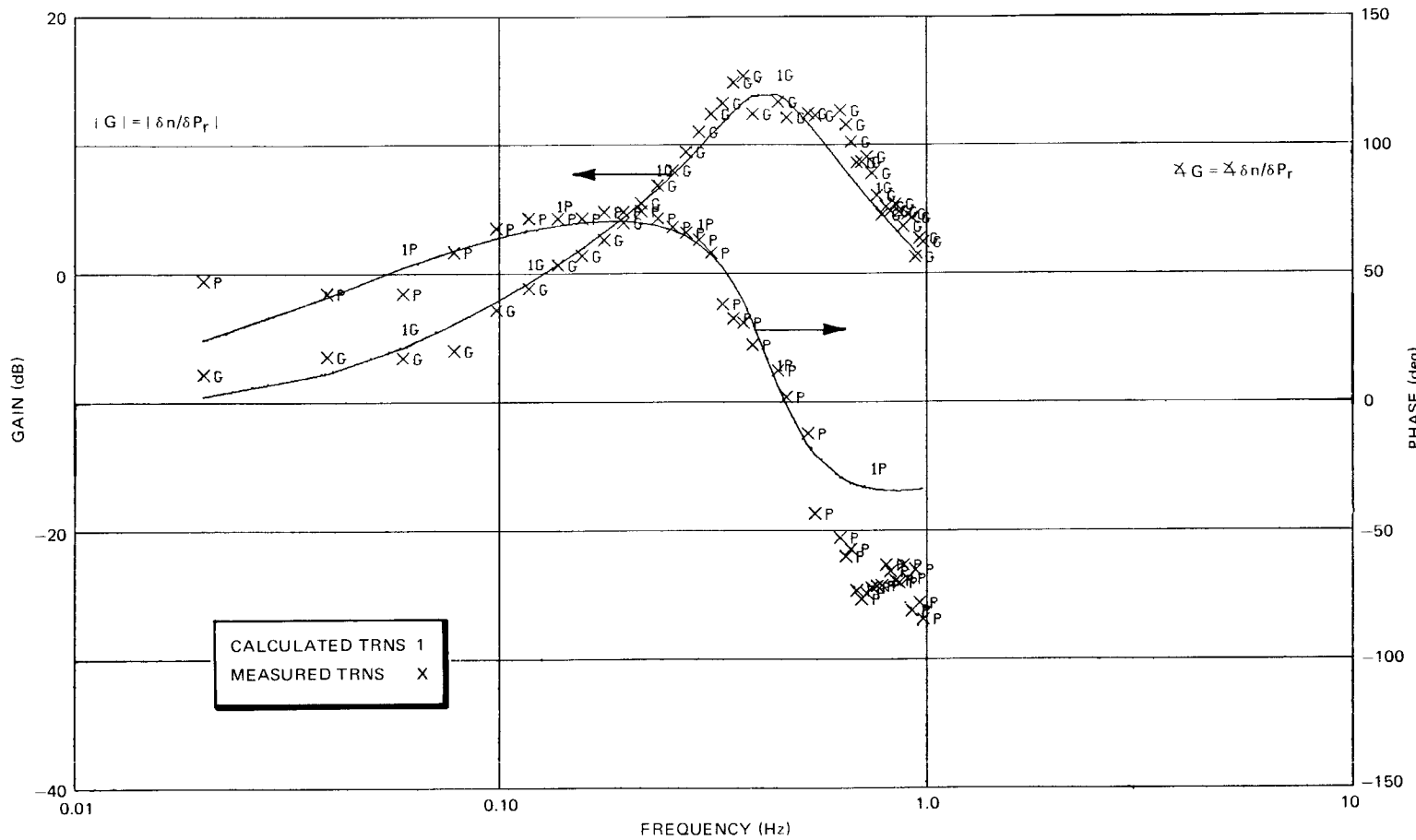


Figure E-17. Peach Bottom-2 EOC2 Low-Flow Stability Test PT2 Transfer Function Model Comparison
(1 Zero/3 Poles)

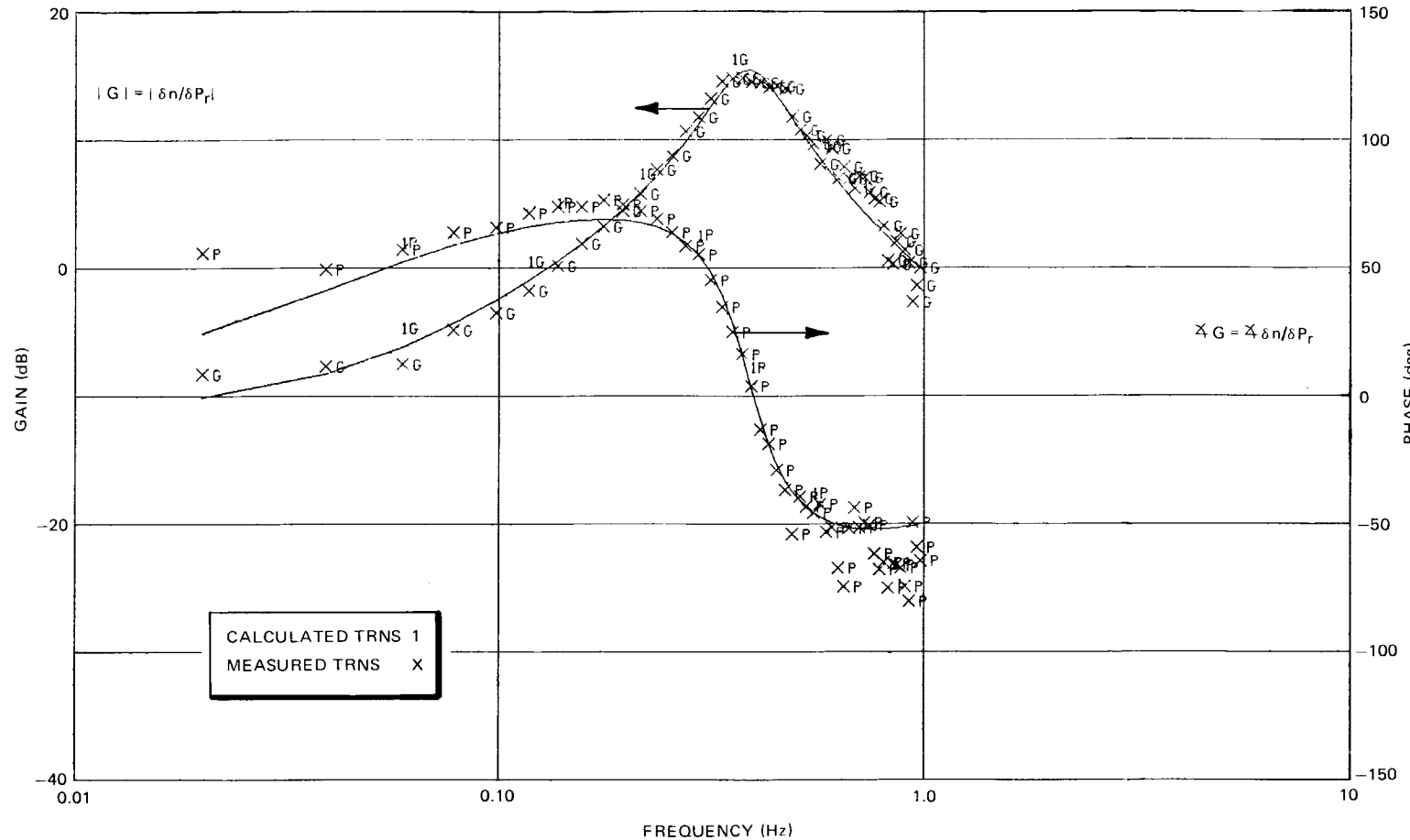


Figure E-18. Peach Bottom-2 EOC2 Low-Flow Stability Test PT4 Transfer Function Model Comparison
(1 Zero/3 Poles)